BEHAVIOUR OF CEMENTITIOUS SUBBASE LAYERS IN BITUMEN BASE ROAD STRUCTURES

BY

MORRIS DE BEER

Presented as partial fulfillment of the requirements for the degree M(Eng)
in the Faculty of Engineering, University of Pretoria

PRETORIA, NOVEMBER 1985

SUMMARY

The process of designing cementitious layers (weakly and strongly cemented) against fatigue distress in road structures is well accepted. Research and field investigations with the aid of the Heavy Vehicle Simulator (HVS) revealed, however, that almost all weakly cemented subbase layers undergo non-traffic and traffic-associated cracking and eventually degradation of the cemented material into a granular state (postcracked phase). It is therefore very important to analyse these layers in the postcracked phase and to incorporate the results of this analysis in the design, for both new and rehabilitation designs. The investigations revealed that the rate of degradation of these materials is largely dependent on traffic loading and the moisture conditions within the pavement layers.

The purpose of this study is to investigate the behaviour of weakly cemented subbase layers in road structures mainly under a bitumen base between 90 mm and 140 mm thick. This behaviour includes both precracked and postcracked phases. It is shown that the fatigue life of bitumen base layers is mainly governed by the condition of the weakly cemented subbase layers.

In Chapter 1 a brief historical review is given of the development of fatigue distress criteria of the cementitious layers. It is shown that the maximum horizontal tensile strain at the bottom of these layers is the main distress criterion in the precracked phase. Unconfined compressive strength and durability requirements are also discussed.

Some aspects of the current design methods are outlined in Chapter 2. The concept of equivalent granular states in the post-cracked phase of cementitious layers was derived from HVS test findings. However, before this document no behavioural prediction models were available to quantify accurately the postcracked state of these layers. The actual mechanisms of distress were also not clear.

In Chapter 3, a detailed investigations and analysis of ten different HVS tests at four different sites in Natal are discussed. The purpose of the analysis, is firstly to illustrate the powerful method of full-scale accelerated HVS-type testing and secondly to indicate the importance of the upper subbase layer, the initial condition of the in-situ structure, the importance of water conditions within the pavement structure, and finally the different states of behaviour of this type of road structure, including predictions of future behaviour based on linear elastic theory. The characteristics of the weakly cemented upper subbase layer are shown to be of paramount importance in the final behaviour of these structures.

In Chapter 4 a method of analysing the behaviour of mainly weakly cemented layers in the postcracked phase is proposed. This method arises from the HVS testing discussed in Chapter 3, and may be regarded as the most important improvement on the current method discussed in Chapter 2. The analysis incorporates the determination of the effective elastic moduli of weakly cemented subbase layers, including both the wet and the dry periods during the structural design period of these layers.

In Chapter 5 the effect of relatively weak interlayers within asphalt base structures is discussed and evaluated. The analysis incorporates the relative position and thickness of the interlayer during both wet (low modulus) and dry (high modulus) conditions.

A summary and detailed discussion, together with recommendations for future research, are given in Chapter 6. The need for the incorporation of durability (erodibility) criteria for weakly cemented materials is also discussed. More research should be done on the effects of accelerated curing compared with normal curing methods. This investigation includes aspects of soil-lime-cement reactions together with delayed compaction techniques to reduce shrinkage cracking. The need for better quality control as well as improved construction techniques for weakly cemented materials is also discussed.

This thesis also contains two appendices. In the first of these detailed photographic records of the different HVS tests and performances are given. In the second appendix an example of an input computer program to plot the three dimensional behavioural model is given.

OPSOMMING

Die proses om sementerende lae (swak- en sterkgesementeerd) teen verswakking vanweë vermoeiing in padstrukture, te ontwerp, is allerweë goed.

Veldondersoeke en navorsing wat met behulp van die Swaarvoertuigna-bootser (SVN) uitgevoer is, het egter aangetoon dat byna alle swakgesementeerde stutlae kraakvorming ondergaan wat aan nie-verkeersverwante en verkeersverwante invloed te wyte is en gevolglik aanleiding gee tot die degradering (afbreking) van die gesementeerde materiaal tot 'n korrelrige materiaal (nakraakfase). Dit is dus baie belangrik om hierdie lae tydens die nakraakfase te ontleed en in die ontwerp vir sowel nuwe as vernuwingsontwerpe, in te sluit. Die ondersoeke het getoon dat die tempo van degradering van hierdie materiale in 'n groot mate afhanklik is van die verkeersbelasting en die vogtoestande in die plaveisel.

Die doel van hierdie studie is om ondersoek in te stel na die gedrag van die swakgesementeerde stutlae in padstrukture, onder hoofsaaklik 'n bitumenkroonlaag wat tussen 90 mm en 140 mm dik is. Hierdie gedrag sluit die voor- sowel as nakraakfase van die swakgesementeerde stutlae in.

In Hoofstuk 1 word 'n bondige historiese oorsig gegee van die ontwikkeling kriteria vir verswakking vanweë vermoeiing vir gesementeerde lae. Daar word aangetoon dat die belangrikste verswakkingskriterion in die voorkraakfase van hierdie lae die maksimum horisontale trekvervorming op die bodem van die laag is. Onbegrensde druksterkte en duursaamheidsvereistes word ook bespreek.

Sekere aspekte van die huidige ontwerpmetodes word in breë trekke in Hoofstuk 2 bespreek. Die konsep var ekwivalente korrelrige toestande in die nakraakfase van sementerende lae is uit SVN-toetsresultate afgelei. Daar bestaan egter geen vroeëre gedragsvoorspellingsmodelle wat die nakraaktoestand van hierdie lae akkuraat kan kwantifiseer nie. Die werklike verswakkingsmeganismes was ook nie duidelik nie.

In Hoofstuk 3 word 'n gedetailleerde ondersoek en ontleding van tien verskillende SVN-toetse wat op vier verskillende terreine in Natal uitgevoer is, bespreek. Die doel van die ontleding is eerstens om die kragtige metode van volskaalse versnelde SVN-tipe toetswerk aan te toon; tweedens om die belangrikheid van die boonste stutlaag, die aanvanklike toestand van die in situ-struktuur, die invloed van watertoestand in die plaveisel en laastens die verskillende gedragstoestande van hierdie tipe padstruktuur tesame met toekomstige gedragsvoorspelling gebaseer op die linieêre elastisiteitsteorie, aan te toon. Daar word aangetoon dat die eienskappe van die swakgesementeerde boonste stutlaag van pertinente belang is in die finale gedrag van hierdie strukture.

'n Metode om die gedrag van hoofsaaklik swakgesementeerde lae in die nakraakfase te ontleed, word in Hoofstuk 4 voorgestel. Hierdie metode spruit voort uit die SVN-toetswerk wat in Hoofstuk 3 bespreek is, en kan beskou word as die mees belangrikste verbetering aan die huidige metode wat in Hoofstuk 2 bespreek word. Die ontledings sluit hoofsaaklik bepaling van die effektiewe elastisiteitsmoduli van swakgesementeerde stutlae in met inbegrip van sowel die nat as droë periodes gedurende die beplande struktuurgebruiksduur van hierdie lae.

In Hoofstuk 5 word die effek van relatief swak tussenlae in asphaltkroonlaagstrukture bespreek en geëvalueer. Die ontleding sluit die relatiewe posisie en dikte van die tussenlaag gedurende die nat (lae modulus) sowel as die droë (hoë modulus) toestand in.

'n Opsomming en gedetailleerde bespreking, tesame met aanbevelings vir toekomstige navorsing, word in Hoofstuk 6 aangegee. Die behoefte vir die insluiting van duursaamheidskriteria (erodeerbaarheid) vir swakgesementeerde materiale word ook bespreek. Meer navorsing behoort ook gedoen te word op die uitwerkings van versnelde nabehandeling in vergelyking met normale nabehandelingsmetodes. Hierdie ondersoek sluit aspekte in oor grond-kalk-sementreaksies tesame met vertraagde verdigtingsmetodes om krimpingskrake te verminder. Die behoefte aan beter gehaltebeheer asook verbeterde konstruksietegnieke vir swakgesementeerde materiale word ook bespreek.

Hierdie proefskrif bevat ook twee bylaes. In die eerste bylae word omvattende fotografiese verslae van die verskillende SVN-toetse en -werkverrigting gegee. In die tweede bylae word 'n voorbeeld gegee van 'n rekenaarinvoerprogram waarmee die driedimensionele gedragsmodel gestip kan word.

ACKNOWLEDGEMENTS

The author would like to express his sincere thanks to the following persons and departments:

The Chief Director, Dr. S H Kühn, National Institute for Transport and Road Research of the Council for Scientific and Industrial Research, for the opportunity to do this study and complete this thesis.

My Group Head and co-supervisor at the NITRR, Dr. Charles R Freeme, for his sincere interest, innovative discussions and comments on the concepts and contents of this thesis.

My supervisor, Professor Philip F Savage, for his interest, advice and valuable discussions and comments on the contents of this thesis.

Messrs. M D Loesch, Graham Haldane, C E L Viljoen and L Marks and their technical teams for their assistance with the substantial amount of HVS and field data collection. Without their help it would have been impossible to complete this work.

The Regional Office of the Department of Transport in Pietermaritzburg for their coöperation and support during this study.

Mesdames Y E Diering and B E Saler of the Drawing office for their help in the preparation of the drawings.

All my other colleagues in the Pavement Engineering Group for their help and assistance during this study.

A special word of thanks to my wife, MARION for her continued support, interest and encouragement during this study.

EN dan my grootste dankbaarheid aan God wat my ook hierin gelei het.

CONCEPTS ARE UNLIMITED
CONCEPTS ARE IMPRESSIVE
BUT ITS ONLY DATA THAT WORKS!

AAN :

MY HARDWERKENDE EN VOORBEELDIGE OUERS :

PEARL EN T.A.P. DE BEER

DANKIE.

CONTENTS

CHAPTER 1

A BRIEF HISTORICAL REVIEW ON FATIGUE OF CEMENTITIOUS LAYERS IN ROAD STRUCTURES

CONTENTS

1.1 INTRODUCTION

Much work has been done on the fatigue characteristics of concrete and strongly cemented materials. (Pretorius, 1970; Otte, 1972). Most of the authors realised that cementitious layers in the road structures should be designed so that it is not overstrained at the bottom; using the induced tensile strain at the bottom of the layer as distress criterion, rather than tensile stress. (Kaplan, 1963; Otte, 1978). This approach was mainly used to design cementitious base course layers for road structures. When the "upside down" designs developed in the late 1970's, cementitious layers were used for the subbase layers. During the period prior to 1979, relatively strongly cemented materials were used for the base and subbase layers. Shrinkage or thermal cracking owing to excessive levels of drying shrinkage stresses, exceeding the tensile strength of the uncracked material, was intensively studied and reported on by various authors (Marais, 1973; Groth, 1973; Biesenbach, 1973; Vail, 1973; Blight, 1973 and Pretorius, 1973). When these strongly cemented layers were used as subbase layers under relatively thick (100-200 mm) bitumen bases, reflection cracking caused great concern (Freeme et al 1974, 1979, 1982). These reflection cracks formed excellent paths for free water ingress which eventually leads to rapid pavement deterioration (Otte, 1973).

During the late 1970's and early 1980's there was a strong move away from strongly cemented layers to unbound granular layers (Freeme, et al 1979). It was however soon realized that the latter type of design resulted in relatively thick bitumen base layers being required to support the load.

Economical analyses (Freeme et al, 1980) indicated however that bitumen base pavements with weakly* cemented subbase

---

* The terms "strongly" and "weakly" are intended to reflect the initial 7-day strength (ucs) characteristic of the cemented layer whereas the terms "well" and "poorly" will be used to reflect workmanship or degradation.

layers can be cheaper than those with granular subbases. This is accomplished by a reduction in the thickness of the bitumen base layer. These new economic designs could save up to 25 per cent compared to the conventional designs of 1980 (Freeme et al, 1984). It must be stressed that the strong move towards weakly cemented materials was mainly to overcome the drying shrinkage cracking, experienced with the relatively strongly cemented materials and not to reduce strength. Proper definition of the difference between "weakly" and "strongly" cemented materials is given in Chapter 2. During the early 1980's a few experimental sections were constructed as well as normal high class traffic pavements in Natal using these economic designs.

Since that time, much of the national road structures included weakly cemented (lime, slag-cement or cement treated) subbase layers, usually 300 mm thick, built in two layers each 150 mm thick. Recent investigations on the behaviour of cementitious subbase layers in South Africa, using the Heavy Vehicle Simulator, (HVS) demonstrated that these subbase layers experience relatively early fatigue distress in the form of cracks. The investigations indicates that these layers provide adequate support during the postcracked phase. The HVS tests indicated that for such pavements more than 80 per cent of the "life" of the cementitious subbase layers occurs in the postcracked phase.

In this chapter a short review is given on the fatigue characteristics of the earlier "strongly cemented" materials.

1.2 HISTORICAL REVIEW

Pretorius (1970) studied and discussed "Design Considerations for Pavements Containing Soil Cement Bases" in the 1970's.

The most valuable part of his work, concerning this thesis, was the development of fatigue relationships and obtaining elastic and strength properties for strongly cemented materials.

He stated, concerning fatigue of cementitious material that:

> "The fatigue characteristics of the soil-cement and the factors that influence its fatigue behaviour are therefore major factors to consider in the design of a pavement containing a soil-cement base".

Because of the importance of above statement, a fatigue investigation resulted in a fatigue-life versus strain relationship, illustrated in Figure 1.1. The relationship between life (N) and initial maximum flexural microstrain (ε_i); is:

$$N = \left(\frac{142}{\varepsilon_i} \right)^{20.3} \quad \ldots\ldots\ldots\ldots\ldots\ldots\ldots\ldots\ldots\ldots \quad (1.1)$$

The relation can be used to indicate that flexural strains from 70 to 130 microns results in a fatigue-life spectrum of 10 to one million applications of load before any micro fatigue cracking is initiated at the bottom of soil-cement beam specimens. See also Figure 1.1.

He further showed that the Poisson's ratio and volumetric micro strains for soil cement varies with stress level, between 0,1 and 0,5, and less than zero to 600, respectively. Linear relationships between unconfined compression strength (UCS) and tensile strength were also obtained. There was, however a difference between the relationship obtained from direct tension and flexture tests. The simple beam theory was used for his calculations, although he was aware of the fact that the modulus of elasticity in tension is less than the modulus in compression (anisotropy). The ratio of compressive to tensile flexural strength is larger than 5. Pretorius mentioned also that the aggregate- mortar bond is the weak link in the strength of cement treated materials. Other researchers (Jones, 1965; Taylor and Broms, 1964; HSU, 1963; Kaplan, 1963; Shah and Winter, 1966), also reported in depth on this subject.

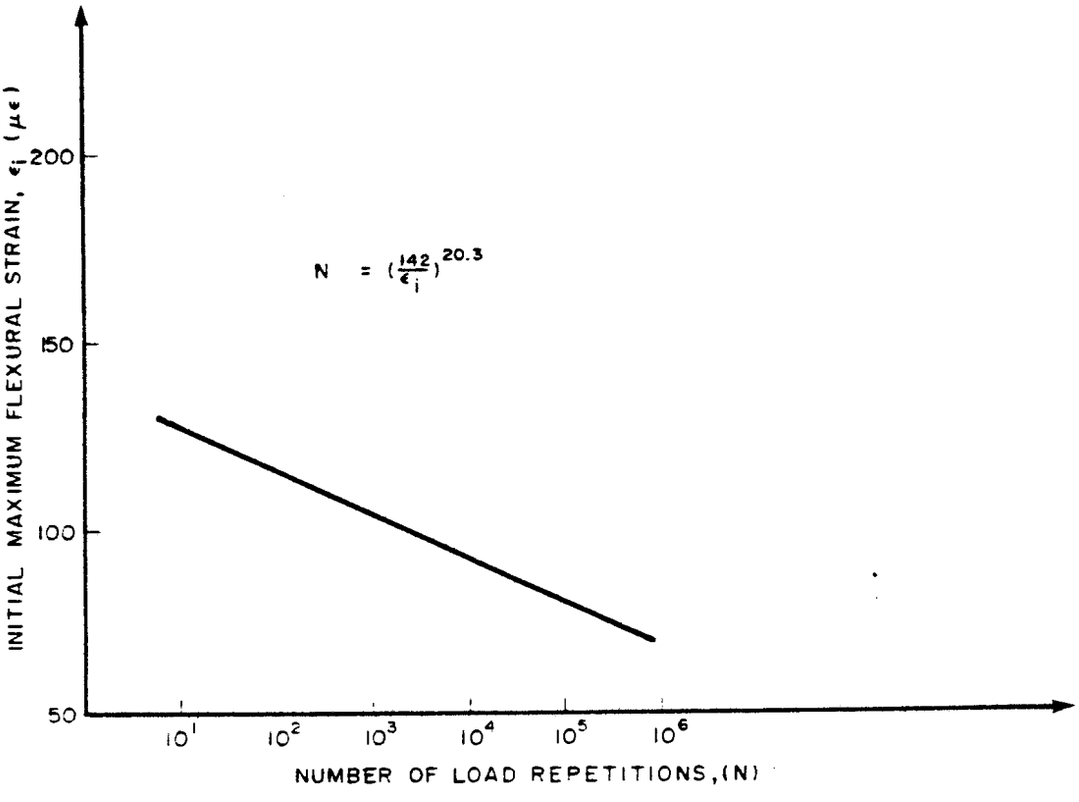

FIGURE 1.1

FATIGUE LIFE OF FLEXURAL SPECIMENS (PRETORIUS, 1970)

The modulus of elasticity and the unconfined compressive strength of the material tested by Pretorius for the fatigue relationship were 19300 MPa and 7MPa respectively, with a A-1-0 non-plastic AASHO classification.

During the period 1972 to 1978, Otte worked in this field in South Africa and proposed a fatigue relationship. From literature this fatigue relationship was adopted and is now in use in the South African design method (Otte, 1978; Walker et al, 1977; Freeme et al, 1982). No fatigue work on cementitious materials was done by Otte. The fatigue relation adopted is illustrated in Figure 1.2. This relationship is:

$$N_f = 10^{9,1\ (1\ -\ \frac{d.\varepsilon}{\varepsilon_b})} \quad \ldots\ldots\ldots\ldots\ldots\ldots\ldots\ldots\ldots \quad (1.2)$$

were N_f = Number of repetitions at strain ε_s to crack initiation. It differs from the previous equation given by Pretorius (eq 1.1), in that the strain at break, ε_b, is incorporated with the strain induced at crack initiation, ε_s. Eq 1.1 incorporates only the initial maximum flexural strain, ε_i, which is comparable to ε in eq 1.2, without any modification for shrinkage cracking (Freeme, et al 1982). The modified strain is:

$$\varepsilon_s = d.\varepsilon \quad \ldots\ldots\ldots\ldots\ldots\ldots\ldots\ldots \quad (1.3)$$

where d = Factor from Table 1.1
ε = Traffic induced micro strain

A comparison between the fatigue relationship suggested by Otte, and the relationship obtained by Pretorius is given in Figure 1.3. It is important to note that eq 1.2 should be compared without the d-factor because Pretorius's result does not include factors for shrinkage in cemented material. It is further important to note that a proper method to compare the two different relationships is to assume a

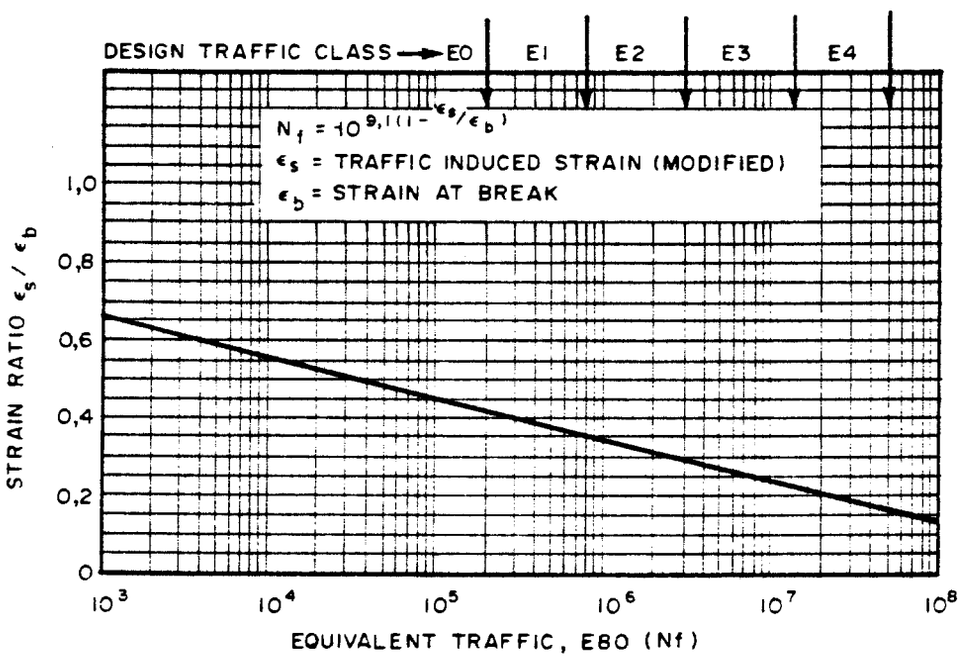

FIGURE I.2

RECOMMENDED FATIGUE RELATION ADOPTED FOR CEMENTITIOUS MATERIALS IN SOUTH AFRICA (FREEME, 1982)

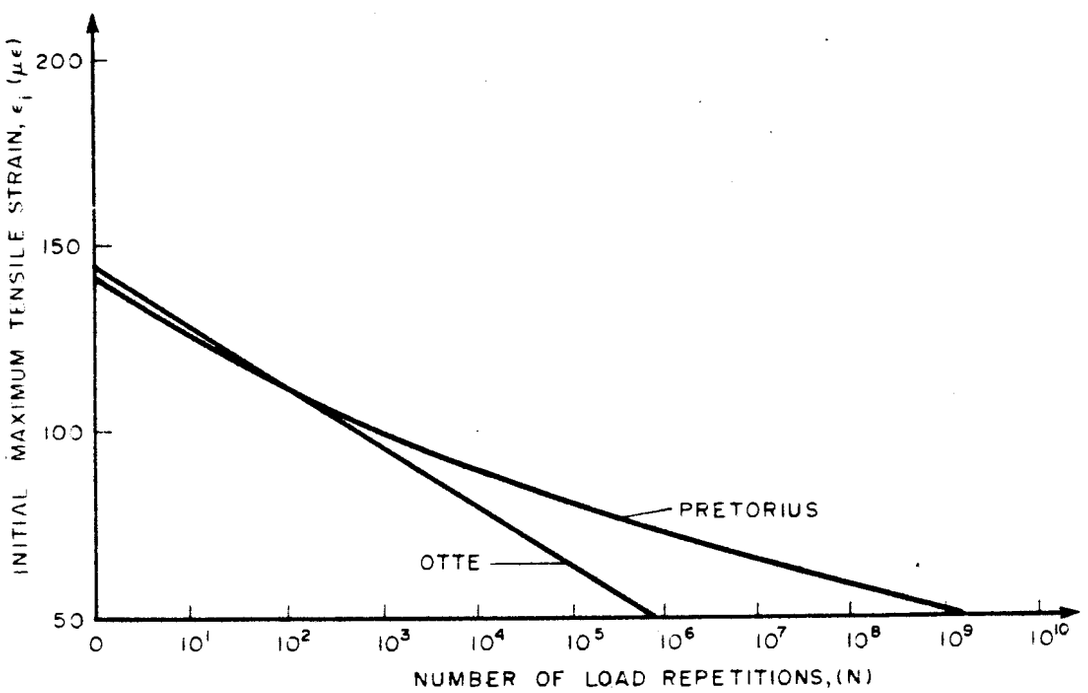

FIGURE 1.3

COMPARISON BETWEEN THE FATIGUE RELATION PROPOSED BY PRETORIUS (1970) & OTTE (1978)

TABLE 1.1 - Factor, d, for modifying the tensile strain induced in cemented materials to allow for the presence of shrinkage cracking (Freeme, et al 1982)

Type of Cracking	Unconfined compressive strengths (MPa)	Factor, d, for total thickness of cemented material (mm)	
		<200	>200
Weakly Cemented:			
Moderate cracking: crack widths less than 2mm			
(eg natural materials	0,75 - 1,5	1,1	1,2
with lime or 2-3% cement	1,5 - 3,0	1,15	1,3
Strongly cemented:			
Extensive cracking: crack widths more than 2mm (eg high quality natural gravels and crushed stone with 4-6% cement)	3-12	1,25	1,4

The tensile strains at break, ε_b, for cementitious material with different unconfined compressive strengths are given in Table 1.2.

TABLE 1.2 - Tensile strain at break recommended for the standard cemented-material categories (Freeme, et al 1982)

Unconfined compressive strength (MPa)	Material type Cemented	Tensile strain at break (ε_b) ($\mu\varepsilon$)
6 - 12	Crushed stone (C1)	145
3 - 6	Stone/gravel (C2)	120
1,5 - 3	Gravel (C3)	125
0,75 - 1,5	Gravel (C4)	145

strain at break for the Pretorius material, ε_b = 142 με. Equation 1.1 indicates that with initial maximum strain of 142 με, the fatigue life is zero. Work done by Otte (1978), indicates however that for similar material to that of Pretorius, an average strain at break of 145 με could be used. Figure 1.3 indicates that the two relationships are consistant for induced strains greater than 100 με, but for induced strains lower than 100 με the relationship suggested by Otte is more conservative.

1.3 FAILURE CRITERION

Pretorius (1970) stated that "no simple failure criterion for the strength of soil-cement under general biaxial stresses exists at the moment". Kaplan (1963) concluded that his test results on concrete suggested that the initiation of cracking may be more dependant on strain as distress determinant rather than on stress. It was also suggested that engineers should develop a better understanding of strain in general rather than stress, because strain values are more consistant than stress in cementitious materials (Otte 1972, 1978). The traffic-induced strain concept was adopted in the South-African design method in the 1970's (Walker et al, 1977), and is still in use, using eq 1.2. Kekwick (1980) concluded in his work on strongly cemented soil slabs that:

> "The general behaviour of the test slabs under load, together with the tensile responses of laboratory-scale specimens and a review of pertinent literature, has led to the adoption of a limiting tensile strain criterion as a fundamental material parameter regarding performance in a pavement system. The limiting strain, defining the extent of elastic material response, represents a maximum allowable deformation to which the material can be subjected in order to sustain many applications of load. This is considered to be a fundamental characteristic of the concrete for highway application with the implication that induced tensile strains greater than the limiting value will lead to structural deterioration".

The author agrees with the above statements but according to the work given in this thesis it holds for less than approximately 20 per cent of the total life of a cementitious subbase layer. According to HVS testing, which will be described later, more than 80 per cent of the "life" of a cementitious subbase layer occurs in the postcracked phase.

During this phase large blocks of cementitious material continue to crack untill the average block size reaches approximately the layer thickness. When this happens the vertical compressive strength (resistance to shear) and erodibility of the cementitious material starts to govern the rut development (permanent deformation on the surface). The initial fatigue distress phase (precracked) does not contribute to any significant amount towards rut development. Because "failure" of a road structure is defined mainly using terminal rut development criteria on the surface, the fatigue distress phase could only be seen as part of the structural rather than functional distress of a road structure, and occurs within 20 per cent of the total life of the structure. The author agrees with Otte that fatigue distress can initiate functional failure through pumping. It is however accepted that the initiation of permanent deformation on the road surface does not start with the first traffic-induced crack at the bottom of the cemented layers.

1.4 OTHER RESEARCHERS (1972 to 1976)

Other researchers: Raad (1976), Van Vuuren (1972), Marais (1973) also worked in the field of cementitious materials. The following section summarise their contributions briefly:

Raad (1976) applied the Griffith and modified Griffith theories to the failure of cement-treated materials. He proposed a new approach to the fatigue life of cement-treated materials which incorporates the biaxial loading condition. He proposed a relationship between the principal major and minor stresses (σ_1 and σ_3) and the tensile strength of the

material (T) and then defined a stress level F/T

$$\text{where } F = \frac{(\sigma_1 - \sigma_3)^2}{8(\sigma_1 + \sigma_3)} \quad \text{when } \sigma_1 + 3\sigma_3 \geq 0 \quad \ldots\ldots\ldots \quad (1.4)$$

Note: + for compressive stresses
- for tensile stresses

$$F = -\sigma_3 \quad \text{when } \sigma_1 + 3\sigma_3 < 0 \quad \ldots\ldots\ldots\ldots \quad (1.5)$$

He proposed a relationship between the stress level F/T and the number of load repetitions to failure (N_f) which is independent of the shape, width (time of loading or duration) and frequency of the applied stress pulses. He applied the relationship to some published work on fatigue of cement-treated materials and it seems to fit the laboratory results obtained by several researchers much better than the simple relationship of stress or strain level versus the number of load repetitions. The application of his laboratory study to pavement design still needs further evaluation, especially after the indication by Walker et al, (1977) that it does not really apply to the behaviour of actual pavements.

Using layered elastic theory and a strain criterion, Van Vuuren (1972) calculated load equivalency factors for fracture in cement-treated materials and demonstrated that they where dependant on the structural layout of the pavement. He calculated equivalency values ranging from 0,1 to 10 000 for cement-treated layers. Otte (1978) concluded that the existing concept of expressing an axle load spectrum as a certain number of equivalent 80 kN axles for a pavement with cement-treated layers is probably incorrect, not applicable and should preferably not be used. It was suggested that each of the different wheel load intensities in the expected traffic spectrum be accommodated when performing the design. Since the number of expected load repetitions cannot be accommodated by calculating E80, some other way has to be devised to accommodate it. It was suggested that Miner's cumulative damage law (Miner, 1945) should be assumed to be

valid and that a procedure similar to that developed by the PCA (1966) for the design of concrete pavements be followed.

Marais (1973) reviewed testing and design criteria for cement-treated bases. From his study it is concluded that unconfined compressive strength and durability tests should be done on these materials. This is in accordance with a study in the USA concerning suitable design criteria for cement-treated layers. In 1967 the extent of use of various design criteria was as shown in Table 1.3. The table shows that the most popular criteria were 7-day unconfined compressive strength and durability.

A review by Williams (1973) of British experience concerning lean concrete roadbases, revealed that no durability criteria were used for their treated materials. However, it is the author's belief that because of the relatively high amount of cement used in lean concrete mixtures, excessive lack of durability is not a problem. The durability problem arises mainly were "soil-cement" or weakly cemented materials are considered, especially fine grained materials. The author believes that this should be investigated in depth in South Africa.

TABLE 1.3 - Extent of use of different design criteria (Marais, 1973)

Design Criteria	Number of States specifying	% of Total
Durability criteria (both freeze-thaw and wet-dry tests) and unspecified compressive strength which increases with age and cement content (PCA criteria)	10	21,8
Durability criteria in addition to a definite 7-day unconfined compressive strength requirement	8	17,4
7-day unconfined compressive strength only	19	41,3
7-day unconfined compressive strength generally with occasional durability tests	2	4,3
7-day unconfined compressive strength in addition to freeze-thaw criteria only	3	6,5
Freeze-thaw durability criteria only in conjunction with increasing unconfined compressive strength	1	2,2
minimum cement content only	1	2,2
CBR criteria	1	2,2
Resistance (R-value) criteria	1	2,1
Total	46	100,0

1.5 SUMMARY

According to this review, most of the research on the behaviour of relatively strongly cemented layers in road structures, constitutes the fatigue characteristics under repetitive loading. It is concluded that the main distress criterion is the maximum horizontal tensile strain at the bottom of such layers. Biaxial stress conditions however were also investigated in the laboratory, but uncertainty exists in the applicability thereof in practice. Investigations into the load equivalency of cementitious layers indicated a very wide range (0,1 to 10 000) for cement treated layers, and that equivalency should be incorporated in the design. It was further shown interestingly enough that in the USA various design criteria during the 1960's were used. Of these the 7-day UCS and durability were the most popular.

1.6 DISCUSSION

In South Africa, during the late 1970's and early 1980's cementitious layers were designed in accordance with its fatigue characteristics using the theoretical procedure, Otte (1978). Provision was also made for thermal stresses and shrinkage, by increasing the induced tensile strain at the bottom of the layer. If the ratio between the modified induced strain (ε_s) and the strain at break (ε_b) are less than 0,3, the cementitious layer should at least withstand one million strain repetitions without fatigue distress. (Otte, 1978) Extensive Heavy Vehicle Simulator (HVS) testing on weakly cemented subbase layers revealed relatively early fatigue distress, afterwhich these layers undergo advanced fatigue distress and break up into the postcracked phase. In this phase, however the layer still provides adequate support in relatively dry conditions (Freeme et al, 1984). The author considers that the behaviour of these materials in the postcracked phase must be incorporated into the design, including the rehabilitation design throughout the life of these types of pavements. It will be shown later on that almost 90 per

cent of the "life" of the weakly cemented layers occurs in the postcracked phase.

Another very important aspect to consider with cementitious materials stabilized with lime, cement, lime/slagment etc., is the important difference between "modification" and "cementation" (Clauss, 1982). It is however beyond the scope of this dissertation to discuss the rather complicated chemistry of soil cementation or modification.

The difference in "strength" and "durability" of cementitious materials is also important and this will be discussed in Chapter 3.

1.7 REFERENCES

PRETORIUS, P C (1970). Design considerations for pavements containing soil-cement bases. Ph.D thesis, University of California, Berkeley, California.

OTTE, E (1972). The stress- strain properties of cement-treated materials. M.Sc. thesis, University of Pretoria (in Afrikaans).

KAPLAN, M F (1963). Strains and stresses of concrete at initiation of cracking and near failure. ACI Journal, Proceedings V.60, No.7 pp. 8573-879.

OTTE, E (1978). A structural design procedure for cement-treated layers in pavements. DSc thesis, University of Pretoria, South Africa.

MARAIS, G P (1973). Transvaal Experience with Cement-treated crushed rock bases. NIRR-PCI Symposium on Cement-treated Crusher-run bases, Johannesburg, February, 1973.

GROTH, P J (1973). The history and performance of Cement-treated crusher-run bases in Natal. NIRR-PCI Symposium on Cement-treated crusher-run bases, Johannesburg, February, 1973.

BIESENBACH, W J (1973). Cement-treated bases in the Cape Province. NIRR-PCI Symposium on Cement-treated Crusher-run bases, Johannesburg, February, 1973.

VAIL, J W (1973). A review of the factors affecting the drying shrinkage cracking of cement-treated crusher-run bases. NIRR-PCI Symposium on Cement-treated crusher-run bases, Johannesburg, February, 1973.

BLIGHT, G E (1973). Theoretical deductions from observed crack patterns in roads with cement-treated bases. NIRR-PCI Symposium on cement-treated crusher-run bases, Johannesburg, February, 1973.

PRETORIUS, P C (1973). Shrinkage and traffic induced stresses in cement-treated crusher run bases. NIRR-PCI Symposium on cement-treated crusher-run bases, Johannesburg, February, 1973.

FREEME, C R and MARAIS, C P (1974). Traffic associated cracking of asphalt pavements. Proc 2nd Conf. on Asphalt Pavements for Southern Africa, Durban, 1974.

FREEME, C R, and STRAUSS, J A (1979). Towards the structural design of more economical pavements in South Africa. Proc. 3rd Conf. on Asphalt Pavement for South Africa, Durban.

FREEME, C R, MAREE, J H and VILJOEN, A W (1982). Mechanistic Design of Asphalt Pavements and Verification using the Heavy Vehicle Simulator. Proc. of the 5th Int. Conf. on Structural Design of Asphalt Pavements, Delft, Holland, August 1982, vol 1, p 156-173.

Otte, E (1973). The performance of two pavements containing cement-treated crusher-run bases. NIRR-PCI Symposium on Cement-treated crusher-run bases, Johannesburg, February, 1973.

FREEME, C R, OTTE, E and MITCHELL, M F (1980). The economics of pavement type selection. National Transport Commission Department of Transport, Pretoria, April, 1980.

FREEME, C R and WALKER, R N (1984). Economic design of bituminous pavements. Proc. 4th Conf. on Asphalt Pavements for South Africa, Cape Town.

JONES, R (1965). Cracking and Failure of Concrete Test Specimen Under Uniaxial Quasi- Static Loading. International Conference on the Structure of Concrete and Its Behaviour Under Load, Imperial College, London, September 28-30.

TAYLOR, M A and BROMS, B B (1964). Shear bond strength between coarse aggregate and cement paste or mortar. ACI Journal, Proceedings V. 61, No. 8 pp. 54-98.

HSU, T C (1963). Mathematical analysis of Shrinkage Stresses in a Model of Hardened Concrete. ACI Journal, Proceedings V. 60, No. 3, pp. 371-389.

SHAH, S P and WINTER, G (1966). Inelastic behaviour and fracture of concrete. American Concrete Institute, Publication SP-20, p. 5.

OTTE, E (1978). A structural design procedure for cement-treated layers in pavements. DSc thesis, University of Pretoria, South Africa.

WALKER, R N, PATERSON, W D O, FREEME C R and MARAIS, C P (1977). The South African mechanistic pavement design procedure. Paper accepted by Fourth Int. Conf. on the Structural Design of Asphalt Pavements.

KEKWICK, S V (1980). Tests on wet-lean concrete in relation to use for road construction. Ph.D thesis, University of Surrey, 1980.

RAAD, L (1976). Design criteria for soil-cement bases. Ph.D thesis, University of California, Berkeley, California.

VAN VUUREN, D J (1972). Discussion on paper by Brown and Pell. Proc. Third Int. Conf. on the Structural Design of Asphalt Pavements, vol. II, p. 172.

MINER, M A (1945). Cumulative damage in fatigue. J. of Applied Mechanics, vol. 12, September, p.A-159.

PCA (1966). Thickness Design for Concrete pavements (ISOIO. 02P). Portland Cement Association.

MARAIS, L R (1973). Testing and design criteria for cement-treated bases. NIRR-PCI Symposium on Cement-Treated Crusher-Run Bases, Johannesburg, February.

WILLIAMS, R I T (1973). Lean Concrete Roadbases - A review of British Experience. NIRR-PCI Symposium on Cement-treated Crusher-Run Bases, Johannesburg, February.

CLAUSS, K A (1982). Stabilization properties of dry processed, waste, carbide lime. NITRR Report RS/2/82 (Unpublished), November, 1982.

CHAPTER 2

ASPECTS OF THE CURRENT DESIGN METHOD OF CEMENTITIOUS SUBBASE LAYERS IN SOUTH AFRICA

CONTENTS

2.1 INTRODUCTION

In order to understand the actual behaviour of road pavements, it is essential to define the necessary parameters controlling the behaviour of the pavement. The concept of different states for the same structure during its service life was introduced. Freeme (1984) defined the behavioural states of the pavement structures encountered in South Africa. The author was involved in especially the developing of the understanding of the behavioural states of weakly cemented subbase layers under bitumen bases in Natal, South Africa. It was found that these cementitious layers undergo marked changes in state during their behaviour as structural elements in the pavement. It is therefore important to take this into account during the design stage.

2.2 BACKGROUND

As discussed in Chapter 1, a variety of economical pavements with asphalt bases was proposed during the late 1970's, based on mechanistic design principles, Freeme et al (1979). During this period it was believed that better use could be made of the properties of asphalt bases by placing them over gravel subbases rather than strongly cemented subbases. It was believed that less conservative fatigue criteria could lead to thinner asphalt bases. According to Freeme (1984) significant advances were made in the design of bitumen base pavements. According to economic comparisons made in 1980 (Freeme et al, 1984) weakly cemented subbase layers appeared to be cheaper than granular subbase layers, based on the present worth of cost (PWOC) method. Because of the economic implications especially for the high traffic class (E4)* roads, a number of experimental sections, based on the proposed economical designs were constructed during 1980 to 1982 in Natal. The purpose of this dissertation, however, is not to discuss the economic implications but to investigate the behaviour of the

---

*E4 : 12 to 50 million E80s, NITRR (1985).

weakly cemented subbase layers and their influence on the rest of the structure in terms of their structural and functional lives. Suggestions of how to take account of the different behavioural aspects during the design and rehabilitation stage are made.

2.3 PRESENT DESIGN PHILOSOPHY FOR CEMENTITIOUS MATERIALS IN SOUTHERN AFRICA

As discussed in Chapter 1, the method adopted in South Africa was to limit the horizontal tensile strain at the bottom of cementitious layers (strongly and weakly cemented) as proposed by Otte (1978). More recently the concept of precracked and postcracked states for these layers was discussed by Freeme (1984). From HVS testing and field behaviour of these layers, it was soon realized that most of the structural and functional life of pavements occur while the cementitious base- or subbase layers were in the postcracked state.

The behaviour of cementitious layers is best explained by initially discussing changes in its effective modulus which occur with time (traffic). A typical example of changes in modulus a C2 quality material (See Table 2.1) will be discussed.

These changes are shown diagrammatically in Figure 2.1(a). Initially in the precracked phase the effective modulus will be relatively high (3 to 4 GPa) and the layer will behave much as a slab of concrete, i.e. "very stiff" state. However, shrinkage cracks and load associated cracking can reduce the effective modulus even though discrete large blocks of the material still retain the high modulus of the original cemented (stabilized) material. The effective modulus can continue to drop to lower values in the order of 500 MPa, at which time the discrete blocks will be fairly small and could form a mosaic. The behaviour at this stage is then very similar (equivalent) to that of high quality granular material but the structure changed into the "flexible" state. The eventual modulus in this state will depend on the quality of

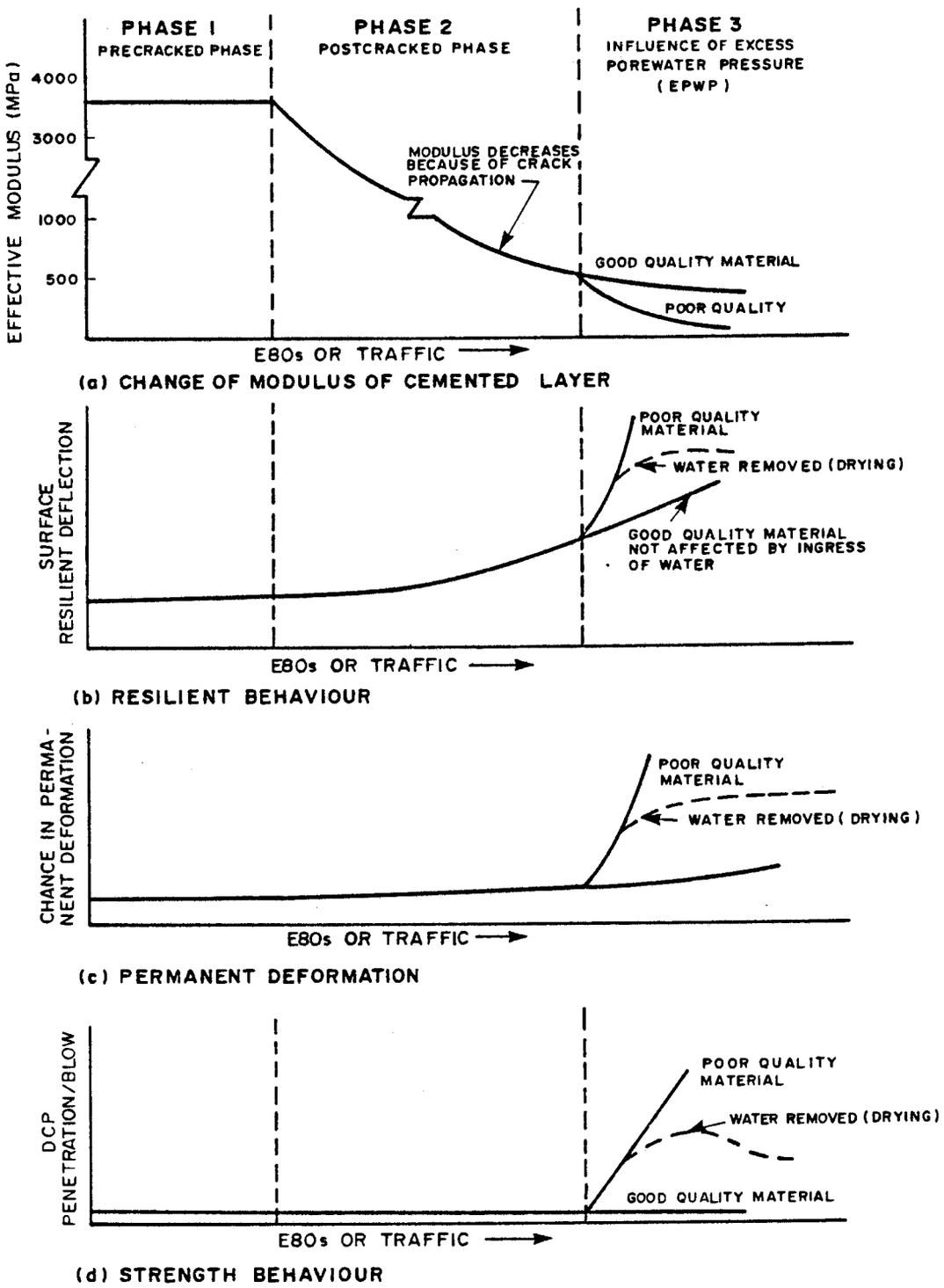

FIGURE 2.1

INDICATORS OF THE BEHAVIOUR OF CEMENTED (C2 QUALITY) LAYERS (AFTER FREEME, 1984)

the material originally stabilized, the cementing agent, the effectiveness of the mixing process, the absolute density achieved, the extent and degree of cracking and the sensitivity to excess porewater pressure (EPWP).

The ingress of water can significantly affect the modulus in this state through the development of excess porewater pressures (EPWP) and this stage has been designated Phase 3. In some cases the layer may behave as a good-quality granular material with a modulus of 200 to 500 MPa, whereas in other cases the modulus will be as low as 50 to 200 MPa. The net result of the cementitious layer reducing to these very low modulus values (50 MPa) will usually be inadequate support of any upper layers in the structure or inadequate cover over the lower layers or both.

These changes in modulus are reflected in the resilient behaviour of the cementitious material (see Figure 2.1(b). Initially the relative deflection between the top and bottom of the slab could be small and will increase as cracking develops. In Phase 3 the resilient deflection can increase markedly. The plastic behaviour is also distinctive in that initially in Phases 1 and 2 there is little or no increase in deformation (see Figure 2.1(c). However, in Phase 3, in the granular state, there can be a marked increase in deformation through densification, shear and/or erosion. If the source of the water is removed and the material dries, its behaviour can again improve, (rate of change in deformation decrease).

In general surface resilient deflection is a good indicator of the state of cementitious layers; low deflections indicate high moduli and visa versa. However, in Phase 3 the resilient deflection will not necessarily be a good indicator of large deformation, since this depends on the moisture sensitivity of the material (erodibility). This however will be discussed in more detail in Chapter 3.

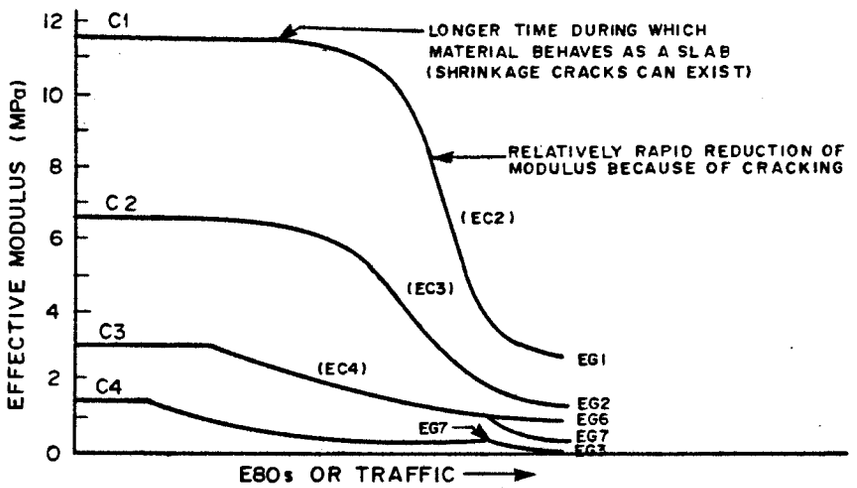

FIGURE 2.2

SHEMATIC DIAGRAM OF RELATIVE BEHAVIOUR OF CEMENTED LAYERS OF DIFFERENT QUALITY (FREEME, 1984)

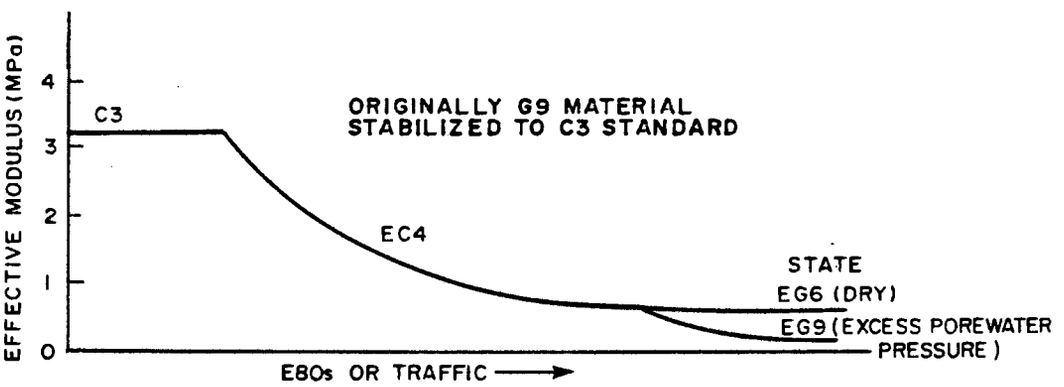

FIGURE 2.3

SCHEMATIC REPRESENTATION OF THE EQUIVALENT BEHAVIOUR OF A CEMENTED MATERIAL (FREEME, 1984)

The relative behaviour of cementitious materials of different qualities and strengths is indicated in Figure 2.2. Generally high strength materials (such as a C1)* will start off with a high modulus compared with that of a lower strength material (e.g. a C4 material). In the normal situation the higher strength materials will also tend to retain the high modulus state for a longer period. Initially the cementitious layers will crack because of shrinkage and these cracks may or may not be detrimental to the pavement. However, when further cracking occurs, the rate of decrease of modulus is generally very rapid. If measurements are made of the deflection during this period, when the decrease in modulus occurs the material will be found to be equivalent to that of lower strength cementitious materials (e.g. equivalent C2 quality, EC2).

The eventual equivalent state of the material is granular, upon breaking down into the smaller particle sizes (relative to layer thickness). The quality of the equivalent granular material depends on the original granular material, the degree of densification achieved, the degree of interlock and particle strength. Generally, the higher the quality of material initially stabilized the higher will be the eventual equivalent modulus, if properly constructed. The equivalent behaviour of a cemented material is shown diagrammatically in Figure 2.3.

The effective moduli of cementitious materials are defined for four states : that is

(a) Before extensive cracking (precracked phase); although shrinkage cracks may and probably do exist the block size is large relative to layer thickness,t (block size >5t), and the material acts as a slab similar to a concrete slab. In this state the layer should be designed against fatigue and the propagation of cracks.

---

*The codes for cemented materials are defined in Chapter 1, Table 1.2 (p1.8) and in Table 2.1 of this chapter.

(b) Loading or the environment, or both, have reduced the block size, but the behaviour is still predominantly controlled by the large blocks of material relative to layer thickness; ($5t < \text{block size} < t$). In this state the designer should again design against fatigue and further propagation of cracks. (See Section 2.4.2)

(c) The block size has decreased to blocks small in relation to layer thickness, and the material is equivalent to that of a granular material (block size predominantly $\leq t$).

If the material is, in a dry state then the relevant safety factor (See Section 2.4.3) for the equivalent granular material should be used for design.

(d) The cementitious material has broken down into a granular state equivalent to (c), but the material is in a "wet" state. The reduced moduli should be used for design, using also the safety factor approach.

These moduli are given in Table 2.1.

2.4 PRESENT DESIGN METHOD FOR CEMENTITIOUS LAYERS IN SOUTH AFRICA

The design phases which must be considered for this class of material can be divided into three phases. These are :

(a) Design against the effects of excessive shrinkage cracking.
(b) Design to control the effects of fatigue and propagation of cracks of the cementitious material while in the slab state.
(c) Design to control the possible shear deformation of the layer in an equivalent granular state.

TABLE 2.1 - Moduli of cemented materials (Freeme, 1984)

Original code	UCS (MPa)* precracked state	Parent material		Precracked state GPa (range)	Postcracked states (MPa)				
					Large Blocks	Small Blocks			
						Dry state	Equiv. code	Wet state	Equiv. code
C1	6-12	Crushed stone	G2	14 (7-30)	3 000	600	EG1	500	EG1
		Crushed stone	G3	12 (6-30)	2 800	600	EG1	400	EG2
C2	3-6	Crushed stone	G2	10 (4-14)	2 500	500	EG1	300	EG2
			G3	8 (14-14)	2 400	450	EG2	250	EG3
		Gravel	G4	6 (3-12)	2 200	450	EG2	200	EG3
C3	1,5-3	Gravel	G4	5 (3-10)	2 000	400	EG3	180	EG4
			G5	4,5(3-9)	2 000	350	EG4	160	EG5
			G6	4 (2-8)	2 000	300	EG4	140	EG6
			G7	3,5(2-7)	1 500	250	EG5	120	EG7
			G8	3 (2-6)	1 200	200	EG5	90	EG8
C4	0,75-1,5		G4	4 (2-7)	2 000	350	EG3	180	EG4
			G5	3,5(2-6)	2 000	300	EG4	160	EG5
			G6	3 (2-6)	2 000	250	EG4	140	EG6
			G7	2,5(1-5)	1 000	200	EG5	120	EG7
			G8	2 (1-4)	1 000	170	EG5	90	EG8
			G9	1,5(0,5-3)	500	150	EG6	70	EG9
			G10	1 (0,5-2)	500	125	EG6	45	EG10

Poisson's ratio 0,35

* 7-day UCS, Method A14, TMH1, (See ref. NITRR (1979)).

TABLE 2.2 - Factor, d, for modifying the tensile strain induced in cemented materials to allow for the presence of shrinkage cracking (Otte, 1978)

Type of cracking	Unconfined compressive strengths (MPa)	Factor, d for Total thickness of cemented material (mm)	
		<200	>200
Weakly cemented:			
Moderate cracking; crack widths less than 2 mm			
(e.g. natural materials	0,75 - 1,5	1,1	1,2
with lime or 2-3 % cement)	1,5 - 3,0	1,15	1,3
Strongly cemented:			
Extensive cracking; crack widths more than 2 mm			
(e.g. high-quality natural gravels and crushed stone			
with 4-6 % cement)	3 - 12	1,25	1,4

2.4.1 Shrinkage Cracking

Shrinkage cracking : Cemented (strongly and weakly cemented) materials generally crack through shrinkage as a result of drying and thermal stresses. This is taken into account in design by increasing the traffic-induced strain, ε, by a factor, d, which can be obtained from Table 2.2. The increased value is termed (after Otte, 1978) the modified strain, ε_s, viz.:

$$\varepsilon_s = d \cdot \varepsilon. \quad \ldots\ldots\ldots\ldots\ldots\ldots\ldots\ldots\ldots\ldots\ldots\ldots \quad (2.1)$$

The effects of shrinkage cracks on the layers above and

below the cemented layer must also be given consideration. For the layer above the activity of the crack is of importance since high movements (activity) may be present at the crack. At present, research is being done to determine not only the movements at cracks but also how to take account of this effect for rehabilitation design, Freeme (1984).

2.4.2 Fatigue and crack propagation (after Otte, 1978)

The maximum tensile strain at the bottom of the layer is adopted as the criterion for controlling cracking under traffic. The material is very sensitive to the magnitude of tensile strain and has a limited range of fatigue life, (precracked phase).

The equivalent traffic required to cause initiation of cracking is determined from Figure 2.4. This requires computation of the strain ratio ($\varepsilon_s/\varepsilon_b$), where ε_b is the tensile strain at break given in Table 2.3.

TABLE 2.3 - Tensile strain at break recommended for the standard cemented-material categories

Code	Cemented material: UCS (MPa)	Material type cemented	Tensile strain at break ε_b ($\mu\varepsilon$)
C1	6-12	Crushed stone	145
C2	3-6	Stone/gravel	120
C3	1,5-3	Gravel	125
C4	0,75-1,5	Gravel	145

Fatigue properties : The fatigue life of relatively strongly* materials under repeated flexure can be expressed by the following

* This relationship is also adopted for weakly cemented i.e. C3 and C4 materials in the precracked state.

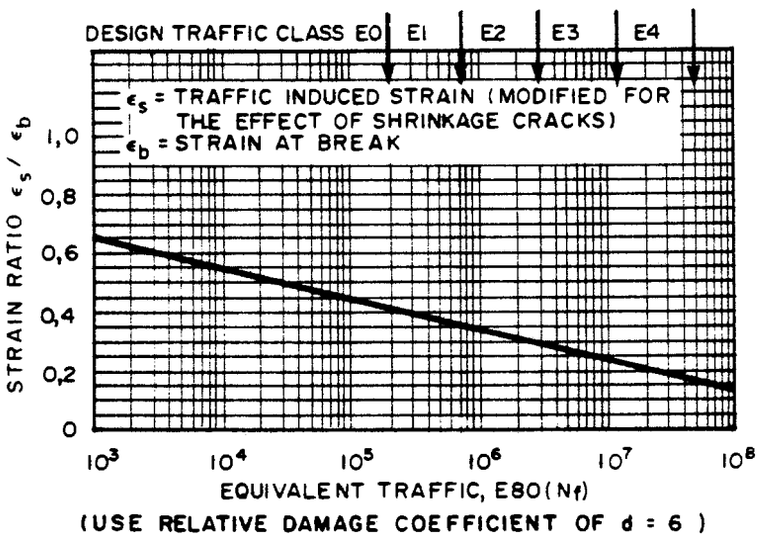

FIGURE 2.4

RECOMMENDED STRAIN RATIO FOR CEMENTED LAYERS – CRACK INITIATION –

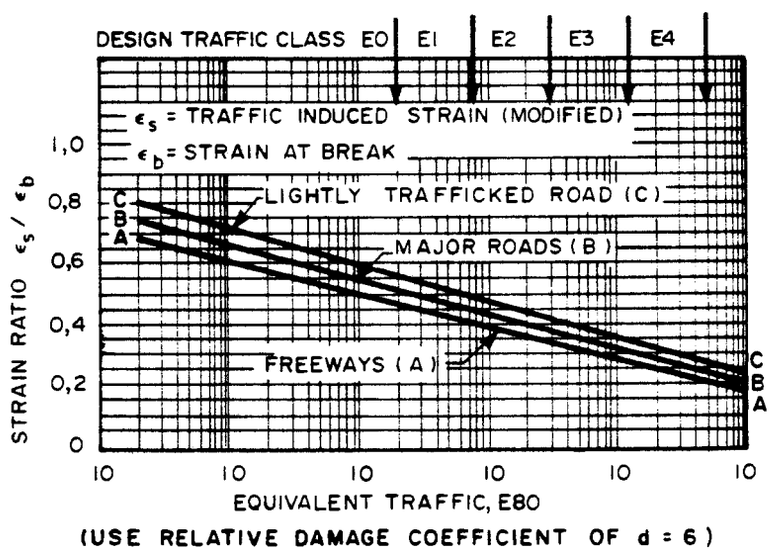

FIGURE 2.5

ALLOWABLE STRAIN RATIOS FOR CEMENTED LAYERS. – VISIBLE CRACKS AT THE SURFACE –

$$N_f = 10^{9,1\,(1 - \varepsilon_s/\varepsilon_b)} \quad \ldots\ldots\ldots\ldots\ldots\ldots\ldots \quad (2.2)$$

where N_f = number of repetitions at strain ε_s to crack initiation.

A shift factor is applied to account for time between initiation of cracking and cracks appearing at the surface. Table 2.4 shows the applicable shift factors for the different road categories and for different layer thicknesses while from Figure 2.5, the equivalent traffic required before cracks appear can be determined directly from the strain ratio. In order to convert different axle loads to the standard E80, it is recommended to use a relative damage coefficient, d = 6, in the precrackedphase*. It must be emphasized that the precracked phase is the phase where the slabstate of the cementitious layer controls the behaviour of the pavement.

TABLE 2.4 - Shift factors** for cemented layers (Freeme, 1984)

Layer thickness (mm)	Road category		
	A	B	C
Bases and subbases			
100 - 200	1,2	2,0	3,0
Subbases >200	3,0	5,0	7,5

* To convert the number of load repetitions other than 40 kN (80kN axle) the relative damage formula, $F = (\frac{P}{40})^d$ is used, with d = 6.

** The calculated fatigue life is multiplied by the appropriate shift factor

2.4.3 Cementitious layer in the equivalent granular state

A cemented layer can crack under the action of traffic into smaller particle sizes relative to the layer thickness. Often there is still very good interlock between the particles and effectively the material behaves as an equivalent granular material, even though it will not meet the specification for the granular material.

According to Freeme (1984), the criteria applicable to granular materials should apply for granulated cementitious materials. It is worthwhile to discuss the distress criterion for granular materials in the following section, as it is proposed to apply to cementitious materials in the equivalent granular state.

An important concept here is that if a material is in an equivalent material state, then the criteria for that state apply, i.e. if cementitious material is in the granular state, say EG4 state, then the approach is to use safety factors to control deformation of the material (e.g. safety factors and Mōhr-Coulomb strength parameters of cohesion, c, and angle of internal friction, Ø, for a G4 material apply, Maree (1982)).

2.4.3.1 Granular materials

Granular materials exhibit distress in the form of cumulative permanent deformation or inadequate stability. Both distress modes are related to its shear strength which is expressed in terms of the Mōhr-Coulomb strength parameters of cohesion, c, and angle of internal friction, Ø.

The use of the safety factor, F*, as defined in the equation (Maree 1982) below, safeguards the layer against shear failure or gradual shear deformation by limiting the shear stresses to a safe level.

$$F = \frac{\sigma_3 \overbrace{\left|K(\tan^2 (45 + \phi/2) - 1\right|}^{\text{Ø-term}} + \overbrace{2Kc \tan (45 + \phi/2)}^{\text{c-term}}}{(\sigma_1 - \sigma_3)} \quad ..(2.3)$$

where σ_1 and σ_3 = calculated major and minor principal stresses acting at a point in the layer. (Compressive stresses are positive while tensile stresses are negative.)

c = cohesion

Ø = angle of internal friction

K = constant = 0,65 for saturated conditions
= 0,80 for moderate conditions
= 0,95 for normal dry conditions

The values of c and Ø and the c-term and Ø-term in eq. 2.3 are given in Table 2.5. Values are given for the material in the dry state (∿ 45 per cent of saturation) and the wet state (∿ 90 per cent of saturation).

According to eq. 2.3 the safety factor depends on σ_1 and σ_3. These two stresses depends more on contact pressure and contact area, than on wheel load, thus is F indirectly affected. The safety factor depends therefore more on the contact pressure and it is therefore recommended that a 40 kN dual wheel at 520 kPa contact pressure be used. The safety factors should be calculated at the mid-depth of the granular layer, under one of the wheels and at the centre of the dual wheels.

---

* The safety factor, F, must not be mistaken for the "F" of the relative damage formula discussed on page 2.12.

TABLE 2.5 - The shear properties of granular materials (Maree, 1982)

Material, Code	Moisture State	Cohesion, c (kPa)	Internal Friction, Ø (Degrees)	Ø-term	c-term
High density	dry	65	55	8,61	392
crushed stone, G1	wet	45	55	5,44	171
Moderate density	dry	55	52	7,06	303
crushed stone, G2	wet	40	52	4,46	139
Crushed stone and	dry	50	50	6,22	261
soil binder, G3	wet	35	50	3,93	115
Base quality	dry	45	48	5,50	223
gravel, G4	wet	35	48	3,47	109
Subbase quality	Moderate	40	43	3,43	147
gravel, G5	wet	30	43	3,17	83
Low quality	Moderate	30	40	2,88	103
subbase gravel, G6	wet	25	40	1,76	64

The allowable safety factor varies according to the road category and the design traffic. Table 2.6 gives the recommended safety factors for the design traffic classes (also shown in Figure 2.6).

For cementitious materials in the equivalent granular state of G7 to G10, the material should be treated as an equivalent subgrade. In cases where a lens of the material is sandwiched between two stiff layers, the safety factor approach is desirable for analysing the lens. At present, values for c and Ø for materials of this standard have not been determined but estimates are given in Table 2.7.

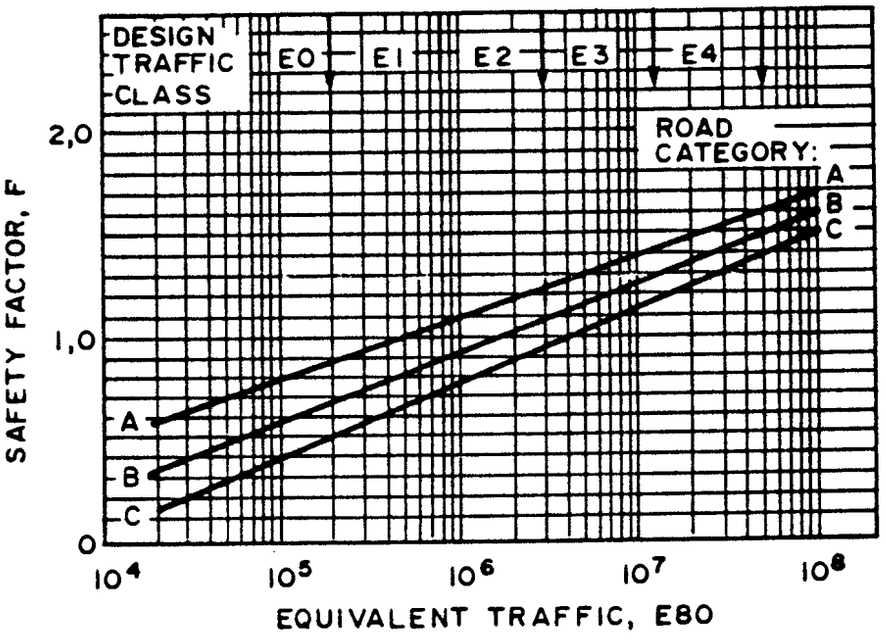

RECOMMENDED VALUES OF RELATIVE DAMAGE COEFFICIENT TO COMPUTE EQUIVALENT TRAFFIC

d= 4 FOR A CATEGORY ROAD
d= 3 FOR B CATEGORY ROAD
d= 2 FOR C CATEGORY ROAD

FIGURE 2.6

RECOMMENDED SAFETY FACTORS FOR GRANULAR MATERIALS (G1 TO G6) (FREEME, 1984)

TABLE 2.6 - The safety factor recommended for granular material (Maree, 1982)

Road Category	Design Traffic Class	Minimum Allowable Safety Factor
A	E4	1,60
	E3	1,40
B	E3	1,30
	E2	1,05
	E1	0,85
C	E2	0,95
	E1	0,75
	E0	0,50

TABLE 2.7 - Estimates of values of c and Ø for soils (G7 to G10)

Material Code	Moisture State	Cohesion, c (kPa)	Internal Friction, Ø (Degrees)	Ø-term	c-term
G7	dry	25	35	2,51	91
	wet	20	35	1,40	50
G8	dry	25	30	1,85	82
	wet	20	30	0,95	45
G9	dry	25	28	1,63	79
	wet	20	28	0,80	43
G10	dry	25	25	1,34	75
	wet	20	25	0,60	41

2.5 DISCUSSION AND CONCLUSIONS

Although the concept of equivalent granular states for cementitiuos layers was derived from the findings of HVS research on cementitious layers in road structures, the actual quantification of all the necessary components to result in accurate predicted behaviour for these layers had not been done prior to this dissertion. The proposed method to use assumed c and Ø values for the equivalent granular states, however, applied with different levels of success by different people and organisations. A suggested way to improve the validity of the concept is to analyse the HVS results in such a format that pavement behaviour and behavioural states can be directly or indirectly predicted from field results. However the South African design method is unique in utilizing the concept of different states of the pavement during its service life. The main reason for this advantage in design is the availability of the HVS. An attempt will be made by the author to further evaluate the above-mentioned concept using recent HVS and laboratory results on weakly cemented materials. (Lime treated) These tests were conducted by the author during the period January 1983 to 1985. Most of the HVS tests had been done on asphalt base and cementitious subbase pavement structures in Natal on National routes, N2 and N3. These tests were carried out on four different structures with basically the same initial design. In order to understand the behaviour of the cementitious subbase layers it is therefore necessary to investigate these layers not as separate structural units only, but to study the influences of these layers on the rest of the structural layers in the total system (structure), including the asphalt layers. The reason for this approach is that the different pavement layers behave as a system and the behaviour of each layer is dependant on the behaviour of the layer above or below. The behaviour of the cementitious subbase layers in different states will be frequently highlighted. It is believed that the upper subbase layer, in this design, is the most critical structural layer and mainly governs the performance of the structure. This will be evaluated and discussed further in Chapter 3.

The effect of strength build-up because of the cementing action with time as well as factors such as the effect of delayed compaction to reduce cracking were not evaluated during this study. It is however accepted that these factors are very important and should be investigated further in the future. This includes the durability of these materials.

2.6 REFERENCES

FREEME, C R (1984). Symposium on : Recent findings of Heavy Vehicle Simulator testing. ATC 1984, NITRR, South Africa.

FREEME, C R and STRAUSS, J A. (1979). Towards the Structural design of more economical pavements in South Africa. Proc. of the third Conf. on Asphalt Pavements for southern Africa, Durban, Vol.1.

FREEME, C R and WALKER, R N. (1984). Economic design of bituminous pavements. Proc. of the Fourth Conf. on Asphalt Pavements for southern Africa - CAPSA84, Cape Town, Vol 1.

NATIONAL INSTITUTE FOR TRANSPORT AND ROAD RESEARCH (1985). Structural design of interurban and rural road pavements. Pretoria, TRH4, CSIR.

OTTE, E (1978). A structural design procedure for cement-treated layers in pavements. DSc thesis, University of Pretoria, South Africa.

NATIONAL INSTITUTE FOR TRANSPORT AND ROAD RESEARCH (1979). Standard Methods of Testing Road Construction Materials. Technical Methods for Highways, No. 1, CSIR, Pretoria, RSA. 1979, ix + 183 pp.

MAREE, J H (1982). Aspekte van die ontwerp en gedrag van Padplaveisels met korrelmateriaalkroonlae. D.Sc. Dissertation (in Afrikaans). University of Pretoria, Pretoria.

CHAPTER 3

EVALUATION AND ANALYSES OF A NUMBER OF HEAVY VEHICLE SIMULATOR TESTS AND RESULTS

CONTENTS

Contents continued Page

3.1 INTRODUCTION AND BACKGROUND

Prior to this effort of full scale research, not much work has been done to quantify the behaviour of weakly cemented layers in road structures. The current South African mechanistic design method heavily rely upon the fatigue relationship proposed by Otte (1978) mainly in the precracked phase. With the use of the HVS the limitations of the design and theoretical evaluation method was soon realized. The concepts of precracked and postcracked and also equivalent granular state of cementitious layers (Freeme et al, 1984) are direct results of HVS research. The purpose of this chapter is to describe the behaviour of weakly cemented subbase layers including its influence on the other layers (surfacing, base and subgrade) in the road structure. Four (4) HVS tests, done by the author during the period January 1983 to December 1984, will form the basis of evaluation and discussion. The research include mainly work done on bituminous base structures (Freeme, 1979, 1984) found in the Province of Natal, South Africa.

The basic pavement design specifies a 40 mm asphalt surfacing, bitumen base (80-135 mm thick) on two weakly stabilised subbase layers, each 150 mm thick. Beneath the subbase layers the selected subgrade (150-300 mm thick) and the subgrade occur. The four sites tested with the HVS included in this chapter are at Mariannhill, National Route 3, Section 1 (N3/1); Figtree, National Route 2, Section 24 (N2/24); Umgababa, National Route 2, Section 24 (N2/24) and Van Reenen's Pass, National Route 3, Section 6 (N3/6). Reference will also be made to other related HVS tests and findings. In this thesis only a comprehensive summary is given of the tests and results of above-mentioned tests. The detailed descriptions and evaluations of each test are given elsewhere (De Beer, 1984(a),(b); 1985(a),(b)). Photographic records of these HVS tests are given in Appendix A

3.2 SUMMARY OF HVS TESTS AND RESULTS AT MARIANNHILL, N3/1

Three separate HVS tests were done at this site. These tests include dry tests and water introduction into the sublayers and also on one section the asphalt was artificially heated for specified periods during the testing. The state and condition of each layer in the structure were monitored before, during and after testing. Resilient deflections and permanent deformations of each layer were measured with the multi-depth deflectometer (MDD). Surface profiles across the test sections were measured using a straight edge and electronic profilometer. Surface deflections were measured with the road surface deflectometer (RSD), which is a modified Benkelman beam (De Beer, 1984(a)).

3.2.1 Road structure and subbase material

The road structure at Mariannhill is shown in Figure 3.1. The design specified 40 mm AC; 125 mm BC; 150 mm C3; 150 mm C4; 250 mm G4; G7 in situ material. These material codes are according to TRH14 (NITRR, 1985). The variation in layer thicknesses are also shown in the figure.

Both the upper and lower weakly stabilized subbase layers consists of wheathered granite and were classified using the Highway Research Board's (HRB) classification system as A1-b(0) before stabilization. Lime ($Ca(OH)_2$) was used for the stabilization. In the upper subbase an average of 2,4 per cent (by mass) and in the lower subbase an average of 2,1 per cent lime were added. The parent plasticity (before stabilization) varied between semiplastic and 5 per cent. Average relative compactions of 97,6 and 96,8 mod. AASHTO were obtained for the upper and lower subbase, respectively. The unconfined compressive strengths (UCS) after 24 hours curing at 70 to 75 °C were 2,4 MPa and 2,5 MPa for the upper and lower layer, respectively. Minimum UCS's of 1,5 MPa and 0,75 MPa were specified for the upper and lower layer. According to these results both layers could be classified

• LAYER THICKNESS AND MATERIAL CODE ACCORDING TO TRH14

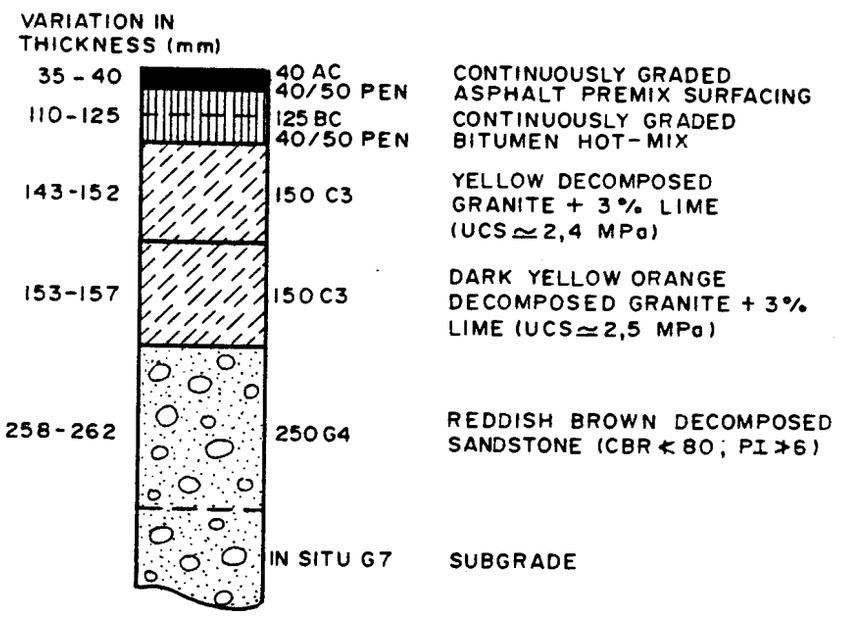

FIGURE 3.1

PAVEMENT STRUCTURE AT MARIANNHILL HVS SITE

using the material codes in TRH14 (NITRR, 1985) as C3-material (UCS: 1,5 MPa to 3,0 MPa). The base layer consisted of 50/50 Pen. hot-mix asphalt (continuously graded) and the selected and subgrade layers of decomposed sandstone.

3.2.2 Selection of HVS test sections

Prior to HVS testing an extensive road surface deflection survey was conducted and was reported elsewhere, De Beer (1984(a)). The survey indicated that the deflection ranges between zero and 0,21 mm, with an average site deflection was 0,12 mm with a standard deviation of 0,03 mm.* The locations of the three selected test sections as well as the deflections are illustrated in Figure 3.2(a) and (b).

An important observation gained from the deflection survey was that although the deflections on the selected subgrade were relatively low (0,8 mm) during construction, the final deflections on the surface were reduced to an average of 0,12 mm. The construction of 2 x 150 mm thick weakly cemented subbases, 1 x 125 mm thick bitumen base and 40 mm thick asphalt surfacing, were seen to reduce the deflection on the selected subgrade by approximately seven times, one year after construction.

This is a relatively good illustration of the design principle covering the subgrade with successive layers to reduce stresses (deflections) on the subgrade layers. It is believed that the cementitious properties of the weakly cemented subbase layers are the main contributor to this reduction in deflection. An important question concerning the permanency of these cementitious properties with time and or traffic loading must be adequately answered. An attempt will be made to discuss and formulate the answer to above question, using mainly the results obtained with the aid of the HVS.

---

* Average were calculated from three transverse and four longitudinal positions - a total of approximately 490 points.

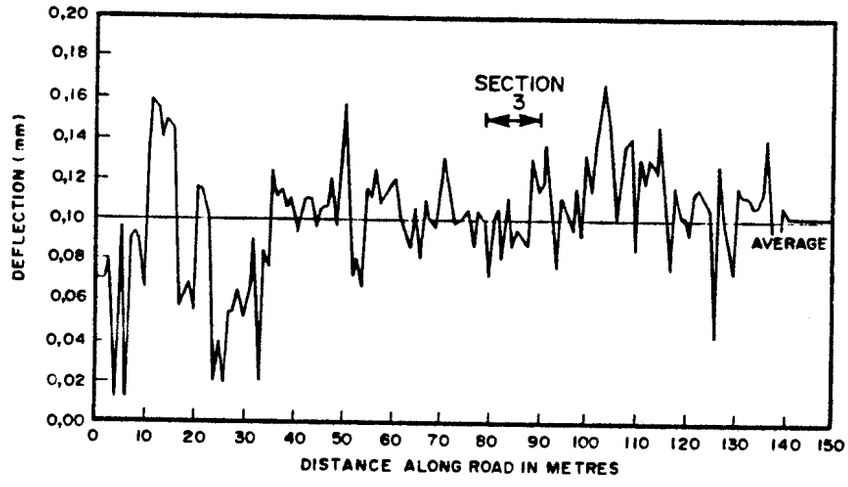

(a) INNER NORTHBOUND LANE (HVS TEST SECTION 3)

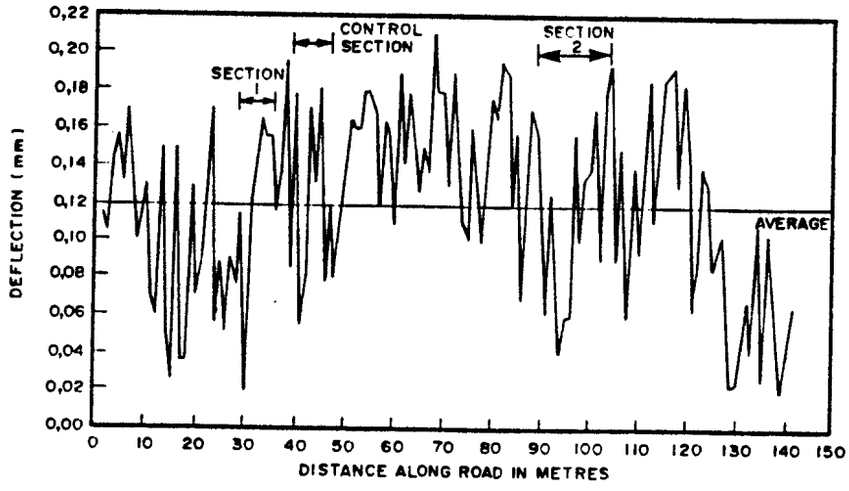

(b) OUTER NORTHBOUND LANE (HVS TEST SECTIONS 1 AND 2)

FIGURE 3.2

BENKELMAN BEAM DEFLECTION OF THE ROAD SURFACE AND POSITION OF THE DIFFERENT HVS TEST SECTIONS

It is believed that subbase layers are major structural elements in the pavement structure, because of their part in the reduction in surface deflection. Experience has shown that almost all cementitious layers experienced cracking owing to traffic loading and changing environmental conditions. Fairly early after construction shrinkage cracks develop owing to the loss of water as well as thermal conditions. During the development of non-traffic associated cracking or thereafter, construction traffic is allowed. Because of the dynamic action resulting from moving loads as well as subsurface water conditions, a gradual break down or "fracturing" of the cementitious layers occurred. Some layers experience "active" and some layers "inactive" cracks. The active crack is one which resulted in high relative horizontal and vertical movements (Rust, 1985). The inactive crack hardly experience any movements. The activity of a crack depends also on its support and interlock which is not always constant. Cracks on the surface often started off as inactive cracks and becomes very active with traffic loading depending on a range of factors such as :

(i) loading (rate and magnitude)

(ii) excessive porewater pressure and tyre pressure

(iii) cementitious characteristics of the cementitious layer

(iv) wet- and dry durability (erodibility)

(v) support conditions underneath the cementitious layer

(vi) temperature of asphalt

(vii) fatigue characteristics of the cementitious layer and block sizes,

(viii) compressive strength of the layers in the structure, etc.

It should be possible with an HVS to quantify the gradual breakdown of the cementitious subbase layers. It should also be possible to discover the effects of the initial reduction in vertical resilient deflection on subgrade layers. The increase in resilient deflection during the

pre- and postcracked phases of the cementitious subbase layers can be monitored using multi depth deflectometers (MDD). The behaviour with an excess of porewater pressure in the postcracked phase of the structure should also be studied.

A typical layout of a test section is illustrated in Figure 3.3.

3.2.3 Permanent deformation

The average change in permanent deformation (rut development) on the three test sections at various moisture, temperature and loading conditions is illustrated in Figure 3.4. The individual test programmes for each section are summarized in Table 3.1.

As a standard for comparison it was decided to compare directly the change in permanent deformation on the three sections with the number of equivalent standard axles (E80s). A constant damage exponent of d = 4 was used in the equivalency formula, $(\frac{P}{40})^d$. The value of 4 does not necessarily represent the "true" damage exponent for this structure. The aim of these tests, however, was not to determine an accurate damage exponent, although some differences were noticed in the rate of change in the permanent deformation on the surface, using different wheel loads. The permanent deformation of each section will be discussed separately.

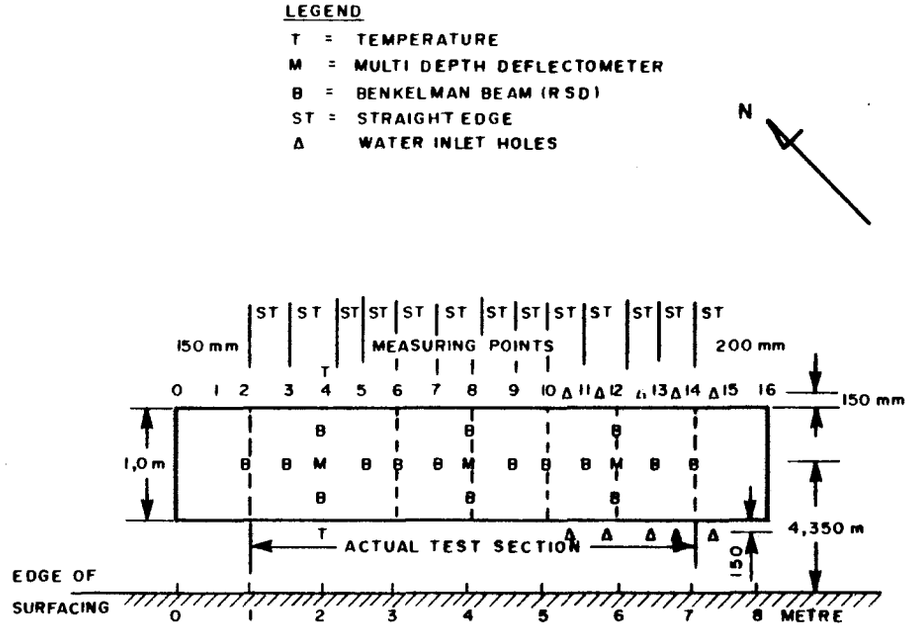

FIGURE 3.3

A TYPICAL LAYOUT OF AN HVS TEST SECTION

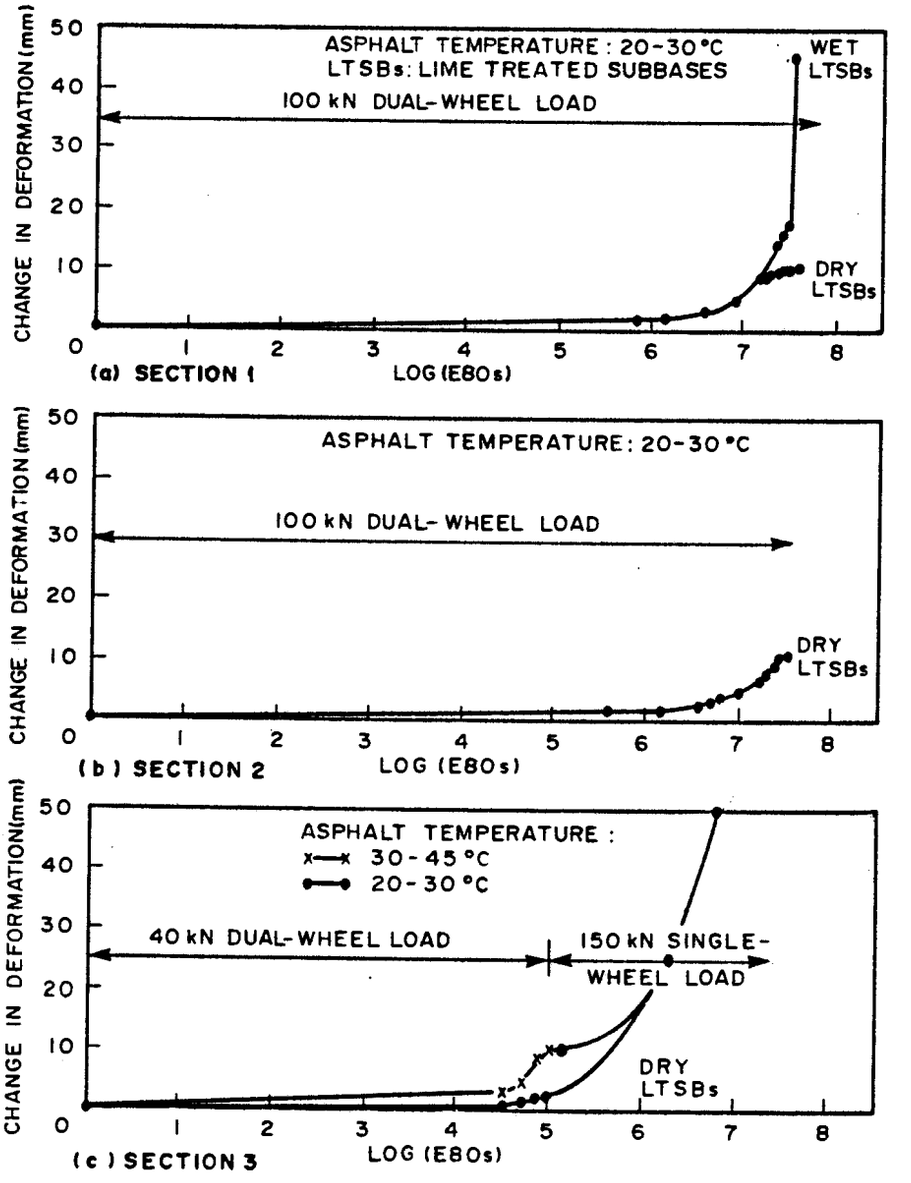

FIGURE 3.4

AVERAGE CHANGE IN PERMANENT DEFORMATION ON THE THREE TEST SECTIONS AT VARIOUS STAGES OF TRAFFICKING

TABLE 3.1 - Test programmes of the three test sections

Section	Trafficking load (kN)	Moisture Condition	Asphalt Temperature (°C)	Actual Repetitions	Remarks
1	100	Dry	20 - 30	520 000	Total test section
	100	Dry	20 - 30	175 000	Half of test section
	100	Wet	20 - 30	175 000	Half of test section
				695 000	Total repetitions applied
2	100	Dry	20 - 30	830 000	Overlapping of test sections
3	40	Dry	20 - 30	96 000	Half of test section (Pts 9 - 15)*
	40	Dry	30 - 40	96 000	Half of test section (Pts 0 - 8)*
	150	Dry	20 - 30	34 000	Total test section
				130 000	Total repetitions applied

* Pts : Measuring points on test section (longitudinal)

When considering the change in permanent deformation in Figure 3.4 on Section 1, which was tested with 100 kN dual wheel loading, the terminal level of 20 mm deformation was not reached during the test in the dry state (normal conditions) of the weakly cemented subbase layers, (LTSBs).* During the dry state, the rutting originated mainly within the asphalt base and surfacing layer. An average rut of

* LTSBs : Lime treated subbase layers

13 mm was measured at the end of the test in the dry state. The rate of change of rutting was calculated to be approximately 0,5 mm/ME80*. During the wet test (i.e. the cracked subbases saturated), moisture-accelerated distress (MAD)** was experienced. The origin of the rutting was seen to gradually change from the asphalt layers to the upper stabilized subbase layer, LTSB(1), in the wet state. At the end of the test an average rut of 45 mm was measured on the wet section. The asphalt surfacing and base layer were extensively cracked owing to fatigue. Pumping occurred almost immediately after the cracks appeared on the surface of the test section. (See photographic record of the tests in Appendix A.) The asphalt temperature varied between 20 and 30 °C which was the normal daily variation during the time of testing.

A total of 27 million E80s (ME80s) were applied to the dry test section, of which 6,8 ME80s were applied on the wet section. After completion of the tests the stabilized subbase layers were extensively cracked. The upper subbase layer was more fractured than the lower subbase layer. In the wet state, the former was granulated and the latter only fatigue cracked.

---

* ME80s : million E80s

** The terms in this report : wet, saturated and moisture accelerated distress (MAD); all refers to a condition in the sublayers, especially between the asphalt and upper subbase layer, were excess porewater pressure developed during HVS testing.

The permanent deformation shown in Figure 3.4 is related to standard E80. In Figure 3.5 the average deformation of the road surface at various stages of trafficking on Sections 1 and 2, is given against actual 100 kN repetitions. Water was introduced from the surface to a depth of 440 mm on one half of the test section. Deformations were measured with a 2 m straight edge. A longitudinal permanent deformation profile of the surface of the section is shown in Figure 3.6. The relative positions of the water inlet pipes used to introduce water into the structure are also shown in the figure. Maximum deformations of 90 mm were recorded during this test after the introduction of water. Subsequent cracking of the asphalt and pumping from the subbase layers were seen. The deformation, however, was not uniform across the wet section.

Permanent deformations at different levels within the road structure were measured with the Multidepth deflectometers (MDDs). Three MDDs were installed on Section 1, as shown in previous Figure 3.3. The average permanent deformation of the road surface at the three MDD positions at various stages of trafficking on Section 1 is illustrated in Figure 3.7(a). A maximum of 82 mm was measured at MDD12.

Subsurface permanent deformations measured with the MDDs at the three positions are shown in Figures 3.7(b), 3.7(c) and 3.7(d). At MDD4 (Figure 3.7(b)), the bottom of the asphalt base layer deformed approximately one millimeter, which was obviously the permanent deformation of the top of the upper stabilized subbase. The permanent deformation in the middle and bottom of the stabilized subbases were 0,3 mm and less, which is negligible. In Figure 3.7(c) the permanent deformation in the sublayers measured with MDD8 is shown. The upper MDD was situated 60 mm from the surface, within the asphalt base layer. At this level deformations of up to 4 mm were measured. The second MDD level was at 320 mm, a location which is in the middle of the two subbase layers (i.e. the top of lower subbase). At this level the permanent deformation was found to be 0,6 mm and less. Water was

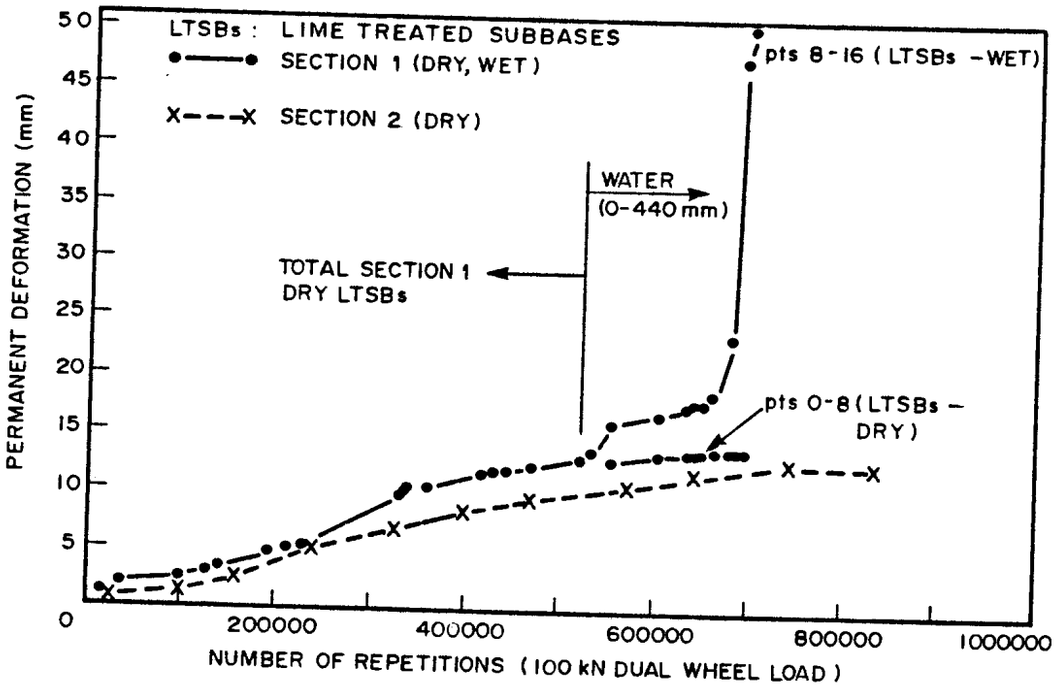

FIGURE 3.5

AVERAGE PERMANENT DEFORMATION OF THE ROAD SURFACE AT VARIOUS STAGES OF TRAFFICKING ON SECTIOIN 1 AND SECTION 2

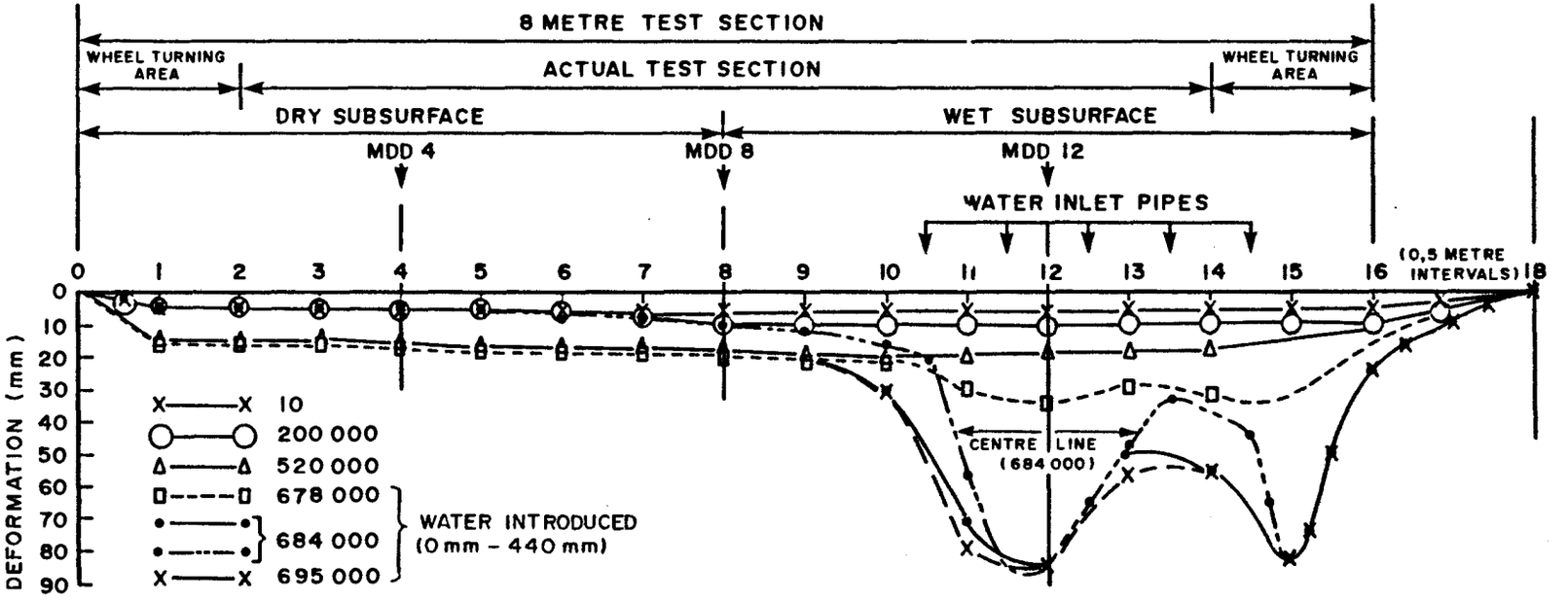

FIGURE 3.6

MAXIMUM LONGITUDINAL PERMANENT DEFORMATION ON THE SURFACE OF HVS SECTION 1 AT VARIOUS STAGES OF TRAFFICKING

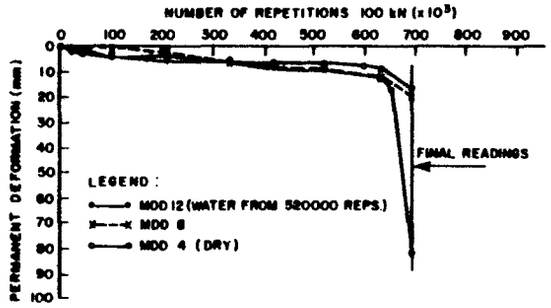

(a) DEFORMATION OF THE ROAD SURFACE AT THE THREE MDD POSITIONS AT VARIOUS STAGES OF TRAFFICKING

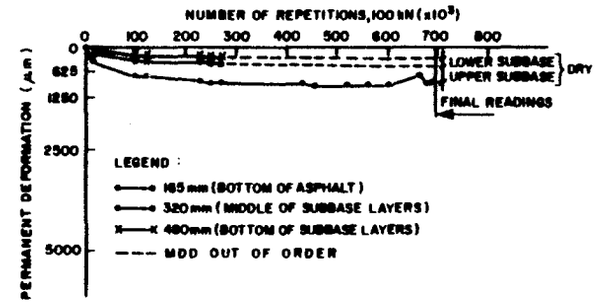

(b) DEFORMATION IN THE SUB-LAYERS AT MEASURING POINT 4

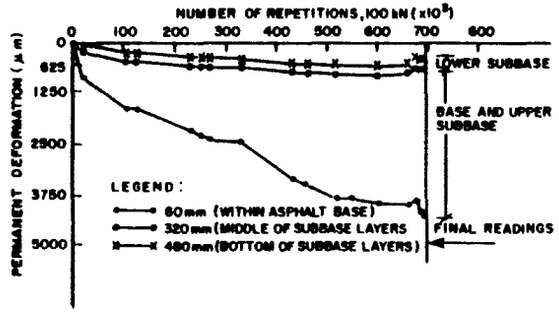

(c) DEFORMATION IN THE SUB-LAYERS AT MEASURING POINTS 8

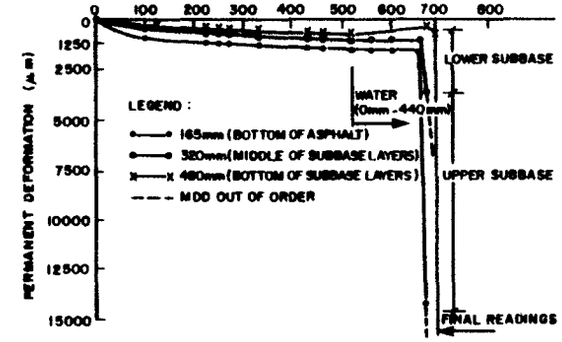

(d) DEFORMATION IN THE SUB-LAYERS AT MEASURING POINTS 12

FIGURE 3.7

AVERAGE PERMANENT DEFORMATION MEASURED WITHIN THE TEST SECTION WITH THE MULTI-DEPTH DEFLECTOMETER (MDD) AT VARIOUS STAGES OF TRAFFICKING

introduced into the sublayers after 520 000 repetitions. This was done approximately one meter from MDD8 towards MDD12. The effect of the water was seen after approximately 678 000 repetitions, see previous Figure 3.6.

In Figure 3.7(d), the permanent deformation in the sublayers measured with MDD12 is shown. During the dry state, the permanent deformation at the bottom of the asphalt and within the weakly cemented layers resulted in values of approximately 1,3 mm and 0,6 mm, respectively. This compares fairly consistent with those measured at MDD8 and MDD4. During the wet state, however, dramatic increases in the permanent deformations were recorded at the bottom of the asphalt and within the weakly cemented subbase layers. At the end of the test the magnitude of these deformations exceeded the measuring range of the MDDs. At approximately 650 000 repetitions, the deformations were 14 mm at the bottom of the asphalt (i.e. top of upper subbase), and 3,5 mm in the middle of the subbase layers (i.e. top of lower subbase layer). At the bottom of the lower subbase the deformation was approximately 0,6 mm. This result indicated a decrease in thickness of the stabilized subbase layers, especially the upper subbase. The subbase layer can only deform (loss in thickness) due to shear, densification or erosion. It is however believed that shear and erosion contributes largely to the deformations after the stabilized layer experienced fatigue and "crushing" failure in the dry state. It is believed that the simultaneous action of the shear and erosion within the upper subbase layer resulted in subsequent excessive permanent deformations of the road surface. An effect of the erodibility of these subbase layers is excessive pumping of fine subbase material through extensive fatigue cracking within the asphalt layer. (See photographic record in Appendix A). During this phase a state of excess of porewater pressure is believed to be the main reason for distress. These pressures equal or exceeds the tyre pressure during the test, which was in this case

approximately 700 kPa. Such forces are very destructive and are the main reason for failures if erodible subbase material exists in structures containing thick asphalt or concrete bases.

Section 2 was tested only in the dry state, with the ambient asphalt temperature varying between 20 °C and 30 °C. The average change in deformation is illustrated in the previous Figures 3.4(b) and 3.5. The trafficking dualwheel load was 100 kN. Relatively good agreement between Section 1 and Section 2, with respect to change in asphalt deformation in the dry state was obtained. A total of 32 ME80s were applied to Section 2 and an average rut of 12 mm was measured at the end of the test. The comparable rut depth was 13 mm on Section 1.

The layout of Section 2 was similar to Section 1. Overlapping in a longitudinal direction of the section was done twice. The overlapping distance was approximately two metres. The permanent deformation shown in Figure 3.4(b) was measured on the part of the section which received the maximum number of repetitions, i.e. 830 000, at 100 kN dualwheel load. The permanent deformation measurements against actual repetitions are shown in Figure 3.5. The rate of increase in asphalt deformation compared favourably with the rate of deformation measured on Section 1, during the dry subbase conditions. Test pits made across Section 2 after completion of HVS testing confirmed that early fatigue cracking of both stabilized subbase layers after approximately 94 000 repetitions with the 100 kN dualwheel occurred. The upper subbase experienced advanced cracking, in a similar way to that found on Section 1.

Because asphalt deformation occurred on Section 1 and 2 with 100 kN wheel loads during the temperature range of 20 °C to 30 °C and with the material in the dry state, it was decided to test a third section at a standard dualwheel load of 40 kN at elevated temperatures.

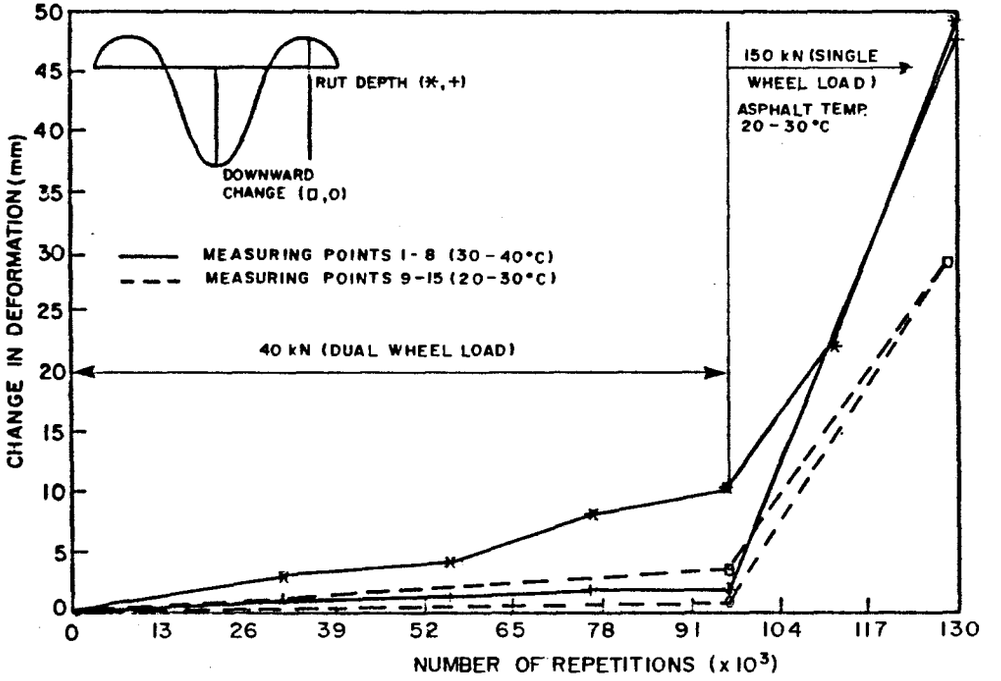

FIGURE 3.8

AVERAGE DEFORMATION OF THE ROAD SURFACE AT VARIOUS STAGES OF TRAFFICKING AT INDICATED WHEEL LOAD AND ASPHALT TEMPERATURE ON SECTION 3

This was done by introducing heat on one half of the test section using heaters. Two ranges of temperature were achieved on Section 3 namely 20 °C to 30 °C and 30 °C to 40 °C. The hotter asphalttest continued up to 96 000 E80s. (See Figures 3.4(c) and 3.8.) The average rut depths measured at 96 000 E80s were 2 and 10 mm for both the normal and hot temperature ranges. These results indicated that if temperatures between 30 - 40 °C were experienced for long periods of time together with relative heavy loading, excessive asphalt deformation will occur. It is, however, believed that the higher temperature range together with heavy loading would only prevail for very short periods of time, and therefore excessive asphalt deformation is not expected during the service life of this structure.

An excessively high singlewheel load (150 kN) test followed the higher temperature test on Section 3. The asphalt temperature during this latter test varied between 20 and 30 °C. The objective of the latter test was to study any permanent deformation (or distress) which may occur in the dry state of the weakly stabilized subbase layers. After 34 000 actual repetitions (i.e. 6,7ME80s)*, the average rut was 50 mm. This rutting occurred in the short space of time throughout a single night. In Figure 3.8, the average deformation of the road surface at various stages of trafficking is shown. A difference in rut depth of approximately 10 mm was measured on the surface after the temperature test, at 96 000 E80s. It is believed that the relatively young age of the asphalt surfacing caused the deformation, (± 6 months untrafficked). Excessive deformation occurred during the 150 kN test (50 mm rut) after 34 000 repetitions. After discovering the origin of the rutting, it was observed that more than 80 per cent of the rutting originated within the asphalt surfacing and base layer. This indicates that the support layers (stabilized

---

* $d = 4$ in $(\frac{P}{40})^d$

subbases) are adequate, but the asphalt layers are sensitive to overloading (i.e. wheels with high contact pressures, 1 450 kPa). No fatigue cracks were found at the bottom of the asphalt base layer after the test. The two stabilized subbases were cracked, but still provided adequate support. The upper subbase, however, was more fractured than the lower stabilized subbase, a condition which was also observed on both the previous test sections.

3.2.4 Transverse surface profiles

Section 1 and 2 were trafficked with 100 kN dualwheel loads and Section 3 with a 40 kN dualwheel load up to 96 000 repetitions after which the wheel load was changed to 150 kN singlewheel load. The average transverse profiles of the road surface at various stages of trafficking on the three sections is shown in Figure 3.9. The results indicate a distinctive difference in profiles after trafficking with 100 kN dualwheel and 150 kN singlewheel load. Although the behaviour of the stabilized subbases were virtually the same (cracking and crushing), the asphalt surfacing and base layer appeared to be more sensitive to loading in terms of permanent deformation when the subbases remains dry. It is believed that the higher bearing capacity of dry subbases contributes largely to this.

3.2.5 Road surface deflection (RSD) and radii of curvature (RC)

In Figure 3.10, a comparison of the average radii of curvature (RC) and road surface deflection (RSD) of the three test sections, is shown. Similar results were seen on the three test sections in the dry state. The curvature decreased from more than a 1 000 to 250 m, whilst the deflection increased from 0,18 to 0,6 mm. In the wet state (Section 1) the curvature decreased from 230 to less than 100 m, whilst the deflection increased from 0,5 to more than 1,5 mm. According to Freeme et al (1984) this road structure reached the flexible state after approximately 7 ME80s,

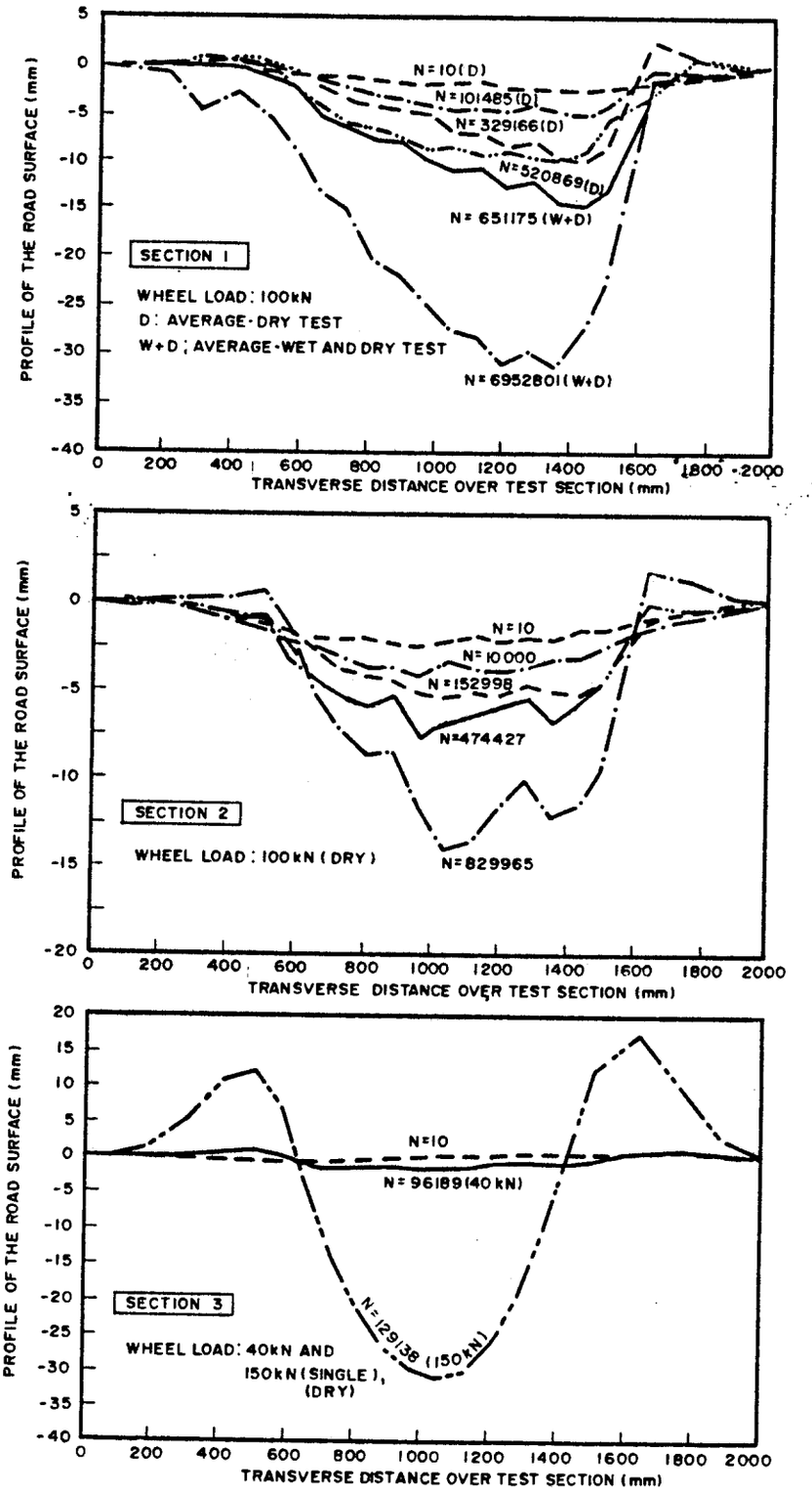

FIGURE 3.9

AVERAGE TRANSVERSE PROFILE OF THE ROAD SURFACE AT VARIOUS STAGES OF TRAFFICKING ON THE THREE SECTIONS

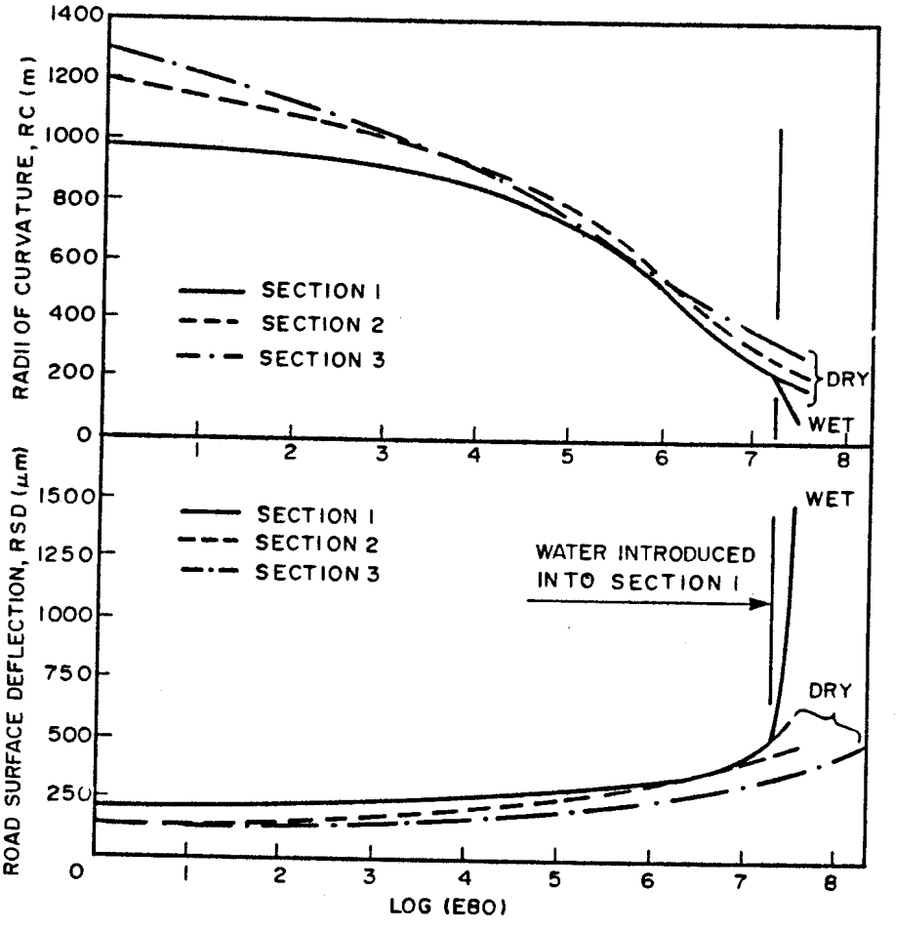

FIGURE 3.10

COMPARISON OF THE AVERAGE RADII OF CURVATURE AND ROAD SURFACE DEFLECTION MEASURED ON THE THREE TEST SECTIONS AT MARIANNHILL, N3/1

during dry conditions (0,4 mm $\leq$ RSD $\leq$ 0,6 mm). The very flexible state is possible only during saturated conditions especially of the upper weakly cemented subbase, when fractured (RSD>0,6 mm). Owing to increase in cracking and fracturing of the upper stabilized subbase, the layer's sensitivity to water, i.e. breakdown, softening and potential for pumping (erodibility) increased.

In Figure 3.11(a), (b) and (c) average longitudinal road surface deflections at various stages of trafficking on the three sectors are shown. In Figure 3.11(c), the deflections under a 40 kN dual wheel load on Section 1 are illustrated. The results indicate the effect of the excess porewater pressure within the subbases of this section, reflected by the rapid increase in deflections from approximately 651 000 repetitions in the wet state. Lower deflections resulted on the dry part of the section. The same irregularity the deflection measurements existed as with the permanent deformation resulted on this section. See previous Figure 3.6. This is an indication of variability in road behaviour. It is further believed that non-erodibile upper subbase material could decrease the risk rapid increase in RSD and subsequent failure. In Figure 3.11(b) the deflections resulted on Section 2 are shown. This section was trafficked in the dry state only. After approximately 830 000 repetitions with the 100 kN wheel load the maximum deflections were approximately 0,55 mm. If a damage exponent of 4 is used to convert these repetitions to E80s, almost 33 x 10^6 E80s had been applied to this section without cracking or serious deformation. This indicates the relatively high structural capacity of this type of pavement in the dry state. It is believed that the weakly cemented subbase layers are the main structural elements in this structure, causing the relatively low surface deflections, even after 30 x 10^6 E80s. The asphalt mixes also proved to withstand excessive permanent deformation during normal trafficking and prevailing temperature.

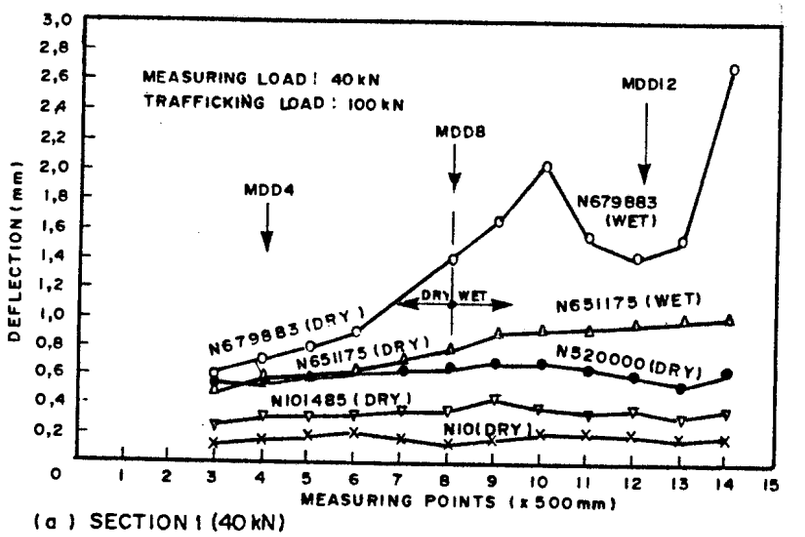

(a) SECTION 1 (40 kN)

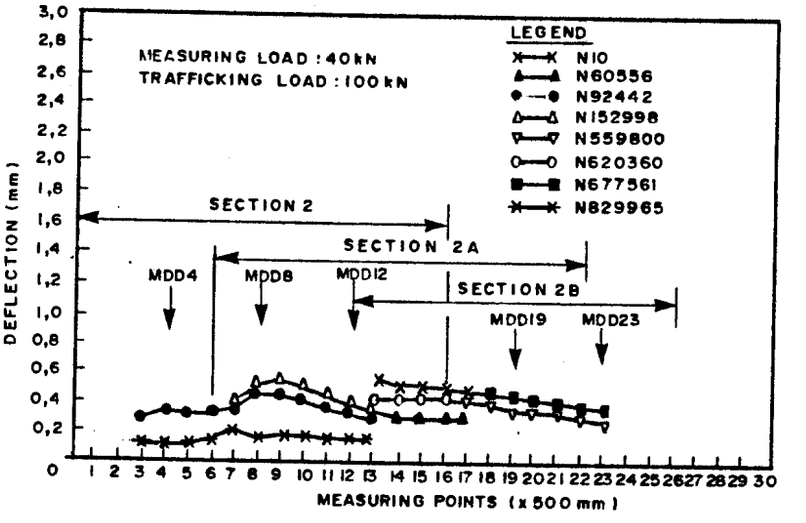

(b) SECTION 2 (40 kN)

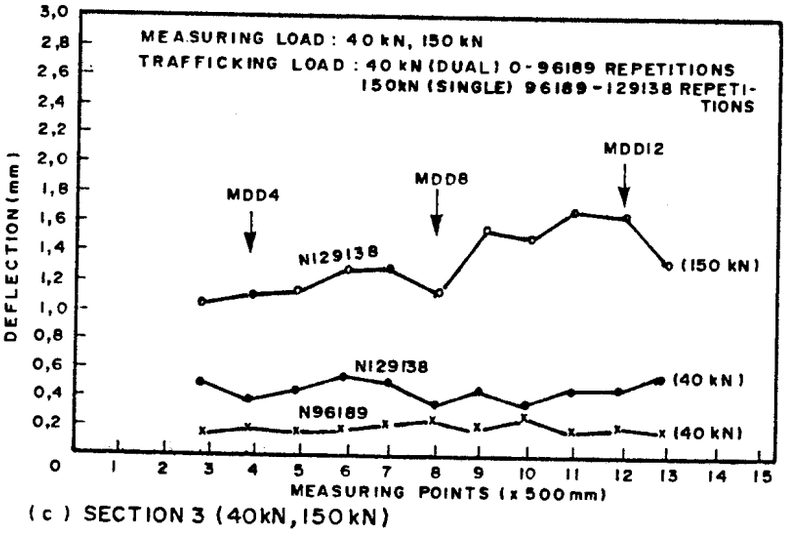

(c) SECTION 3 (40kN, 150 kN)

FIGURE 3.11

AVERAGE LONGITUDINAL ROAD SURFACE DEFLECTION UNDER THE INDICATED WHEEL LOADS AT VARIOUS STAGES OF TRAFFICKING ON THE THREE SECTIONS

In Figure 3.11(c), the deflections resulted on Section 3 are illustrated. At the end of this test the 40 kN deflections were less than 0,66 mm, which compared favourable with those measured on the previous sections. The surface deflection under a 150 kN single wheel load varied between 1,0 mm and 1,6 mm.

These deflections are indicative of the sensitivity of this pavement structure to heavy overloading when the weakly cemented subbase layers both in the precracked and post-cracked phases when dry.

In order to evaluate the elastic response of the pavement structure, it was decided to measure the surface deflection at various wheel loads. Loads from 20 kN to 100 kN were used on Section 1 and 2 and single wheel loads from 20 kN to 200 kN were used on Section 3. The average road surface deflection and radii of curvature (RC) of the three sections are illustrated in Figure 3.12(a), (b) and (c). All the sections behaved linear elastic for wheel loads up to 70 kN, i.e. : the deflection doubles as the wheel load doubles. Initially (N = 10), wheel loads higher than 70 kN resulted in non-linear elastic responses (softening) from the sections. This "softening" however changed to "stiffening" after the HVS trafficking, which is also a non-linear elastic response. The RC results appears to be more linear with increase in trafficking. The linearity of RC however appears not to be an indication of linear elastic response of the pavement structure. Relatively high RC's were measured under a 40 kN wheel load, at the end of the HVS test (250 m - 500 m). In Figure 3.12(a), the resilient response of the control section is also indicated and is consistent with the results measured on the other sections. It is again believed that the main structural element in this structure, to reflect such linear elastic behaviour is the two weakly cemented subbase layers, even in a cracked state (dry).

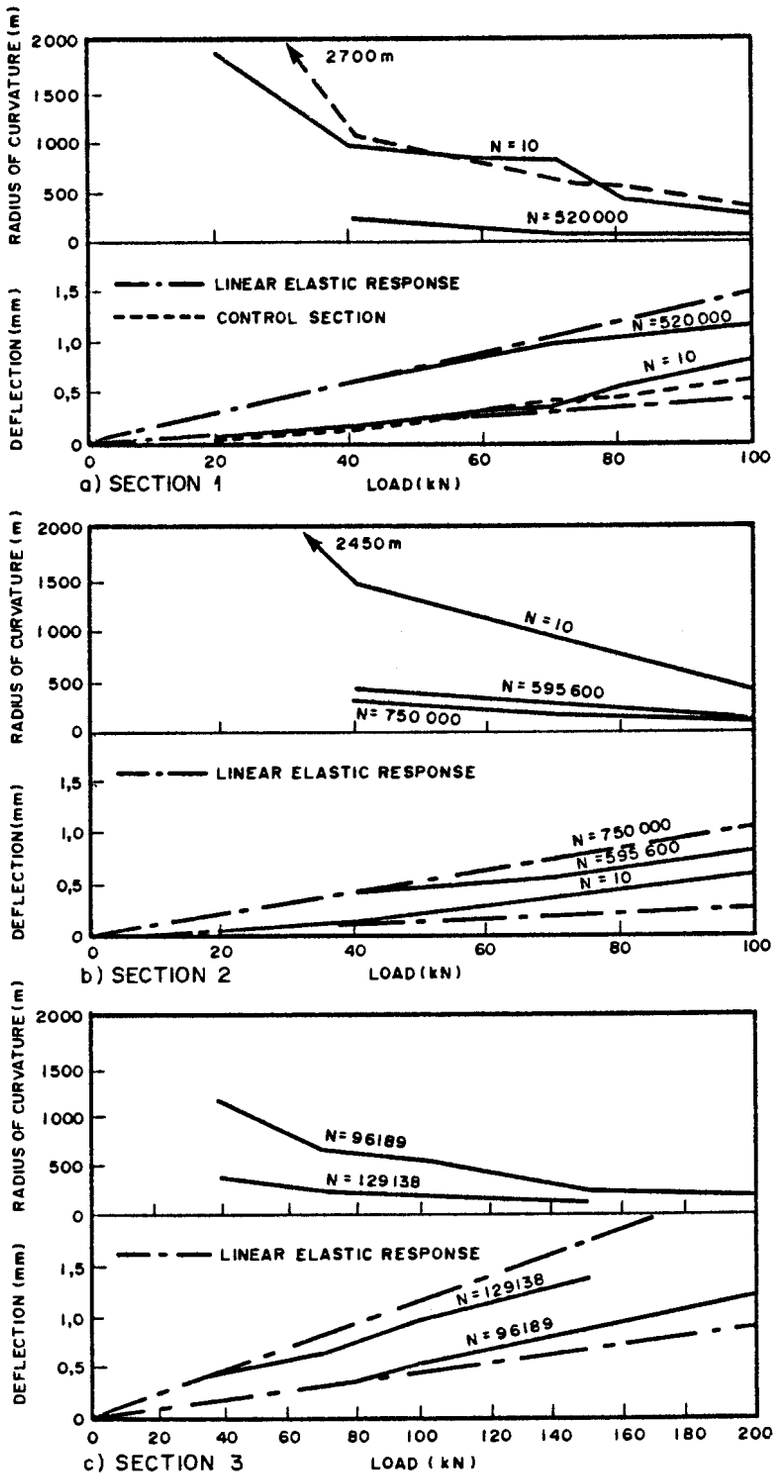

FIGURE 3.12

AVERAGE ROAD SURFACE DEFLECTION AND RADII OF CURVATURE UNDER VARIOUS DUAL WHEEL LOADS ON THE THREE TEST SECTIONS AT DIFFERENT STAGES OF TRAFFICKING

3.2.6 Resilient depth deflections

Resilient depth deflections were measured with the aid of MDD's. The average MDD depth deflection measurements at various stages of trafficking on the three test sections under a 40 kN dualwheel measuring load are illustrated in Figure 3.13. The figure indicates relatively small relative deflections resulting from both weakly cemented subbase layers. The majority of surface deflections are attributable to the selected subgrade layer downwards. Higher relative deflections were also measured within the asphalt layers. During the wet state (Section 1 only), the relative deflection in all the layers, subbase included, increased markedly. (See EPWP* state (MDD12) in the figure). The resilient structural capacity of the cemented layers is reflected by the comparatively low relative deflections. According to De Beer, 1984(a) the behaviour of all the layers in this structure is linear elastic (axle loads up to 80 kN). It is therefore concluded that linear elastic analysis of this pavement structure would probably be better than non-linear analyses.

According to beam flexural strength tests, visible cracks in the stabilized subbase material appeared at deflections ranging between 0,1 mm and 0,3 mm (De Beer, 1984(a)). From this information it is quite possible that when these levels of deflection were reached during the HVS tests, cracking occurred within the stabilized layers. It is therefore possible that cracking of the weakly cemented subbase layers occurred when the deflections on top of the selected subgrade increased (rapidly) beyond the 70 kN wheel load. Test pits made after HVS trafficking revealed some crack patterns printed on top of the selected subgrade layer which can only be the result of cracked subbase layers.

---

* Excess Porewater Pressue

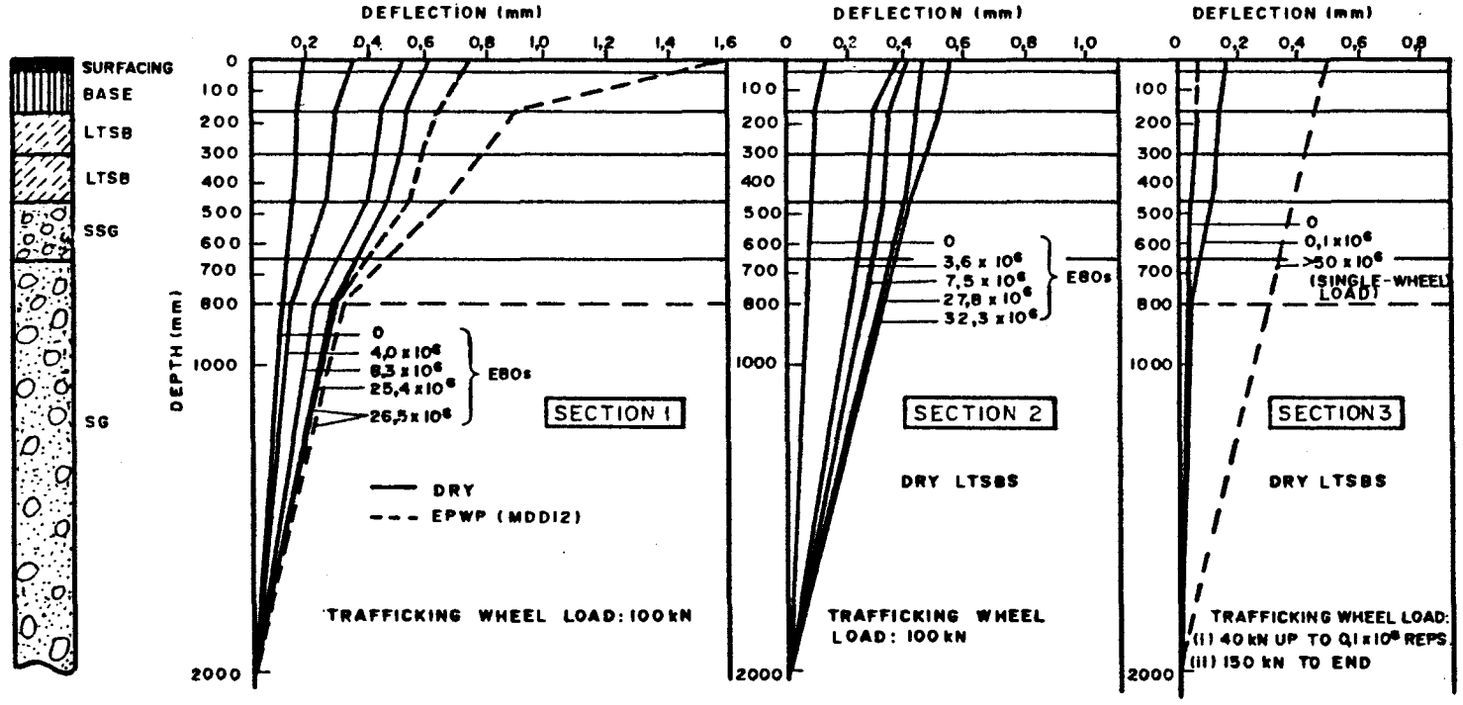

FIGURE 3.13

AVERAGE MDD MEASUREMENTS AT VARIOUS STAGES OF TRAFFICKING ON THE THREE TEST SECTIONS UNDER A 40kN DUAL - WHEEL LOAD

The deflection on the top of the weakly cemented subbase layers increased from approximately 0,2 mm to 0,58 mm during the dry state on Section 1. During the EPWP state the deflection increased to approximately 0,95 mm. At the bottom of the lower cemented layer (top of selected subgrade layer) the deflection increased to approximately 0,7 mm which can be compared to the initial 0,8 mm RSD measured on the selected subgrade layer after construction. This is an indication of the enormous reduction (almost 100 per cent) in load carrying capacity of the upper layers during the EPWP state.

The surface deflection under the 40 kN dual wheel load increased from 0,15 mm to almost 1,6 mm during the dry and wet states at MDD 12. The higher resilient deflections is an indication of the loss in the structural capacity owing to excess porewater pressure which existed not only on top of the upper subbase layer, but also within the layer. Because the layer developed an advanced state of cracking in the dry state, (confirmed by cracked recovered subbase material after HVS tests), voids existed which were then filled (saturated) with water. With the trafficking wheel load (overburden pressure) the EPWP state develops. Enormous pressures are created thereby "blowing the upper pavement layers into pieces"! In this state (Section 1), the support from the subbase layers decreased, with the asphalt layers consequently becoming overstrained. This resulted in excessive fatigue cracking of the asphalt, pumping and finally excessive rutting on the surface. See photographic record of HVS tests in Appendix A.

3.2.7 Mechanistic analyses

Mechanistic analyses were done on the structure, using the RSD and MDD results. The linear elastic analysis was done with the ELSYM 3 programme together with failure criteria proposed by Freeme et al (1984). The MDD deflections were used to calculate effective elastic moduli values of the

different layers. The moduli values and assumed Poisson's ratio values were then used to calculate stresses and strains in the simulated model.

Moduli values, measured and calculated deflections for the different test sections and different stages of trafficking are summed in Tables 3.2, 3.3 and 3.4. Good agreement exists between the measured and calculated deflections.

The initial effective stiffness of the asphalt surfacing and base layer varied between 4 000 and 1 500 MPa. In the dry state, the effective stiffness decreased to a range of 1 250 and 570 MPa. In the wet state, however, the value decreased almost to 12 MPa. The asphalt layer experienced fatigue cracking and stripped during the wet test.

The modulus of the upper stabilized subbase, varied initially between 9 900 and 7 400 MPa. After 25 ME80s the value decreased to a range of 1 000 to 800 MPa. In the wet state the value decreased to 260 MPa. The effective elastic modulus of the lower stabilized subbase, varied initially between 3 600 MPa and 3 000 MPa. The modulus decreased to a range of 700 to 400 MPa after 25 ME80s. In the wet state, the modulus decreased to 200 MPa. During the high single-wheel load test (150 kN) in the dry state, the modulus decreased also to almost 200 MPa.

The modulus of the subgrade layers ranged initially between 110 and 450 MPa. This value decreased to a range of 40 to 60 MPa after 25 ME80s. The modulus, however, did not decrease during the wet state, but increased from 41 to 50 MPa, showing a slight "stress stiffening" behaviour probably because the subbase layers lost its load bearing capacity resulting in higher stresses to be transferred to the subgrade layers.

TABLE 3.2 - The calculated effective elastic moduli values together with the measured and calculated depth deflections at various stages of trafficking on Section 1.

DEPTH (mm)	LAYER	HVS TRAFFIC (ME80s)																	
		0			4			8,3			25,4			26,5 (semi-wet-MDD8)			26,5 (wet-MDD12)		
		Deflection (μm)		E (MPa)	Deflection (μm)		E (MPa)	Deflection (μm)		E (MPa)	Deflection (μm)		E (MPa)	Deflection (μm)		E (MPa)	Deflection (μm)		E (MPa)
		Measured	Calculated		Measured	Calculated		Measured	Calculated		Measured	Calculated		Measured	Calculated		Measured	Calculated	
0	Surface & Base	180	177	2 799	350	346	800	500	493	790	600	594	750	746	734	500	1 670	1 612	12
165	LTSB(1)	160	159	7 428	280	279	2 200	430	430	2 200	530	530	800	637	636	550	890	886	260
315	LTSB(2)	155	155	3 599	265	267	2 058	415	416	1 190	490	496	672	584	585	350	760	757	200
465	Selected subgrade	150	150	110	255	257	74	400	401	44	465	471	41	543	543	40	660	666	50

Note : E = Effective Elastic Modulus

TABLE 3.3 - The calculated effective elastic moduli values together with the measured and calculated depth deflections at various stages of trafficking on Section 2

Depth layer (mm)		HVS Traffic (ME80s)													
		0			3,6			7,5			27,8			32,3		
		Deflection (µm)		E (MPa)	Deflection (µm)		E (MPa)	Deflection (µm)		E (MPa)	Deflection (µm)		E (MPa)	Deflection (µm)		E (MPa)
		Measured	Calculated		Measured	Calculated		Measured	Calculated		Measured	Calculated		Measured	Calculated	
0	Surface & Base	131	131	1 470	386	386	565	405	405	860	441	441	5 640	514	514	5 850
165	LTSB(1)	94	94	9 898	282	282	7 050	343	343	4 000	434	434	1 075	506	508	126
315	LTSB(2)	90	91	2 999	278	278	8 600	336	336	2 900	416	416	410	457	457	79
465	Selected	85	85	251	274	275	53	328	328	49	397	396	40	408	410	48

Note : E = Effective Elastic Modulus

TABLE 3.4 - The calculated effective elastic moduli values together with the measured and calculated depth deflections at various stages of trafficking on Section 3

Depth layer (mm)		HVS Traffic (ME80s)								
		0			0,1			>50		
		Deflection (µm)		E (MPa)	Deflection (µm)		E (MPa)	Deflection (µm)		E (MPa)
		Measured	Calculated		Measured	Calculated		Measured	Calculated	
0	Surface & Base	75	71	4 000	165	162	1 600	500	484	1 250
165	LTSB(1)	58	58	8 000	127	127	8 898	450	449	900
315	LTSB(2)	53	54	3 300	123	124	7 798	415	417	226
465	Selected subgrade	50	50	450	120	121	140	375	378	56

Note : E = Effective Elastic Modulus

The tensile and compressive strain values, together with the appropriate failure criteria, were used to predict the life expectancies (structural capacities) for the different layers in the structure. In Table 3.5 a summary of the different strain parameters (distress determinants) used, are given.

In Table 3.6 the strain values for the different sections at various stages of testing are given. Similar strain values were obtained on Section 2 and 3. The strains increased rapidly during the EPWP state on Section 1.

The predicted E80s (using the current failure criteria) to result in visible cracking on the surface of the layers and limit subgrade deformation for the three sections are summarized in Table 3.7. The values were derived using the mechanistic design method proposed by Freeme et al (1984). The HVS results indicated that the strains initiated at the bottom of the relatively stiff (high moduli) layers, i.e. asphalt and cementitious layers, are not constant. It varies with the number of load repetitions. The rate of increase in these strain values are a strong function of the moisture and crack state of the layer itself and the support from the other layers in the structure.

TABLE 3.5 - Summary of different strain parameters used in the analysis

Layer	Strain Parameter	Remarks
Surfacing and base	Horizontal tensile, ε_t	Bottom of layer (crack initiation)
Upper stabilized subbase	"	"
Lower stabilized subbase	"	"
Selected and subgrade layer	Vertical compressive, ε_v	Top of selected layer (limit permanent deformation.)

TABLE 3.6 - A summary of the calculated strain values at various stages of trafficking in the different layers of all three test sections

(a) SECTION 1

ME80s (HVS)	Bottom of			Top of
	Asphalt ε_t (με)	LTSB(1) ε_t (με)	LTSB(2) ε_t (με)	Selected Layer ε_v (με)
0	8	21	36	-39
4	38	36	74	-82
8,3	30	63	108	-119
25,4	135	102	165	-188
26,5(SW)*	203	179	242	-293
26,5(W)	360	331	421	-596

(b) SECTION 2

ME80s (HVS)	Bottom of			Top of
	Asphalt ε_t (με)	LTSB(1) ε_t (με)	LTSB(2) ε_t (με)	Selected Layer ε_v (με)
0	0,4	21	33	-39
3,6	Nil	7	33	-35
7,5	8	28	63	-67
27,8	83	94	115	-139
32,3	156	146	134	-284

(c) SECTION 3

ME80s (HVS)	Bottom of			Top of
	Asphalt ε_t (με)	LTSB(1) ε_t (με)	LTSB(2) ε_t (με)	Selected Layer ε_v (με)
0	12	18	23	-29
0,1	4	10	25	-27
>50	132	173	174	-244

* SW : Semi-wet : Subbases wet but not saturated

W : Wet : Subbases saturated (excess porewater pressure state)

TABLE 3.7 - Predicted E80s to cracking and limit subgrade deformation on the three test sections

(a) SECTION 1

Applied E80s (HVS) (ME80s)	Predicted E80s* to :			
	Cracking on the surface of			Limit subgrade strain at the top of selected layer
	Asphalt	LTSB(1)	LTSB(2)	
0	>50 x 10^6	>50 x 10^6	9 x 10^6	>50 x 10^6
4	>50 x 10^6	>50 x 10^6	300 000	>50 x 10^6
8,3	>50 x 10^6	1,8 x 10^6	3 000	>50 x 10^6
25,4	>50 x 10^6	600 000	0	>50 x 10^6
26,5 (SW)	8 x 10^6	0	0	>50 x 10^6
26,5 (W)	600 000	0	0	100 000

(SW) See Table 3.8 (W) See Table 3.8

(b) SECTION 2

Applied E80s (HVS) (ME80s)	Predicted E80s to :			
	Cracking on the surface of			Limit subgrade strain at the top of selected layer
	Asphalt	LTSB(1)	LTSB(2)	
0	>50 x 10^6	>50 x 10^6	21 x 10^6	>50 x 10^6
3,6	>50 x 10^6	>50 x 10^6	21 x 10^6	>50 x 10^6
7,5	>50 x 10^6	>50 x 10^6	1,2 x 10^6	>50 x 10^6
27,8	20 x 10^6	21 000	120 000	>50 x 10^6
32,3	8 x 10^6	0	27 000	>50 x 10^6

(c) SECTION 3

Applied E80s (HVS) (ME80s)	Predicted E80s to :			
	Cracking on the surface of			Limit subgrade strain at the top of selected layer
	Asphalt	LTSB(1)	LTSB(2)	
0	>50 x 10^6	>50 x 10^6	>50 x 10^6	>50 x 10^6
0,1	>50 x 10^6	>50 x 10^6	>50 x 10^6	>50 x 10^6
>50	3 x 10^6	0	0	>50 x 10^6

* Shift factors from Freeme et al (1984), A Category road.

According to Table 3.7, after 25 ME80s, the strain level (effective horizontal tensile strain, (ε_t)) in the asphalt was relatively low and the structural capacity was calculated to be in excess of 50 ME80s. After the introduction of water, the fatigue life reduced to approximately 600 000 E80s. Surface cracks on the asphalt occurred however just after the introduction of water into the subbase layers. According to the prediction of cracking for weakly cemented subbase layers, the lower subbase layer should develop fatigue cracking long before the upper subbase layer. The HVS tests proved that the real situation is visa versa. The upper subbase was in an advanced state of fatigue cracking, than that observed in the lower subbase layer. Field inspections revealed that the interface between weakly cemented layers was relatively smooth and of utmost importance. If a smooth surface exists between these layers, the two subbases does not react as a solid beam (thickness 300 mm), but reacts as two separate beams (2 x 150 mm) placed on top of one other with relatively low horizontal friction at their interface. It can be shown mechanistically that relatively high horizontal strains will be experienced at the bottom of the upper layer by inserting a thin zero modulus layer between the two subbases. (See Chapter 5 later). The advanced state of fatigue cracking in the upper layer can then be explained. The main disadvantage in the current mechanistic design criteria for fatigue life of treated layers lies in the fact that strain values at the bottom of treated layers change with trafficking. Because of this behaviour, it is meaningless to predict structural capacities for the different layers, especially cementitious layers, using the current procedure, unless the real strain value at that time is known. According to the prediction on Section 2, (See Table 3.7) surface cracking on the asphalt layer will occur after approximately 40 ME80s (32 + 8 ME80s), provided the horizontal strain at the bottom of the asphalt layer being kept at a value of approximately 160 με (Table 3.6). The same reasoning holds for the weakly cemented subbase layer on Section 2. No cracking is expec-

ted in the upper layer after 8 ME80s, provided the strain level being kept constant at 28 με. This is possibly correct, but the practice indicates that the strain value is not a constant. Therefore the limitations of the current design and evaluation criteria are realized. A "performance expectation chart" must be constructed to enable future predictions rather than the use of the current "design curves", based on actual induced strain vs repetitions history.

The deformation criteria proposed by Freeme et. al. 1984 for the subgrade layers in this type of design proved to be adequate. The changes in the vertical strains are relatively small and therefore no real deformation problems for this layers are foreseen.

According to Tables 3.2 and 3.3, the vertical deflection at the bottom of the lower subbase varied initially from 0,09 mm to 0,50 mm during the dry state. The relative deflection within the two layers varied between 0,04 mm and 0,10 mm. This is accompanied by effective elastic modulus changes of > 5 000 to less than 500 MPa in the dry state. In the EPWP state the relative deflection increased to 0,9 mm and the modulus decreased to 200 MPa, on Section 1. (The relatively low moduli values calculated for the dry subbase layers on Section 2 (Table 3.3) after 32,2 ME80s are believed to be due to malfunctioning of the MDD's.) The moduli values for the subbase layers after 27,8 ME80s were more reasonable varying between 400 to 1 000 MPa in the dry state. In terms of moduli it is concluded that the weakly cemented subbases still provided good structural support at the end of the test in the dry state. This was also found with a high standard crushed stone base pavement in Transvaal, Van Zyl (1983).

3.2.8 Layer densities and moisture contents

Inspection trenches made after HVS testing enabled densities and moisture contents to be measured. Comparisons of trafficked vs untrafficked sections were also done. The position of these trenches on Section 1 are illustrated in Figure 3.14. In Figure 3.15 cross section profiles at the two trenches on Section 1, are illustrated. A distinct difference was observed between the dry (wall A) and wet (wall D) sections. The origin of the surface permanent deformation (rut) during the wet state (EPWP) was within the granulated upper weakly cemented subbase. During the dry state only fatigue distress occurred within both weakly cemented subbase layers. It was not possible to measure any decrease in density of the weakly cemented subbase layers during the dry state of testing, however, increases of approximately 1,5 to 3,2 per cent were measured in the upper and lower subbase layers, respectively. The insitu moisture contents varied between 9,6 per cent for the upper subbase and 13,8 per cent of the lower subbase layer. During the wet state however a decrease of 4,3 per cent in density of the upper subbase was measured. In the lower subbase (not granulated) a slight increase of 0,6 per cent was measured. The average moisture content of the upper subbase was 9,2 per cent. The reason for this relatively low moisture content is that moisture samples were taken approximately two weeks after the end of the test, therefore natural drainage resulted in moisture contents more or less equal to the moisture contents in the dry state at the time of sampling. An increase of 4,8 per cent in density was observed within the selected layer. It is believed that the decrease in density (strength) of the upper subbase, causes increased load transfer to the selected layer, which compacted under traffic resulting in relatively higher densities.

X DCPs
• MDD
* MAXIMUM RUT - 80mm

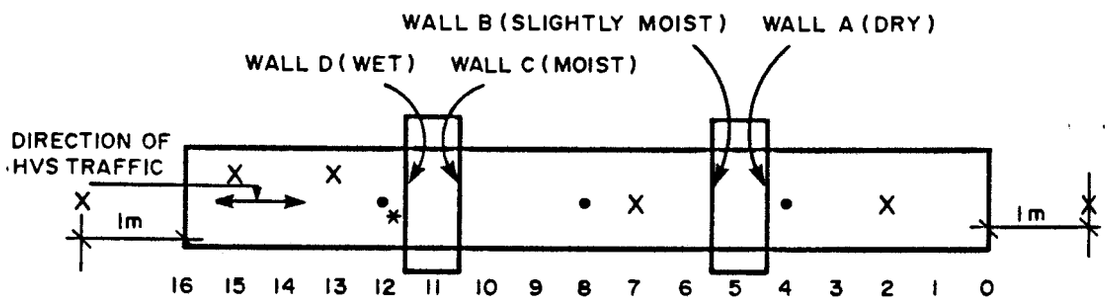

FIGURE 3.14

POSITIONS OF THE TWO TRENCHES EXCAVATED ON TEST SECTION 1

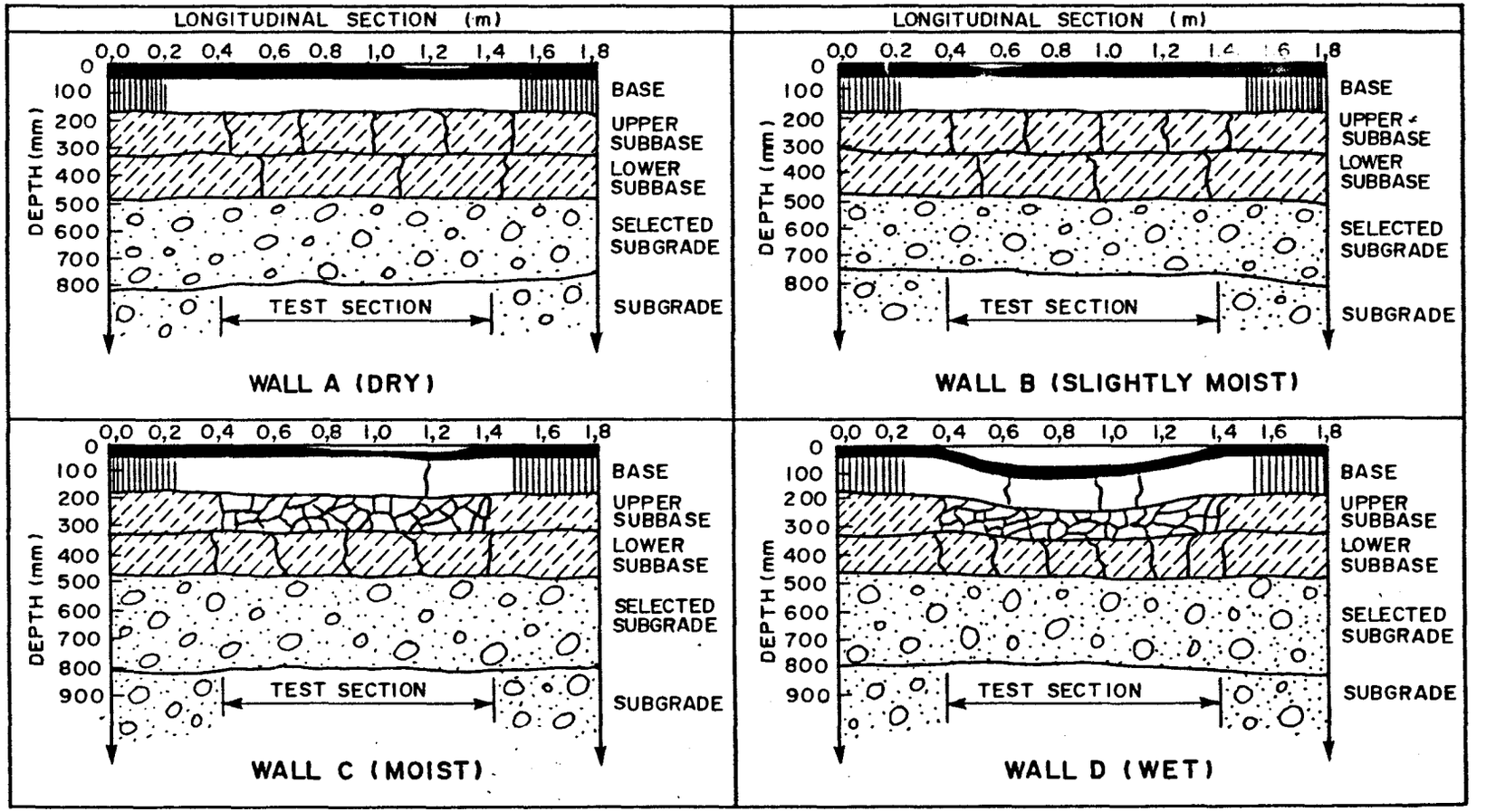

FIGURE 3.15

CROSS SECTION PROFILES AT THE TWO TRENCHES ON SECTION 1

On Sections 2 and 3 similar densities and moisture contents were measured as in the dry state on Section 1. It is interesting to note that during the high single wheelload (150 kN) test on Section 3 the density of the asphalt increased by approximately 5 per cent. It is believed that the relatively stiff weakly cemented subbase layers provided strong support to the load therefore resulting in the densification of the asphalt layers. No decrease in density was measured within both subbase layers although these layers were fatigue cracked into small blocks (approximately 150 mm x 150 mm). The density in the selected and subgrade layers increased by 2,4 and 3,2 per cent, respectively. According to the mod. AASHTO values, the density increased from 94 per cent to 96 per cent in the selected layer and 98 per cent to 101 per cent in the subgrade layer. On Section 3 (150 kN test), 1 to 2 per cent lower moisture content values were measured within the selected and subgrade layers and were associated with the more dense areas (trafficked areas). A cross profile made on Section 3 is illustrated in Figure 3.16. The profile was made at the position of maximum rut (60 mm) on the section. More than 80 per cent of the permanent deformation on the surface occurred within the asphalt surfacing and base layer only. It was however not possible to distinguish accurately between the surfacing and the base layer. Between 10 and 20 mm permanent deformation occurred on the surface of the upper cemented layer, and a maximum of 10 mm occurred within the selected subgrade layer. The two subbase layers were cracked, with the upper subbase more fractured than the lower subbase layer. The lower layer experienced only fatigue cracking.

3.2.9 Permeability test results (MARVIL)

In order to supplement the density results on the weakly cemented subbase layers, it was decided to measure water permeability on the two subbase layers, using the Marvil apparatus (Viljoen and Van Zyl, 1983). This was done in

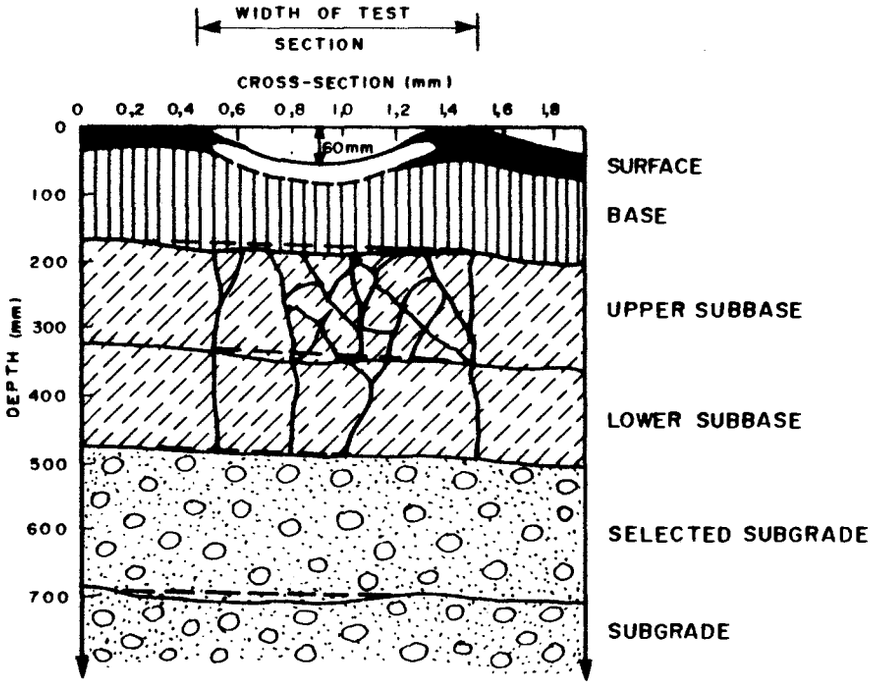

FIGURE 3.16

CROSS PROFILE OF SECTION 3 AT THE POSITION OF MAXIMUM RUT

situ (on the trafficked material) as well as on recovered blocks of weakly cemented material after trafficking on Section 2 only. The in situ permeabilities were done from the top of the layers. The permeabilities on the recovered blocks were done from the bottom of the layers. The recovered block of material was turned upside down before the measurement. The permeabilities were done at the same temperature and with the same source of water. Road surface temperature ranging between 20 - 30 °C (on the asphalt) at the time of testing. Permeabilities were also done on the asphalt layer but this layer proved to be relatively impermeable using the MARVIL instrument. The permeability results are illustrated in Figure 3.17. In Figure 3.17(a), the permeability measured on the upper subbase are illustrated. Relatively higher permeabilities were obtained from the bottom of the recovered blocks of subbase material. The blocks however were handled very carefully and the higher rate is believed to be a result of invisible hair cracks (fatigue) at the bottom of the weakly cemented layers. The figure also indicates relatively higher permeabilities on the blocks where the higher number of repetitions were applied, although there is not clear evidence that increases in permeability occurred with number of repetitions. In Figure 3.17(b) the permeabilities measured on the lower subbase at various stages of trafficking are illustrated. Relatively higher permeabilities also resulted on the recovered blocks of subbase material. Relatively lower permeabilities, however, were measured in the lower subbase. This confirms the relatively higher degree of cracking observed within the upper subbase. The in situ dry densities and nuclear moisture content values are also indicated on the figure.

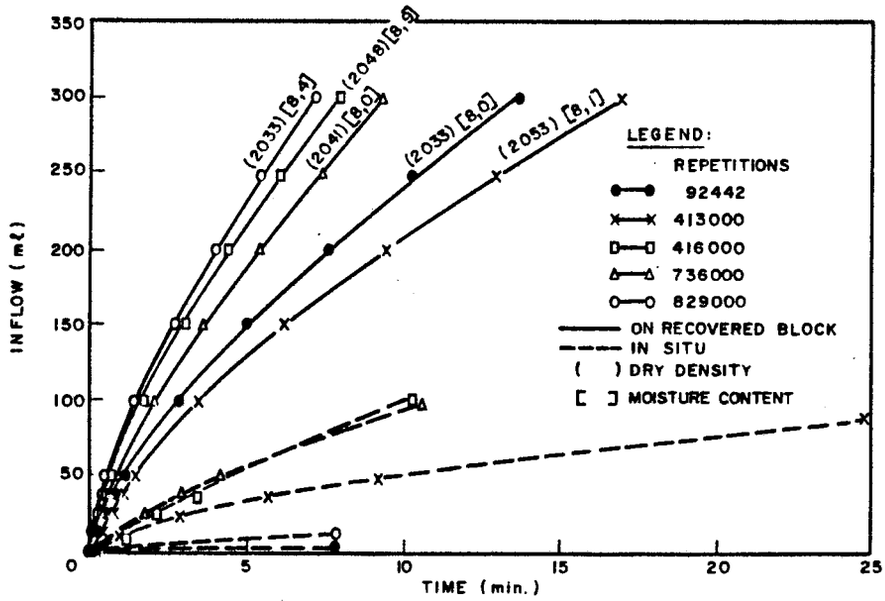

(a) UPPER STABILIZED SUBBASE

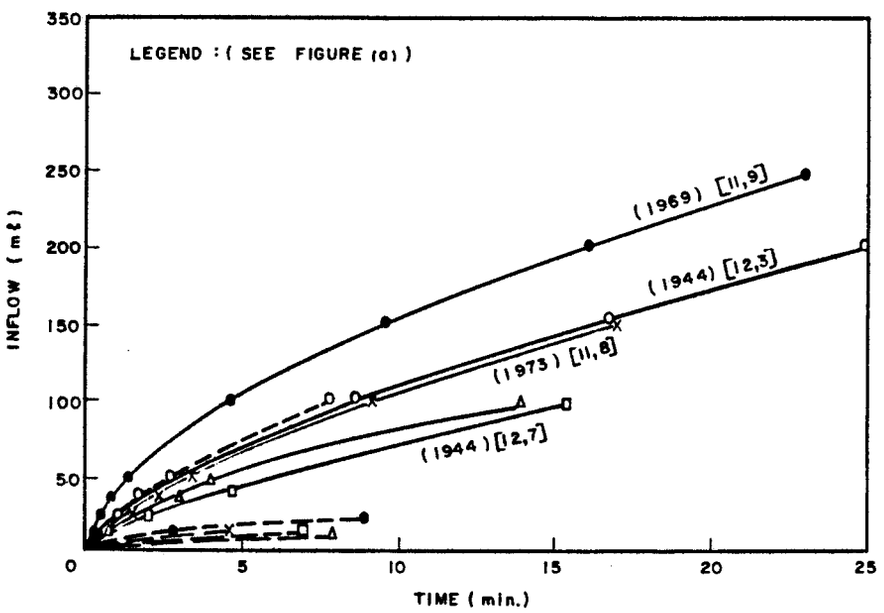

(b) LOWER STABILIZED SUBBASE

FIGURE 3.17

MARVIL PERMEABILITIES MEASURED ON THE STABILIZED SUBBASES ON SECTION 2 AT VARIOUS STAGES OF TRAFFICKING

3.2.10 Dynamic Cone Penetrometer (DCP) test results

Dynamic cone penetrometer (DCP) tests were done on the dry and wet parts of Section 1. The DCPs were done from the top of the upper subbase. The main objective with this tests was to quantify the state of the individual pavement layers in terms of DCP value (i.e. shear strength). The average penetration rate was approximately 0,8 mm per blow in the upper subbase in the dry state. The penetration rate outside the trafficked section was approximately 0,5 mm per blow. See Table 3.8. These are very low penetration rates (i.e. higher strengths) but the higher rate of 0,8 mm per blow within the test section is an indication of weakening of the upper subbase owing to traffic. The average penetration rates within the lower subbase, selected subgrade and subgrade, however, were 1,5; 7,5 and 2,5 mm per blow, respectively.*

On the wet section, the penetration rate of 2,2 is the same than those measured crushed stone base pavements in Transvaal (Maree, 1982).

The results indicates that traffic loading causes break up or cracking of the stabilized layers (loss in shear strength). The average block size (diameter) measured from the upper subbase material on the dry section was approximately 250 mm. On the wet section the upper subbase was granulated and the particle sizes average at nominal diameter of approximately 50 mm. Horizontal cracking was also observed within the upper subbase layer, after trafficking.

---

*It is important to note that the DCPs were done in order to quantify the state of the subbase layers rather than to quantify the balance of the structure. Therefore the balance curves proposed by Kleyn et al (1983) are not included in this study.

In Table 3.8 a summary of DCP penetration rates observed on the three test sections, is given.

TABLE 3.8 - Average DCP penetration rates for the three Sections in mm per blow

Section	Subbase layer	Position*		Number of repetitions	Wheel load (kN)
		Inside	Outside		
1	Upper (dry)	0,8	0,5	695 000	100
	Lower (dry)	1,5	1,1	695 000	100
1	Upper (wet)	2,2	0,5	520 000(dry);175 000(wet)	100
	Lower (wet)	1,5	0,5	520 000(dry);175 000(wet)	100
2	Upper (dry)	0,6	0,5	830 000(dry)	100
	Lower (dry)	2,0	<0,5	83 000(dry)	100
3	Upper (dry)	1,1	0,6	96 000(40kN);34 000(150kN)	40,150
	Lower (dry)	2,0	2,0	96 000(40kN);34 000(150kN)	40,150

* Relative to HVS test section

From the table it can be concluded that although the penetration rates were relatively low, the highest penetration rate of 2,2 mm per blow was measured in the upper subbase after the wet test on Section 1. During trafficking in the dry state, penetration rates increased between 20 to 180 per cent in the upper subbase and 30 to 400 per cent in the lower subbase. It is believed that the in situ moisture content of the lower subbase is the major factor contributing to the higher percentage increase in penetration rates, in that moisture content is a critical parameter in the shear strength of soil materials. As no marked differences in the moisture contents within and without the sections were obtained, the increase in penetration rates in the upper subbase is believed to be mainly due to trafficking.

3.2.11 Block sizes of cracked weakly cemented subbase material

The majority of the HVS results indicated that cracking (postcracked phase) of cementitious materials is a reality. (See also photographic record of HVS tests in Appendix A). Because of the geometry of the layers in the structure and the loading, the material initially break up or crack owing to fatigue (beam bending concept).

At the stage, when the average block size (diameter) reaches the layer thickness, t, the probability of further fatigue distress is almost zero. The only mode of further break up is therefore fracturing, crushing and/or shear, depending also on the porewater pressure in or on the material. In Table 3.9 an indication of different block sizes is given for the upper subbase layer at various stages of trafficking.

TABLE 3.9 - Different block sizes resulted in the upper subbase at various stages of trafficking on the structure

Number of repetitions*		State of cracking	Estimated Block Size (diameter)	
100 kN	40 kN (E80s)		Dry	EPWP**
0	0	Precracked	Slab	Slab
92 000	$3{,}6 \times 10^6$	Postcracked	4 t	4 t
520 000	20×10^6	Postcracked	3 t	2 t
830 000	32×10^6	Postcracked	1,5 t	<0,3 t (Granulated)

* 40 kN repetitions (E80s) calculated with d = 4, in $(\frac{P}{40})^d$

t = layer thickness (t = 150 mm in this case)

** EPWP = Excess Porewater Pressure

On Section 1 it was observed that after block sizes reached dimensions of approximately 1,5 t - 2 t in the dry state, only 34 000 repetitions at 100 kN wheel load (1,4 x 10^6 E80s) is needed in the EPWP state to change the material into a granulated state (block size $\leq$ 0,3 t). The lower subbase only break down to sizes of the layer thickness even in the EPWP state because the stress level is markedly reduced at this depth in the pavement structure. It is interesting to note that Otte (1978) also found that cementitious base layers do crack and that the average block sizes reached equals approximately the layer thickness. In this case the base layer was 100 mm thick and blocks of 100 mm x 100 mm were recovered after HVS trafficking.

3.2.12 Summary of some indicators of behaviour

In order to summarize this pavement's behaviour and to indicate the important function of the weakly cemented subbase layers (especially the upper subbase), Figure 3.18 was compiled. The figure indicates resilient and permanent changes of the pavement structure with increase in traffic loading and change in moisture condition. The most dramatic change in the behaviour of the pavement structure occurred when the moisture state and condition of the upper stabilized subbase changed. It can be concluded that any remarkable change within the state of the upper weakly cemented subbase layer will be reflected by these indicators. This is also true for resilient behaviour such as surface deflection (RSD) and radius of curvature (RC). The indicators for permanent changes in behaviour are permanent deformation (rut), shear strength (DCP) and dry density. These indicators provide relatively valuable information, especially after a state of an excess porewater pressure existed within the upper subbase of pavement structure.

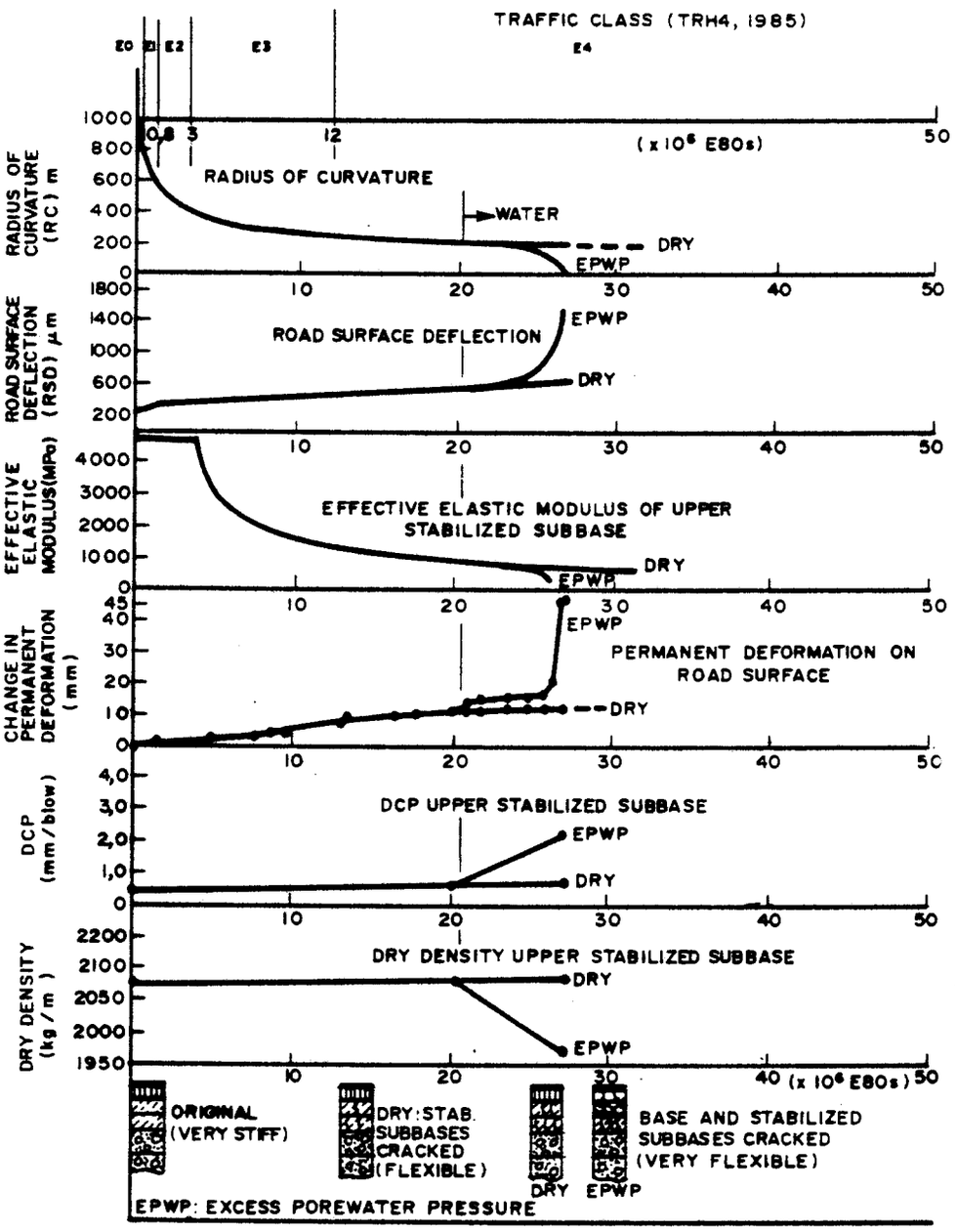

FIGURE 3.18

INDICATORS OF THE STATE OF THE PAVEMENT STRUCTURE AT VARIOUS STAGES OF TRAFFICKING AND MOISTURE CONDITIONS AT MARIANNHILL

These indicators can be used to observe and quantify the state of the individual pavement layers at various stages of trafficking. The pavement structure changed its state from an initially very stiff structure to flexible or very flexible depending on the loading and environmental conditions, such as accumulated water (EPWP), or high asphalt temperatures. These paths of behaviour during the "life" of the structure are well defined, and are illustrated in Figure 3.19. The flow diagram in the figure is self explanatory. Generally the pavement structure will change from very stiff to flexible and it is possible to change to very flexible if a state of excess porewater pressure does exist within the upper subbase layer. If this condition is removed (drying of the layer) the structure can reverse to the flexible state, but with the upper subbase in a granulated (dry) state. The asphalt layer will probably be fatigue cracked. Provision should however be made to prevent the structure following any of the EPWP paths by adequate construction, drainage provision, regular inspections and timely maintenance (i.e. cracksealing, etc.).

3.2.13 Pavement state and radius of curvature

The following section describes the state of the pavement defined including radius of curvature (RC).

The measured average road surface deflection (RSD) and radius of curvature (RC) for various stages of trafficking for measuring points 3 to 8 (dry test on Section 1) are given in Table 3.10. The trafficking dualwheel load was 100 kN. The HVS traffic was converted to E80s using a damage exponent of d = 4. This value was used for convenience, and does not represent an accurate damaging value for this structure as was previously discussed (Section 3.2.3).

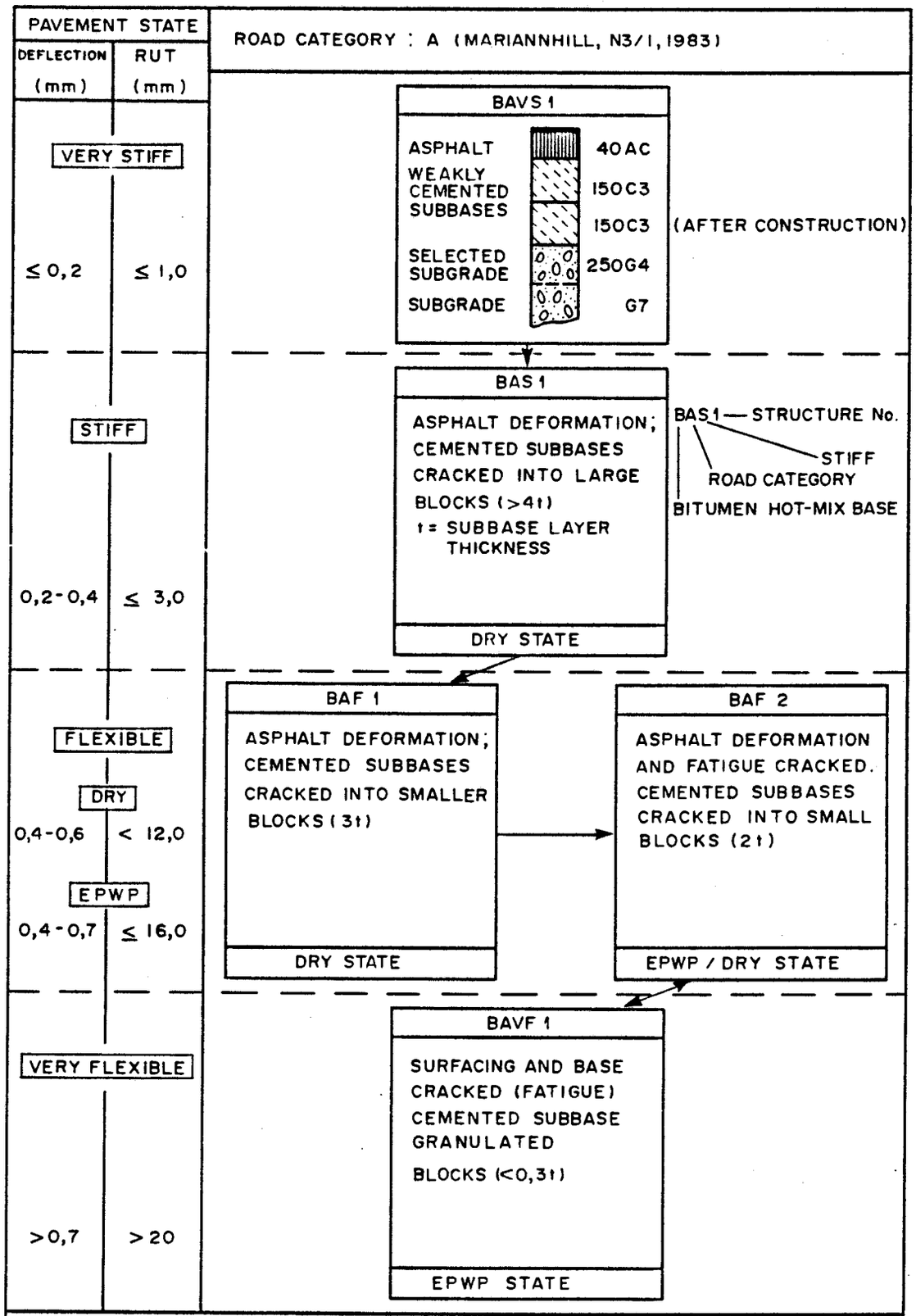

FIGURE 3.19

DIFFERENT PAVEMENT STATES DURING THE HVS TESTS ON THE PAVEMENT STRUCTURE AT MARIANNHILL

The results given in the table are also illustrated in Figure 3.20. The figure indicated an increase in RSD and decrease in RC. After 5 x 10^6 E80s gradual, almost linear, changes in RSD and RC occurred. As mentioned earlier the states of behaviour of pavement can be defined as very stiff, stiff flexible, very flexible in terms of surface deflection Freeme et al, (1984). The state of the pavement are defined in Table 3.11.

TABLE 3.10 - Average measured RSD and RC values at measuring points 3-8 on test Section 1 at various stages of trafficking

E80s (x 10)^6	RSD (µm)	Standard deviation (µm)	RC (m)	Standard deviation (m)
zero	119	67	987	217
1,48	306	49	484	296
3,96	320	41	540	194
8,31	459	52	276	58
12,83	527	46	289	99
16,30	550	23	255	61
20,28	589	32	227	36
25,4	600	67	250	93
26,5	750	85	150	178
		51(19)		137(86)

When these deflection boundaries are applied to the associated radius of curvature, it is possible to broaden the definition of the state of the pavement including radius of curvature, see Figure 3.21.

The appropriate radius of curvature and surface deflection for the different states are given in Table 3.12.

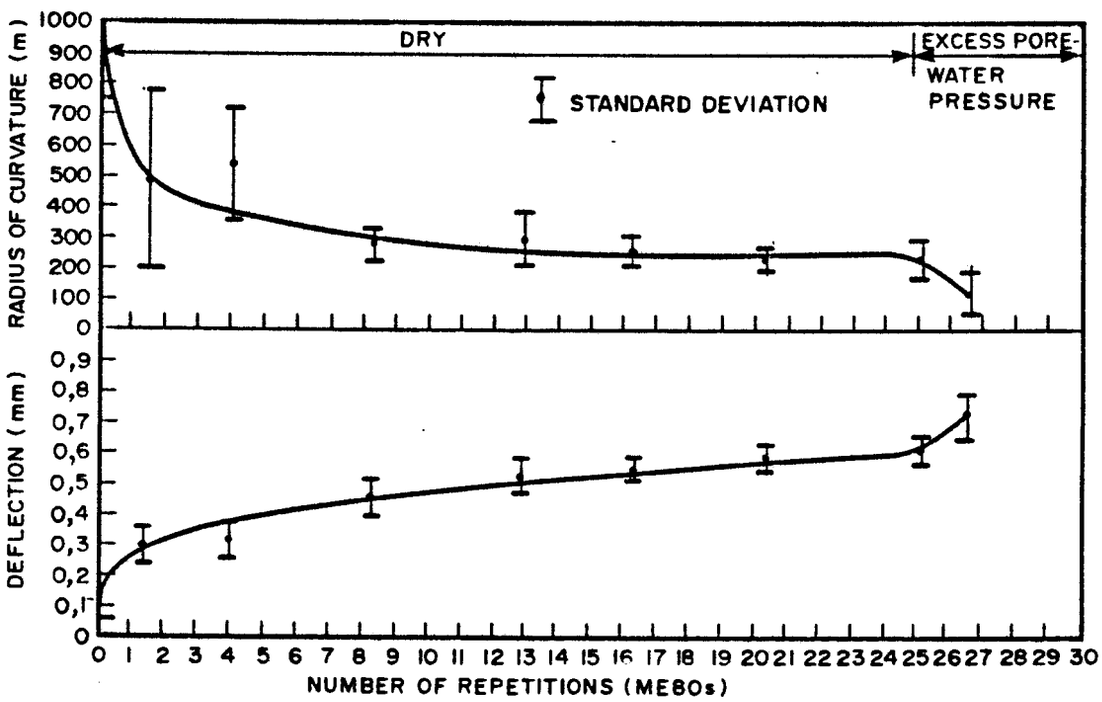

FIGURE 3.20

AVERAGE ROAD SURFACE DEFLECTION (RSD) AND RADIUS OF CURVATURE (RC) UNDER A 40kN DUAL WHEEL LOAD

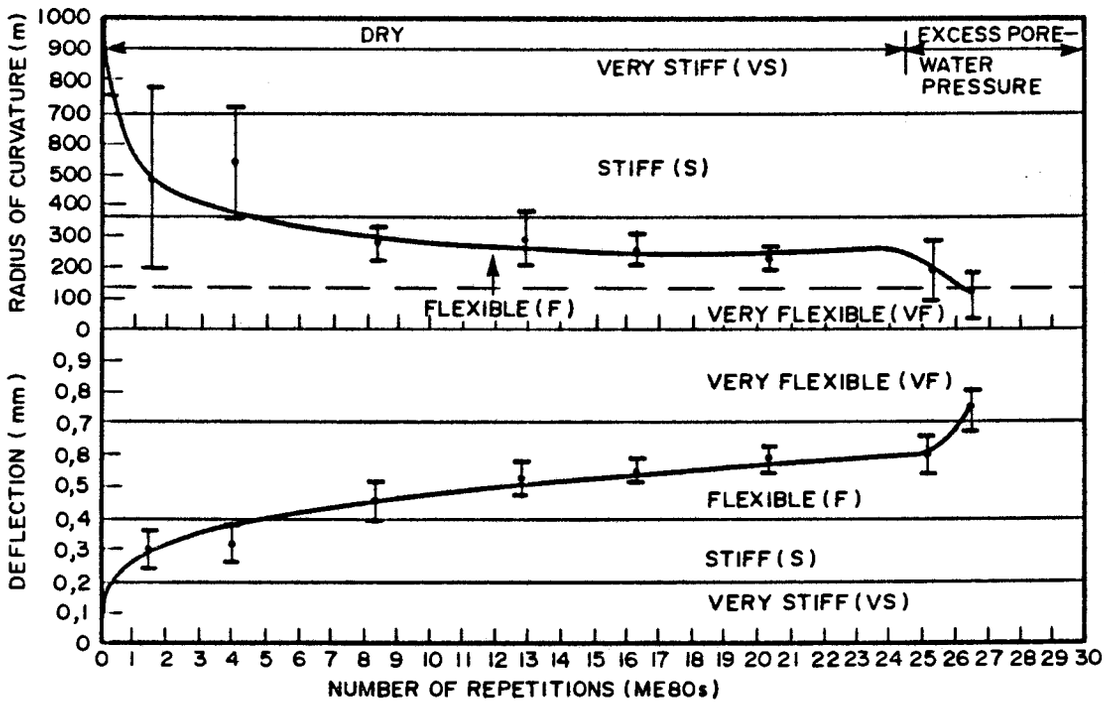

FIGURE 3.21

AVERAGE ROAD SURFACE DEFLECTION (RSD) AND RADIUS OF CURVATURE (RC) MEASURED UNDER A 40kN DUAL WHEEL LOAD

3.2.14 Development of a resilient behavioural model

This section describes the development of a three dimensional model to describe the resilient behaviour of the structure, using the effective elastic modulus of the upper stabilized subbase, E, the road surface deflection under a 40 kN wheel load, RSD, and the radius of curvature, RC. As indicated in Table 3.2, Figure 3.15 and Figure 3.18, the road surface deflection is largely dependent on the effective elastic modulus of the upper weakly cemented subbase. To construct the model it was necessary to obtain mathematical relationships between road surface deflection, modulus and radius of curvature. The measured values used to obtain the relationships are given in Table 3.13.

TABLE 3.11 - Definition of states of the pavement behaviour (After Freeme et al, (1984)

State	Approximate deflection range (mm)	Comments
Very stiff	<0,2	Pavement behaviour predominantly controlled by very high modulus (>5 000 MPa). Cemented subbase layers acting as slabs.
Stiff	0,2 - 0,4	Pavement behaviour controlled by cemented subbase layers with high moduli (>3 000 MPa). Subbase layers could be cracked but blocks tends to be larger than 1 m in diameter.
Flexible	0,4 - 0,7	Pavement behaviour controlled by layers with reasonably high moduli (800 - 3 000 MPa). Cementitious subbase layers cracked into smaller blocks. Diameter of blocks 1,5 x layer thickness (t).
Very flexible	>0,7	Pavement behaviour controlled by materials flexible in the granular state usually with low moduli (<800 MPa). Subbase layers tends to be susceptible to excess porewater pressure.

TABLE 3.12 - Road surface deflection and radius of curvature in the different states of behaviour

State	RSD (mm)	RC (m)
Very stiff (VS)	<0,2	>700
Stiff (S)	0,2 - 0,4	350 - 700
Flexible (F)	0,4 - 0,7	150 - 350
Very flexible (VF)	>0,7	<150

TABLE 3.13 - Measured and calculated values used to obtain the relationships

RSD (μm)*	RC (m)**	E (MPa)**
180	1 000	7 428
350	450	2 200
500	270	2 200
600	250	800
746	150	550
1 670	50	260

* Results from Table 3.2

** Results from Figure 3.10

In Figure 3.22, the relationships between RSD and E, and RSD and RC are given. Confidence limits are also indicated on the figure, because the real mathematical functions are not purely hyperbolic. The confidence limits were derived using the standard deviation of the constants, obtained from the products of RSD and E and RSD and RC, respectively. These values are indicated in Table 3.14.

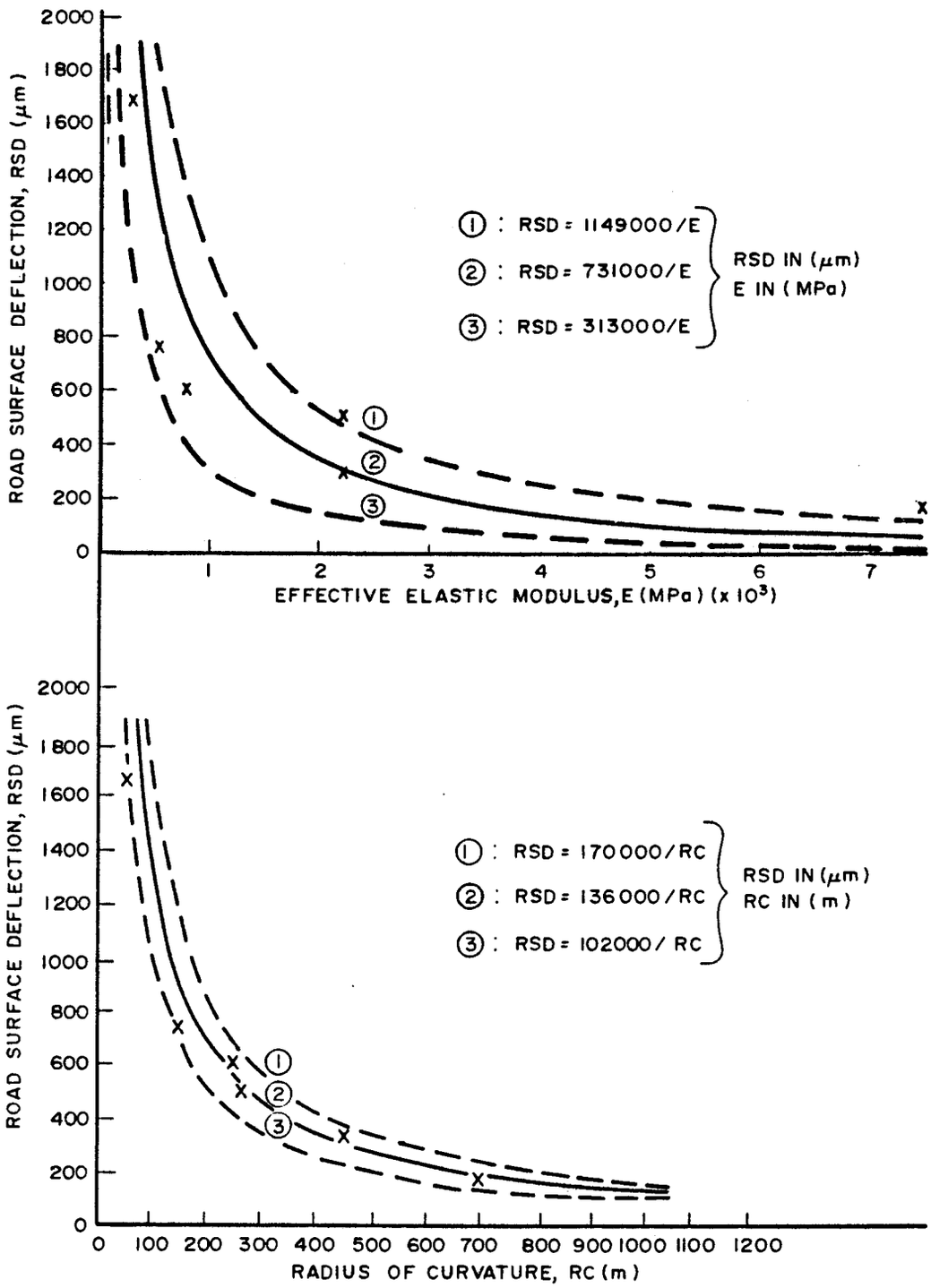

FIGURE 3.22

RELATIONSHIP BETWEEN ROAD SURFACE DEFLECTION, ELASTIC MODULUS OF THE UPPER SUBBASE AND RADIUS OF CURVATURE

TABLE 3.14 - Constants used in the hyperbolic relationships

	RSDxRC (µm.m) ($x10^3$)	RSDxE (µm.MPa) ($x10^3$)
	180,0	1 337,0
	157,7	770,0
	135,0	1 100,0
	150,0	480,0
	111,9	264,0
	83,5	434,2
Average	136	731
Standard deviation	±34	±418

The average values (constants in hyperbolic relationships) 136 000 and 731 000 were used to calculate both curves number two (2) in Figure 3.22. The other curves i.e., confidence limits, are calculated using the average values plus and minus the standard deviation, respectively. From these calculations, the relationship between the RSD and RC appears to be more accurate than RSD versus E. The accuracy of the relationships are indicated when the RSD is plotted against the constant divided by the independant variable, i.e. E and RC. See Figures 3.23 and 3.24. The relationships between RSD and C/E and K/RC are indicated, where C and K are the different constants. If the previous relationships were pure hyperbolic, the latter relationships should both be linear. In this case both relationships appears to be parabolic. The calculated relationships are :

$$RSD = 7{,}428 \times 10^{-1}\ C/E - 5{,}668 * 10^{-5}\ (C/E)^2 \quad .... \quad (3.1)$$

where C = 1 149 000 (Upper Confidence limit)
= 731 000 (Average)
= 313 000 (Lower Confidence limit)
with RSD in (µm) and E in (MPa).

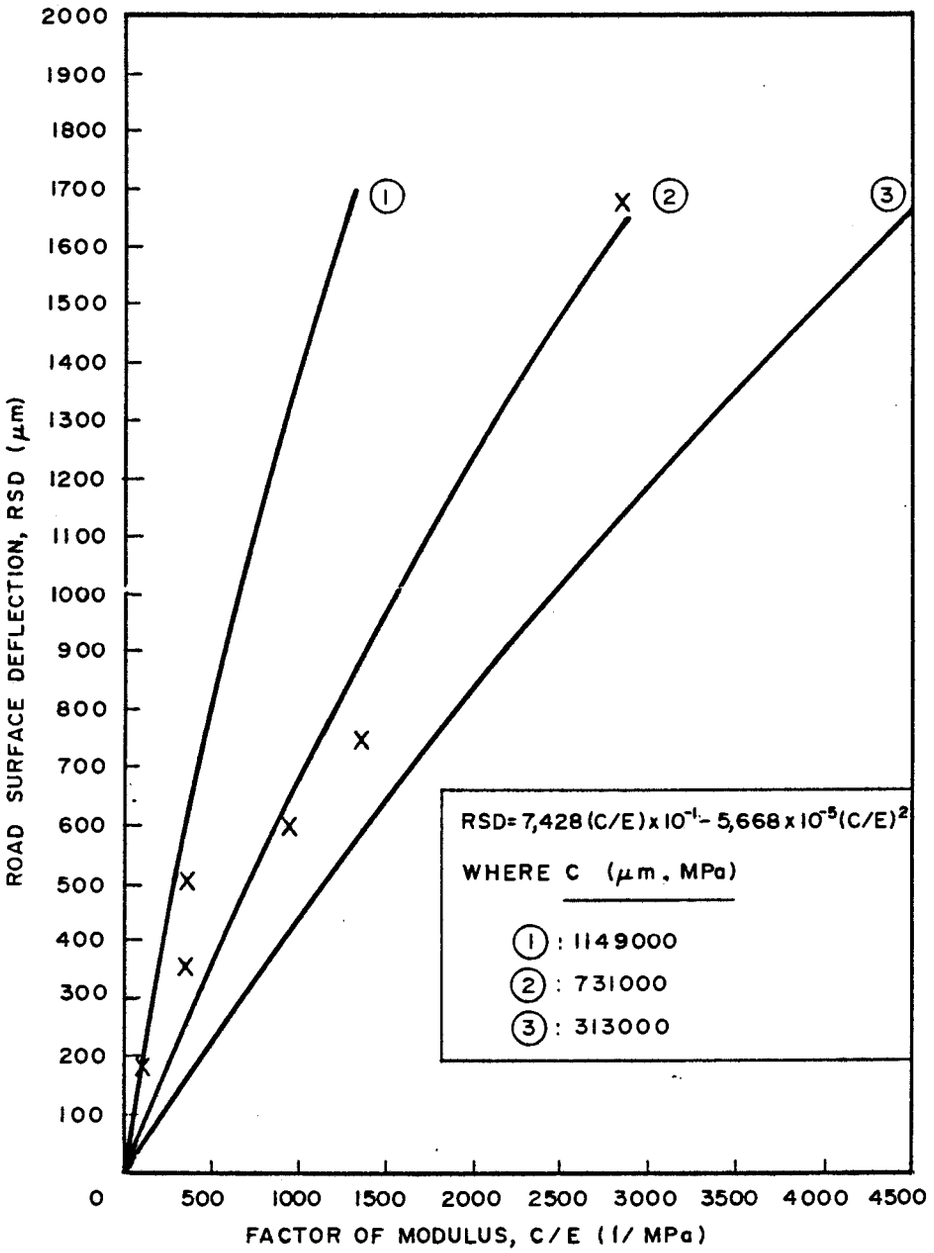

FIGURE 3.23

RELATIONSHIP BETWEEN ROAD SURFACE DEFLECTION (RSD) AND EFFECTIVE ELASTIC MODULUS (E) OF THE UPPER SUBBASE

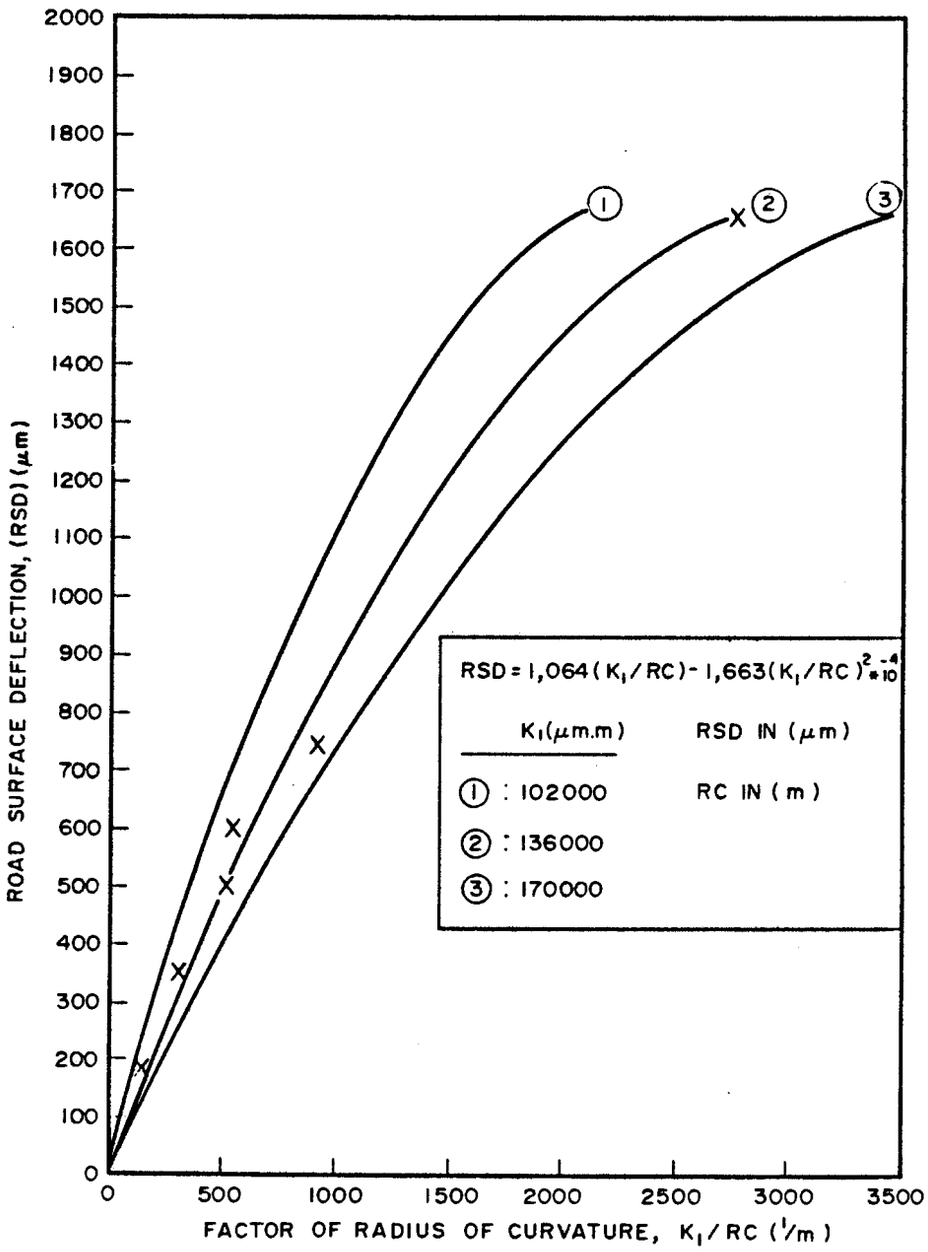

FIGURE 3.24

RELATIONSHIP BETWEEN ROAD SURFACE DEFLECTION (RSD) AND RADIUS OF CURVATURE (RC)

and RSD = 1,064 (K/RC) - 1,663 * 10^{-4} $(K/RC)^2$ ..... (3.2)

where K = 102 000 (Upper Confidence limit)
= 136 000 (Average)
= 170 000 (Lower Confidence limit)
with RSD in (μm) and RC in (m).

The regression analyses for above relationships are given in Tables 3.15 and 3.16.

TABLE 3.15 - Regression analysis for RSD versus C/E

Polynomial regression of degree 2

Dependent variable is RSD
Independent variable is C/E

Exponent	Reg. Coef	Std. error coef	Computed t
1	.74280612	.19351785	3.83843717
2	-.00005668	.00007786	-.72791937

Intercept 0.00000
Multiple correlation ..... .95839
R-squared ..... .91851
Std. error of estimate 193.74918

TABLE OF RESIDUALS

Data No	RSD Observed	RSD Estimated	Residual	Std. Resid.
1	180.000	72.552	107.448	.555
2	350.000	240.557	109.443	.565
3	500.000	240.557	259.443	1.339
4	600.000	631.419	-31.419	-.162
5	746.000	887.141	-141.141	-.728
6	1670.000	1640.424	29.576	.153

TABLE 3.16 - Regression analysis for RSD versus K/RC

Polynomial regression of degree 2

Dependent variable is RSD
Independent variable is K/RC

Exponent	Reg. Coef	Std. error coef	Computed t
1	1.06429973	.07931453	13.41872250
2	-.00016630	.00003170	-5.24536416

Intercept	0.00000
Multiple correlation	.99451
R-squared	.98905
Std. error of estimate	71.01897

TABLE OF RESIDUALS

Data No	RSD Observed	RSD Estimated	Residual	Std. Resid.
1	180.000	141.669	38.331	.540
2	350.000	306.465	43.535	.613
3	500.000	493.898	6.102	.086
4	600.000	529.764	70.236	.989
5	746.000	828.256	-82.256	-1.158
6	1670.000	1664.512	5.488	.077

The tables indicate relatively good multiple correlations, i.e. 95 and 99 per cent for RSD versus E and RSD versus RC respectively. The standard errors of the RSD estimate are 193,7 µm and 71 µm respectively. The relationship between RSD and K/RC appears to be fairly accurate.

In order to establish the three dimensional model, the relationship between E and RC was also studied. This relationship appears to be a relatively accurate parabola. Multiple correlation is 97 per cent with a standard error in E of 586 MPa.

The relationship obtained is :

$$E = 5{,}528\ RC + 2{,}510 * 10^{-3}\ (RC)^2 \quad \ldots\ldots\ldots\ldots\ldots \quad (3.3)$$

with E in (MPa) and RC in (m).

The regression analysis of E versus RC is given in Table 3.17. The relationship is illustrated in Figure 3.25.

To develop the behaviour model only two of above equations are necessary, i.e. equation 3.2 and 3.3. The RSD and E values are calculated from different RC values. Equation 1 was left out on purpose because of the relatively high standard error involved.

In order to obtain a three dimensional plot of the three variables i.e. RSD, RC and E, a computer program, DISSPLA, available at CSIR computer centre was used. The data input program and results are given in Appendix B. In Figure 3.26 the computer plot of the model is illustrated.

As the original results include the EPWP state, the rapid change in resilient behaviour is well illustrated by the sharp curvature of the model in this state. In the dry state the model indicates gradual change in resilient behaviour. As previously discussed (Section 3.2.5), this pavement structure behaved almost linear elastic throughout, for normal loading. Therefore it was decided to call the curved surfaces in the model the "ELASTIC SURFACE" and the plane parallel with the RSD, i.e. orthogonal to the RC-E plane, the "ELASTIC WALL". Any behaviour which does not coincide with the elastic line is therefore not linear elastic. In other words, the behaviour on the elastic line indicates linear elastic behaviour. In this pavement

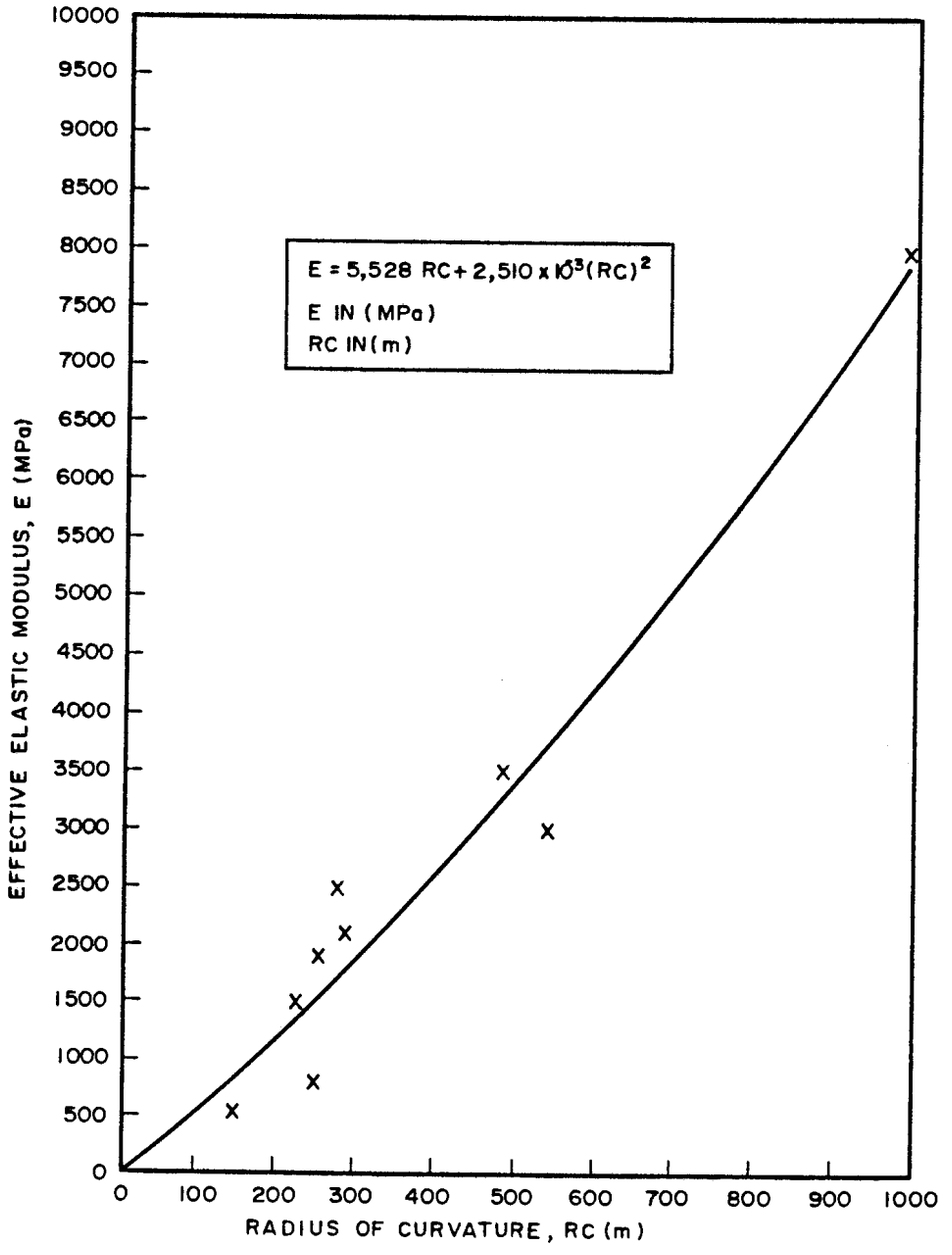

FIGURE 3.25

RELATIONSHIP BETWEEN EFFECTIVE ELASTIC MODULUS OF THE UPPER SUBBASE AND THE RADIUS OF CURVATURE

structure the dry "cut off" point appears to be at an RSD value of approximately 600 m. (Dry cut-of is defined as the maximum deflection reached in the dry state on the road surface. (See Figures 3.10 and 3.26.)

TABLE 3.22 - Regression analysis of E versus RC

Polynomial regression of degree 2

Dependent variable is E
Independent variable is RC

Exponent	Reg. Coef	Std. error coef	Computed t
1	5.52787639	1.09818279	5.03365783
2	.00251021	.00142015	1.76756148

Intercept	0.00000
Multiple correlation	.97361
R-squared	.94792
Std. error of estimate	585.62815

TABLE OF RESIDUALS

Data No	E Observed	E Estimated	Residual	Std. Resid.
1	8000.000	7901.381	98.619	.168
2	3500.000	3263.523	236.477	.404
3	3000.000	3717.030	-717.030	-1.224
4	2500.000	1716.911	783.089	1.337
5	2100.000	1807.211	292.789	.500
6	1900.000	1572.835	327.165	.559
7	1500.000	1384.176	115.824	.198
8	800.000	1538.857	-738.857	-1.262
9	550.000	885.661	-335.661	-.573

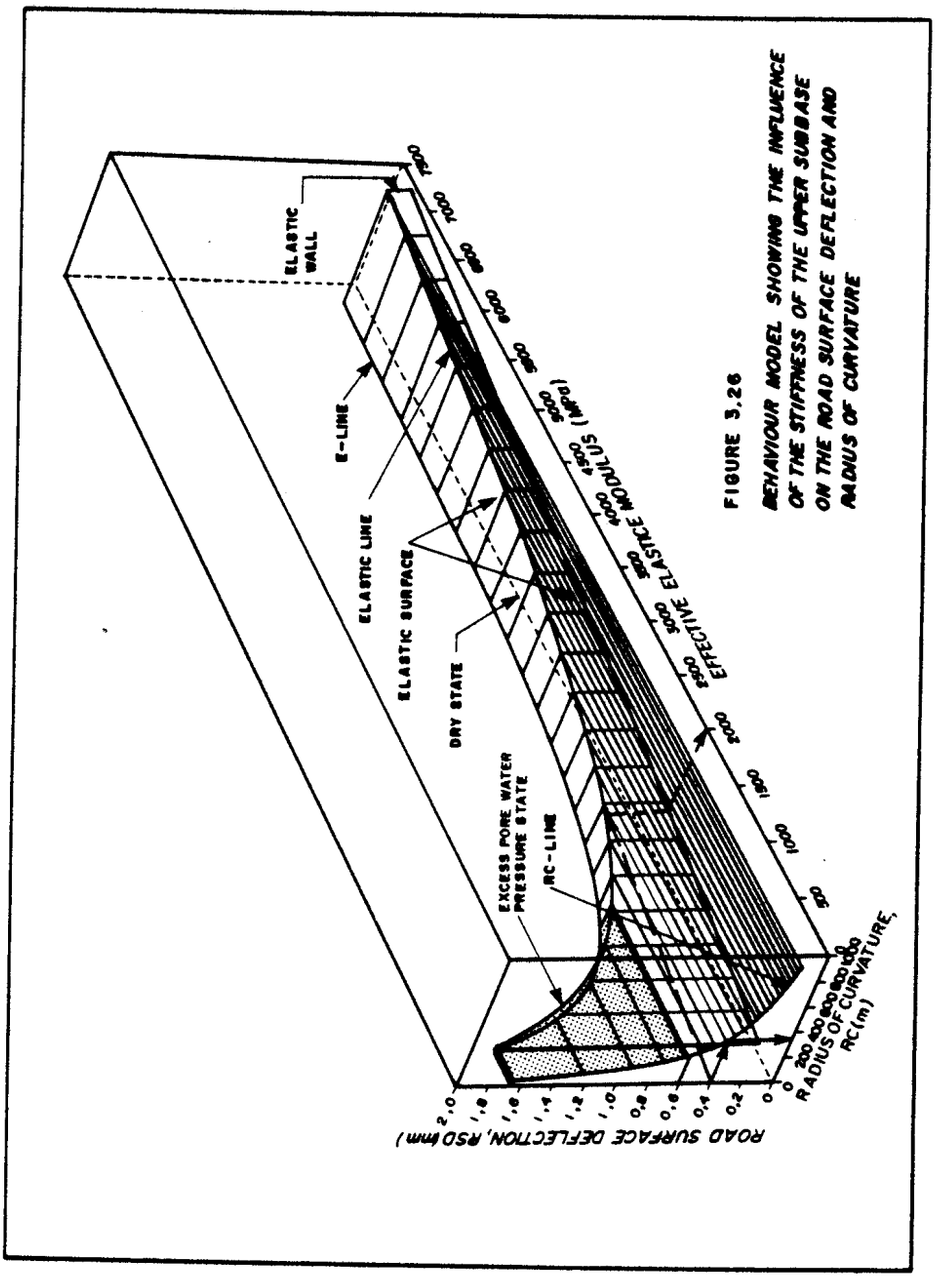

FIGURE 3.26
BEHAVIOUR MODEL SHOWING THE INFLUENCE OF THE STIFFNESS OF THE UPPER SUBBASE ON THE ROAD SURFACE DEFLECTION AND RADIUS OF CURVATURE

The model, which is illustrated in Figure 3.26 describes the resilient behaviour during the normal loading (traffic) in the dry and excess porewater pressure states in terms of effective elastic modulus of the upper subbase, surface deflection and associated radius of curvature. It can be used as an visual aid to understand the complex field of pavement behaviour. The model can also be used to determine two of the unknowns if one of the three variables is known by entering the model with the known (measured or guessed) value on the appropriate axis. The mathematical relationships can also be used for calculation purposes.

3.2.15 Summary and conclusions of HVS test at Mariannhill, N3/1

This part of Chapter 3 describes the main results obtained from HVS testing on a bitumen base pavement structure at Mariannhill, in Natal. The weakly cemented lime stabilized subbases were constructed of locally available weathered granitic material. Permanent deformation and resilient behaviour were observed on three test sections, both in the normal moisture (dry) and excess porewater pressure states. Moisture accelerated distress (MAD) was observed during the excess porewater pressure (EPWP) state within the upper subbase layer. Good behaviour was observed in the dry state and it is expected that this type of structure will be structurally adequate to carry E4 traffic without major rehabilitation necessary. It is however important to monitor pavement state in order to adequately design timely minor rehabilitation, such as cracksealing, drainage improvement etc. According to mechanistic analyses, the horizontal strain values initiated at the bottom of the asphalt and lime treated layers appeared to increase non linearly, with a marked increase during the moisture accelerated distress (MAD) phase. During this phase fatigue distress of the asphalt and subsequent pumping from the upper subbase are possible. Care should be taken in specifying cementitious subbase materials to be non-erodible. (De Beer, 1985(c)) The surface deflection and radius of curvature appear to be

relatively good indicators of behaviour of this type of structure, both in the dry and wet states.

Permeability tests on the recovered stabilized subbase layers indicated higher permeabilities at the bottom of the layer than at the top of the layer. This is believed to be a demonstration of the beam bending concept resulting in a higher degree of cracking at the bottom of these layers after trafficking.

DCP results indicated relatively high penetration rates within the upper subbase after trafficking, especially after the excess porewater pressure state. It was also possible to quantify the state of cracking of the weakly cemented subbase layers. The different states of behaviour of this pavement structure are described using a flow diagram which may be useful in future rehabilitation design. It was also shown that the state of the pavement can also be defined including the radius of curvature.

A behavioural model of this pavement structure was developed using three parameters, i.e. road surface deflection, radius of curvature and the effective elastic modulus of the upper subbase. It was indicated that mainly the effective modulus of the upper subbase governs the deflection on the road surface, especially during the excess porewater pressure state. The results shows that the modulus, road surface deflection and radius of curvature are interrelated. The model or the mathematical relationships can be used to obtain any of two unknowns in the model.

3.3 SUMMARY OF HVS TESTS AND RESULTS AT FIGREEE, N2/24

The objective of the HVS tests at this site was the same as that at Site 1 at Mariannhill. However, the tests and analysis were hampered by a longitudinal settlement crack through all the layers. (It finally appeared on the surface of the test section during HVS trafficking). It is, however, be-

lieved that the results obtained will be very useful in evaluating the influence of such non-traffic-associated cracks on the future behaviour of this type of pavement design including weakly cemented subbase layers. Slope instabilities often cause cracks in road structures in Natal (De Beer, 1983). Two sections were tested at this HVS site. Detailed evaluation of the test results at this HVS site is given elsewhere (De Beer, 1984(b)).

3.3.1 Road structure

The road structures as designed and as tested are illustrated in Figure 3.27. The main differences between the two structures are:

(a) vertical crack through all the layers, including the fill material,

(b) soft and moist zone on the sides of the crack as well as a ± 70 mm soft and moist sandy layer at the bottom of the lower weakly cemented (lime-treated) weathered granite subbase layer. This layer was partially carbonated according to a chemical test (Netterberg, 1984). At distances away from the vertical crack, the soft horizontal layer was also evident. The vertical crack was discoloured and visible through all the layers in the structure.

3.3.2 HVS test programme

The two HVS test programmes are summarized in Table 3.18.

3.3.3 Permanent deformation

The average permanent deformation of the road surface at various stages of trafficking on the two test sections is illustrated in Figures 3.28 and 3.29. Figure 3.28 indicates a gradual increase in asphalt deformation on Section 1 in the dry state for the first 520 000 repetitions (20 ME80s).

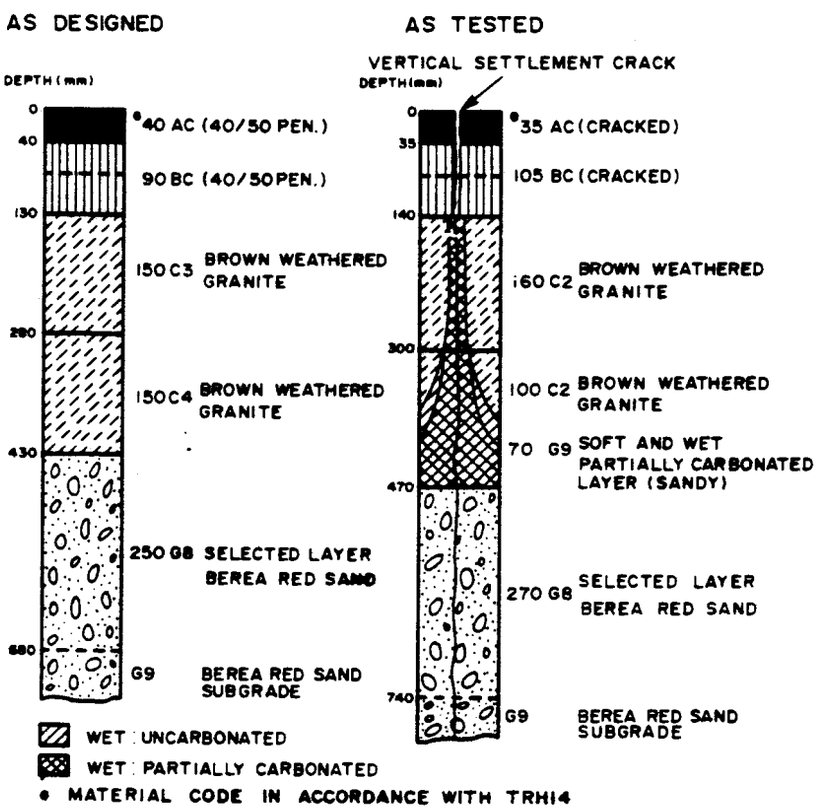

FIGURE 3.27

PAVEMENT STRUCTURE AT FIGTREE HVS SITE

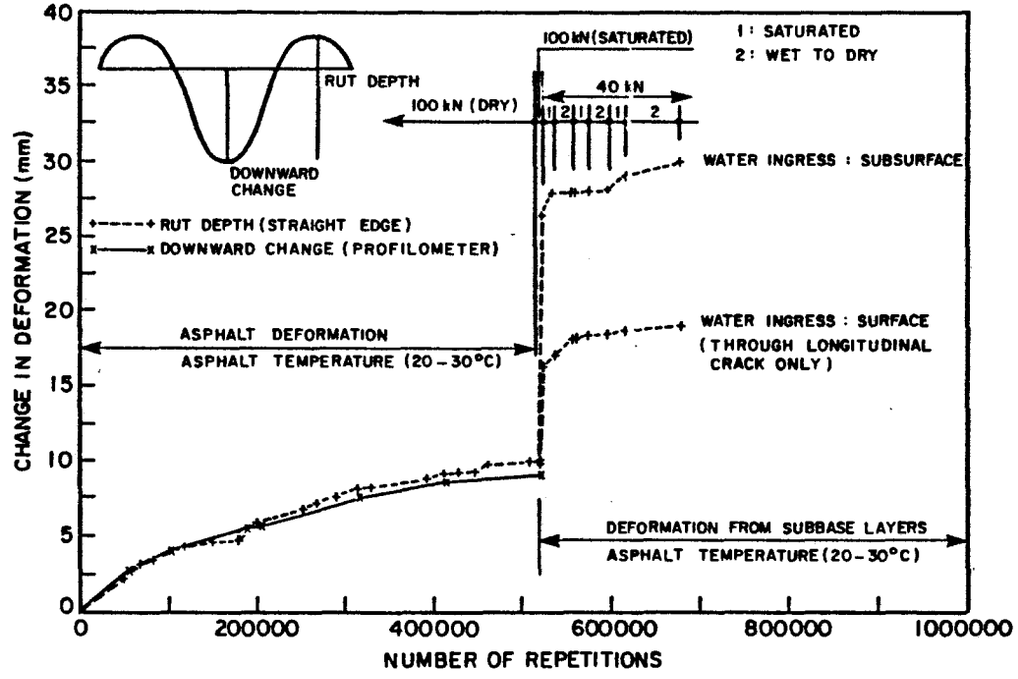

FIGURE 3.28

AVERAGE DEFORMATION OF THE ROAD SURFACE AT VARIOUS STAGES OF TRAFFICKING ON SECTION 1 AT INDICATED WHEEL LOAD

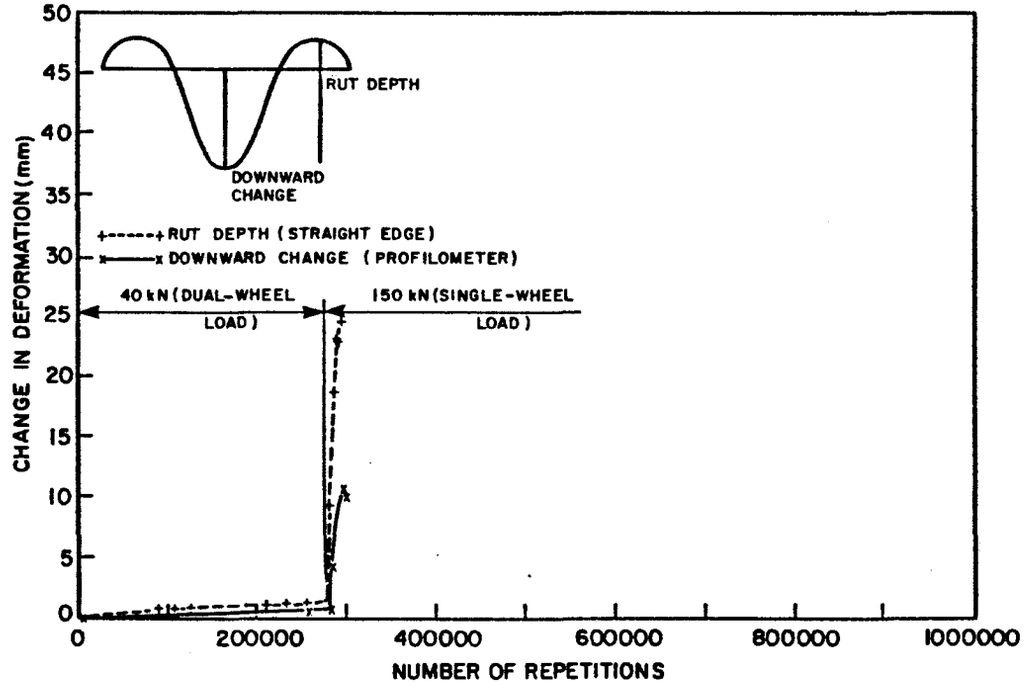

FIGURE 3.29

AVERAGE DEFORMATION OF THE ROAD SURFACE AT VARIOUS STAGES OF TRAFFICKING ON SECTION 2 AT INDICATED WHEEL LOAD

TABLE 3.18 - Test programme of Section 1 and Section 2

Section	Traffic loading (kN)	Moisture condition	Asphalt temperature (°C)	Actual repetitions	Remarks
1	100	Dry*	20-30	520 000	Total section tested (8 m)
	100	Saturated**	∿30	3 108	Subsurface water ingress, both sides of the test section, (one half of the section)
	100	Wet	20-30	3 108	Water ingress mainly from the surface through the longitudinal crack in the asphalt
	40	Wet to saturated	20-30	156 382	Subsurface water ingress every alternate 24 hours both sides of the test section (4 m)
				679 490	Total number of repetitions applied to test section
2	40	Dry	20-30	280 494	
	150***	Dry	20-30	17 255	
				297 749	Total number of repetitions applied to test section

* "Dry" is indicative of the normal in-situ moisture condition in the sublayers. (≤ optimum moisture content)

** "Saturated" in this thesis is indicative of a condition where excess porewater pressure exists within the structure of the test section, especially between the asphalt and upper subbase layers.

*** Singlewheel load 150 kN, tyre pressure 1448 kPa and dualwheel loads 40, 100 kN, tyre pressure 690 kPa.

After 520 000 repetitions the average rut was 9 mm. After the introduction of water the rut increased to 20 mm and 30 mm on the two parts of the test section*. A decrease in the rate of deformation was observed after the dualwheel load was decreased from 100 kN to 40 kN, and after the application of water was varied.

Figure 3.29 indicates a relatively low increase in asphalt deformation after 280 000 repetitions (E80s) on Section 2. The deformation increased to an average of 2 mm in the dry state with 40 kN dual-wheel load trafficking. The dualwheel load was changed to a singlewheel load of 150 kN and the deformation increased to an average of 25 mm after a further 17 255 repetitions. After studying the origin of the rut, it was concluded that more than 60 per cent of the rut originated in the asphalt layers. Similar behaviour was found at the previous HVS site (Mariannhill) where more than 80 per cent of the rut originated from the asphalt layers. (Testing temperature between 20 °C and 30 °C).

3.3.4 Road surface deflection (RSD) and radii of curvature (RC)

The average RSD and RC under a 40 kN dualwheel load on Sections 1 and Section 2 are illustrated in Figure 3.30. It is important to note that both saturated conditions and excessive loading, even in the dry state, resulted in an increase in the deflection and a decrease in the RC. With normal trafficking, however, it is believed that this structure will not reach the very flexible state under dry conditions.

---

* Pressurized water (1 to 2 m) was introduced into the sublayers of the structureon both sides of the test section, for half the length of the test section.

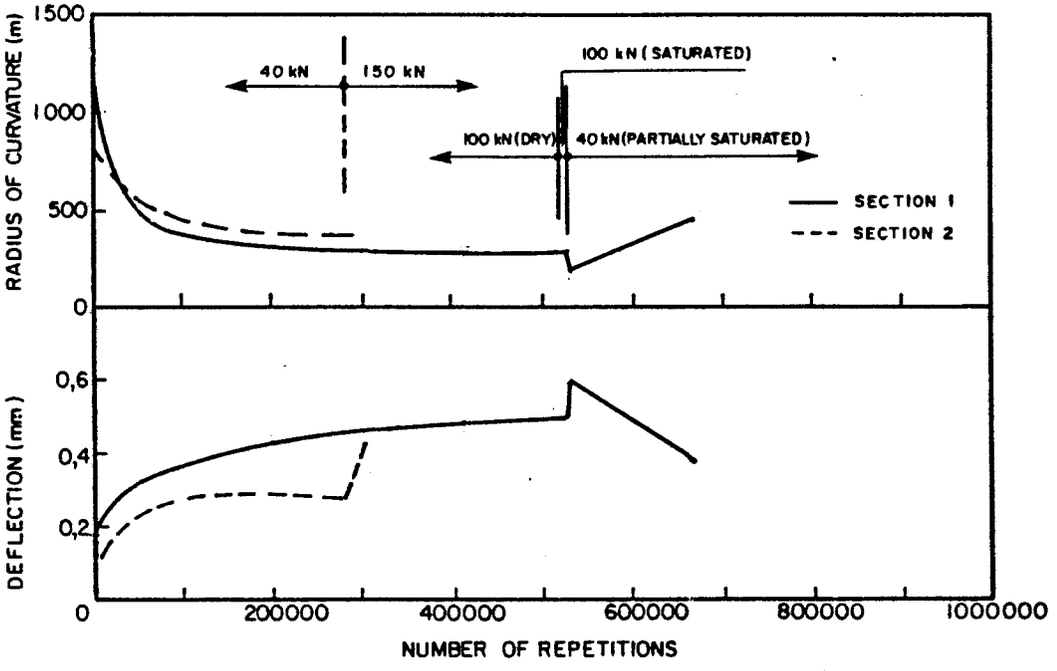

FIGURE 3.30

AVERAGE RSD DEFLECTION AND RADIUS OF CURVATURE (RC) UNDER A 40 kN DUAL-WHEEL LOAD ON SECTIONS 1 & 2

It is, however, important to seal any cracks on the surface, including the settlement cracks found on this route, to prevent water ingress and rapid carbonation of the weakly cemented layers.

3.3.5 Resilient depth deflections

The average MDD depth deflections at various stages of trafficking on Sections 1 and 2 are illustrated in Figure 3.31. The figure indicates that at the end of the dry state more than 60 per cent of the surface deflection originated in the selected layer downwards on both test sections. Less than 10 per cent originated in the asphalt layers. The remaining 30 per cent of the deflections originated in the weakly cemented subbase layers. However, the deflections were small. In the saturated state the contributions to the surface deflection changed from 60 to 50 per cent in the selected layers downwards, 10 to 15 per cent in the asphalt layers, and 30 to 35 per cent in the stabilized subbase layers. These results were similar than those found at Mariannhill.

3.3.6 Summary and conclusions of HVS test at Figtree, N2/24

From the HVS results of tests on Section 1 an average permanent deformation of 20 mm in the asphalt is not expected within the design life of this pavement; however, 10 mm is expected after approximately 20 ME80s (± 25 years after the opening of the road). It is important to note that after 10 years the weakly cemented subbase layers will be cracked and possibly fractured.

The HVS, however, proved that fatigue cracking will not occur in the asphalt layer during the design life of this road structure if the subbases remain dry. Early fatigue cracking will be experienced in both the weakly cemented subbase layers, especially the upper layer. However, this will not result in immediate functional failure of the

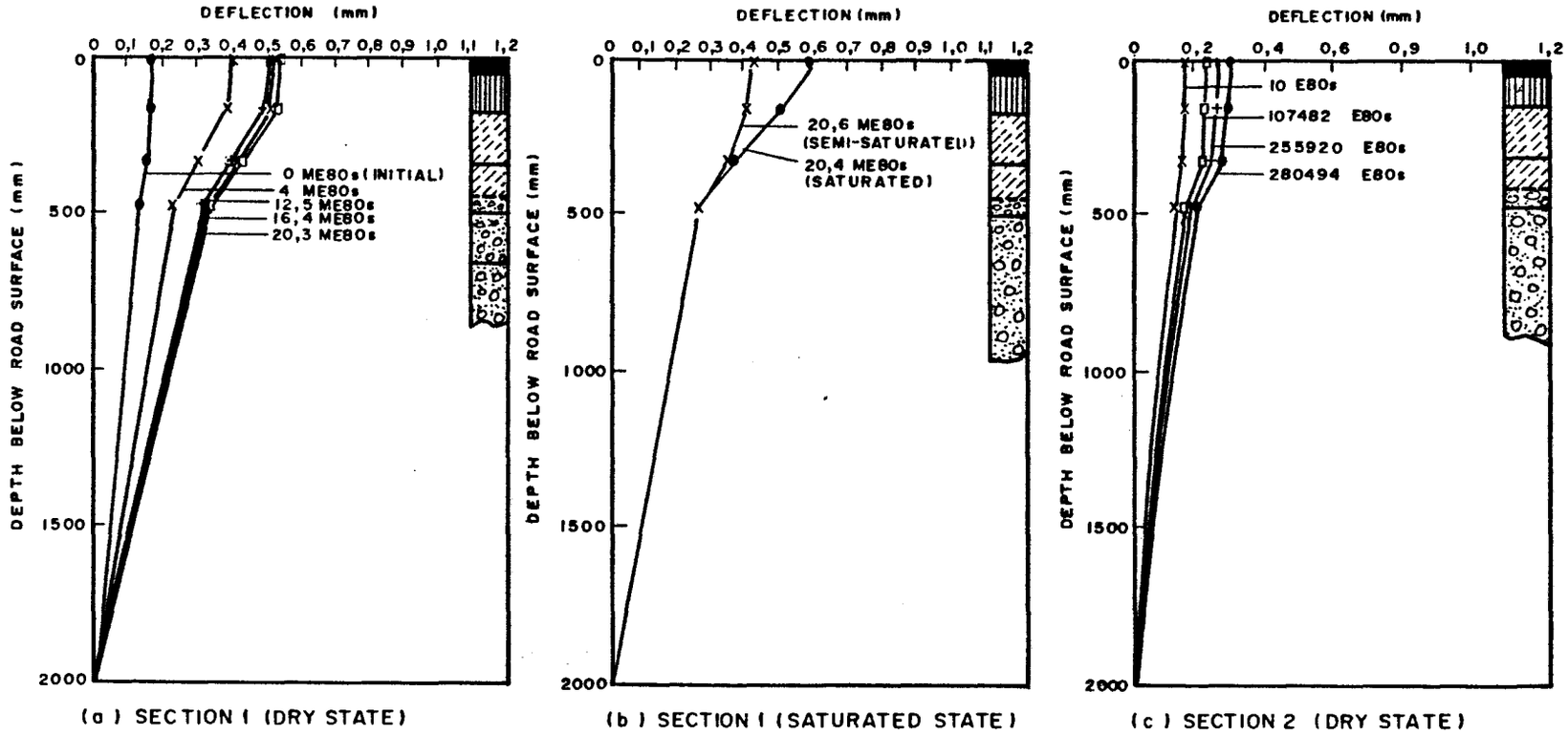

FIGURE 3.31

AVERAGE MDD DEPTH DEFLECTIONS AT VARIOUS STAGES OF TRAFFICKING ON SECTIONS 1 & 2

structure (relatively short precracked phase, mainly because of the longitudinal crack).

From the limited HVS test results it appears that the weakly cemented (uncarbonated) weathered granite material used in this structure behaves relatively better than the weathered granite used at the previous site (Mariannhill), although the effective elastic moduli values for the stabilized subbases were relatively low. The effective elastic moduli values of the upper subbase varied between 10 000 MPa and 70 MPa and for the lower subbase between 114 MPa and 30 MPa, respectively. It is believed that the reason for the very low moduli values is the existance of the settlement crack in the cemented layers (De Beer, 1984(b)). The weakly cemented granite at Mariannhill appeared to be more sensitive to water (EPWP) than the granite material at this site. It is important to note that the road structure at Mariannhill consisted of well stabilized subbase layers and excellent construction without thick and soft interlayers, carbonation or settlement cracks. There were virtually no differences in ultimate behaviour during the dry states of testing on these two sites. It is believed that the weakly cemented weathered granite material at this site (Figtree), built according to the design (no interlayers, carbonation and/or settlement cracking), will be able to carry the design traffic over the design period (20 to 30 ME80s over 20 years). Lime or cement may be injected into the settlement cracks to retard the carbonation and to decrease the water sensitivity of the subbase material in the vicinity of such cracks. The cracks must also be sealed to prevent water and air from penetrating into the road structure.

More care should be taken in constructing cemented layers to avoid uncemented soft and wet interlayers, since these cause a dramatic reduction in the fatigue life of the stabilized and asphalt layers of this design. Quality control should include the carbonation test proposed by Netterberg, 1984. On fill foundations cementitious and asphalt layers should be built only after most of the primary consolidation and

settlement have taken place to avoid detrimental cracking in the main structural layers of these road structures, including weakly cemented subbase layers.

It can be concluded that the existance of the vertical crack and the soft zone influenced the measurement of the relative deflections and hence the calculation of the effective elastic modulus of the weakly cemented subbase layers. This leads to very short fatigue lives of the asphalt layers. The origin of the rutting occurred within the soft zone in the vicinity of the crack and not from the weakly cemented subbase layers, (see Figure 3.32), therefore this type of weakness within these structures must be minimized.

3.4 SUMMARY OF HVS TESTS AND RESULTS AT UMGABABA, N2/24

At this site the two weakly cemented subbases consisted of lime treated Berea Red sand material. The objective of these tests was also to study the behaviour of the subbase layers again with and without the introduction of water into the structure. Detailed evaluation of the test results at this HVS test site is also given elsewhere (De Beer, 1985(a)).

3.4.1 Road structure

The design of the road structure was the same as that of the structure at Mariannhill (Figure 3.1), except that the asphalt base layer was 90 mm thick. The structure was tested without the asphalt surfacing layer. The weakly cemented subbases were constructed of fine grained weakly cemented (lime treated) Berea Red Sand material. Two sections were tested at this HVS site, each in the dry and saturated states.

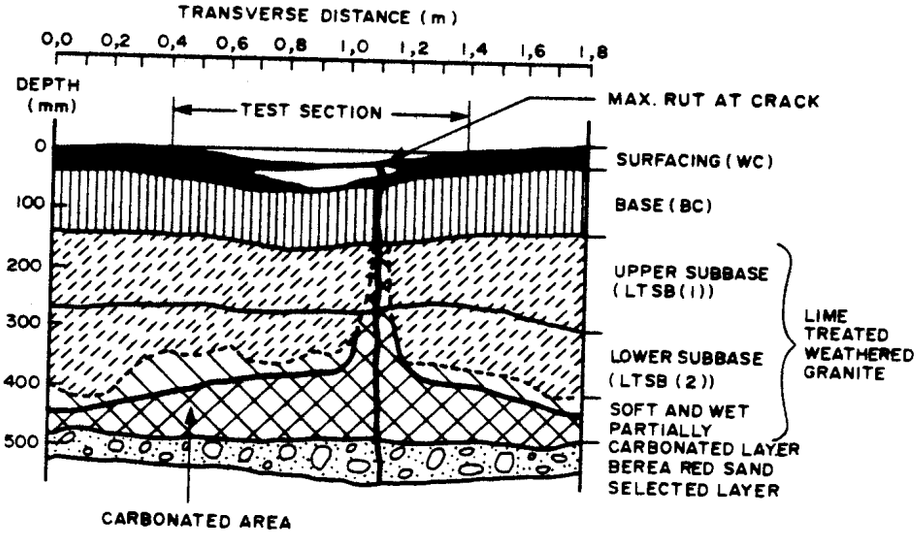

FIGURE 3.32

FINAL TRANSVERSE PROFILE OF SECTION I WHERE SURFACE AND SUBSURFACE WATER WERE INTRODUCED

3.4.2 HVS test programme

The traffic loading and moisture conditions differ for each test and are summarized in Table 3.19. No trafficking was done on the control section, but deflection measurements were taken to supplement the main tests, although measurements were more limited.

Water was introduced into both the test sections towards the end of the tests. The method used was the same as the method used on the previous two sites.

TABLE 3.19 - Test Programme of the tests on Sections 1 and 2 at Umgababa

Section	Traffic loading (kN)	Asphalt temperature (°C)	Actual repetitions	Moisture* conditions
1	80	17 - 25	201 617	Dry
	100	20 - 27	318 383	Dry
	100	20 - 27	2 067	Excess pore-water pressure
	40	20 - 27	45 419	Excess pore-water pressure
2	40	17 - 30	263 000	Dry
	40	17 - 30	106 674	Excess pore-water pressure

*The moisture conditions refers mainly to the moisture condition of the two weakly cemented subbases, especially the interface between the asphalt and upper subbase.

Because the test sections are situated on a relatively steep slope, the total length of the subsurface of both sections was influenced by the excess porewater pressure (EPWP) during HVS trafficking.

3.4.3 Permanent deformation

Figures 3.33(a) and (b) give the average deformation (rut) of the road surface at various stages of trafficking on Sections 1 and 2, respectively. Pressurized water (1 to 2 m) was introduced after approximately 15,6 ME80s on Section 1 and 263 000 E80s on Section 2.

Hardly any rut development occurred in the dry state on either test section. In the state of excess porewater pressure, especially in the interface between the asphalt base and the top of the upper weakly cemented subbase, moisture-accelerated distress (MAD) was initiated. The rate of change in deformation appeared to be linear and varied between 300 and 500 mm per ME80. Typical HVS longitudinal fatigue cracking appeared on the surface of the asphalt layer on the sides of both sections during the MAD phase. Fine subbase material was pumped from the weakly cemented subbase through these cracks and at some MDD holes. Hardly any other fatigue cracks were evident on the surface of the asphalt base layer of either section after the tests.

3.4.4 Road surface deflection (RSD) and radii of curvature (RC)

Figures 3.34(a) and (b) give the RSD responses for the tested sections together with the associated RC. On both test sections a gradual increase in deflection occurred in the dry state. At the start of the excess porewater pressure state, there were mean surface deflections of 0,35 mm and RC of approximately 400 m on both test sections. Neither figure indicates any drastic change in the above-mentioned parameters during the excess porewater pressure state. On Section 1 the deflection increased to 0,40 mm only. Both sections appeared to be in the stiff state after the introduction of excess of porewater pressure. The relatively poor correlation between the surface deflection measurements and subsequent HVS results shows that deflection and RC cannot, in this case, be used as a strong indicator of performance during excess porewater pressure states in this structure.

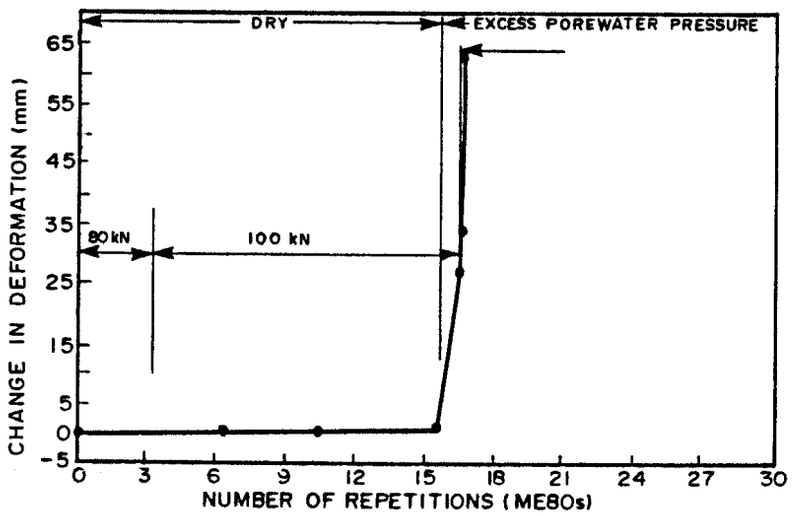

(a) SECTION 1

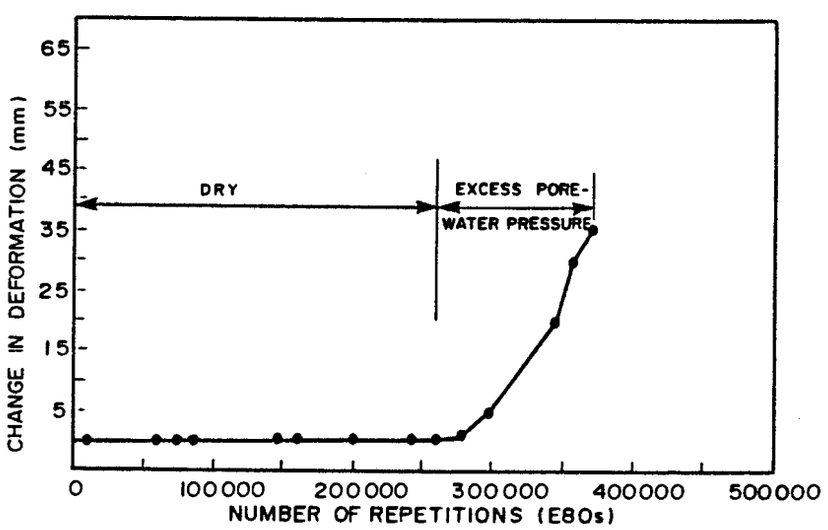

(b) SECTION 2

FIGURE 3.33

AVERAGE DEFORMATION (RUT) OF THE ROAD SURFACE AT VARIOUS STAGES OF TRAFFICKING ON THE TWO SECTIONS

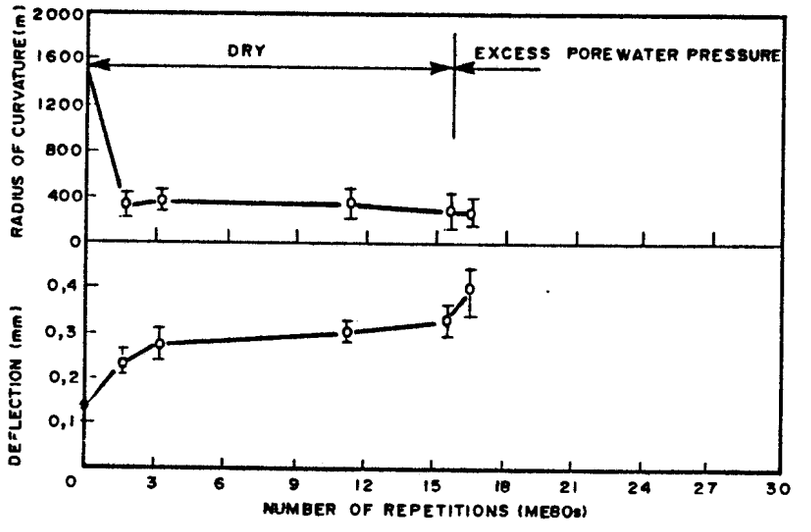

(a) SECTION 1

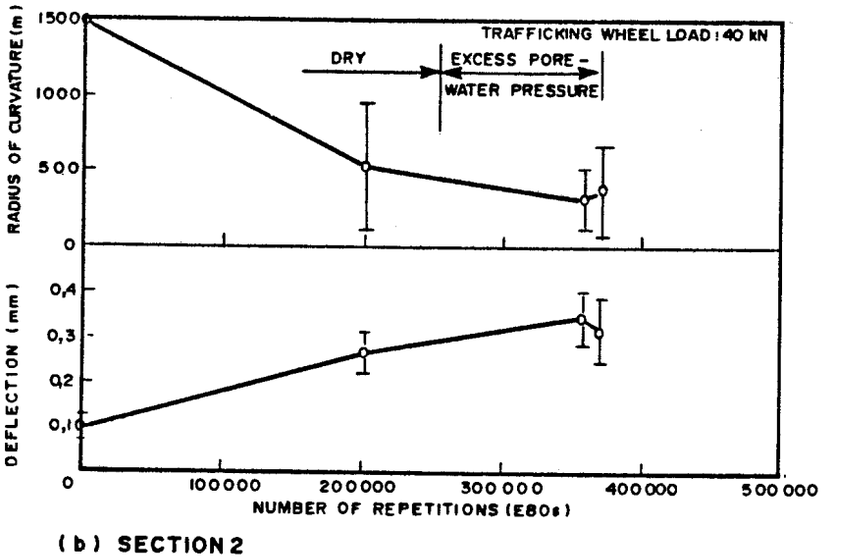

(b) SECTION 2

FIGURE 3.34

AVERAGE RSD AND RC UNDER A 40 kN DUAL-WHEEL LOAD ON THE TWO SECTIONS

3.4.5 Resilient depth deflections

Figures 3.35(a) and (b) give the average MDD depth deflection under a 40 kN dualwheel load at various stages of trafficking on the two sections. The figure indicates a well balanced pavement structure in terms of depth deflection, even in the MAD state. The stiffness of every layer tends to decrease with trafficking (MDD depths represent layer interfaces). The major part of the surface deflection is attributable to the selected layer downwards (405 mm and below), which contributes some 75 per cent of the total surface deflection. In the case of Mariannhill and Figtree the percentages were approximately 50 to 80 and 65, respectively.

3.4.6 Visual observations and discussions

Visual changes on both test sections were almost the same in the dry and excessive porewater pressure states. In the dry state hardly any change was noted on either of the sections. A rapid change in permanent deformation with minor surface fatigue cracking was evident on both sections in the excess porewater pressure state.

Figure 3.36 shows a profile of Section 2, taken after completion of testing, at the position of maximum rut. The major part of the permanent deformation inside the test section was due to the loss of weakly cemented upper subbase layer material. The material was pumped towards the sides of the test section between the bottom of the asphalt and the top of the weakly cemented subbase layer. The failure mechanism was clearly indicated by the horizontally displaced material (pumped layer). The same mechanism of failure was evident in another seven similar profiles inspected on the two sections after HVS testing. The displacement of the top of the upper layer was attributable to this layer's lack of resistance to erosion in the excess

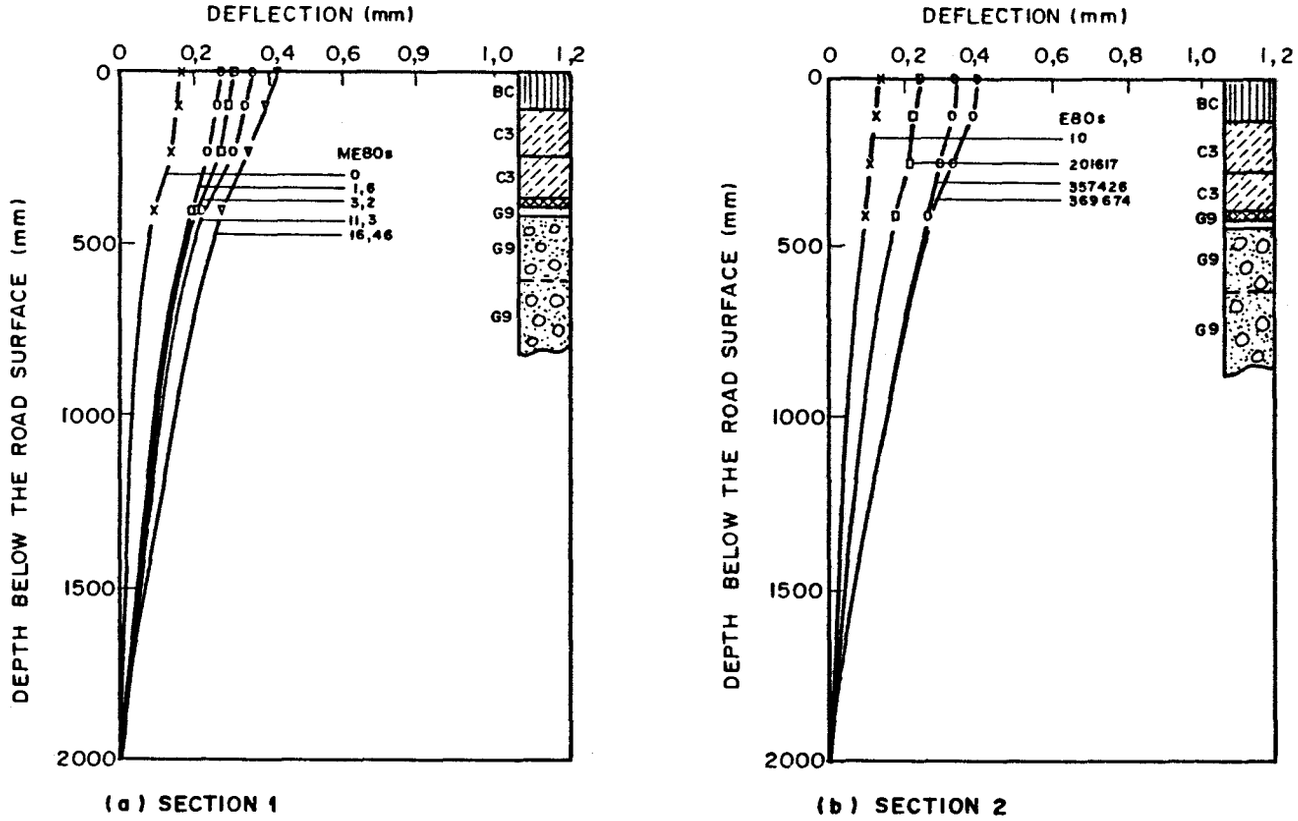

FIGURE 3.35

AVERAGE MDD DEPTH DEFLECTION UNDER A 40 kN DUAL-WHEEL LOAD AT VARIOUS STAGES OF TRAFFICKING ON THE TWO SECTIONS

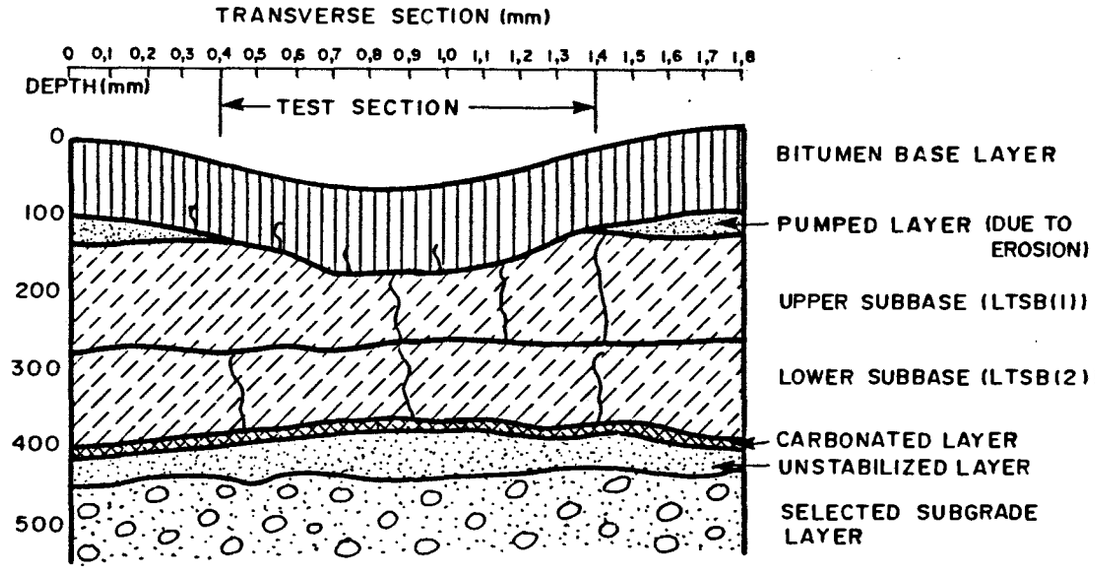

FIGURE 3.36

PROFILE OF HVS TEST SECTION 2 TAKEN AT POINT II AT UMGABABA

porewater pressure state. It is worthwhile to note that the pumped material as well as the top of the subbase were uncarbonated before and during the testing.

It is proposed that a durability test should be developed to quantify the erodibility of cementitious material. Work in this regard has already been started at the NITRR. (De Beer, 1985(c))

Because of the different failure mechanisms encountered on this HVS site, the limitations in the current mechanistic design method are realised because durability criteria for weakly cemented materials are not considered at this stage.

3.5 SUMMARY OF HVS TESTS AND RESULTS AT VAN REENEN'S PASS, N3/6

It was decided to include in this thesis the test results of this HVS site because very important behavioural characteristics were found. In this case the design was the same as for the previous three sites, i.e. asphalt base of approximately 100 mm thick, asphalt surfacing 40 mm thick on top of two weakly cemented subbase layers, of 150 mm thick each. The subbases consists of blended river gravel and sandstone, treated with 1,5 per cent lime and 1,5 per cent slag. Because this was a rehabilitation project the sandstone of the old road was re-used together with new river gravel material. The old asphalt was also re-used (recycled) with a ratio of 70 per cent virgin to 30 per cent new conventionally continuously graded asphalt. The recycled (hot processed) asphalt was layed separately in two layers of 65 mm and 45 mm, respectively. Detailed analyses and evaluation of this HVS test site is given elsewhere (De Beer, 1985(b)).

Inspection test pits prior to HVS testing revealed that the weakly cemented upper subbase was not in a cemented state but rather in a granular state. In another test pit the upper 50 to 75 mm of the upper subbase was relatively strongly cemented. In both test pits, however, the lower subbase was

also relatively strongly cemented and probably of C3/C2 quality.

The main objective of the HVS testing at this site was to evaluate the structural behaviour of the recycled asphalt base and secondly to predict the future behaviour of the rehabilitated pavement. Because of the type of design (i.e. weakly cemented subbases) the behavioural characteristics in view of this thesis is of utmost importance because relatively early fatigue distress and excessive rutting of the asphalt layers occurred after HVS trafficking. This distress was shown to be directly a function of the support from the upper subbase both in the dry and in the excess porewater pressure (EPWP) state. In the dry state relatively early fatigue distress occurred. When water was introduced (EPWP state) after the cracking occurred, excessive rapid change in permanent deformation (rutting) and pumping occurred.

The construction of the rehabilitated pavement was completed during 1981/82 and HVS testing was done from January 1983 to July 1983.

The overall evaluation included Lacroix deflection and Dynamic Cone Penetrometer (DCP) surveys in the slow lanes (both directions) of this route. The three HVS test sections were selected on the basis of these results. One section was representative of the weaker 10 to 15 per cent of the structure.* The other two sections represented the remaining 85 to 90 per cent. The total length of the rehabilitation project was approximately 24 km of which 17,5 km included recycled asphalt in the base. The other 6,5 km included conventional asphalt in the base layer. The substructure was virtually the same for both parts of the route.

---

* Based on the length of the route with relatively high deflections and high DCP values.

3.5.1 Section 1

Section 1 was representative of the weaker 10 to 15 per cent of the route.

The pavement structure of this section is shown in Figure 3.37(a). A test pit dug near Section 1 before the HVS testing and trenches excavated across the test section after the HVS test confirmed that the upper subbase was not weakly cemented and rather in a granular (poor) state. The granular state was first suspected after DCP measurements of over 5 mm per blow in this layer. The lower subbase was relativele stronger cemented and remained in a solid state after the HVS testing, without major cracking or granulation.

The section was trafficked with a 70 kN dualwheel load and fatigue cracks appeared on the surface after about 58 800 repetitions. After 60 000 repetitions a well defined crocodile crack pattern was established. After 280 000 repetitions the surface was extensively cracked, and at this stage the temperature of the asphalt layer was increased, by means of heaters, from an average ambient level of 25 °C to 45 - 50 °C.

At this temperature permanent deformation occurred mainly the semi-gapgraded asphalt surfacing. The rate of increase in deformation, however, was not critical when compared with that in other similar tests done in Natal (Freeme et al, 1982). The measured permanent deformation versus the number of 70 kN load repetitions is shown in Figure 3.37(b)

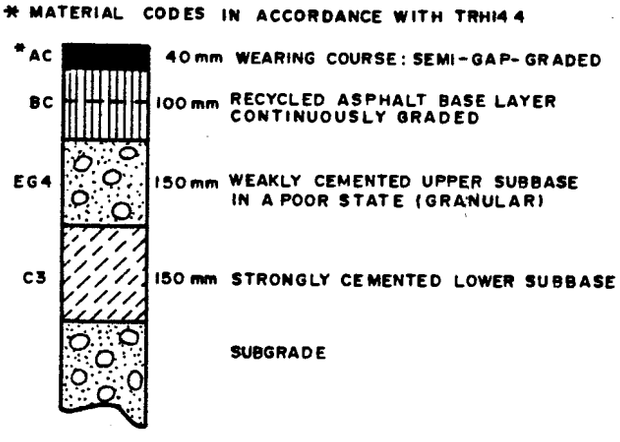

(a) PAVEMENT STRUCTURE: WEAKER 10-15% OF ROUTE (HVS TEST 1)

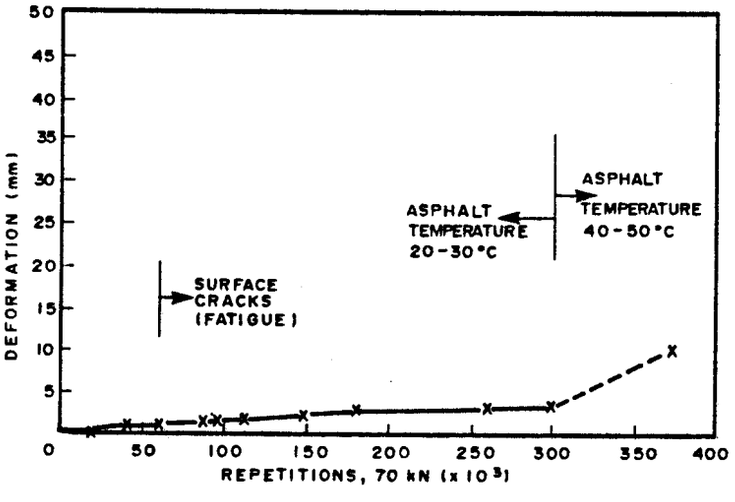

(b) PAVEMENT DEFORMATION MEASURED ON SECTION 1

FIGURE 3.37

PAVEMENT STRUCTURE REPRESENTATIVE OF THE WEAKER 10—15% OF THE ROUTE TOGETHER WITH THE PERMANENT DEFORMATION AND CRACKING BEHAVIOUR RESULTING FROM THE HVS TEST UNDER DRY CONDITIONS

The HVS test results from Section 1 and a mechanistic evaluation indicated that fatigue cracks would appear on the weaker 10 to 15 per cent of the route within the following two to three years. No excessive permanent deformation is expected if the structure remains dry. The elevated temperature test showed that high temperatures in the asphalt under heavy traffic loading would not be critical with regard to permanent deformation of the asphalt surface and base layers.

3.5.2 Section 2

Sections 2 and and 3 were representative of 85 to 90 per cent of the route.

The fatigue cracking behaviour of the asphalt layer of Sections 2 and 3 was studied further at normal ambient temperatures. Water was also introduced to study the reaction of the pavement structure to excess porewater pressure (EPWP) in the subbase of Section 2.

A test pit dug between Sections 2 and 3 before the HVS testing and trenches excavated across Section 2 after the HVS test showed that the upper subbase was in a better condition than that on Section 1. The pavement structure at Sections 2 and 3 is shown in Figure 3.38(a). The upper 50 to 75 mm of the upper subbase was strongly cemented (C2). The rest of the layer was weakly cemented and in a granulated (poor) state, as was found on Section 1.

On Section 2 a 70 kN dualwheel load was used for the first 100 000 repetitions, after which the load was increased to 100 kN for the remainder of the test. Fatigue cracks appeared on the surface after a total of 301 000 repetitions. (See Figure 3.38(b)).

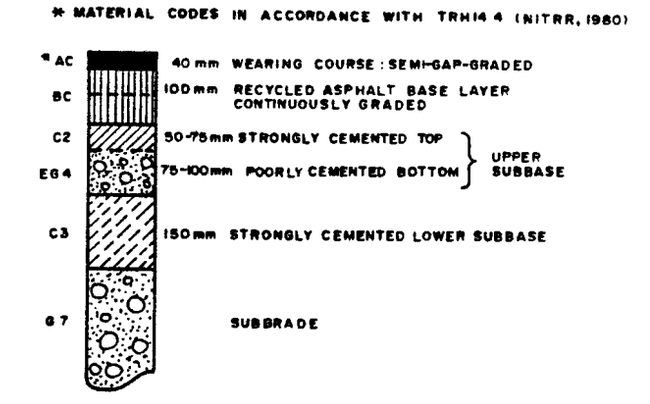

(a) PAVEMENT STRUCTURE : REMAINING 85-90% OF ROUTE (HVS TEST 2 AND 3)

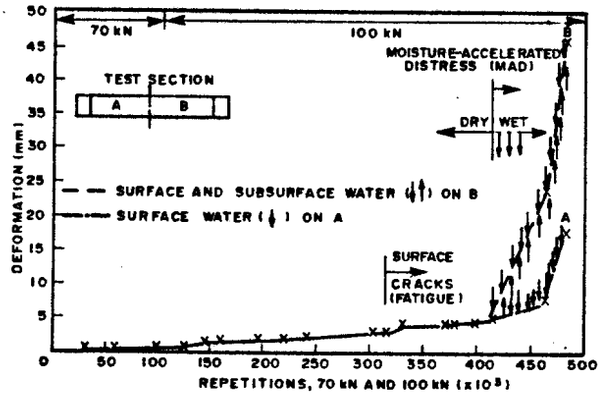

(b) PERMANENT DEFORMATION MEASURED ON SECTION 2

FIGURE 3.38

PAVEMENT STRUCTURE REPRESENTATIVE OF 85-90% OF THE ROUTE TOGETHER WITH THE PERMANENT DEFORMATION AND CRACKING BEHAVIOUR RESULTING FROM THE HVS TEST UNDER DRY AND WET CONDITIONS

Section 3 was first trafficked with a 40 kN dualwheel load for 800 000 repetitions and then with a 100 kN load for the remainder of the test. After 200 000 repetitions of the 100 kN load, fatigue cracks were visible on the surface.

The fatigue response of the pavement structure at Sections 2 and 3 was better than that found at Section 1. The HVS tests showed that fatigue cracks should not be experienced on the rest of the route (which is equivalent to Sections 2 and 3) within the next ten years or so with normal traffic (E80 growth rate of 10 per cent). Mechanistic analysis was used to predict a fatigue-crackfree period of 10 to 15 years. (See Section 3.5.5 later).

The influence of the ingress of water into the subbase layers, after the occurrence of fatigue cracks in the asphalt base and surfacing layers, was also studied. Water was sprayed on the cracked Section 2 and then subsurface water was introduced into the subbase layers. The introduction of water into the pavement structure initiated moisture-accelerated distress (MAD) (see Figure 3.38(b)), which demonstrates the necessity of preventing the ingress of water into this pavement. The excessive permanent deformation that followed was mainly due to loss of fine material, through pumping (EPWP), from the upper subbase layer.

The permanent deformation and cracking on Section 3, were similar to those experienced on Section 2 in the dry state. No water was introduced into this section.

With the ingress of water under normal traffic loading the results on Section 2 showed that the terminal level of permanent deformation (20 mm) would probably occur within four years, and within two to three years if the subdrainage was poor. Sealing of the asphalt surface with a proven waterproof seal as soon as the cracking appears was strongly advised. Local maintenance to improve the subdrainage was also advised in areas with poor subdrainage.

3.5.2.1 Observation of fatigue distress of the asphalt layers

Section 2 was initially trafficked with a 70 kN, dualwheel load as was done on Section 1. Because of the relatively better (strongly cemented) upper 50 to 75 mm of the upper subbase, no crack pattern was established after 100 000 repetitions in the dry state. It was then decided to increase the wheel load to 100 kN. A similar fatigue crack pattern as on Section 1 was established after 216 000 repetitions with the 100 kN wheel load. The permanent deformation at that stage was approximately 3 mm. See previous Figure 3.38. During this stage of trafficking the fatigue crack length was measured regularly to establish a crack growth curve for this pavement structure. The crack length (CL) is defined as the total length of cracks on the surface of the test section, in metres. The crack growth is illustrated in Figure 3.39.

The figure illustrated the crack length (CL) versus number of actual repetitions. After approximately 316 000 total repetitions, 50 m of cracks were measured. A marked increase in crack length (125 m) occurred in a very short period of trafficking ($\pm$3 000 repetitions), after which the rate of increase in crack length decreased. A final length of approximately 200 m of crack was measured on the test section. It can be concluded from this information that rapid fatigue crack growth from the bottom of the recycled asphalt base layer to the surface will occur.

As previously mentioned water was continuously sprayed on the surface of the cracked section using a spray bar, in order to simulate normal rain conditions on this pavement. Virtually no rapid rut development occurred for at least 100 000 repetitions (100 kN) in this state, alghouth slight pumping was observed. After a total of 416 000 actual repetitions, pressurized subsurface water was introduced, using a set of inlet pipes both side of the

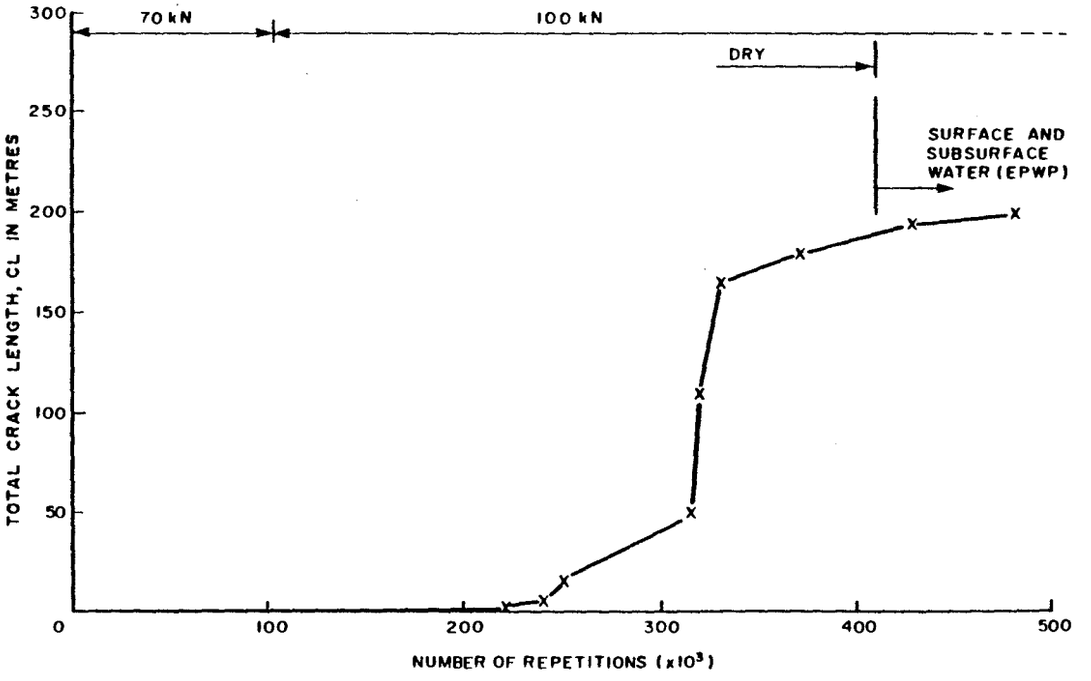

FIGURE 3.39

FATIGUE CRACK GROWTH ON THE ASPHALT SURFACE OF TEST SECTION 2 AT VARIOUS STAGES OF TRAFFICKING WITH INDICATED DUAL WHEEL LOADS

test section. This was done only at one half of the length of the test section (See part B, Figure 3.38).

Excessive pumping started at 416 000 actual repetitions over the total section with increasing effect on where subsurface water was also introduced. The test was ended with an average rut depth of 45 mm on part B and 15 mm on part A. (See previous Figure 3.38)

The final crack pattern observed on the section is illustrated in Figure 3.40. Part A experienced a crack pattern consisting of relatively large blocks. The average diameter of the blocks was approximately 150 mm which was also the total thickness of the asphalt layers. This block size was called the A-blocks. On this part of the section only surface water was applied during trafficking. The average rut depth at the end of the test was approximately 15 mm on this part of the section. The maximum rut depth however was 65 mm at point 6. At point 2 a local rut of 40 mm was measured. See Figure 3.40.

On part B of the section, two block sizes were mainly observed. On two local areas, points 8 to 11 and points 13 to 16 on the left of the section (facing the section from point zero), the A-block size (average diameter approximately 150 mm) was observed. The rest of the section experienced smaller blocks with average diameter of approximately 90 mm. This was called the B-blocks. Maximum rut depths were established on two of the A-block areas, viz: 90 mm and 70 mm at points 9 and 14, respectively. Where the smaller blocks were formed the average rut depth was less than 40 mm. A local maximum rut of 55 mm, however, was measured at point 9.

Inspection test pits after testing revealed that the fatigue cracks were through to the bottom of the asphalt base layer in the areas consisting of A-block sizes. In the area (part B) receiving subsurface water excessive

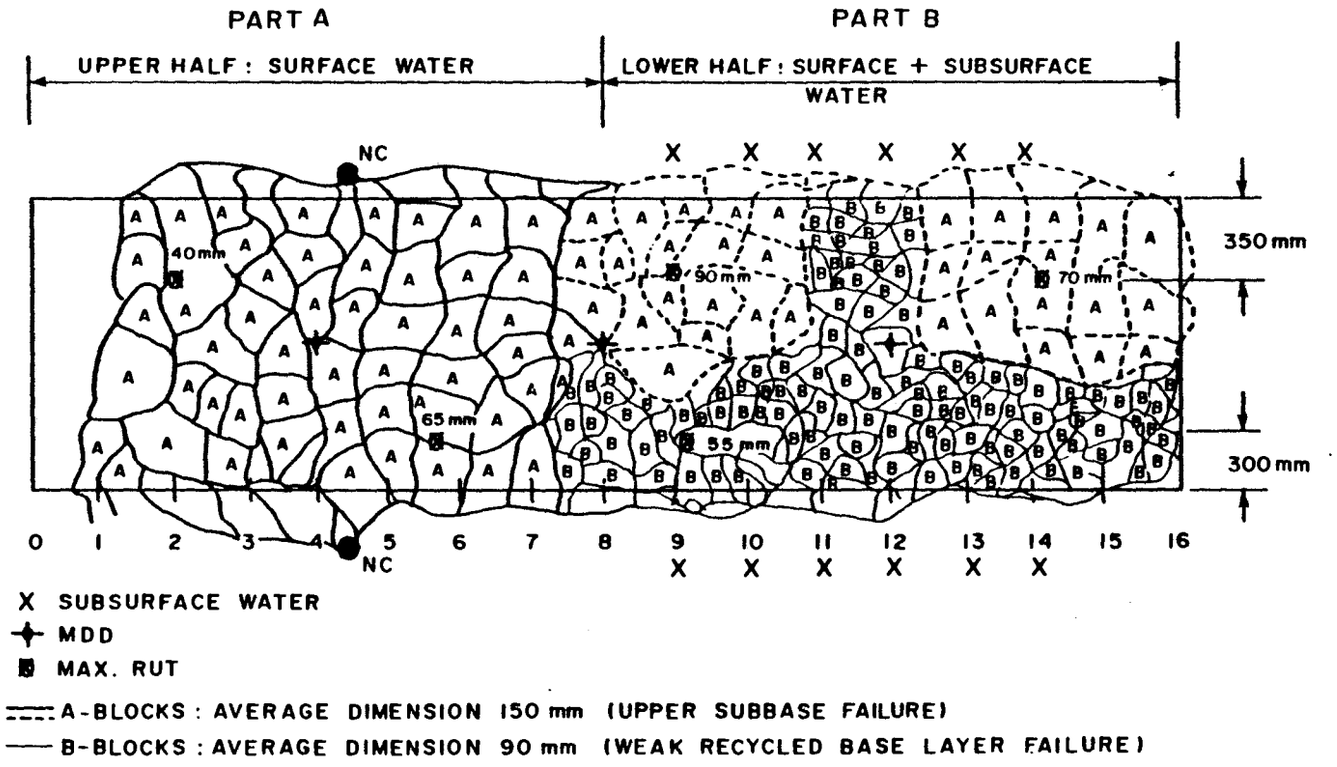

FIGURE 3.40

FINAL CRACK AND RUT PATTERN OBSERVED ON SECTION 2 AFTER WATER APPLICATION AND HVS TRAFFICKING

pumping occurred vertically through these cracks from the granulated upper subbase layer, hence the large permanent deformations of 70 mm to 90 mm. In the areas consisting of the B-blocks, the fatigue cracks were not through the lower 50 to 75 mm of the recycled asphalt base layer, but extended only approximately 90 mm from the surface to within the recycled base layer. As a result virtually no pumping from the upper subbase occurred in this area. It is further interesting to note that the upper subbase at this position was in a relatively strongly cemented state. It is believed that the influence of the stronger upper subbase support in this case was such that weaknesses within the recycled asphalt base layer were accentuated, hence the smaller blocks and fracturing of the asphalt. This distress occurred a depth approximately equal to the average diameter of the blocks (90 mm) on the surface. It is further interesting to note that it appears that the average diameter of the blocks on the surface, owing mainly to fatigue, approaches the depth of the weaker layer. In this case two "weak layers" were identified, viz: the upper subbase (granulated) under the A-blocks, and secondly a weak sone within the asphalt base layer where the B-blocks were observed. In each case the "weak layer" was situated at a depth equal to the average block size on the surface. If the block diameter approaches the layer thickness, "rocking" of the block occurs, without further fatigue distress because the blocks are simply too small to bend. This block size was called the "optimum block size", which is actually the smallest diameter which could occur owing to fatigue distress. A cross section of Section 2, illustrating above mentioned failure mechanisms, is illustrated in Figure 3.41. The figure is self explanatory.

Because the relatively poor state (granular) of the upper subbase at this site was known prior to HVS testing, it was decided to make a test pit through all the layers in the structure, approximately 800 mm away from the one end

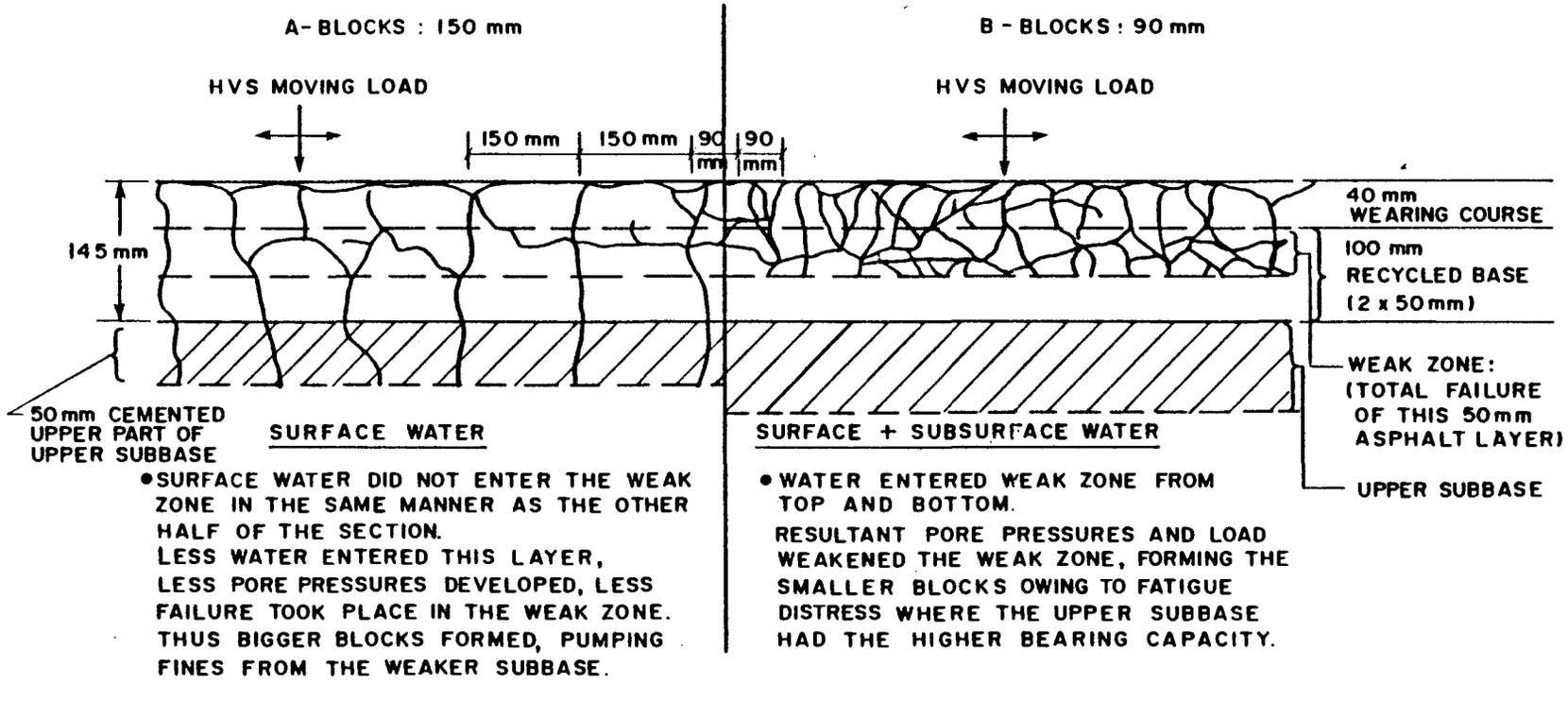

FIGURE 3.41

THE TWO FAILURE MECHANISMS EXPERIENCED ON HVS TEST SECTION 2

of Section 2. See Figure 3.42. This was done in order to study horisontal pumping resulting during the excess porewater pressure (EPWP) state in Section 2. A substantial amount of fine upper subbase material was horizontally pumped and was observed in this test pit during the test. Fine subbase material was flowing out of the weak zone within the recycled asphalt base layer as well as from the upper subbase. This observation is indicative of the enormous pressures which develop during traffic loading in the road structure when free water is allowed to be within relatively poor layers.

3.5.3 Road surface deflection (RSD) and radii of curvature (RC)

The road surface deflection (RSD) and radius of curvature (RC) at various stages of trafficking measured on Section 1 are illustrated in Figure 3.43(a). The average initial RSD was 0,48 mm and increased to approximately 0,61 mm at the time of the appearance of fatigue distress on the surface of the asphalt (after approximately 60 000 repetitions, 70 kN dualwheel load). The final RSD was approximately 0,80 mm after 370 000 actual 70 kN repetitions, which is 3,5 x 10^6 E80s if a damage exponent d=4 is used. A relatively low initial RC of 110 m was calculated from the RSD measurements. The final RC was approximately 80 m. These relatively low RC values (and high RSD) are indicative of the relatively weak initial state of this pavement structure at Section 1. According to the previous Tables 3.11 and 3.12 this structure varies from flexible (F) to marginal very flexible (VF) in the dry state. The effect of high temperature in the asphalt layers with respect to RSD and RC is negligible.

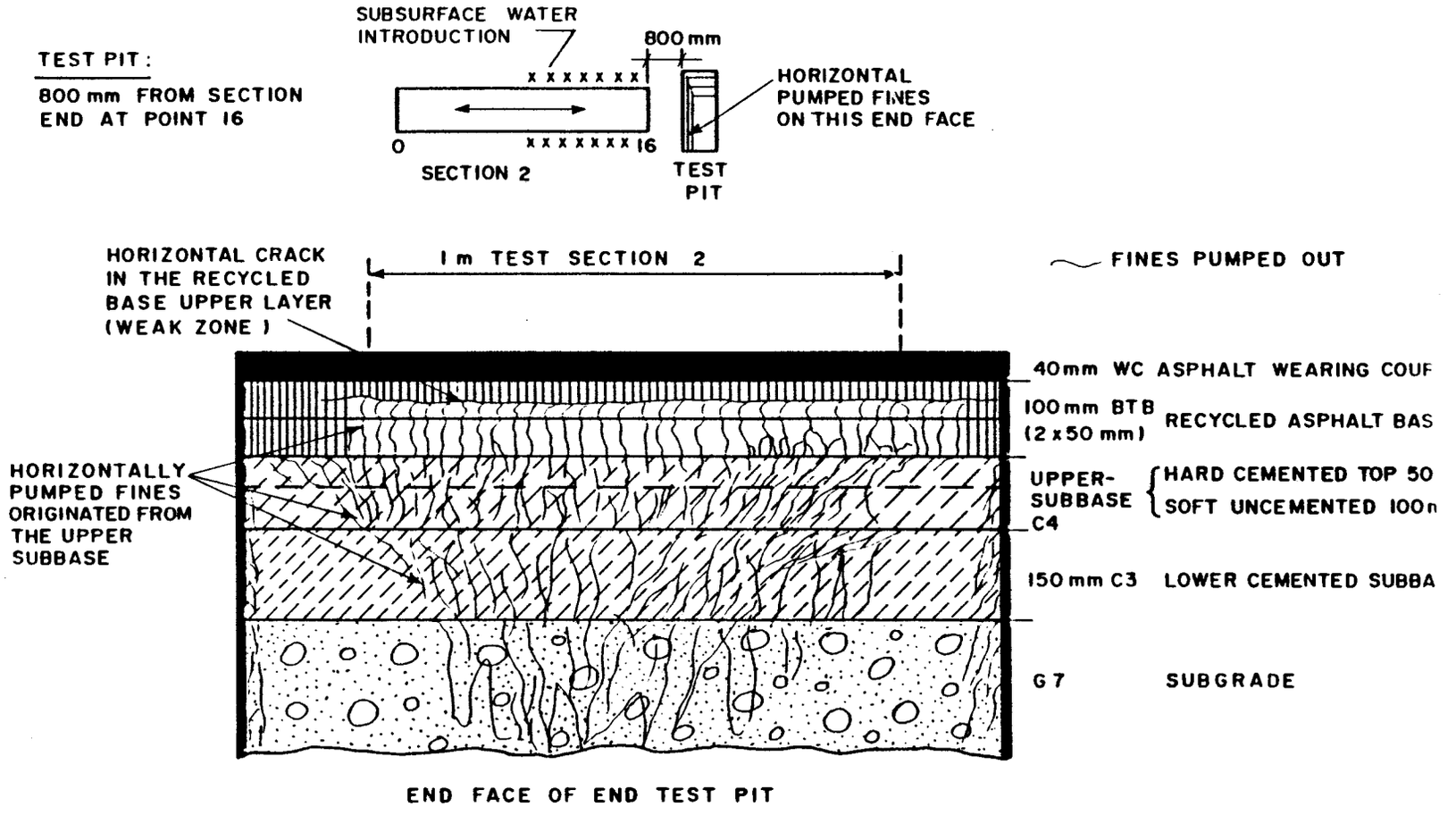

FIGURE 3.42

HORIZONTAL PUMPING OBSERVED IN THE TEST PIT, 800 mm AWAY FROM SECTION 2

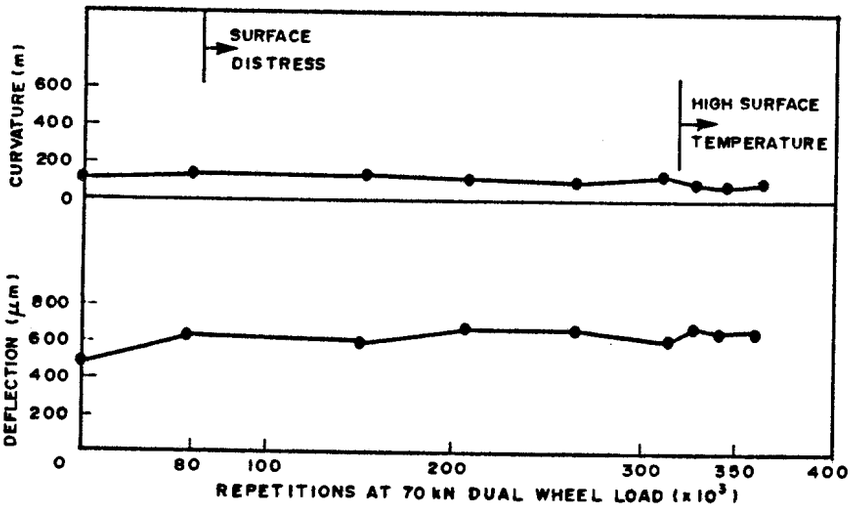

(a) SECTION 1

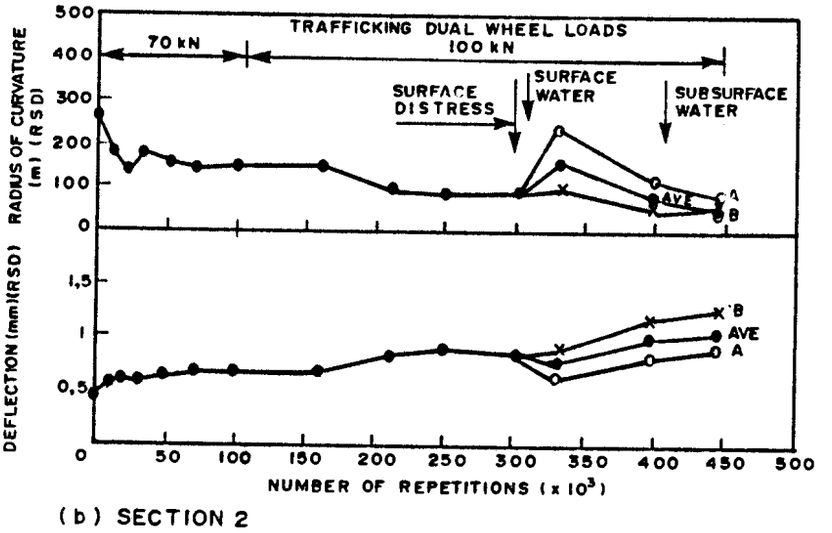

(b) SECTION 2

FIGURE 3.43

AVERAGE ROAD SURFACE DEFLECTION AND RADIUS OF CURVATURE UNDER A 40 kN DUAL WHEEL LOAD ON SECTION 1 AND SECTION 2

The average RSD and RC under a 40 kN dualwheel load on Section 2 are illustrated in Figure 3.43(b). The initial RSD and RC were 0,44 mm and 230 m, respectively. These values were both better than those measured on Section 1, although it is also relatively low compared with the previous structures at Mariannhill, Figtree and Umgababa. The RSD increased to approximately 0,80 mm and the RC decreased to almost 80 m when fatigue cracks appeared on the surface of the section. This "end state" compares favourable with those found on Section 1. During the application of water, the effect was not rapid changes in these indicators, (RSD and RC) mainly because of the originally poor state of the structure. Part B of the section (surface and subsurface water) experienced the highest RSD (approximately 1,25 mm) and the lowest RC (approximately 50 m) at the end of the test. This section changed also from flexible (F) to very flexible (VF). The slight decrease in RSD and increase in RC at the end of the test on part A of the section is believed to be partly due to difficulty in measurements (irregular surfaces) and interlocking* of the asphalt blocks (150 mm) during trafficking. It was noted during the trafficking that less rocking of the individual blocks occurred during repetitions 300 000 to 400 000. The netto effect however on the total section (part A and part B) was that the rocking of the blocks increased to the end of testing.

3.5.4 Resilient depth deflections

The average MDD depth deflections under a 40 kN dualwheel load at various stages of trafficking on Section 1 are illustrated in Figure 3.44(a). The figure indicates relatively high depth deflections, which was also reflected in the relatively high RSD values. According to this result, approximately 50 per cent of the RSD resulted from the

---

* Similar to those found with interlocking block paving (Clifford, 1985).

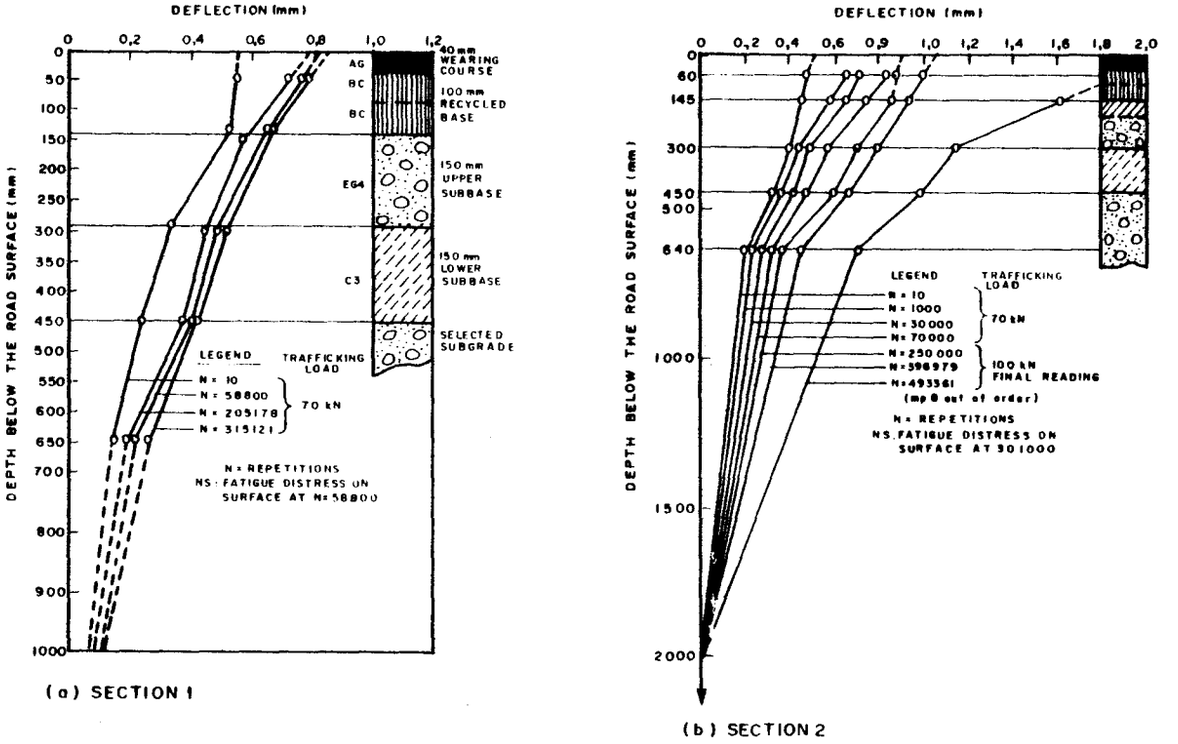

(a) SECTION 1

(b) SECTION 2

FIGURE 3.44

AVERAGE MULTI-DEPTH DEFLECTION UNDER A 40kN DUAL WHEEL LOAD AT VARIOUS STAGES OF TRAFFICKING ON SECTIONS 1 AND 2

selected subgrade layer, downwards. The other 50 per cent resulted from the surfacing, base and the two subbase layers. Relatively high deflections (0,15 mm to 0,20 mm) were measured in the upper subbase (145 mm to 300 mm) and the selected subgrade (450 mm to 640 mm). Only slight variations in deflection were measured with increase in traffic and it is believed that the initially poor state of the upper subbase contributes largely to these high deflections. A relatively small relative deflection (0,10 mm) was measured within the lower subbase layer, which was relatively strongly cemented.

The individual contributions to the RSD from the different layers are given in Table 3.20. The table indicates increases in contribution from the asphalt and selected subgrade layers, and decreases in the contributions of the two subbase layers. Not much difference were noted between the state at 58 800 repetitions, and the end of the test.

The results also indicates that initially 35 per cent of the RSD originated from within the upper subbase. This value decreased to 16 per cent during the first 58 800 repetitions. At the end of the test, only 14 per cent of the RSD originated from this layer owing to possible compaction under HVS traffic. The contribution from the selected subgrade layer increased from 45 per cent to 52 per cent and these of the asphalt layers from 3 to 22 per cent. This relatively high increase in relative deflection probably indicates a weakening of the recycled asphalt base layer during trafficking.

The average MDD for Section 2 under a dualwheel load of 40 kN at different depths below the road surface for various stages of trafficking is illustrated in Figures 3.44(b).

TABLE 3.20 - Layer contributions to the RSD on Section 1

Layer	Beginning of test	At 58 800 reps. (Fatigue distress)	End of test
Surface and base course	3%	22%	25%
Upper subbase	35%	16%	14%
Lower subbase	17%	10%	9%
Selected subgrade	45%	52%	52%

The figure also indicates that marked increases in the deflections of all the layers during the first 70 000 repetitions of the 70 kN wheelload occured. The RSD measurements along the centre line of the section indicate that the RSD increased from point 4 to point 12 on this section throughout the test. See Figure 3.45. This was mainly caused by the higher subgrade deflections experienced at measuring point 12. There was however no clear indication that fatigue distress started earlier at the vicinity of point 12 than on the rest of the section. This could be an indication that the fatigue crack development in this case is rather a function of the upper subbase support than the subgrade support. The low RC also indicated that inadequate support resulted from the upper subbase.

In Figures 3.46(a) and (b) the initial and final MDD deflections on part A (MDD4) and part B (MDD12) are illustrated, respectively. Both figures indicates further weakening of the upper subbase. A relatively marked increase in the deflections of all the layers at MDD12 (surface and subsurface water) was experienced. It is believed that there are mainly two reasons for the higher deflections measured with MDD12. Firstly the initial deflections at MDD12 were

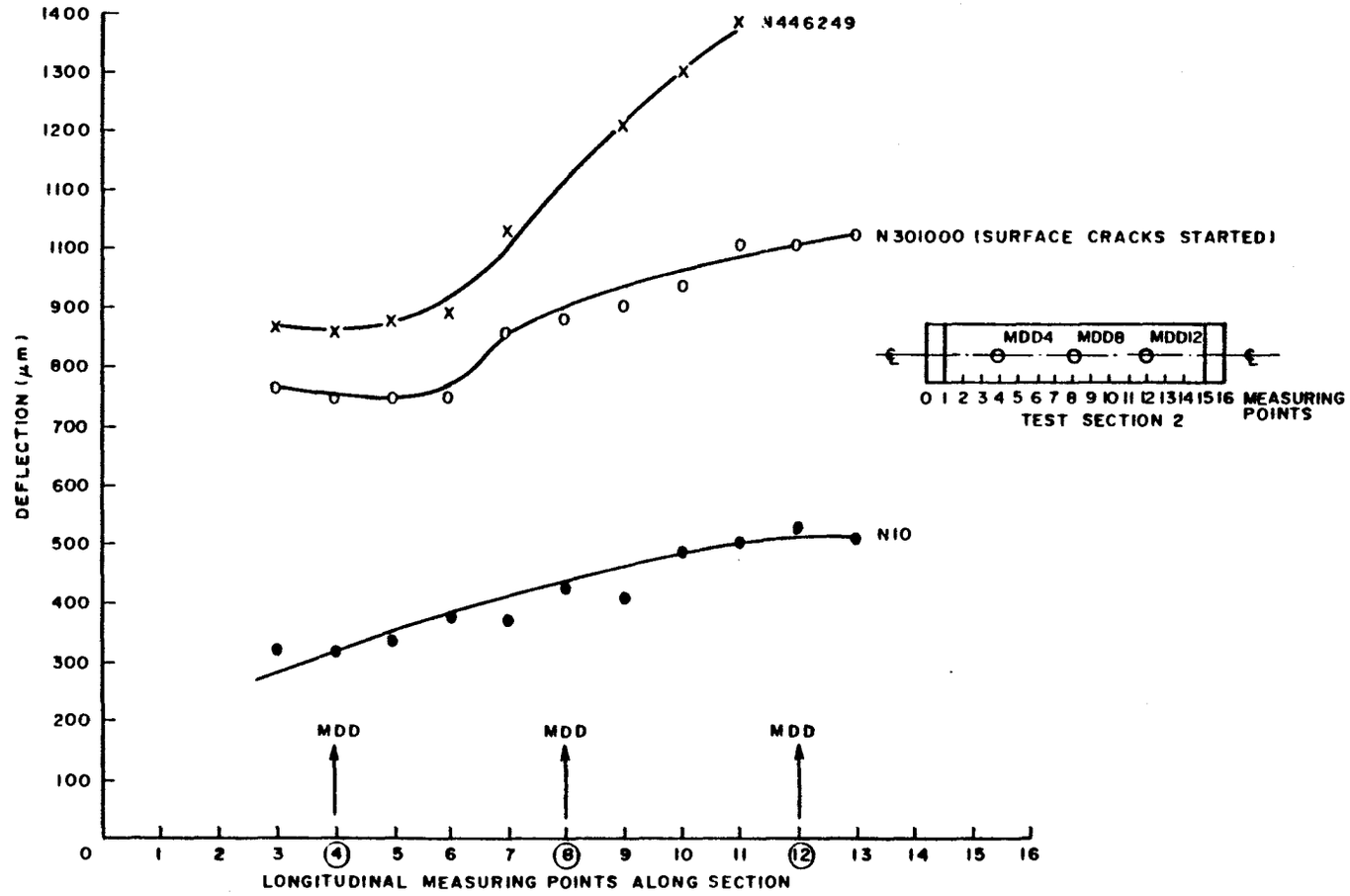

FIGURE 3.45

ROAD SURFACE DEFLECTIONS UNDER A 40kN DUAL WHEEL LOAD ON THE CENTRE LINE DURING VARIOUS STAGES OF TRAFFICKING ON SECTION 2

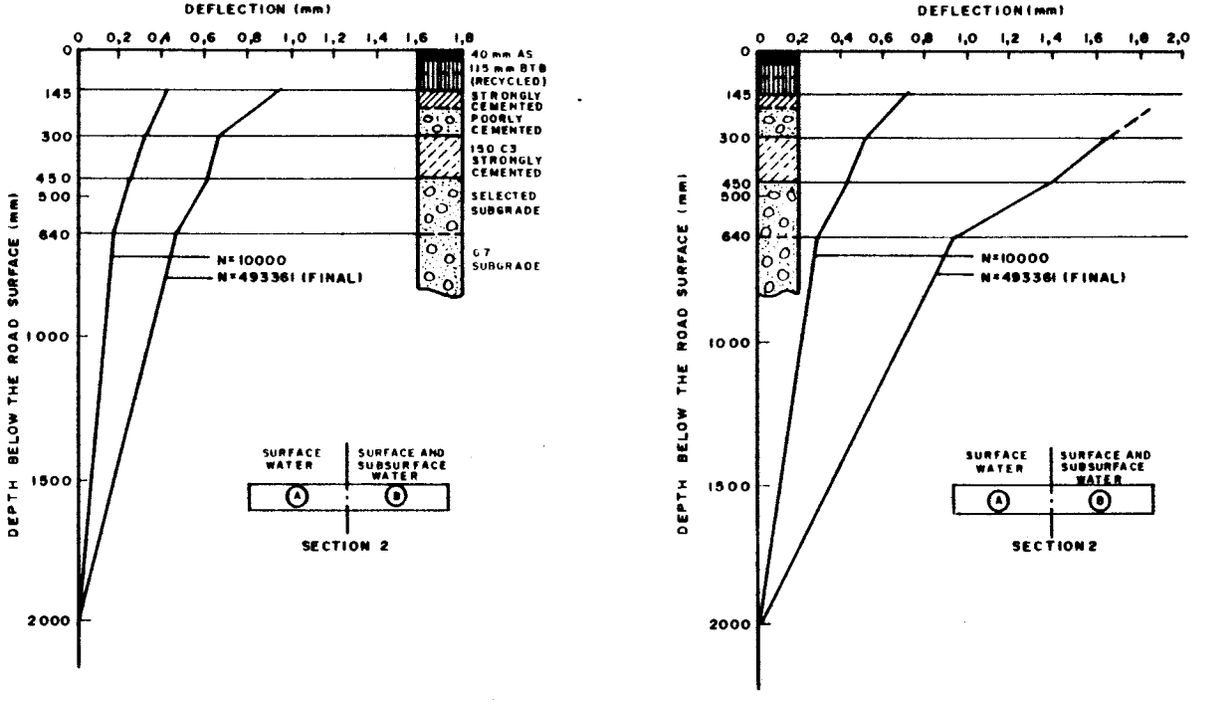

(a) MDD4 (b) MDD12

FIGURE 3.46

INITIAL AND FINAL MULTI-DEPTH DEFLECTIONS UNDER A 40 kN DUALWHEEL LOAD AT MDD4 (PART A) AND MDD12 (PART B)

higher from the start of the test. Secondly, it is believed that the subsurface water played a major role in decreasing strength of especially the granular upper subbase, therefore more support was needed from the lower layers, resulting in higher subgrade and hence total deflections.

3.5.5 Mechanistic analyses

As was done with the MDD deflection results at the previous three sites, mechanistic analyses were also done on the results at this HVS site. In addition vertical stress analyses indicated that the highest stresses occurred within the recycled asphalt base layer and increase markedly with increase in wheel load (De Beer, 1985(b)). This observation is believed to be indicative of the severe stress conditions that the asphalt experienced during trafficking on this structure (weak upper subbase support). Both fatigue distresses (bigger and smaller blocks - see Section 3.5.2.1) in the asphalt are believed to be directly a result of this condition. It is however appreciated that the linear elastic model is based on a few important assumptions such as homogeneity; isotropy etc., nevertheless this rather simple modelling can be used to indicate very important behavioural characteristics.

3.5.5.1 Effective elastic moduli

The different effective elastic moduli values for the three test sections are given in Tables 3.21, 3.22 and 3.23. The moduli values were calculated at 40 kN wheel-load at 520 kPa tyre pressure. The modulus of the asphalt wearing course in this case was kept constant at 3 000 MPa during the analyses. This was done because no relative deflections were measured in this layer. The results in the tables indicates very low moduli values for both weakly cemented subbase layers. On Section 1 (Table 3.21) the modulus values ranging from 32 MPa to 55 MPa. On Section 2 (Table 3.22) the values ranging from 46 MPa to

TABLE 3.21 - Effective elastic moduli for the different pavement layers for various stages of trafficking at 40 kN dual wheel load on Section 1

Number of repetitions With a dual wheel Load of 70 kN (N)	Wearing course* (MPa)	Base (MPa)	Upper subbase (MPa)	Lower subbase (MPa)	Selected layer (MPa)	Subgrade (MPa)
Average values for points 4, 8 and 12:						
10	3 000	1 563	38	55	72	182
58 800	3 000	1 206	35	51	27	123
261 009	3 000	1 228	32	51	27	139
333 847	3 000	684	55	54	29	145

* Modulus (stiffness) of wearing course was kept constant during analysis of all three sections.

TABLE 3.22 - Effective elastic moduli for the different pavement layers at various stages of trafficking at 40 kN dual wheelload on Section 2

Number of repetitions (N) (70 and 100 kN)	Wearing Course (MPa)	Base (MPa)	Upper Subbase (MPa)	Lower Subbase (MPa)	Selected Layer (MPa)	Subgrade (MPa)
Average values for points 4, 8 and 12:						
10	3 000	1 490	89	115	55	133
10 000	3 000	1 236	75	95	36	106
100 000	3 000	1 019	58	92	26	74
211 460	3 000	847	48	68	19	60
301 488	3 000	787	46	73	17	52
396 979 (EPWP)	3 000	572	120	66	15	44
446 249:						
for points 4	3 000	876	44	123	39	51
8 (EPWP)	3 000	18	59	71	25	85
12	3 000	679	24	43	12	44

TABLE 3.23 - Effective elastic moduli at 40 kN dual wheelload for the different layers at various stages of trafficking on Section 3

Number of Repetitions (N)	Wearing Course (MPa)	Base (MPa)	Upper Subbase (MPa)	Lower Subbase (MPa)	Selected Layer (MPa)	Subgrade (MPa)
10 000	3 000	1 245	152	238	41	122
216 023	3 000	1 235	135	198	35	111
713 114	3 000	1 186	106	179	29	98
866 379	3 000	476	136	180	27	85
996 813	3 000	71	167	232	43	115

115 MPa and on Section 3 the values ranging from 106 MPa to 238 MPa. Comparing these moduli values to those of the previous three sites it is very low. The reason is believed to be the initial state of especially the upper subbase which was mainly granulated approximately equivalent to G4 (EG4) or lower quality material. The granulated state of this layer was confirmed also after HVS testing when inspection test puts were made. The moduli values of the upper subbase at Section 1 are the lowest of the three sections. This is believed to be due to the relatively strongly cemented 50 mm to 75 mm layer found in the structures of Sections 2 and 3.

In the case of the rather low moduli values of the lower subbase, which was also relatively strongly cemented, it is believed that the MDD levels during instrumentation were not exactly positioned at the layer interfaces because this is virtually impossible from a practical point of view. Because of the relatively weakness of the upper subbase (or selected layer) higher relative deflections were measured in the lower subbase hence the lower

moduli values. It is however believed that the moduli values of the upper subbase are indicative of its relatively weak and granulated state.

This weak upper subbase can therefore be viewed as a weak interlayer between the asphalt and the relatively strongly cemented lower subbase. The effect of interlayers in this type of pavement structure is however analysed in Chapter 5.

Using the modular ratios of the asphalt and upper subbase, which is an indication of balance* in the structure. If the modulur ratios of the initial moduli values of the base and upper subbase are calculated and compared with the sum of the horizontal tensile strains (ε_t)** at the bottom of the treated (asphalt and cemented) layers, a distinct difference in the results at Van Reenen's Pass and the other HVS tests at Mariannhill, Figtree and Umgababa is obtained. See Figure 3.47. The figure indicates that a very high modular ratio (E_1/E_2) of approximately 40 resulted in a relatively high Fdp. Simply this is indicative that the potential for fatigue distress in this structure (mainly the asphalt layers) is very high and that relatively early fatigue cracking is expected at the Van Reenen's Pass structure. In Chapter 5 it is shown that the thicker the interlayer and the weaker (wet and granulated vs cemented) the higher the Fdp.

---

* The higher this ratio the poorer the "balance", the higher the fatigue distress potential, Fdp.

** The scalar quantity of the sum of the maximum horizontal tensile strain at the bottom of the treated layers in the structure is called the "Fatigue distress potential", Fdp, of the structure under consideration (See Chapter 5, Section 5.2.1.2).

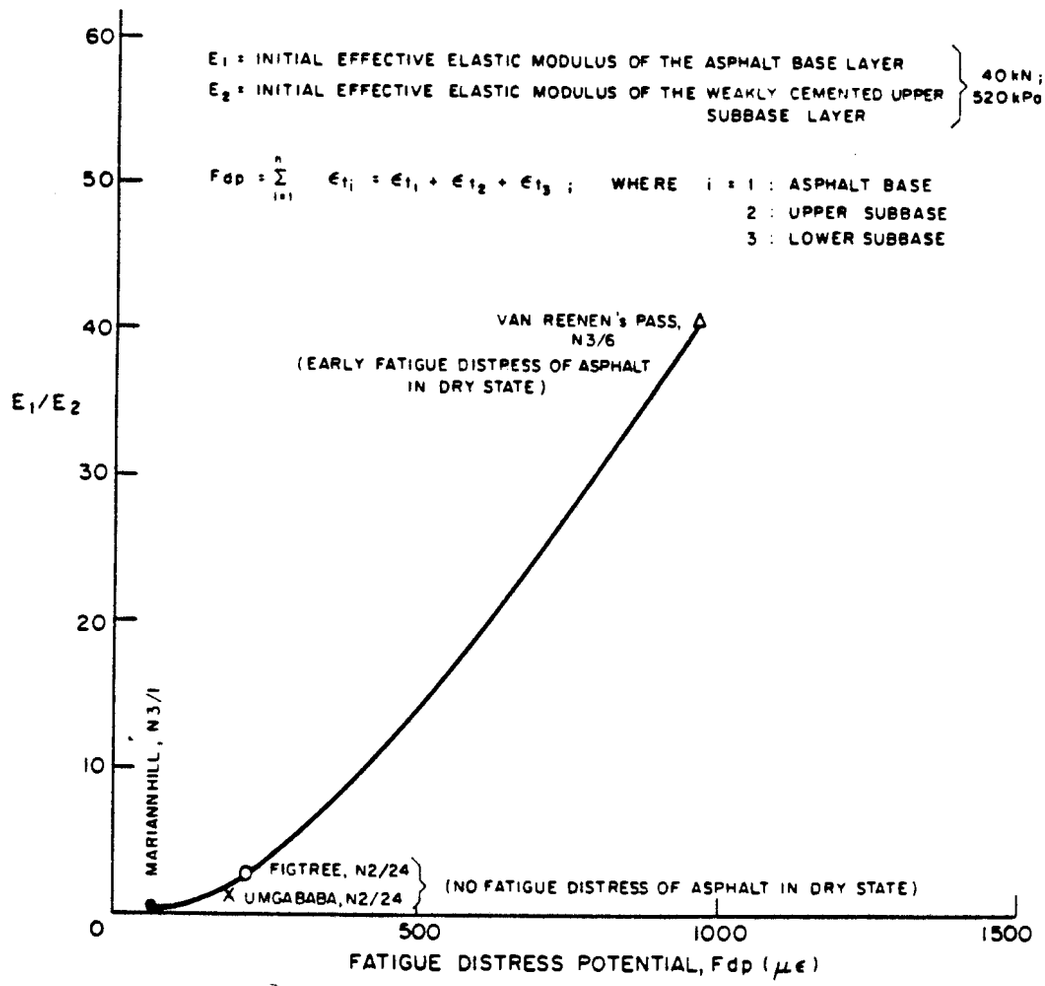

FIGURE 3.47

RELATIONSHIP OF THE INITIAL EFFECTIVE ELASTIC MODULAR RATIO (E_1/E_2) BETWEEN THE ASPHALT BASE AND WEAKLY CEMENTED UPPER SUBBASE LAYER AND THE FATIGUE DISTRESS POTENTIAL (Fdp) AT THE FOUR DIFFERENT H V S SITES.

TABLE 3.24 - Areas likely to have inadequate subbase support

*Locality (km) (Slow lanes)	Lacroix deflection (1982) (mm)	DCP measurements (mm/blow)	Likely condition
Northbound :			
28,5 - 29,5	> 0,4	-	Slope instability
33,7 (fill)	> 0,4	-	-
35,2	> 0,4	2,5 - 5	Weak subbase
36,2 - 36,4	> 0,4	2,5 - 5	Weak subbase
37,5	> 0,4	2,5 - 5	Weak upper subbase
43,5	> 0,4	1,0 - 2,5	Weak upper subbase
46	> 0,4	2,5 - 5	Weak upper subbase
Southbound :			
29,7	> 0,4	-	Slope instability
30,5	> 0,4	-	-
33 - 33,4	> 0,4	-	-
36	∿ 0,2	2,5 - 5	Weak upper subbase
39,4	∿ 0,2	2,5 - 5	Weak upper subbase
46,3	∿ 0,4	2,5 - 5	Weak lower subbase

* Located from start of contract at km 27,0 at the time of construction. Because of renumbering of this route, the kilometer distances changed (increased) by approximately 9,8 km.

3.5.5.2 Prediction of future expected fatigue distress

In order to evaluate the validity of the HVS findings on this site certain predictions for fatigue distress of the asphalt layers were made and was re-evaluated during March 1985. Because this was a rehabilitation project and not a pre-planned HVS experimental section, the HVS findings were used to predict the behaviour of the total road using also the DCP and Lacroix survey results.

Table 3.24 lists pavement areas likely to have inadequate subbase support according to the evaluation performed in 1983. Lacroix deflections and DCP measurements were used

to identify these areas. Deflection levels on these areas were mainly above the 0,4 mm given as a warning level in draft TRH12 (NITRR, 1983). As slope instabilities could well account for some of these high deflections, DCP measurements were used to determine the condition of the weakly cemented subbase layers. It was stressed that slope instability cracks should be sealed immediately after they had occur to prevent the ingress of water into the subbase layers and the failure planes of the unstable slopes.

After the HVS, deflection and DCP results had been analysed, certain conclusions and recommendations were made. A summary of these findings is given below:

The need for major rehabilitation within five years of testing is not foreseen provided timely sealing, local repairs and subdrainage improvements were undertaken.

The expected behaviour and likely need for future sealing is given in Table 3.25.

TABLE 3.25 - Expected behaviour of rehabilitated pavement (De Beer, 1985(b))

Percentage of road affected	Predicted appearance of fatigue cracks :	Sealing likely to be needed before :	If not sealed in time critical deformation (20 mm) is likely to occur owing to ingress of:	
			Surface water in	Surface and subsurface water in
10 - 15	1985-1986	∿ 1988	∿ 1990	∿ 1988
85 - 90	∿ 1993	∿ 1995	∿ 1997	∿ 1995

It is recommended that the pavement be inspected periodically, especially after rainy seasons, to identify the areas with inadequate drainage.

The behaviour of the asphalt layers subbase layers in this pavement structure is a function of the support from mainly the especially the upper subbase. Where the support is adequate, (cemented) the relatively rigid recycled asphalt layer is expected to be able to carry the predicted future traffic without the appearance of serious fatigue distress.

The investigation has shown that the asphalt produced with a 70/30 ratio of reclaimed bitumen to virgin material experienced early distress cracking when there was inadequate support. Total structural and functional failure occurred when water entered this weak layer.

Further in this paragraph a summary is given of the method of predicting when surface cracking (fatigue distress) may be expected on this route.

Two predictions were made regarding the time (in years) expected to elapse before fatigue distress and pumping occured, viz: for the weaker 10 to 15 per cent and for the remaining 85 to 90 per cent of the route.

This elastic simulation previously mentioned was used to calculate the effective horizontal strain values (micro-strain) at the bottom of the asphalt base layer. The expected fatigue life to cracking (visible at surface) on the three sections is given in Table 3.26. The initial effective elastic moduli of the asphalt base layer varied between 1 000 and 2 000 MPa. The effective elastic moduli of the upper subbase varied between 30 and 40 MPa on Section 1 and between 45 and 150 MPa on Sections 2 and 3. (See previous Tables 3.21; 3.22 and 3.23)

TABLE 3.26 - Expected fatigue life to cracking of asphalt base (De Beer, 1985(b))

Section	Dual wheel load (kN)	Strain* (με)	Effective elastic moduli of the asphalt base layer (MPa)	
			1 000	2 000
1	40	400	200 000	50 000
	70	690	20 000	6 000**
2 and 3	40	290	900 000	160 000
	70	520	72 500	16 000
	100	620	33 500	8 250**

* Effective horizontal microstrain

From the results in Table 3.26, fatigue crack damage exponents were determined. At this stage it was assumed that the well known power formula would also hold for fatigue damage to the asphalt. The relation between wheel load and damage is given below:

$$F = \left(\frac{P1}{P2}\right)^{d} \qquad \text{..... (3.4)}$$

where P1 = TEST wheel load (kN)
P2 = STANDARD wheel load, 40 kN (E80)
d = damage exponent.

In order to convert the fatigue lives from Table 3.26 to standard E80s the following method was used:

$$N_{P2} = N_{P1} \times F \qquad \text{..... (3.5)}$$

Thus $F = N_{P2}/N_{P1}$

$$\rightarrow \left(\frac{P1}{P2}\right)^{d} = N_{P2} / N_{P1} \qquad \text{..... from (3.4)}$$

$$\rightarrow d = \frac{\log (N_{P2}/N_{P1})}{\log (P1/P2)} \qquad \text{..... (3.6)}$$

where N_{P2} = Number of equivalent standard repetitions (E80s)

N_{P1} = Number of actual repetitions before cracking on the surface results from wheel load P1.

The different damage exponents calculated from the data in Table 3.26 are given in Table 3.27.

TABLE 3.27 - Damage exponents calculated from the fatigue data

Section	Load (kN)		Effective elastic moduli of base layer (MPa)	
	P1	P2	1 000	2 000
1	70	40	4,11	3,79
2 and 3	70	40	4,50	4,11
	100	40	3,59	3,24

The results in Table 3.27 indicates that there is a relatively small variation in the exponent value, d. Because the prediction would be for a number of full years, it was decided to use an average value, viz: 3,89, with a standard deviation of 0,45, for the damage exponent. The number of equivalent standard axles required to produce surface fatigue distress, calculated with the average value, is given in Table 3.28.

TABLE 3.28 - Number of equivalent standard axles required to produce fatigue cracking visible on the surface of the asphalt

Section	Traffic loading (kN)	Actual repetitions	Standard repetitions (E80s)
1	70	58 800	518 556
2	70	100 000	-
	100	201 000	$7{,}98 \times 10^6$
3	40	801 488	-
	100	195 000	$7{,}69 \times 10^6$

In order to calculate the number of years before cracking occurs (crack-free periods) the following equation was used (NITRR, 1985):

$$Ne = Ni \times fy \quad \ldots\ldots\ldots\ldots\ldots\ldots\ldots\ldots (3.7)$$

Where Ne = cumulative equivalent traffic (E80s)
Ni = initial traffic
fy = cumulative growth factor,

$$\text{where } fy = 365 \left[\frac{(1 + 0{,}01i)\left[(1 + 0{,}01i)^{Y} - 1\right]}{(0{,}01i)} \right] \quad \ldots (3.8)$$

With a compound growth rate of 10 per cent in E80s on this route the prediction (crack-free) period can be calculated. The initial traffic was obtained from traffic weight classifier (TAWC) data obtained in 1982. This data is given in Table 3.29.

TABLE 3.29 - Traffic count and number of E80s calculated for this route

Direction of lane	Axle weight group (tons)	Average daily count (axles)	Daily count E80s*
Southbond	0 - 2	3 708	1
	2 - 4	445	10
	4 - 6	519	83
	6 - 8	237	141
	8 - 10	95	150
	10 - 12	13	45
	12 - 14	0	0
		TOTAL	430
Northbound	0 - 2	3 886	1
	2 - 4	475	10
	4 - 6	716	115
	6 - 8	480	286
	8 - 10	106	168
	10 - 12	9	31
	12 - 14	0	0
		TOTAL	611

* $d = 3{,}89$ in $\left(\frac{P1}{P2}\right)^d$

The average initial daily E80s (Ni) is therefore 521 per lane for this route. To calculate the crack-free periods, equation (3.7) was used, viz:

(a) <u>For 10 to 15 per cent of this route: (HVS Test Section 1)</u>

Ne = 518 556 E80s (from Table 3.28)

Ni = 521 E80s per lane

i = 10 per cent

$\rightarrow fy = 365\ (1,1)\ \left|(1,1)^{y} - 1\right| / 0,1 = Ne/Ni$ From eq.(3.7)

$\rightarrow (1,1)^{Y} - 1 = \left(\frac{518\ 556}{521 \times 4\ 015}\right)$

$\rightarrow \quad y = \log(1,25)/\log(1,1)$

$\rightarrow \quad y = 2,3$ years.

In this case the crack-free period from the time of HVS testing is therefore two to three years.

(b) <u>For the remaining 85 to 90 per cent of the route (HVS Test Sections 2 and 3)</u>

(i) Section 2: $Ne = 7,98 \times 10^{6}$ ..... (from Table 3.28)

$Ni = 521$ ..... (average from Table 3.29)

with $i = 10$ per cent

$\rightarrow y = 16,5$ years

(ii) Section 3: $Ne = 7,69 \times 10^{6}$ ..... (from Table 3.28)

$\rightarrow y = 16,2$ years

For Sections 2 and 3 a conservative estimate (due to uncertainty about the long-term growth rate, i) is that the crack-free period will be longer than 10 years, probably between 10 and 15 years.

The expected behaviour of the rehabilitated pavement is summarized in previous Table 3.25.

3.5.5.3 Validation of predictions and discussions

This route was re-evaluated during March 1985. According to Table 3.25 the prediction was made that fatigue cracking would appear during 1985 on some 10 to 15 per cent of the length of the route under consideration. A visual inspection was undertaken to assess the validity of this prediction.

Before HVS testing a Lacroix deflection survey was done in the slow lanes of the route. Deflection was measured every 5 m. At the HVS site, however, a Benkelman beam deflection survey was done along the 100 m of test site, at 1 m intervals prior to HVS testing. The various deflection results are illustrated in Figure 3.48(a), (b) and (c). The position of the three test Sections are also indicated in the figure. The average deflection of the site was 0,54 mm. (See Figure 3.48(c)). The crack survey in March 1985 revealed that the cracked areas coincides with the high deflection areas were cracked and signs of pumping were present. The crack patterns were typical crocodile fatigue cracking, as experienced with the HVS in 1983.

The Lacroix deflection and DCP results were used to identify possible "weak" areas in the subbases of this route. As previously mentioned, Lacroix deflections were measured along the 24 km of route. Deflections were measured every 5 m and the 95th percentile of each 100 m was calculated. It is accepted that the Lacroix deflectograph tends to measure lower deflections than the Benkelman beam (Coetzee, 1985). In this case the Lacroix deflection should be increased by approximately 20 per cent, plus a constant of 0,13 mm to be added to the Lacroix deflections to match the deflection measured with Benkelman beam. The Lacroix deflections measured during 1982 are illustrated in Figures 3.48(a) and (b). The average deflection (Lacroix) of the HVS site is also

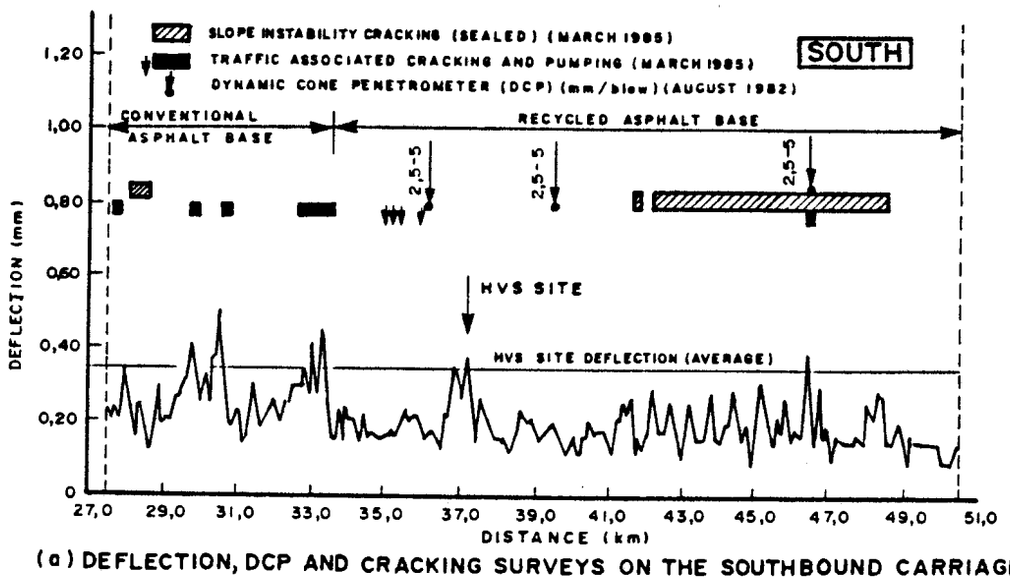

(a) DEFLECTION, DCP AND CRACKING SURVEYS ON THE SOUTHBOUND CARRIAGEWAY

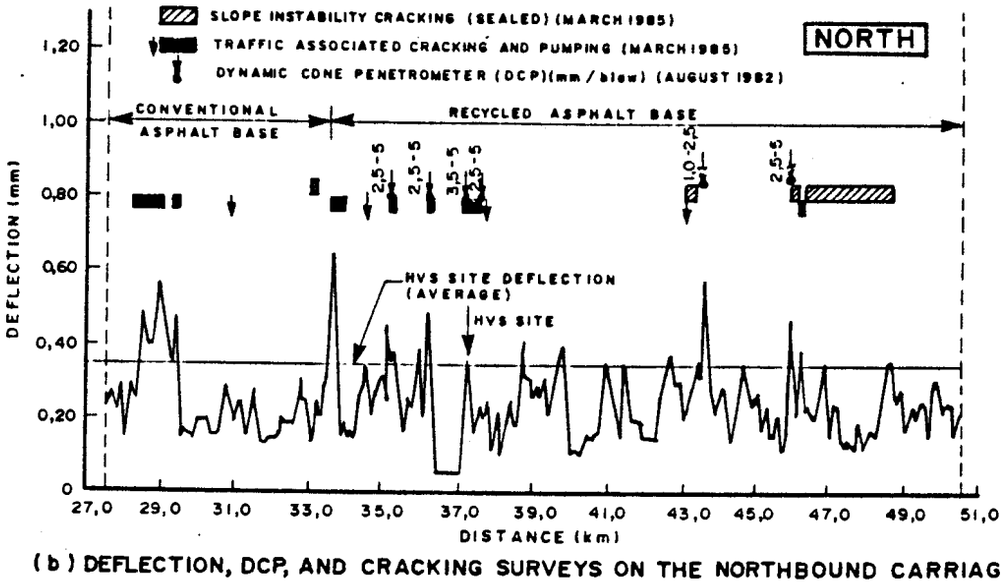

(b) DEFLECTION, DCP, AND CRACKING SURVEYS ON THE NORTHBOUND CARRIAGEWAY

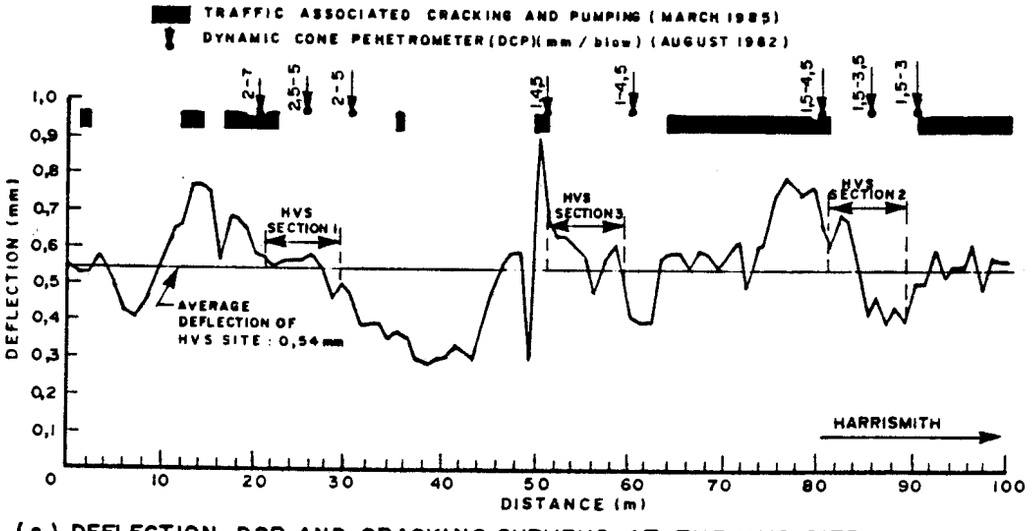

(c) DEFLECTION, DCP AND CRACKING SURVEYS AT THE HVS SITE (NORTHBOUND CARRIAGEWAY)

FIGURE 3.48

RESULTS OF THE DEFLECTION, DCP AND CRACKING SURVEYS DONE AT VAN REENEN'S PASS

illustrated in the figures, including the crack evaluation of March 1985.

As previously mentioned the evaluation includes the section of route (27 km to 33,5 km) which consisted of conventional asphalt base material. It is interesting to note that most of the locations where the Lacroix deflection exceeded a value of 0,35 mm (0,55 mm Benkelman beam), were subjected to traffic associated cracking. Most of those cracking were situated in the outer wheel path. According to the prediction in 1983, 10 to 15 per cent of this route should be subjected to this type of cracking during the period 1985 to 1986.

See previous Table 3.25. The re-evaluation indicated that almost 12 per cent of the length of this route already experienced this type of cracking. (Traffic associated cracking and pumping). A summary of the different percentages of cracking obtained are given in Table 3.30.

TABLE 3.30 - Percentage cracking at Van Reenen's Pass

Section (Base material)	Carriage way (Direction of traffic)	Percentage cracking*
Conventional asphalt	North	2,7
Conventional asphalt	South	4,0
Recycled asphalt	North	4,2
Recycled asphalt	South	1,1
TOTAL		12,0

* Percentage based on length of road affected

It is also worth while to mentioned that the areas likely to have inadequate subbase support according to the prediction made in 1983 (see previous Table 3.24), coincided almost exactly with the cracked areas found in the current investigation.

This re-evaluation also indicated that approximately 23 per cent of the length of this route is subjected to slope instability cracking. Almost 100 per cent of these cracks were sealed. It is, however, important to note that traffic associated cracking did appear at some locations of these cracks also. In general though, the two types of cracking occur independant, provided the slope instability cracks are adequately sealed in good time.

The results from Table 3.30 indicated that approximately 6,7 per cent of the cracking appeared on the area with the conventional asphalt base layer. Furthermore it is interesting to note that the higher deflections measured in 1982 also occurred on these parts, of the route, especially on the southbound carriageway. It is believed that the conventional asphalt contributes largely to this since it is more flexible than the recycled asphalt.

3.6 SUMMARY AND DISCUSSIONS

Ten different HVS tests were summarized in this chapter. The tests were done in Natal, at four different sites with the same design. The HVS tests indicate that the weakly cemented subbase layers experience fatigue cracking and fracturing. However, if the subbases remain dry, neither excessive permanent deformation nor excessive asphalt fatigue distress is expected in the design period (12 to 50 ME80s in 20 years) of these structures. It is believed that this design will be able to carry more than 30 ME80s in the dry state. In the wet state (excess porewater pressure), the durability (erodibility) of the upper subbase governs the functional life of this design. The tests indicate that durability requirements

should take precedence over the strength requirements of these fine-grained weakly cemented materials, (at least the upper subbase). Furthermore it is important to police overloaded vehicles, since asphalt deformation may occur especially at relatively high ambient asphalt temperatures. Any cracks should be sealed immediately and regular drainage maintenance should be done. The weakly cemented weathered granite material, however, is adequate for the subbase layers in these designs. The Berea Red Sand, treated with three to four per cent lime, is not recommended for the upper subbase in this type of design (Umgababa tests).

It can be concluded that the function of the weakly cemented subbase layers in this type of pavement design are not only to protect the subgrade layers against excessive deformation but also and more important to protect the asphalt layer against fatigue distress. It is therefore the author's belief that the upper subbase is one of the most important structural layers in the pavement. Investment should be in this layer because it is more economical from a rehabilitation point of view to repair only the base or surfacing layers.

With the aid of linear elastic modelling (mechanistic analyses in this case) very important behavioural characteristics could be quantified. Of the most important parameters were surface and depth deflections, effective elastic moduli values, horizontal and vertical micro-strains and radius of curvature. The introduction of artificial changes in the moisture state or elavated temperature under controlled conditions enabled the precise defining of the different failure mechanisms encountered at the different sites. The importance of sub-surface drainage to avoid EPWP conditions is again realized. Quality control during the construction of weakly cemented layers is very important and proved to be the key factor for longevity of these layers. Weak interlayers must be avoided (Van Reenen, N3/6). Stable fills must be provided before weakly cemented layers are build (Figtree, N2/24).

Most of the HVS tests indicates that weakly cemented subbase layers undergo cracking and dramatic changes in their effective elastic moduli values occur. From this it appears that the postcracked phase are very important because most of these layers were cracked during most of the testing.

In the following chapter an attempt is made to illustrate an example how to quantify weakly cemented layers during the postcracked phase. It is considered only as an example, but certain principles used are believed to be very important when doing similar analyses.

3.7 REFERENCES

OTTE, E (1978). A structural design procedure for cement-treated layers in pavements. DSc thesis, University of Pretoria, South Africa.

FREEME, C R and STRAUSS, J A (1979). Towards the structural design of more economical pavements in South Africa. Proc. 3rd Conf. on Asphalt Pavements for South Africa, Durban.

FREEME, C R and WALKER, R N (1984). Economic design of bituminous pavements. Proc. 4th Conf. on Asphalt Pavements for South Africa, Cape Town.

FREEME, C R (1984). Symposium on: Recent findings of Heavy Vehicle Simulator testing. ATC 1984, NITRR, South Africa.

DE BEER, M (1984(a)). HVS testing at Mariannhill, N3/1: Detail Report. NITRR Technical Report, RP/11, CSIR, Pretoria.

DE BEER, M (1984(b)). HVS testing of National Road N2/24 between Illovo and Umgababa in Natal (Figtree). NITRR Technical Report, RP/10/84, CSIR, Pretoria.

DE BEER, M (1985(a)). HVS testing of National Road N2/24 at Umgababa in Natal, NITRR Draft Report TP/40/85, Pretoria, CSIR, 1985. (Unpublished).

DE BEER, M (1985(b)). HVS testing and evaluation of the recycled base section at Van Reenen's Pass, N3/6 Upgraded detail report (Unpublished). NITRR Technical Report, TP/135/85, CSIR, Pretoria.

NATIONAL INSTITUTE FOR TRANSPORT AND ROAD RESEARCH (1985). Standards for road construction materials. Draft TRH14, Pretoria, NITRR.

RUST, F C (1985). Load associated crack movement measurements during HVS testing. NITRR Technical Note TP/68/85, Pretoria, CSIR, 1985.

VAN ZYL, N J W and MAREE, J H (1983). The behaviour of a high-standard crushed-stone base pavement during a heavy vehicle simulator test. NITRR Technical Report, RR358, CSIR, Pretoria.

VILJOEN, C E L and VAN ZYL, N J W (1983) The "Marvil" Permeability Apparatus for in situ testing of surfacing and base coarse layers. Technical Note, TP/181/83, NITRR, Pretoria.

KLEYN, E G and VAN HEERDEN, M J J (1983). Using DCP soundings to optomise pavement rehabilitation. ATC, CSIR, Pretoria.

MAREE, J H (1982). Aspekte van die ontwerp en gedrag van padplaveisels met korrelmateriaal kroonlae, D.Sc. thesis, University of Pretoria, Pretoria.

DE BEER, M (1985(c)). Erosion test : Intermediate revised method and first results. Technical Note, TP/6/85, Pretoria, NITRR.

NETTERBERG, F (1984). Rapid Field test for carbonation of lime or cement treated materials. RS/2/84, NITRR, Pretoria.

FREEME, C R, FRANCIS, V C, VILJOEN, A W, and HORAK, E. (1982). The Impetus of Heavy Vehicle Simulator Testing in Natal. Proceedings of the Annual Transporation Convention, August 1982, Pretoria, South Africa.

CLIFFORD, J M. Some aspects of the structural design of segmental block pavements in southern Africa, D.Ing. Thesis, University of Pretoria, 1984.

NATIONAL INSTITUTE FOR TRANSPORT AND ROAD RESEARCH. (1983). Bituminous pavement rehabilitation design, Draft TRH12, CSIR, Pretoria.

NATIONAL INSTITUTE FOR TRANSPORT AND ROAD RESEARCH. (1985). Structural design of interurban and rural road pavements (TRH4). Pretoria, CSIR.

CHAPTER 4

QUANTIFICATION OF CEMENTITIOUS LAYERS IN THE POSTCRACKED PHASE

CONTENTS

4.1 INTRODUCTION

A method to evaluate and quantify the effective elastic modulus of relatively weakly cemented subbase materials in the postcracked state during wet and dry periods is proposed in this chapter. The major tools in the field evaluation of the behaviour were the HVS and a theoretical procedure involving linear elastic simulations of the road structure. The different phases of cracking or states of cementitious layers during its "life" is also described.

In order to put perspective to the use of the theoretical procedure in the evaluation of road structures, Table 4.1 was extracted from work done by Otte (1978). The main elements in pavement design theory are traffic, materials, environment, analyses and modes of distress. The main advantage of the HVS system (full scale testing) is that most of the main elements of the design theory are well defined and can be accurately controlled and measured. One particular field of interest is the study of the modes of distress which can be accurately observed during an HVS test, using both permanent and resilient behavioural indicators. A few of the pertinent modes of distress observed on structures containing cementitious layers are

(a) Asphalt deformation
(b) traffic associated cracking of cementitious layers
(c) traffic associated cracking of asphalt layers
(d) surface deformation originated from the upper cementitious subbase layer owing to the lack of durability of the layer during the excess porewater pressure state,
(e) surface deformation, cracking and pumping owing to a poorly cemented upper subbase layer, and
(f) crushing of weakly cemented layers in the dry state during trafficking.

TABLE 4.1 - The development in pavement design theory (after Otte, 1978)

	California bearing ratio (CBR)	State of California	AASHTO	Theoretical procedure
Traffic:				
Number of load repetitions	Not considered	Any number; is calculated from predicted traffic volume.	Any number; is calculated from predicted traffic volume.	Any number; is calculated from predicted traffic volume but depends on materials, for example . E80 for untreated materials . Maximum wheel load for cementitious materials . Total traffic volume for bituminous surfacing.
Magnitude or unit of loading	Light : 31 kN Medium : 40 kN Heavy : 53 kN	Equivalent 22,2 kN wheel loads.	Equivalent 80 kN axles (E80)	Equivalent 80 kN axles and actual loading.
Materials				
Type considered	Untreated	Treated and untreated	Treated and untreated	All road-building materials; also those still to be developed.
Characterized by	CBR	R-value and gravel equivalency factors.	Structural coefficient	. Elastic modulus and Poisson ratio . Allowable stress and strain
Environment	-	R-value is determined from a saturated sample.	Regional Factor	. Adjustments in elastic modulus and allowable stresses and strains. . Calculates and includes effect of thermal and moisture stresses.
Analysis	Single graph	Equation	Tables and equation	Complex equations - must be solved by computer
Outcome of analysis	Total thickness; and thickness of base and subbase	. Gravel equivalent. . Thickness of various layers in structure	. Structural number . Thickness of various layers	. Number of load repetitions until distress. . Critical position in structure and likely mode of distress. . Probable maintenance requirements
Mode of distress	Deformation of subgrade	Permanent deformation in pavement materials.	Loss of riding quality.	All modes of distress

(g) horizontal interfacial layers (horizontal cracking) within a cemented layer. This leads initially to fatigue distress of the remaining "thin" layers within the main layer. These layers eventually undergo shearing and crushing or fracturing. The end result being a cemented layer with the upper part of the cemented layer crushed (granulated).

As was discussed previously in Chapter 3 each of above modes of distress occurred along a certain paths of behaviour depending on the traffic, materials and environment.

4.2 PRECRACKED AND POSTCRACKED STATES OF CEMENTITIOUS LAYERS

Most of the work done on the design and evaluation of cementitious layers in road structures, Otte (1978) and Freeme et al (1984), accept that cracking is unavoidable in cementitious layers, after construction. This cracking can be divided in non-traffic associated and traffic associated cracking. The non-traffic associated cracking involves cracking due to variations in environmental conditions such as temperature and moisture content. According to Otte (1978), little can be done to avoid these modes of cracking, except that it can be protected by an insulating structural layer on top of the cementitious layer to minimize environmental changes and to dampen reflection cracking. These types of cracking must therefore be accepted and incorporated in the design phase. It is however true that much more research in the field of the soil-cement chemistry and construction processes is needed. Factors to investigate with respect to weakly cemented materials (C3 and C4) are:

(i) Modification(i.e. reducing of the plasticity index (PI))
(ii) Cementation (i.e. hydraulic or pozzalanic action)
(iii) Delayed compaction to reduce cracking due to drying shrinkage.
(iv) Initial consumption of lime (ICL)

(v) Cementing lime content (CLC)

(vi) Modification lime content (MLC)

(vii) Both beneficial and detrimental carbonation of cementitious layers

(viii) Delayed mixing of cement after the addition of lime

(ix) Steam curing vs normal curing, etc.

All of the above factors could have a significant influence on the ultimate behaviour of these layers. It is however believed that if environmental and construction type of cracking are avoided or minimized, that the ultimate lives of these layers and hence of the total structure can be lengthened.

This type of cracking however is more important during the precracked state after which mainly traffic associated cracking occures. Work done by Otte (1978) indicated that relatively small movements (0,1 mm to 0,3 mm) occurs in a cracked treated layer owing to environmental changes in temperature. He stated further that:

> "The outcome of this study was quite unexpected in the light of previous thinking on thermal stresses in treated layers. Previously thermal stresses were considered to be very important but this study has shown it to be true only for uncracked treated layers. Once the cracks have developed the thermal stresses become virtually negligible in comparison with the traffic-associated stresses. Thermal stresses may therefore be considered as unimportant in cracked treated layers."

In this dissertion the author shares the view of Otte and for this reason no further research had been done on any of the HVS sites, with respect to the thermal conditions of cementitious layers, or the influence thereof. It is however true that the HVS tests were done on weakly cemented materials covered with a thick insulating asphalt base layer. Relatively small variations in temperature was however measured within the cementitious layers (5° to 10°C). The effect of

thermal stresses in weakly cemented subbase layers is therefore not considered in the postcracked phase because it is believed that the stresses and therefore movements owing to thermal conditions will be lower than those found in strongly cemented layers.

Mechanistic analyses were used to quantify the precracked and postcracked state of cementitious layers. The postcracked state is defined as the period within which cracks develop by trafficking only i.e. traffic associated cracking. For the purpose of illustration the HVS test at Mariannhill in Natal is discussed. (See Chapter 3). As previously described, stresses and strains were calculated using linear elastic simulations of the structure at various stages of trafficking and pavement behavioural states. The input parameters to these analyses were the multi depth deflections, measured with the MDD. Using this method of evaluation the changes in effective elastic moduli with accumulated traffic of the different layers in the structure are obtained, including those of the cementitious layer. The need to obtain such a relationship was already expressed by Otte (1978). The cementitious subbase materials tested with the HVS were mainly of C3 and C4 quality and in this case appropriate relationships were found for the weakly cemented subbase layers under consideration viz : C3 and C4 materials. The definition of cementitious materials according to TRH14 (1980) are given in Table 4.2.

The relationship between effective elastic moduli of the upper subbase and accumulated trafficking is illustrated in Figure 4.1. An hyperbolic relationship was found for the postcracked phase. The correlation coefficient was approximately 75 per cent. The results from the previous Table 3.4 were used. The relationships are:

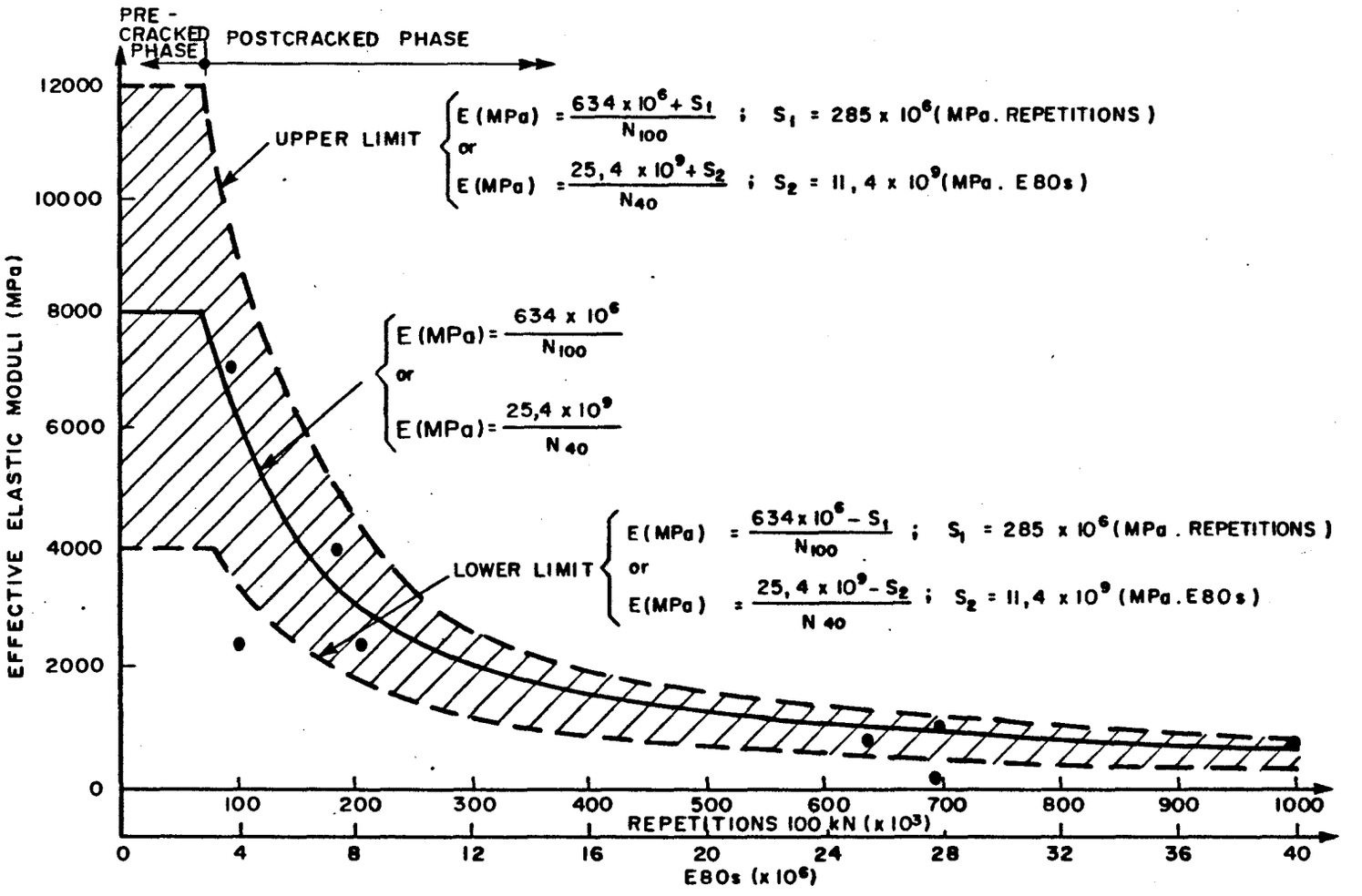

FIGURE 4.1

RELATIONSHIP BETWEEN EFFECTIVE ELASTIC MODULI OF THE CEMENTITIOUS SUBBASE LAYER AND ACCUMULATED TRAFFICKING (DRYSTATE)

TABLE 4.2 - Definition of cementitious materials (NITRR, 1980)

Code	Material	Specifications*					
		UCS at 100% Mod.AASHTO (MPa)	UCS at 95% Mod.AASHTO (MPa)	Aggregate Crushing Strength	Flakiness Index (%)	Sand Equiv. (%)	PI (%)
C1	Cemented crushed stone or gravel	6 - 12	4 - 8	10% FACT: $\geq$ 110kN ACV: $\leq$ 29%	$\leq$ 35	$\geq$ 30	-
C2	Cemented crushed stone or gravel	3 - 6	2 - 4	"	"	"	-
C3	Cemented natural gravel (Max size 63 mm)	1,5 - 3	1 - 2	-	-	-	$\leq$ 6
C4	Cemented natural gravel (Max size 63 mm)	0,75 - 1,5	0,5 - 1,0	-	-	-	$\leq$ 6
C5	Treated natural material	Modified only for Atterberg limits					

* UCS: Method A14, TMH1 (1979)

$$E = 634{,}44 \times 10^6 \pm S_1/N_{100} \quad \ldots\ldots\ldots\ldots\ldots\ldots \quad (4.1)$$

or

$$E = 25{,}4 \times 10^9 \pm S_2/N_{40} \quad \ldots\ldots\ldots\ldots\ldots\ldots \quad (4.2)$$

where E = Effective elastic modulus of upper subbase in MPa

$S_1 = 285 \times 10^6$ (MPa. repetitions), standard deviation

$S_2 = 11{,}4 \times 10^9$ (MPa. E80s), standard deviation

N_{100} = Repetitions of 100 kN dual wheel load

N_{40} = Repetitions of 40 kN dual wheel load, (E80s)

To obtain the upper and lower limits of the moduli, the given standard deviations (S_1 or S_2) is added or subtracted as is indicated in both equations 4.1 and 4.2. These limits are also shown in Figure 4.1. The average value of the moduli is obtained without the standard deviations, i.e.

$$E = 634,44 \times 10^6/N_{100} \quad \ldots\ldots\ldots\ldots\ldots\ldots\ldots\ldots \quad (4.3)$$

or

$$E = 25,4 \times 10^9/N_{40} \quad \ldots\ldots\ldots\ldots\ldots\ldots\ldots\ldots \quad (4.4)$$

The constants in the two equations differs by a multiplying factor of approximately 40, which was obtained assuming a relative damage exponent of 4 for this type of pavement structure in the relative damage expression, $(P/40)^d$. The figure indicates that a constant modulus of 8 000 MPa is proposed during the first 3×10^6 E80s, which is indicative of the precracked state of this layer. This modulus actually varied between 4 000 MPa and 12 000 MPa. It is difficult to measure these moduli in situ with the MDD instrument as very small relative deflections, if any, existed in cementitious layers during this phase. It is believed that some cracking, either traffic or non-traffic associated, in the cementitious layer does exist during the precracked phase, but is rather insignificant compared to that found during the postcracked phase. It is however true that anisotropy in the modulus or deflections of the cementitious layers cannot be measured or obtained by the current method using the MDD instruments. This reality was also appreciated by Otte (1978). The current method of using vertical MDDs in the pavement structure allows only the effect of oblique or horizontal cracking or granulation of the material around the MDD hole to be measured. It is however accepted that this is rather conservative, but it is the best available method of measuring in situ changes in the layer. Any major changes however within the layer can be measured, permitting the changes in effective elastic moduli to be calculated. In this case the moduli of the cementitious upper subbase changed from an average value of 8 000 MPa to approximately 500 MPa. Cracked and almost granulated material

was recovered after the HVS test. Prior to testing intact material was recovered. As was discussed in Chapter 3, changes in the moduli of the other layers in the structure were also observed and calculated. It was therefore possible to define the different stages in the "life" of the road structure using linear elastic simulations. Because the main structural layers in this type of pavement structure (asphalt base, cementitious subbases), were treated materials, the effective horizontal strain was used as distress criterion to evaluate these layers. See also the theoretical procedure outlined in Table 4.1.

To quantify the precracked and postcracked states of the cementitious layer, traffic induced strains obtained from the linear elastic simulations at various stages of trafficking were plotted together with the strain criteria proposed by Otte (1978) and Freeme et al (1984). The comparison between the induced strain during trafficking and the fatigue criterion are illustrated in Figure 4.2. The area under the fatigue curve is defined as the precracked phase or state of cementitious layers. The remaining area (above the curve) is defined as the postcracked phase or state. In this case almost 3×10^6 E80s were applied on the upper subbase layer before major changes occurred within the layer. This effect can best be seen by comparing the slopes of the induced strain-traffic curve during the precracked and postcracked phases in Figure 4.2. On this structure almost 30×10^6 E80s were applied without serious deformation or major decrease in riding quality. The precracked phase encompasses therefore only approximately 10 per cent of the total amount of traffic applied to the structure during the dry state. From this finding the majority of the life of this pavement structure will therefore be in the postcracked phase. The concept of designing against traffic associated cracking in cementitious layers, can result in overdesigning the structure whereby uneconomical thickness of cementitious layer could be obtained. This is in agreement with finding of Otte (1978) where he stated the following:

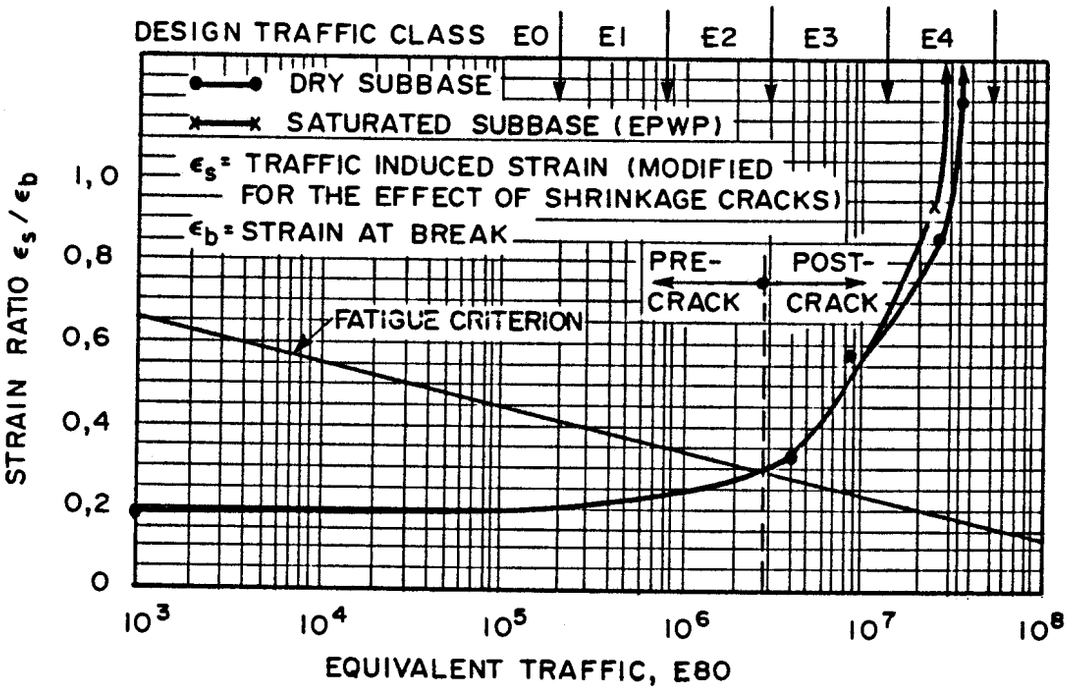

FIGURE 4.2

COMPARISON BETWEEN THE INDUCED STRAIN DURING TRAFFICKING AND THE FATIGUE CRITERION FOR CEMENTITIOUS LAYERS

"A second alternative design approach is to accept the fatigue life concept which implies that cement-treated materials can carry a limited number of load repetitions before failing due to fatigue. In this approach the treated material is considered to undergo traffic-associated cracking once the fatigue capacity of the material has been consumed by the load applications (equations 2.3 to 2.6 in section 2.2.10). During the structural design process it should therefore be endeavoured to ensure that the treated material's fatigue capacity will not be exceeded and that traffic-associated cracking will not occur before the pavement has carried the design traffic. The third alternative design approach, and probably the more practical and even less conservative one, it to accept traffic-associated cracking in the treated layer before the pavement has carried the full design traffic. The period of remaining life after traffic-associated cracking has occurred in the cement-treated layer, will be called the postcracked phase in this thesis. This is a very important phase in the overall design life of pavements with cement-treated layers and, depending on the material properties and traffic conditions, it can vary between 20 to 80 per cent of the total design life - it should therefore not be ignored! To properly analyse and include the contribution of this postcracked phase in the design life is very complex. It is currently only possible to make tentative suggestions on (i) how the postcracked phase can be included during the design, and (ii) the research work still to be done to include it with any degree of confidence."

When it is, however, considered to include the postcracked phase in the design, it is important to ensure that the pavement will not deform excessively with a consequent loss in riding quality during this phase. It is possible that deformation and a loss of riding quality may occur because of the reduction in the elastic modulus of the cementitious layer, especially during the excess porewater pressure state (EPWP), or owing to lack of durability (erosion resistance) of these

layers, as was observed with the HVS test at Umgababa on N2/24, see Chapter 3. It is further possible that the vertical compressive strain within the subgrade layers could increase resulting also in deformation of the surface and subsequent loss in riding quality, especially where only one cementitious layer, 150 mm thick, exists in the structure.

It is therefore vitally important that all the layers in the pavement should be able to carry successfully the remainder of the design traffic after the onset of traffic-associated cracking in the treated layer(s).

4.3 EFFECT OF SUBBASE ON THE OTHER LAYERS IN THE STRUCTURE

In order to study the effect of the change in state of the cementitious upper subbase layer on the other layers in the structure, the induced strains on the asphalt and subgrade layers were compared with their appropriate failure criteria. The maximum horizontal strain at the bottom of the asphalt layer was compared with the fatigue criteria for thick asphalt bases (Freeme, et al, 1984) and the vertical compressive strain on top of the selected layer is compared with the limit subgrade deformation criteria. These comparisons are illustrated in Figures 4.3 and 4.4, respectively. Both figures indicate similar gradual changes to those found with the cementitious layer (Figure 4.2). The change of the slopes of these strain-traffic curves however is much smaller than those found with the cementitious layer. The effect of excess porewater pressure within the upper subbase is more accentuated with the asphalt and subgrade layers. It is thus clear that the ingress of water in the cracked cementitious subbase layer must be avoided as this will lead to excessive deformation, cracking and subsequent loss in riding quality of the pavement (failure).

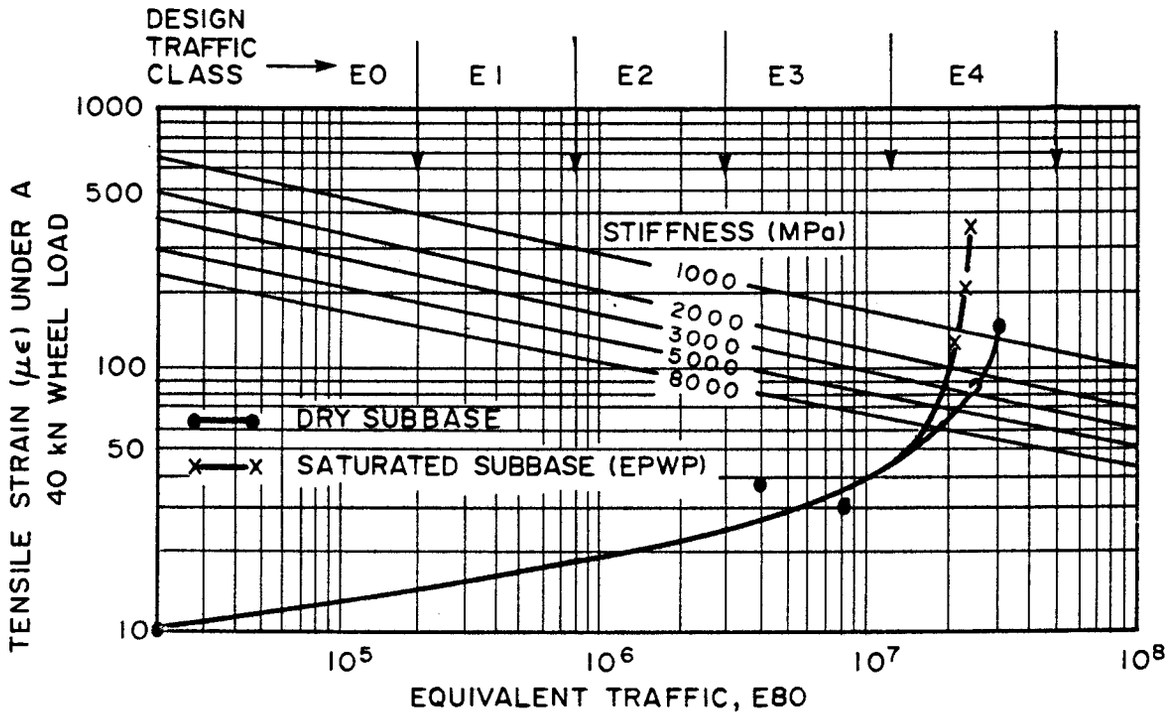

FIGURE 4.3

COMPARISON BETWEEN THE MAXIMUM INDUCED TENSILE STRAIN DURING TRAFFICKING AND THE FATIGUE CRITERIA FOR THICK ASPHALT BASES

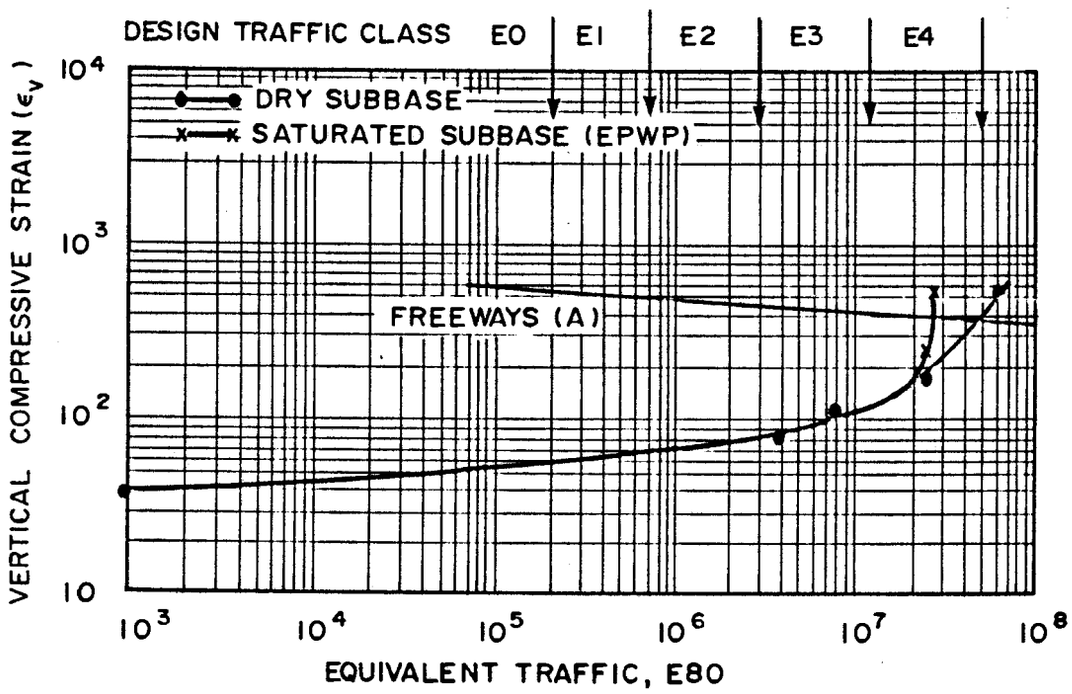

FIGURE 4.4

COMPARISON BETWEEN THE INDUCED VERTICAL COMPRESSIVE STRAIN DURING TRAFFICKING AND THE VERTICAL STRAIN CRITERION TO LIMIT SUBGRADE DEFORMATION OF FREEWAYS (A-CATEGORY)

In the dry state the figures indicate that approximately 30 x 10^6 E80s were applied to the structure before the critical strain limits were reached in the asphalt. In the subgrade layer almost 50 x 10^6 E80s could be accommodated before the critical limit is reached. This is an indication of the degree of protection which the subgrade experiences in this type of design, incorporating weakly cemented subbase layers.

4.4 EFFECT OF WATER ON THE MODULUS OF THE UPPER SUBBASE LAYER

Almost every HVS test done in the wet state, i.e. when water is introduced on or within the road structure being tested, or after the ingress of rain water through surface cracks, moisture accelerated distress (MAD) occurred. The ultimate "life" of the road structure depends heavily upon the rate of progress of this distress and the definition of failure. Because it is not possible at this stage to measure the change in relevant riding quality during a the HVS test, it was decided to define failure when the average deformation measured on the surface of the test section surface equals 20 mm. The importance of decrease in riding quality is appreciated and therefore the difference in functional failure and structural distress of the road must be fully understood. Structural distress in a road leads to functional failure. Structural distress in this dissertion is defined as any major change within the structural layers of the pavement, i.e. cracking, high degree of erodibility (De Beer, 1985) excessive deformation etc. Functional failure occurs when the state of the surface of the pavement in terms of riding quality, changes to unacceptable levels, irrespective of the cause thereof. Most of the HVS tests proved that structural distress occurs rapidly when a state of excess porewater pressure develops within or between the structural layers of the pavement. When the postcracked state of the cementitious layer is considered, fracturing and even granulation of this layer occurred, which was aggravated by the presence of free water in the voids or on the layer. This degradation can quantitatively be incorporated during the design or evaluation

phase of these types of pavement. As with the change in effective elastic moduli of the cementitious layer in the dry state, the change in moduli during the excess porewater pressure state was also measured during HVS testing. These tests indicated that the modulus of the cementitious layer degraded (reduced) at a rate of approximately 360 MPa per 10^6 E80s. This rate of degradation is calculated from the moduli values given in Chapter 3, Table 3.4. The average modulus in the "wet" state, i.e. at MDD8 and MDD12, of approximately 400 MPa was subtracted from the 800 MPa at the end of the "dry" state on Section 1. The rate of degradation is then calculated by dividing this change in modulus by the equivalent applied traffic of approximately 1,1 ME80s. Using this information the "shortest possible life"* of the cementitious layer is calculated. It is however necessary to obtain the earliest time when a state of excess porewater pressure will markedly effect the cementitious layers. It is believed that if non-erodible upper subbase material is used that relatively slow changes in the structural capacity or support value of the cementitious layers will occur during the precracked phase. The effect will become serious only when the rate of degradation in subbase modulus during the excess porewater pressure state exceeds the rate of degradation during the dry state.

---

* The "shortest possible life" of the cementitious layer is defined as the sum of the number of repetitions during the precracked phase and the number of repetitions during the excess porewater pressure state needed in the postcracked phase to reduce the modulus of the layer to zero.

Quantitatively this canging point can be calculated as follows:

from eq 4.4: $E = 25,4 \times 10^9/N$ ..... (4.5)

where N = E80 repetitions

$\therefore \frac{d(E)}{d(N)} = -25,4 \times 10^9/(N)^2$

But $\frac{d(E)}{d(N)}$ = -360 MPa per 10^6 E80s; (measured rate of degradation in wet state).

$\therefore -25,4 \times 10^9/(N)^2 = -360 \times 10^{-6}$

$$N = \sqrt{25,4 \times 10^9/360 \times 10^{-6}}$$

$$= 8,4 \times 10^6 \text{ E80s}$$

Above calculation indicates that when non-erodible materials are used for the cementitious subbase layers, this type of structure can withstand almost E3 class of traffic (i.e. 3 to 12 x 10^6 E80s) irrespective of the presence of water within the pavement. Experience however has taught that the less free water available in the pavement the better. The author believes that although it is possible to calculate the "shortest possible life" of the cementitious layer, that this is over conservative to use in the design phase. Real wet and dry periods should be incorporated, similar to those proposed by Grant, et al (1984), during the total life of the pavement. It is further recommended that the upper limit degradation curve in Figure 4.1 should be used for relatively stronger cemented (C2) materials and the lower limit for weaker (C4) materials. The average degradation curve is recommended for C3 materials. The rate of degradation during the excess porewater pressure state within these materials can be taken as 360 MPa per 10^6 E80s for C2, C3 and C4 materials at this stage, although it is rather conservative for C2 materials.

As previously suggested wet and dry periods during the structural design period of the pavement must be incorporated in the analyses. For example, in this case, if 3 months per year were taken as the "wet" period, i.e. when a state of excess porewater pressure exists within the pavement, the rate of degradation in cementitious subbase moduli is 360 MPa per 10^6 E80s. During the "dry" periods the hyperbolic relationship (eqs. 4.1 or 4.2) must be used to calculate the effective elastic moduli of the cementitious subbase layers. The following example illustrates this principle:

Example : This example illustrates the calculation of the most probable effective elastic moduli values for C2, C3 and C4 materials, both in the "wet" and "dry" states for the cementitious upper subbase layer, incorporating a 3 monthly "wet" period per year:

The following information is given to perform the calculation:

(i) Compound growth rate in E80s, i = 10%

(ii) Cumulative growth factor, fy =

$$fy = 365 \left(\frac{(1+0,01i) \left| (1+0,01)^{Y} - 1 \right|}{(0,01i)} \right)$$

(iii) Analysis period, y. In this example the analysis will be done for each year from year 5 onwards including a 3 monthly wet period per year up to 20 years. Detailed calculations at years 10 and 15 in the "dry" state, and at years 14 and 15 in the "wet" state are given.

(iv) Initial traffic, Ni = 1053 E80s per day per lane

(v) Design distribution factor, Be = 0,95 (NITRR, (1985))

(vi) Non-erodible cementitious subbase material to be used in this design.

(vii) Lower subbase of C4 quality.

Solution:

Analysis for dry state only:

From eq 4.2 the following relationships holds for the moduli values of the three different materials:

(i) $EC2 = 36,8 \times 10^9/E80s$ ..... (4.6)
(ii) $EC3 = 25,4 \times 10^9/E80s$ ..... (4.7)
(iii) $EC4 = 14 \times 10^9/E80$ ..... (4.8)

The cumulative equivalent traffic, Ne, can be calculated from:

$Ne = (NixBe)xfy$ ..... (4.9)
$= (1053x0,95)fy$
$\therefore Ne = 1\ 000\ fy$

for example : y =10 years
$\therefore fy = 6399$
$\therefore Ne = 6,399 \times 10^6$ E80s

The different "dry moduli" values after 10 years can now be calculated by substituting Ne for E80s in each eq. 4.6, 4.7 and 4.8 above:

For example : $EC2 = 36,8 \times 10^9/6,399 \times 10^6 = 5\ 751$ MPa
$EC3 = 25,4 \times 10^9/6,399 \times 10^6 = 3\ 969$ MPa
and $EC4 = 14 \times 10^9/6,399 \times 10^6 = 2\ 188$ MPa

Similarly:
At 15 years the three "dry moduli" values are:

EC2 = 2 885 MPa
EC3 = 1 991 MPa
EC4 = 1 097 MPa

Analyses including "dry" and "wet" alternative states:

To incorporate the 3 monthly wet periods, it is therefore necessary to analyse each year including these wet periods. It was decided to include this period at the start of each year. The cumulative equivalent traffic, associated with each analysis period, were also calculated using eq. 4.9. During the wet periods only (i.e. each 0,25 year of every year), the degradation rate of 360 MPa per 10^6 E80s was used to calculate the reduction in the moduli values.

During the alternative dry periods the previous "dry" degradation rates (hyperbolic relationships) were used. The principle of this calculation method is illustrated in Figure 4.5.

Following the figure, the "wet" moduli values can be calculated as follows:

"Dry" moduli values are : Ea, Eb, Ed and Ef. (See Figure 4.5)
"Wet" moduli values are : Ec, Ee and Eg.
$t_2 - t_1$ = 0,25 years = $t_4 - t_3$ etc. (yearly wet periods)
$t_3 - t_1$ = 1 year = $t_5 - t_3$ etc. (dry and wet periods)
$t_3 - t_2$ = 0,75 year = $t_5 - t_4$ etc. (yearly dry periods)

"Dry" rate of degradation: $E_{dry} = {}^{k}n_{/E80s}$ with n = 1, 2 and 3
where $k_1 = 36{,}8 \times 10^9$ (for C2 material)
$k_2 = 25{,}4 \times 10^9$ (for C3 material)
$k_3 = 14 \times 10^9$ (for C4 material)
.... from eq. 4.2

Therefore Ea = ${}^{k}n_{/E80}$ at t_1; Eb = ${}^{k}n_{/E80}$ at t_2 etc. for the three types of cementitious materials in the "dry" state.

For "wet moduli" values :
Ec = Ea- (E80 at t_2 -E80 at t_1)(360×10^{-6}) MPa ...(E80 in millions)

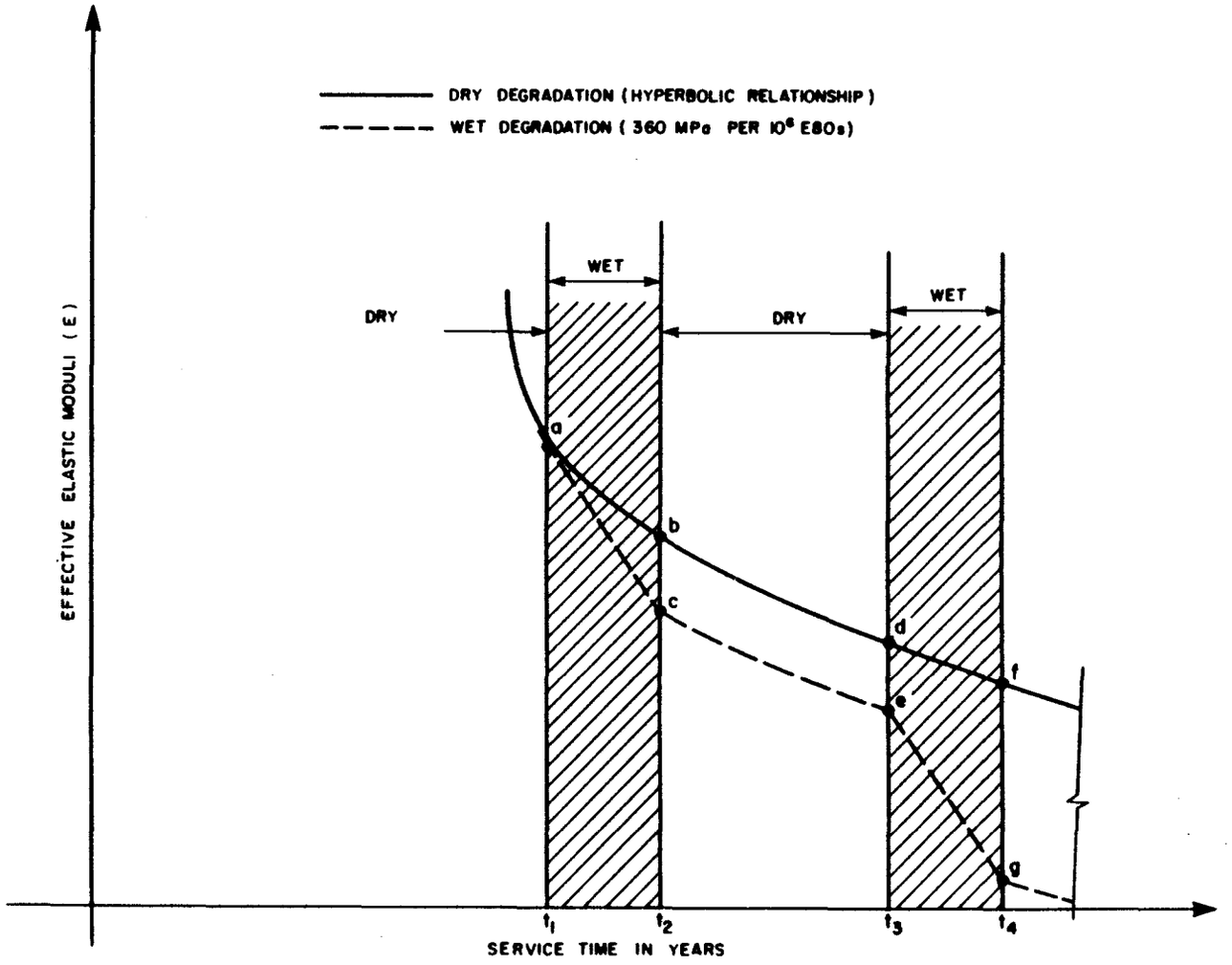

FIGURE 4.5
PRINCIPLE OF CALCULATING WET MODULI VALUES

and Ee = Ed - (Eb - Ec)

= Ed - Eb + Ec

and Eg = Ee - (E80 at t_4 - E80 at t_3)(360 x 10^{-6}) MPa etc.

For example : (i) C2 - Material at year 14:

Edry = Ewet = 36,8 x 10^9/11,232 x 10^6 = 3 276 MPa (No influence of water yet)

at year 14,25: Edry = 36,8 x 10^9/11,60 x 10^6 = 3 172 MPa

and Ewet = (Edry at year 14) - (11,600 x 10^6 - 11,232 x 10^6)(360x10^{-6}) MPa

= (3 276) - (132)

= 3 144 MPa

At year 15 :

Ewet = (E dry at year 15) - (E dry - E wet) at year 14,25

= 2 885 - (3 172 - 3 144)

= 2 857 MPa etc.

Calculation of the accumulative traffic (E80s) at the first stage when "dry" moduli will be affected by water for the different types of cementitious layers, (C2, C3 and C4):

The rate of degradation in moduli during the wet periods is 360 MPa per 10^6E80s. Because the "dry" relationships is hyperbolic, the time when water will first effect the moduli of the cementitious layer can be determined by first order differentiation of the moduli relationships with respect to the number of repetitions, N (E80s):

Thus for C2 : $EC2 = 36{,}8 \times 10^9 / N$

$$\therefore \quad \frac{d(EC2)}{d(N)} = -36{,}8 \times 10^9 / (N)^2$$

but $\frac{d(EC2)}{d(N)} = -360 \times 10^6$ (Rate of degradation in wet state)

$$N = \sqrt{\frac{36{,}8 \times 10^9}{360 \times 10^{-6}}}$$

i.e. for C2: $N|_{C2} = 10{,}11 \times 10^6$ E80s

For C3 : $N|_{C3} = 8{,}40 \times 10^6$ E80s
and C4 : $N|_{C4} = 6{,}24 \times 10^6$ E80s

From above calculation it is clear that the "weaker" the subbase material, the earlier it will be effected during the excess porewater pressure state. In other words the moduli of the three materials, C2, C3 and C4 will be reduced because of water only after $10{,}11 \times 10^6$, $8{,}4 \times 10^6$ and $6{,}2 \times 10^6$ E80s, respectively. These moduli values will be lower than those calculated for the equivalent dry state. The calculated moduli values incorporating the 3 monthly wet period per year for 20 years are given in Table 4.3.

The values from the table are graphically illustrated in Figure 4.6. If a "failure condition" is defined using a "minimum allowable effective elastic modulus" of the cementitious layer during the design life of the structure, the ultimate lives of the three types of subbases, can be obtained from Table 4.3 or Figure 4.6. These values can also be calculated. A minimum effective elastic modulus of 350 MPa is recommended for all three types cementitious subbase layers. According to this failure criterion, the ultimate lives of the three types of cementitious materials are approximately 20 to 25 years for the C2 material; 20 years for the C3 material and 17 years for the C4 material. See Table 4.3 also. It is however important to note that these lives depends heavily on the initial traffic, the real compound growth rate and the actual wet periods etc.

TABLE 4.3 Effective elastic moduli values for the three types of cementitious materials, incorporating in the dry and wet periods.*

Prediction Period ,y (yrs)	fy	Accum. Traffic, (E80s) ($x10^6$)	Effective elastic moduli (MPa)					
			EC2		EC3		EC4	
			Dry	Wet	Dry	Wet	Dry	Wet
0	-	-	12 000	12 000	8 000	8 000	4 000	4 000
5	2 451	2,451	12 000	12 000	8 000	8 000	4 000	4 000
6	3 098	3,098	11 879	11 879	8 000	8 000	4 000	4 000
6,25	3 269	3,269	11 257	11 257	7 770	7 770	4 000	4 000
7	3 809	3,809	9 661	9 661	6 668	6 668	3 676	3 676
7,25	3 998	3,998	9 205	9 205	6 353	6 353	3 502	3 502
8	4 592	4,592	8 014	8 014	5 531	5 531	3 049	3 049
8,25	4 799	4,799	7 668	7 668	5 293	5 293	2 917	2 917
9	5 452	5,452	6 750	6 750	4 659	4 659	2 568	2 568
9,25	5 680	5,680	6 479	6 479	4 472	4 472	2 465	2 465
10	6 399	6,399	5 751	5 751	3 969	3 969	2 188	2 188
10,25	6 650	6,650	5 534	5 534	3 820	3 820	2 105	2 098
11	7 440	7,440	4 946	4 946	3 414	3 414	1 882	1 875
11,25	7 716	7,716	4 769	4 769	3 292	3 292	1 814	1 776
12	8 586	8,586	4 286	4 286	2 958	2 958	1 631	1 593
12,25	8 890	8,890	4 139	4 139	2 857	2 849	1 575	1 484
13	9 846	9,846	3 738	3 738	2 580	2 572	1 422	1 331
13,25	10 180	10,180	3 615	3 615	2 495	2 452	1 375	1 211
14	11 232	11,232	3 276	3 276	2 261	2 218	1 246	1 082
14,25	11 600	11,600	3 172	3 144	2 190	2 086	1 207	950
15	12 757	12,757	2 885	2 857	1 991	1 887	1 097	840
15,25	13 161	13,161	2 796	2 712	1 930	1 742	1 064	695
16	14 434	14,434	2 550	2 466	1 760	1 572	970	601
16,25	14 879	14,879	2 473	2 306	1 707	1 412	941	441
17	16 279	16,279	2 261	2 094	1 560	1 265	860	360
17,25	16 768	16,768	2 195	1 918	1 515	1 089	835	184
18	18 308	18,308	1 733	2 010	1 387	961	765	114
18,25	18 846	18,846	1 953	1 539	1 348	767	743	0
19	20 540	20,540	1 792	1 378	1 237	656	682	0
19,25	21 132	21,132	1 741	1 105	1 202	443	663	0
20	22 996	22,996	1 600	1 024	1 105	346	609	0

* Dry Period : 0,75 year, each year
Wet period : 0,25 year, beginning of each year.

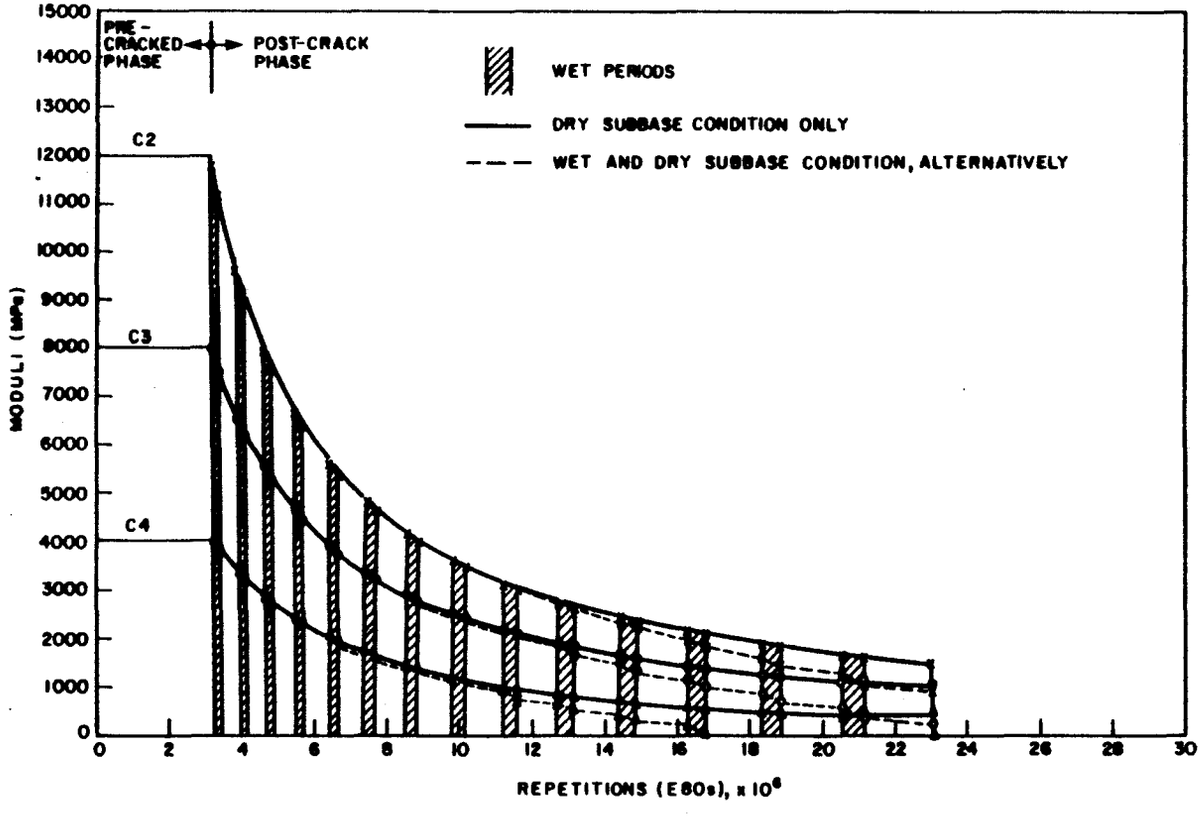

FIGURE 4.6

CHANGE IN EFFECTIVE ELASTIC MODULI OF CEMENTITIOUS SUBBASE LAYERS DURING TRAFFICKING INCLUDING WET AND DRY PERIODS

4.5 CONCLUSIONS AND RECOMMENDATIONS

In this chapter some of the results obtained from HVS testing were evaluated using theoretical procedures, i.e.: linear elastic simulation, in this case. It was shown that the different behavioural states of cementitious layers (precracked and postcracked) in the road structure can be distinguished and quantified using the induced tensile strain at the bottom of these layers in comparison with the fatigue crack criterion proposed by Otte (1978). Comparisons were also made between the failure criteria and induced strain values of the asphaltic and subgrade layers, respectively.

It is concluded that the degradation of the effective elastic modulus during the postcracked phase of the cementitious layer is hyperbolic during the dry state, and linear during the wet (excess porewater pressure) state. A detailed example illustrates the principle of calculating the effective elastic modulus values, incorporating specified wet periods over the structural design life of the structure.

The following relationships are recommended in evaluating or designing pavement structures consisting of a 100 mm thick bitumen base and two 150 mm thick cementitious subbase layers:

Degradation in dry state:

(i) For C2 materials : $EC2 = 36{,}8 \times 10^9/E80s$ ..... (4.10)
(ii) For C3 materials : $EC3 = 25{,}4 \times 10^9/E80s$ ..... (4.11)
(iii) For C4 materials : $EC4 = 14 \times 10^9/E80s$ ..... (4.12)

Rate of degradation during wet state:

$$\frac{d(E)}{d(E80s)} = -360 \text{ MPa per } 10^6 \text{ E80s} \quad \ldots\ldots\ldots\ldots\ldots\ldots \quad (4.13)$$

A lower limit of 350 MPa is recommended as "failure" of a cementitious layer during the postcracked phase. It can further be concluded that:

(i) The "life" of a cementitious subbase layer is strongly dependent on

(a) Real accumulated traffic

(b) Material cementitious quality (C2, C3 or C4)

(c) Environmental conditions - mainly excessive moisture on or within the cementitious layer during the postcracked phase, (wet and dry periods).

(d) Erodibility of the cementitious material.

Last but not least, the traffic associated degradation (i.e. gradual break down of the cementitious layer) must be accepted and incorporated in the design phase. This includes possible rehabilitation design. It was shown that less than 10 per cent of the "life" of these layers are in the precracked phase (i.e. before any traffic induced fatigue distress). In this chapter a quantitative method to describe and define effective modulus elastic values for cementitious subbase layers are proposed.

4.6 REFERENCES

OTTE, E (1978). A structural design procedure for cement-treated layers in pavements. DSc thesis, University of Pretoria, South Africa.

FREEME, C R et al. (1984). State of the art on Heavy Vehicle Simulator testing in South Africa. Symposium on Recent findings of Heavy Vehicle Simulator testing, Annual Transportation Convention, Pretoria, 1984.

NATIONAL INSTITUTE FOR TRANSPORT AND ROAD RESEARCH (1980). Standards for road construction materials. Draft TRH14, Pretoria, NITRR.

NATIONAL INSTITUTE FOR TRANSPORT AND ROAD RESEARCH (1979). Standard Methods of Testing Road Construction Materials. Technical Methods for Highways, No. 1, CSIR, Pretoria, RSA. 1979, ix + 183 pp.

DE BEER, M (1985). Erosion Test : Intermediate revised method and first results. TP/6/85, NITRR, Pretoria.

GRANT, M C and NETTERBERG, F (1984). Determining the cause of distress in pavements with thin bituminous surfacings. Proceedings of the 4th Conference on Asphalt Pavements for South Africa, Vol. 1, Cape Town.

NATIONAL INSTITUTE FOR TRANSPORT AND ROAD RESEARCH (1985). Structural design of interurban and rural road pavements. (TRH4), CSIR.

CHAPTER 5

THE EFFECT OF INTERLAYERS WITHIN BITUMEN BASE STRUCTURES

CONTENTS

5.1. INTRODUCTION

It is often found with the in situ road structure that it differs from the initial design. One of the most important differences is that relatively soft interlayers (lenses) exists between the structural layers of the pavement. These interlayers often causes failures owing to the lack of supporting value especially in the wet state when excess pore-water pressure (EPWP) develops. (De Beer, 1984(a); De Beer, 1984(b); Opperman, 1984; De Beer, 1984(c))

In this case the effects of weak interlayers on the asphalt base pavement design (Freeme, et al, (1984 (a)) are studied. The critical strain parameters of the structural layers of the pavement will be investigated with the aid of linear elastic simulation, using the ELSYM computer program.

Failure potential for fatigue distress and permanent deformation are introduced which indicates which structures are most sensitive to distress, originating mainly from these interlayers. Moduli values for the interlayers are assumed to represent dry and wet conditions. These moduli values are 300 MPa and 50 MPa for the dry and wet conditions, respectively. The moduli for the base, subbases and subgrade layers being kept constant at 3 000, 8 000, 4 000 and 200 MPa, respectively. These moduli values were deliberately chosen to represent the initial state of the pavement structure after construction. A few identified reasons for the existence of these interlayers (which could easily be up to 50 mm or more in thickness) are :

(a) Poor construction;
(b) inadequate layer thickness of stabilised layers, whereby correction layers are introduced;
(c) over or faulty compaction (crushing of top 10-20 mm);
(c) Inadequate mixing depth;
(d) possible carbonation owing to wetting and drying of unprotected stabilised layers (some materials weakens because of carbonation), (Netterberg, 1984).

5.2. ANALYSES

In this analyses four different structures are evaluated. The structures are numbered from 1 to 4. Structure 1 consists of no interlayers representing the designed structure. The rest of the structures (2, 3 and 4) each contain one interlayer, but at a different position. Firstly the effect of the position of a 5 mm interlayer will be studied both in the wet and dry states. Secondly, the effect of the thickness of the interlayer at the bottom of the asphalt (similar to structure 2) will be studied also in the dry and wet states. In this report "dry" and "wet" will be differentiated by the magnitude of the modulus of the interlayer. A modulus of 300 MPa will reflect the "dry" condition and a modulus of 50 MPa will reflect a "wet" condition. The main structural layers however, retain their initial modulus values throughout.

5.2.1 Effect of position of the interlayer

For the purpose of this section of the thesis, the position of the interlayer will be either on top of the upper subbase, between the two subbases or at the bottom of the lower subbase. Because of a limitation in the computer program (ELSYM), a maximum of five layers only can be analysed, therefore only one interlayer per structure could be incorporated.

The effect of these interlayers is described in terms of the fatigue distress parameter, viz. maximum horizontal tensile strain (ε_t) at the bottom of the asphalt or cementitious layers, and in terms of the permanent deformation parameter, viz. vertical compressive strain (ε_v) at the top of the interlayers and the subgrade layer, including all layer interfaces. A dualwheel load of 40 kN at 690 kPa tyre pressure was used in this study. The position midway between the dualwheels was used as the point of analysis.

5.2.1.1 Tensile strain (ε_t) at the bottom of the treated layers

In Figure 5.1 the effect of the 5 mm dry and wet interlayer on the maximum horizontal tensile strain at the bottom of the asphalt base layer is illustrated. The figure indicates maximum strain levels with the interlayer between the asphalt and the upper stabilized subbase, both in the dry and wet conditions. The other structures indicate virtually no significant tensile strains. Above finding is important regarding the fatigue distress potential of the asphalt layer.

The effect of the interlayers on the maximum horizontal tensile strain at the bottom of the upper stabilized subbase layer is illustrated in Figure 5.2. In this case the maximum strains occurred when the interlayer is positioned between the two stabilized subbase layers. Similar strains resulted within the other structures.

The effect of the interlayers on the maximum horizontal tensile strain at the bottom of the lower stabilized subbase layer is illustrated in Figure 5.3. In this case the maximum strains occurred when the interlayer is positioned between the asphalt and the upper subbase. Minimum strains even in the wet state occurred at this position in Structure 3, where the interlayer are positioned between the two subbase layers.

5.2.1.2 Fatigue distress potential, (Fdp)

In order to differentiate between the total sensitivity of the different structures with regard to fatigue distress (for the treated layers only), it is necessary to define a new parameter, called the "Fatigue distress potential". The fatigue distress potential (Fdp) is defined as the sum of the maximum horizontal tensile strains at the bottom of all the treated layers in the structure, viz :

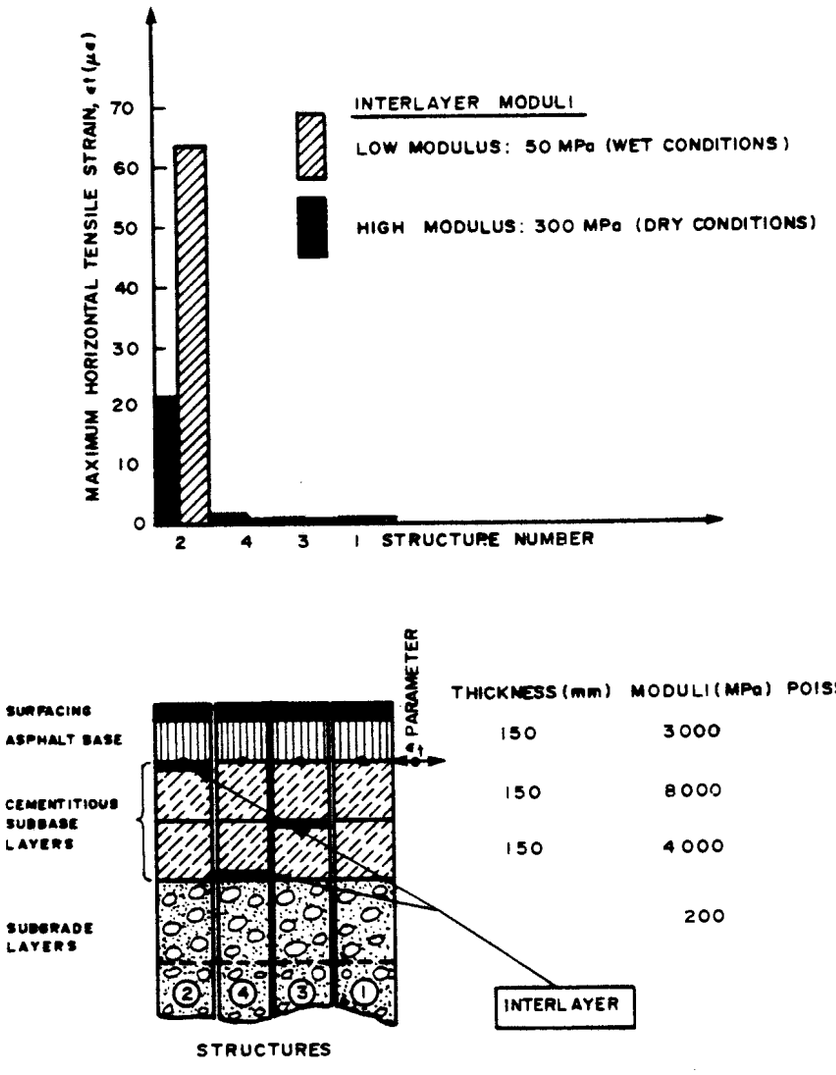

FIGURE 5.1

EFFECT OF 5mm WET AND DRY INTERLAYER ON THE MAXIMUM HORIZONTAL TENSILE STRAIN AT THE BOTTOM OF THE ASPHALT BASE LAYER

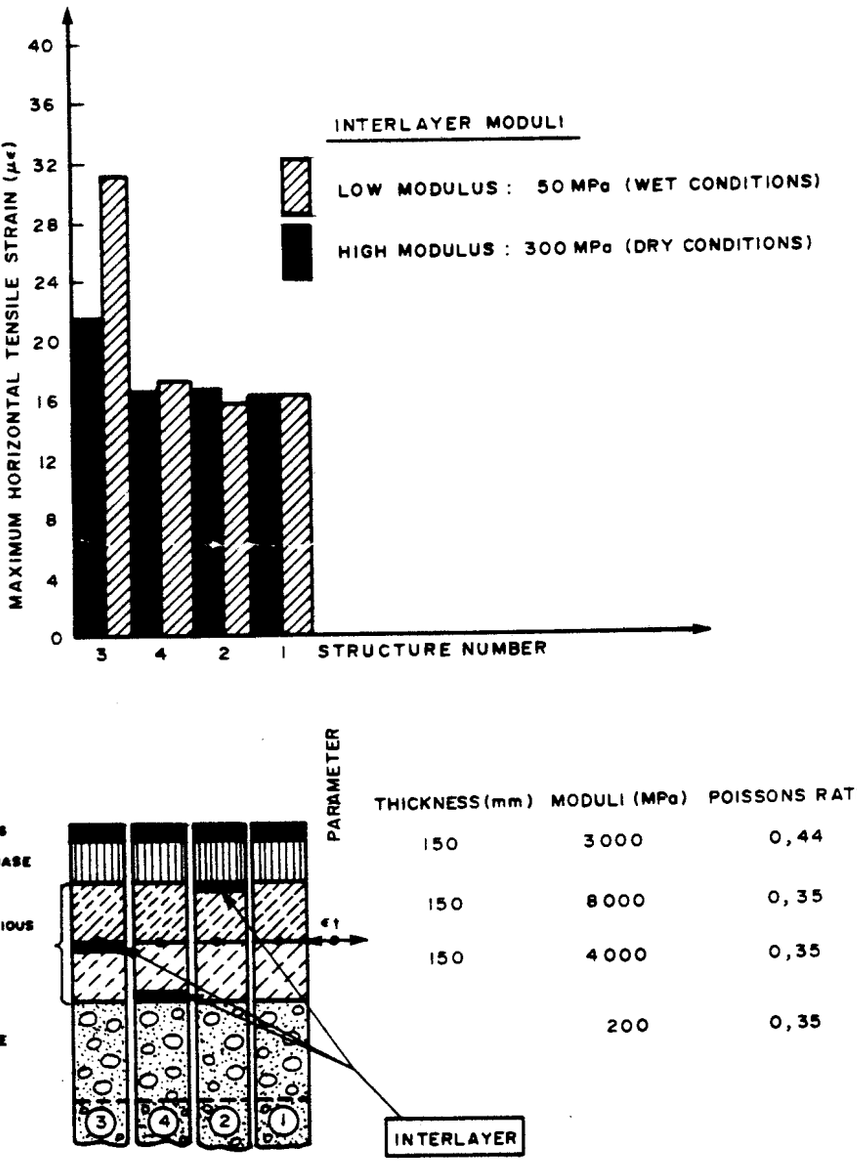

FIGURE 5.2

EFFECT OF 5 mm WET AND DRY INTERLAYER ON THE MAXIMUM HORIZONTAL TENSILE STRAIN AT THE BOTTOM OF THE UPPER CEMENTITIOUS SUBBASE LAYER

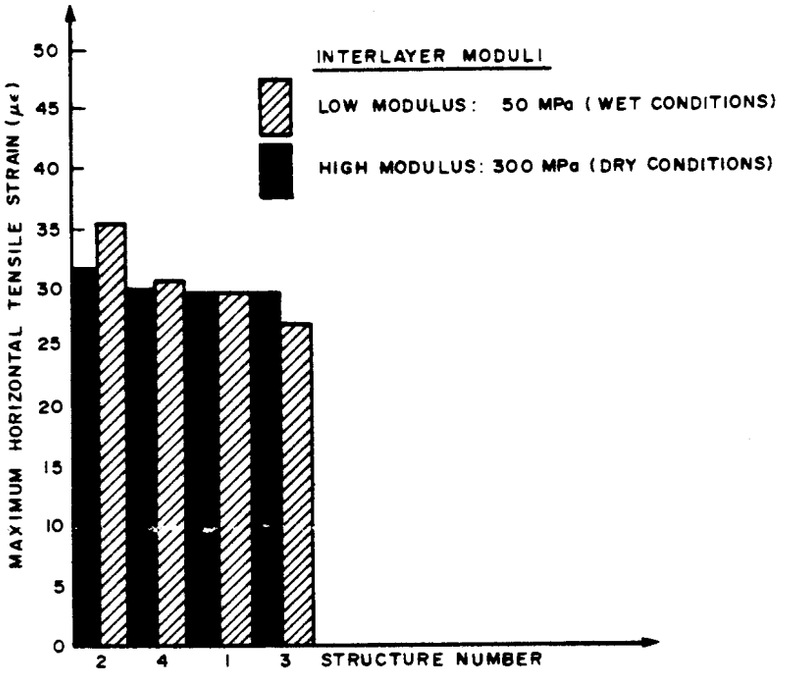

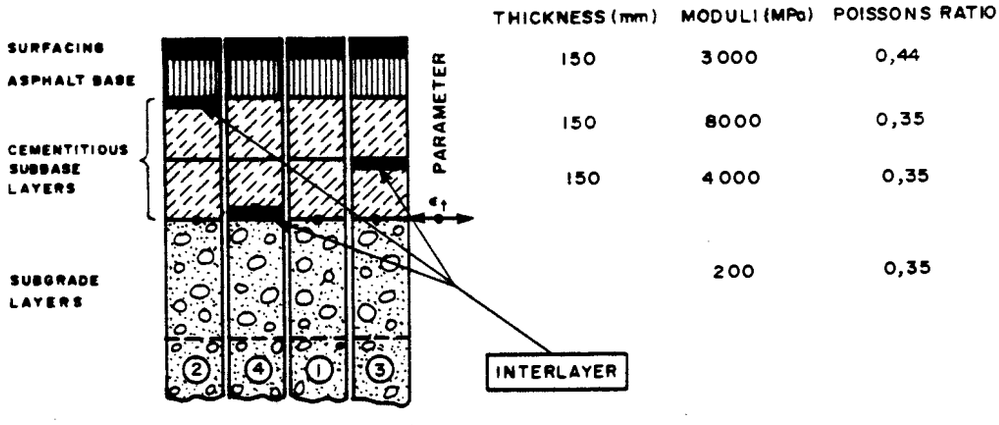

FIGURE 5.3

MAXIMUM HORIZONTAL TENSILE STRAIN AT THE BOTTOM OF THE LOWER CEMENTITIOUS SUBBASE LAYER

$$\text{Fatigue distress potential} = FdP = \sum_{i=o}^{n} \varepsilon_{t_i},$$

n = number of treated layers

The Fdp is measured in microstrain ($\mu\varepsilon$).

The different Fdp's for the four structures analysed are illustrated in Figure 5.4. The figure indicates that Structure 2 is most sensitive to fatigue distress both in the dry and wet conditions. Similar Fdp's were obtained for the three remaining structures. It can be concluded at this stage that an interlayer between the asphalt and upper subbase is relatively more detrimental than interlayers deeper in the structure.

5.2.1.3 Vertical compressive strain, (ε_v)

In order to study the potential for permanent deformation in these structures the vertical compressive strain parameter, ε_v, was used. The vertical compressive strains at the bottom of the asphalt layer (i.e. top of upper subbase - interlayers included) are illustrated in Figure 5.5. The figure indicates a remarkable increase in strain level of Structure 2 when the interlayer is wet. Insignificant strain levels were obtained for the other structures and even for the dry condition in Structure 2.

The vertical compressive strains at the bottom of the upper subbase are illustrated in Figure 5.6. Maximum strains were obtained on the interlayer of Structure 3. Similar strains were obtained for the remaining structures. But here again it is virtually only the wet condition which is significantly higher than the rest.

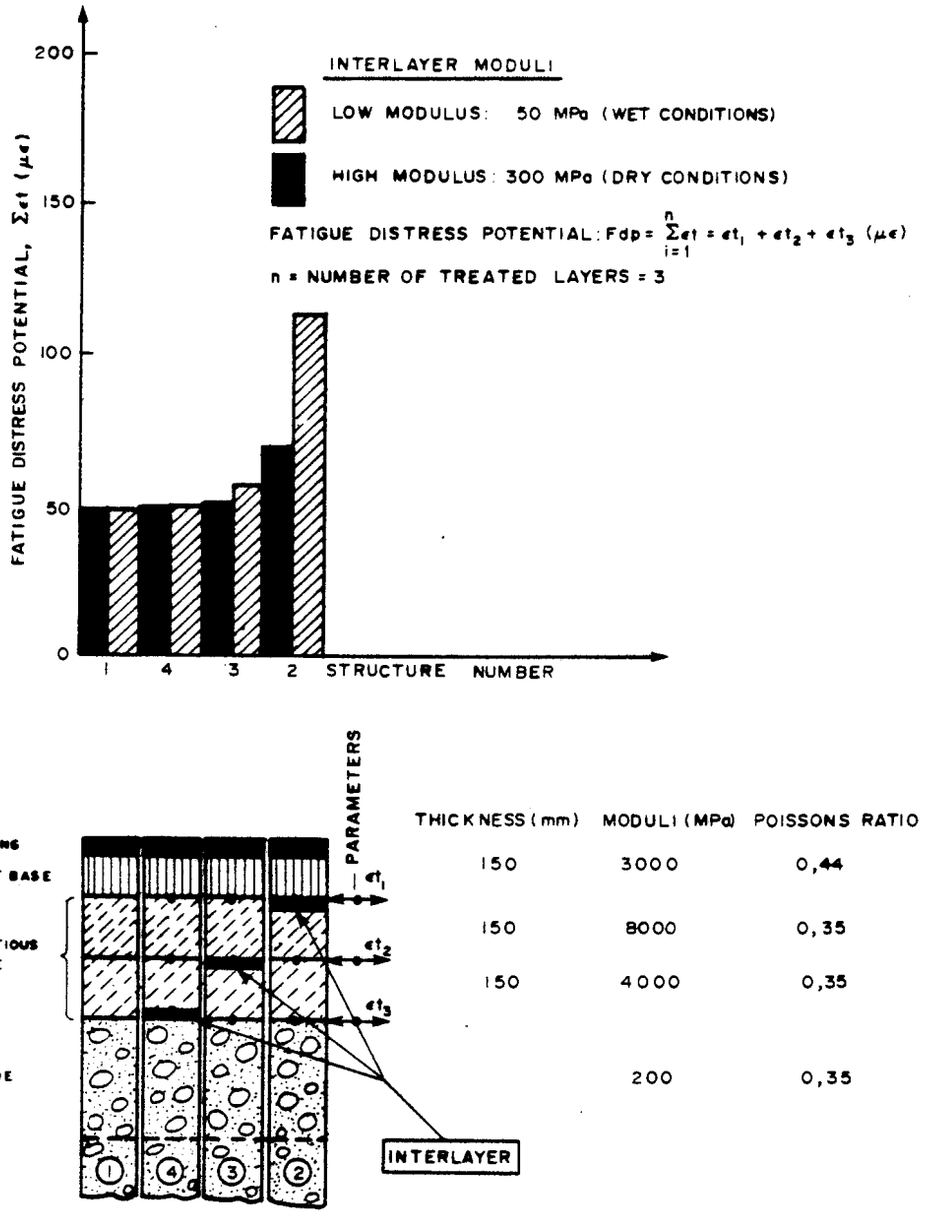

FIGURE 5.4

FAILURE DISTRESS POTENTIALS OF THE TREATED LAYERS IN THE 4 DIFFERENT STRUCTURES

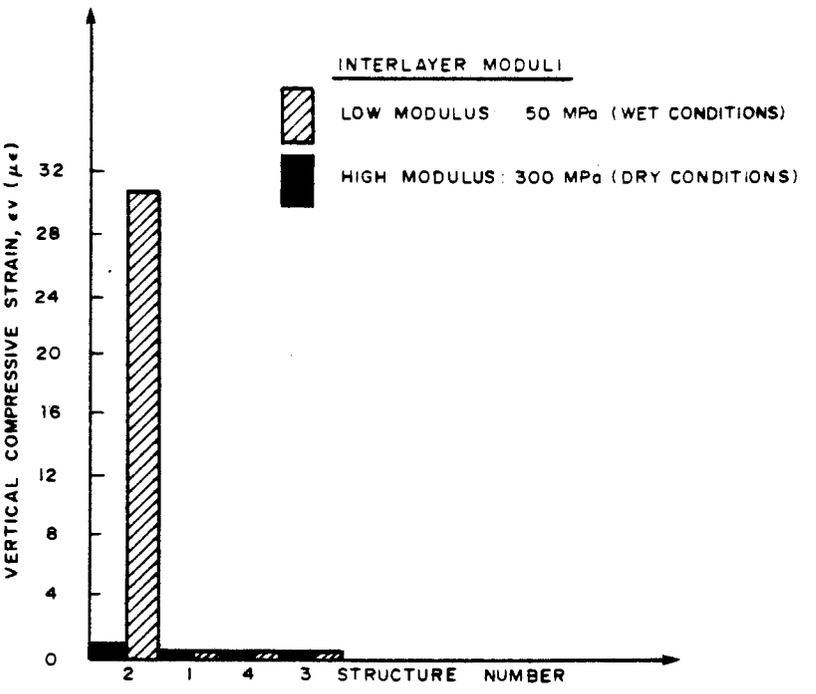

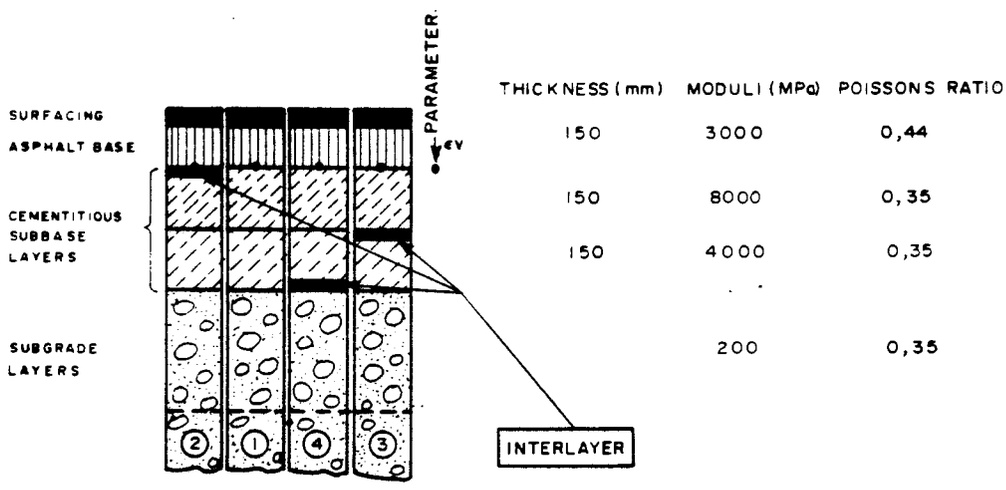

FIGURE 5.5

VERTICAL COMPRESSIVE STRAIN AT THE BOTTOM OF THE ASPHALT LAYER (TOP OF UPPER SUBBASE - INTERLAYER INCLUDED)

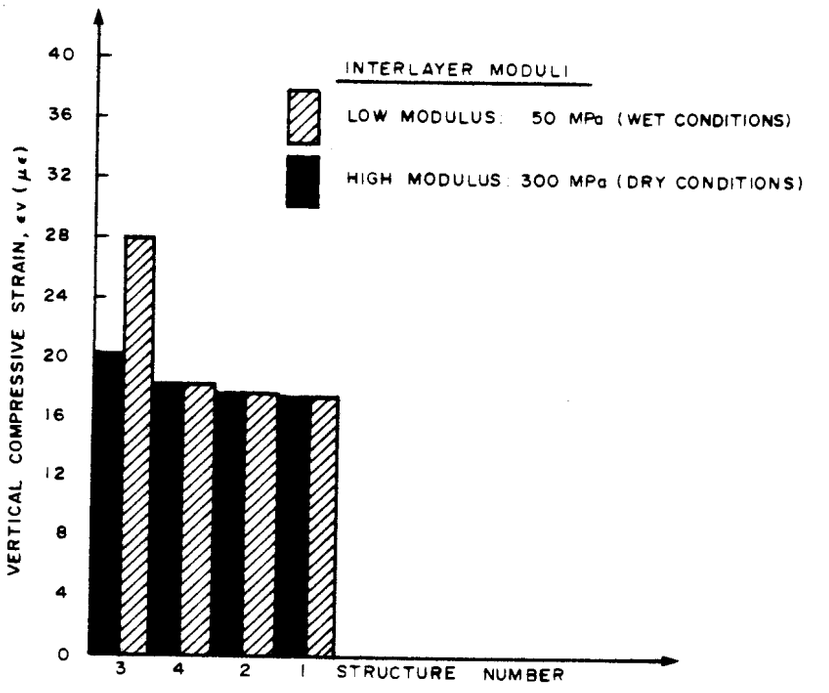

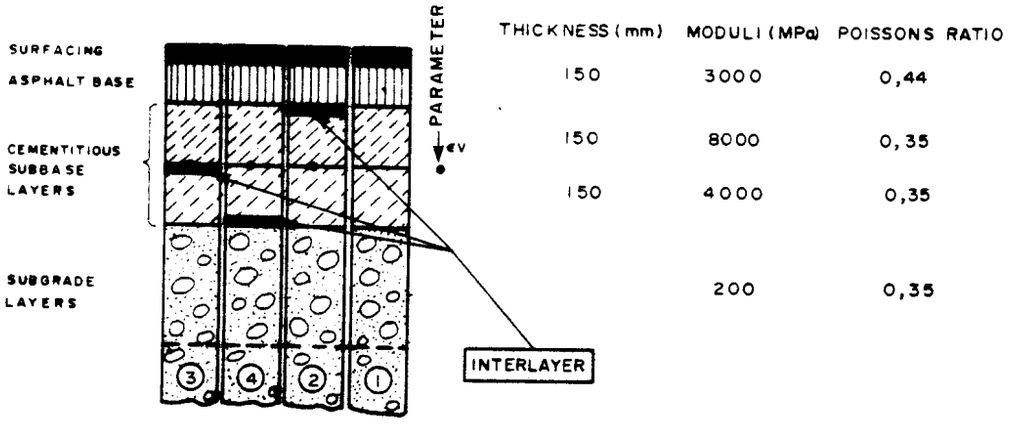

THICKNESS (mm)	MODULI (MPa)	POISSONS RATIO
150	3000	0,44
150	8000	0,35
150	4000	0,35
	200	0,35

FIGURE 5.6

VERTICAL COMPRESSIVE STRAIN AT THE BOTTOM OF THE UPPER SUBBASE LAYER

In Figure 5.7, the vertical compressive strains at the bottom of the lower subbase (top of interlayers and subgrade included) are illustrated. In this case relatively high strain values were obtained with Structure 2, again resulting in the highest strain values both in the dry and especially the wet condition, but very little different from the no interlayer case (Structure 1).

5.2.1.4 Permanent deformation potential, (Pdp)

Similar to the Fdp, it was necessary to define the permanent deformation potential (Pdp) for these structures. The permanent deformation potential is defined as the sum of the vertical compressive strain values at the interfaces of the different structural layers. The vertical compressive strains at the bottom of the interlayers are ignored. Therefore :

$$\text{Permanent deformation potential (Pdp)} = \sum_{i=o}^{n} \varepsilon_{vi},$$

n = number of treated layers.

The Pdp's of the different structures are illustrated in Figure 5.8. The figure indicates that Structure 2 is also most sensitive to permanent deformation with virtually only the wet case being of real significance. Relatively insignificant differences were obtained in the Pdp's of the remaining three structures.

5.2.2 Effect of the thickness of the interlayer

The previous strain analysis indicated that a 5 mm interlayer positioned between the asphalt layer and the upper subbase layer is responsible for resulting in a structure with the highest relative fatigue distress and permanent deformation potentials. It was decided to evaluate this structure further include to the effect of the thickness of the interlayer, both in the dry (300 MPa) and wet (50 MPa) conditions.

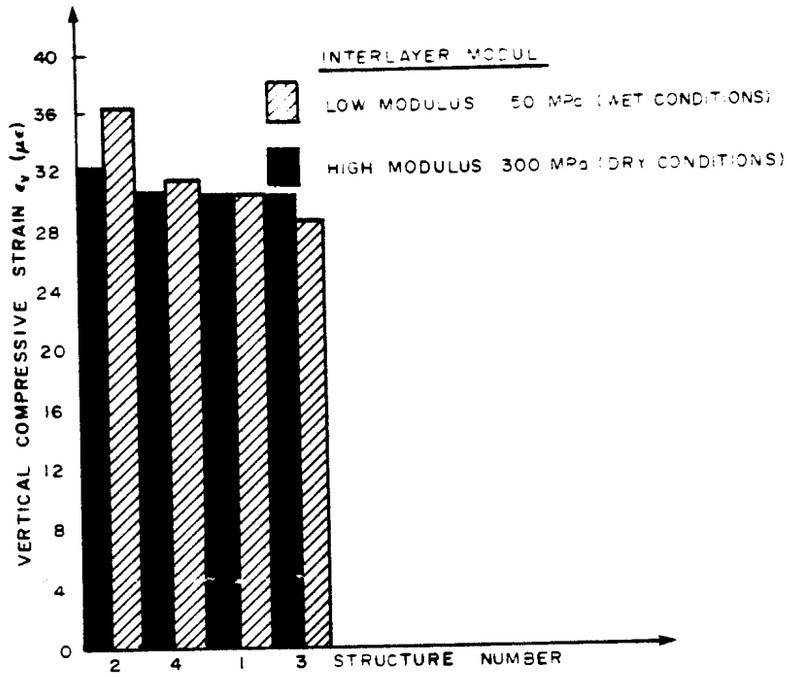

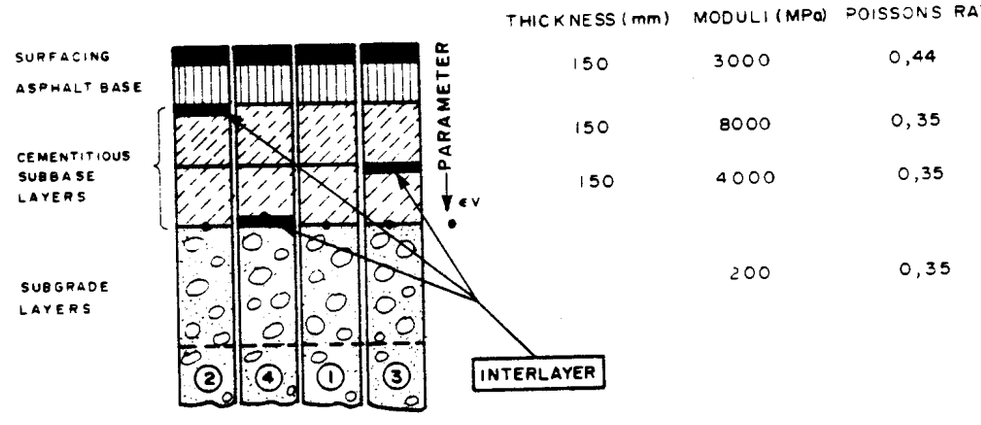

FIGURE 5.7

VERTICAL COMPRESSIVE STRAIN AT THE BOTTOM OF THE LOWER SUBBASE (TOP OF INTERLAYER INCLUDED)

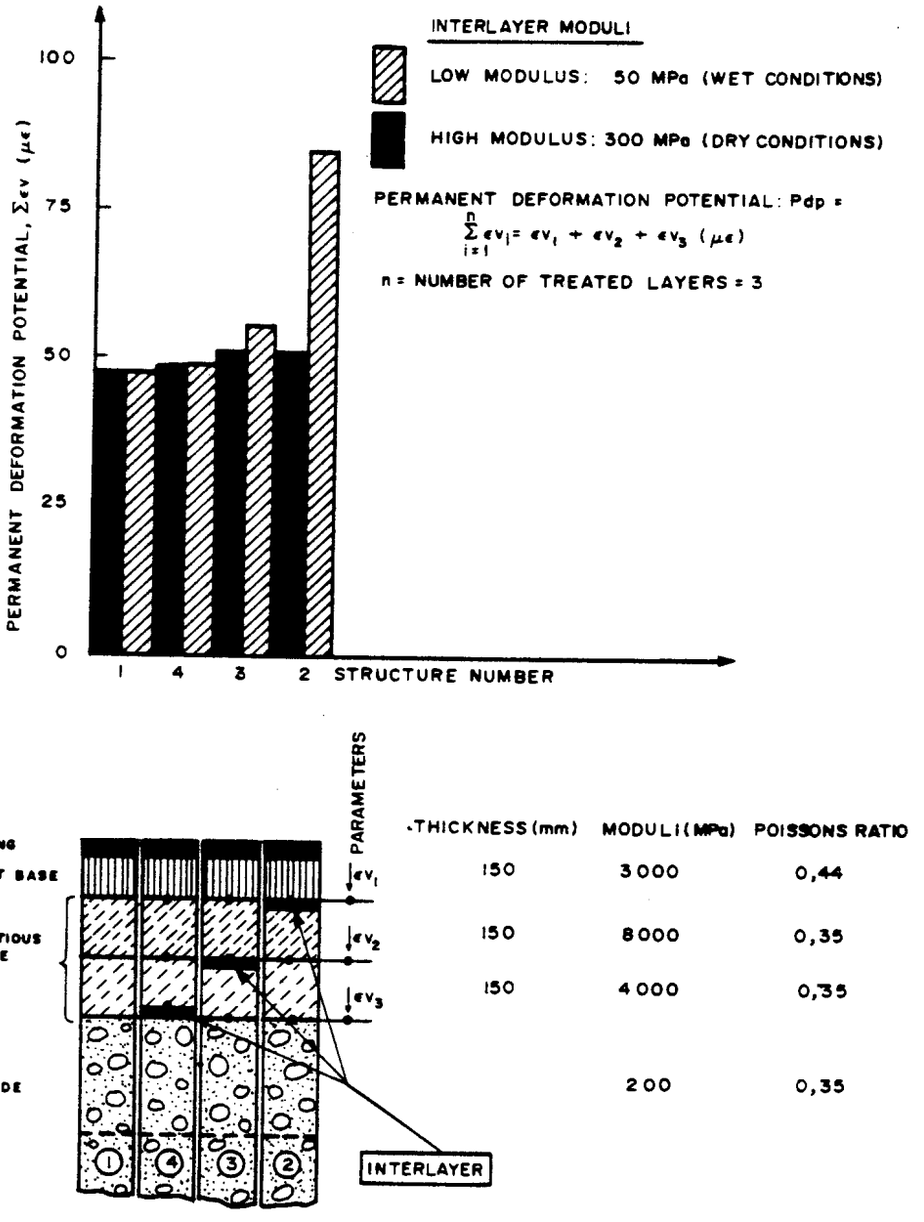

FIGURE 5.8

PERMANENT DEFORMATION POTENTIALS OF THE SOIL LAYERS IN THE 4 DIFFERENT STRUCTURES

5.2.2.1 Tensile strain, (ε_t)

The relationships between the maximum horizontal tensile strain at the bottom of the asphalt layer and the thickness of the interlayer are illustrated in Figure 5.9. The figure indicates relatively rapid increases in strain with layer thickness. The strains resulted from a wet interlayer are more than than those found in the dry state. In the wet state the structural capacity of the asphalt (fatigue life) is reduced by almost 100 per cent with an interlayer 50 mm thick and almost 50 per cent reduction with an interlayer of 20 mm thickness. The horizontal tensile strains at the bottom of the asphalt in the wet state, with interlayer thickness of 20 mm and 50 mm are approximately 115 με and 155 με, respectively. Using these strain values in comparison with the fatigue criteria for asphalt bases (Freeme, et al, 1984 (b)), the relatively short fatigue life in comparison to those in the dry state can be calculated.

In Figure 5.10 the relationships between the maximum horizontal tensile strain at the bottom of both cementitious subbase layers and the thickness of the interlayer are illustrated. In general, the induced strains at the bottom of the lower subbase layer are almost double that induced at the bottom of the upper subbase layer. The upper subbase layer experienced however reduced strains with increase in thickness of the interlayer in both the dry and wet conditions. It is believed that the reason for this reduction in strain level is accomplished by the full friction interface assumed between the two cementitious subbase layers.

The lowest strain values were obtained at the bottom of the upper subbase during the wet conditions (interlayer modulus : 50 MPa). The reverse was true in the lower subbase for interlayer thicknesses less than approximately 30 mm. This indicates longer fatigue lives for both

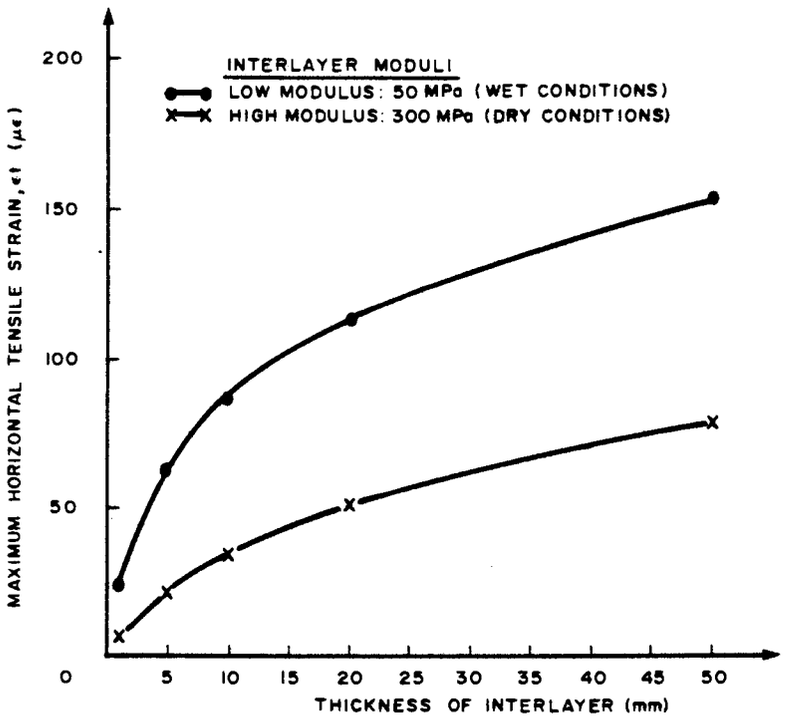

FIGURE 5.9

RELATIONSHIPS BETWEEN THE MAXIMUM HORIZONTAL TENSILE STRAIN AT THE BOTTOM OF THE ASPHALT LAYER AND INTERLAYER THICKNESS

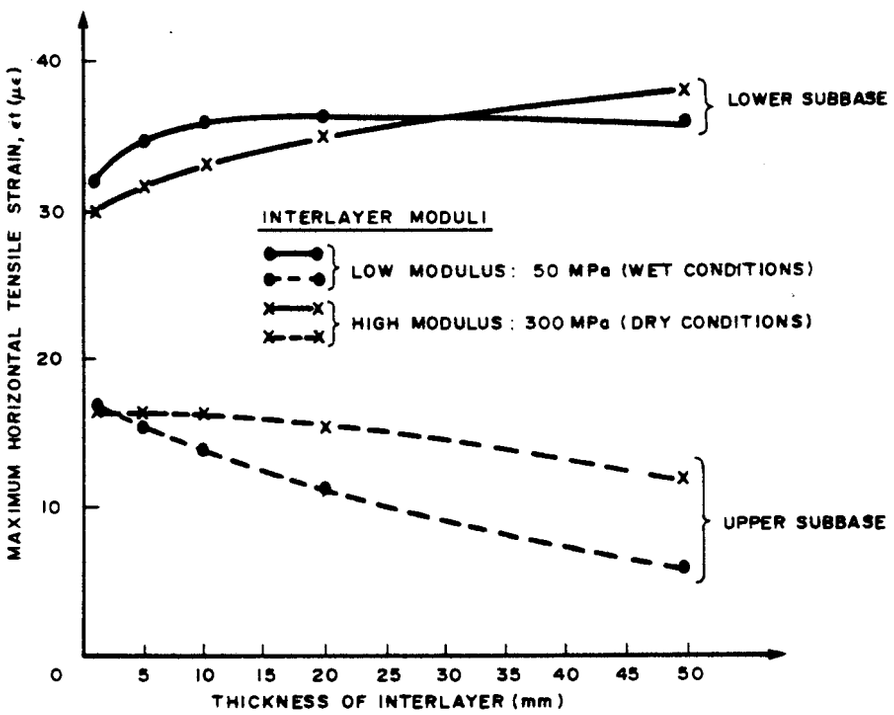

FIGURE 5.10

RELATIONSHIPS BETWEEN THE MAXIMUM HORIZONTAL TENSILE STRAINS AT THE BOTTOM OF THE TWO CEMENTITIOUS LAYERS AND THE THICKNESS OF THE INTERLAYER

cementitious subbase layers when the thickness of the interlayer more than 30 mm thick and relatively soft. It is believed that the soft interlayer acts as a stress absorbing layer thus reducing the deflections (strains) deeper in the structure. The asphalt layer in consequence becomes overstrained.

5.2.2.2 Vertical compressive strain, (ε_v)

The relationships between the vertical compressive strains at the top of both interlayer and the subgrade layer against the thickness of the interlayer are illustrated in Figure 5.11. Very low strain values are experienced by the subgrade layers, both in the wet and dry conditions of the interlayer. On top of the interlayer remarkable strain levels were reached during the wet (50 MPa) state. This becomes serious with interlayer thickness of more than approximately 10 mm. This is an indication of permanent deformation potential of this interlayer. The thicker the interlayer the worse, if wet. This will leads to serious fatigue distress of the asphalt layer, resulting in cracks. Rain water could now enter and will result in consequent further weakening (softening - reducing the modulus) of the interlayer and hence again the asphalt layer.

5.2.2.3 Strain potential

The fatigue distress potentials (Fdp) of the structure with different interlayer thicknesses are illustrated in Figure 5.12. In this case the potential increased rapidly in both wet and dry conditions. The wet condition resulting in strain potentials of 50 to 60 per cent higher than those in the dry state. The figure indicates in general that the thicker the interlayer the higher the fatigue distress potential, both for dry and wet conditions.

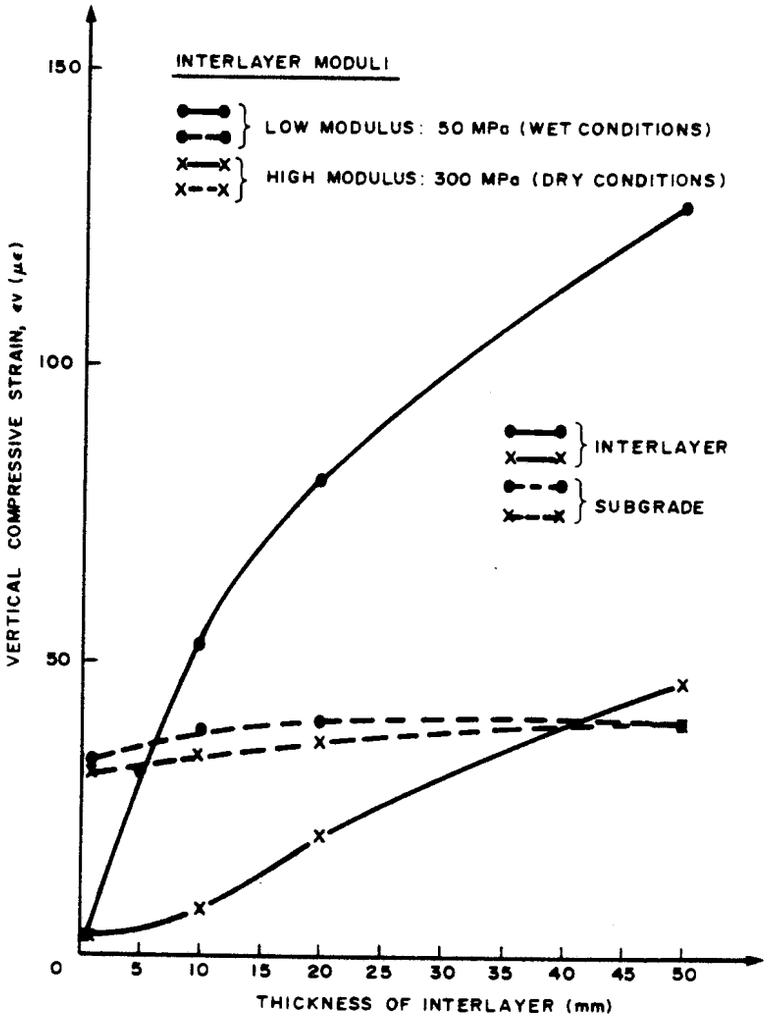

FIGURE 5.11

RELATIONSHIPS BETWEEN THE VERTICAL COMPRESSIVE STRAINS AT TOP OF THE INTER-AND SUBGRADE LAYER AND THE THICKNESS OF THE INTERLAYER

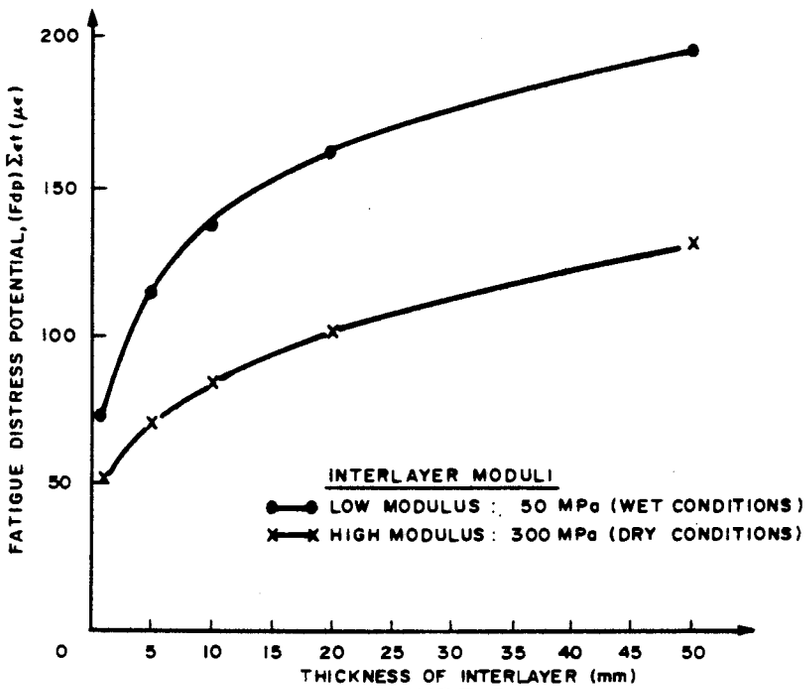

FIGURE 5.12

RELATIONSHIPS BETWEEN FATIGUE DISTRESS POTENTIAL AND THE THICKNESS OF THE INTERLAYER

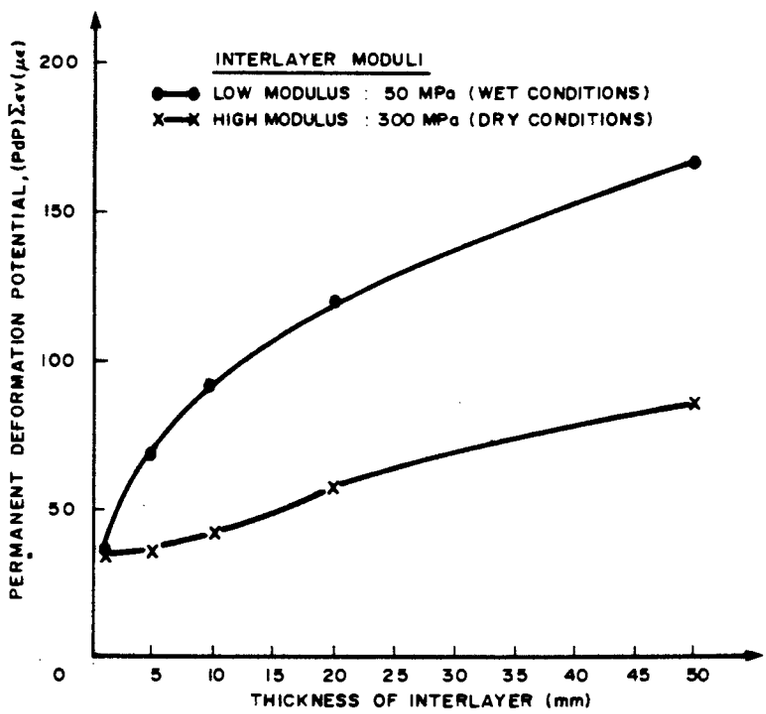

FIGURE 5.13

RELATIONSHIPS BETWEEN THE PERMANENT DEFORMATION STRAIN POTENTIAL AND THE THICKNESS OF THE INTERLAYER

In Figure 5.13, the relationships between permanent deformation potential (Pdp) and thickness of the inter-layer are illustrated. Similar results as with the Fdp were found.

5.3. CONCLUSIONS

From this analitical study it can be concluded that the existence of any interlayer between the upper structural layers of this type of pavement design is detrimental and must be avoided. The thickness of the interlayer and especially its state (dry or wet) is very important. The Fdp and Pdp analyses indicated that the thicker and weaker the interlayer the highest potential for fatigue distress and permanent deformation exists.

It is thus important and the author's belief that interlayers must be avoided especially during the construction process. Layer thickness quality control should be done more carefully. Where cementitious subbase layers are used it is strongly recommended that control of the layer thickness must include the rapid field test for carbonation proposed by Netterberg, 1984. It must be fully understood that this test can identify unstabilized interlayers or carbonated interlayers, including poor mixing (spreading of stabiliser through the layer). It is further important to note that only some materials, not all, weaken as a result of carbonation. This fact is not fully quantified as yet, but is currently being studied in more detail at the NITRR.

This study further emphasizes that one must not only take cognisance of the weakness resulting from interlayers, but also ways and means must be found to optimise the construction processes to narrow the gap between the designed structure and the actual as- built structure. This will lead to even more economical pavement behaviour in future.

5.4 REFERENCES

DE BEER, M (1984(a)). Preliminary investigation of the pumping problem on Section 26 of the N2, Technical Note TP/45/84, NITRR, Pretoria.

DE BEER, M (1984(b)). HVS testing of National Road N2/24, between Illovo and Umgababa, In Natal Figtree - Summary, RP/12/84.

OPPERMAN, R A (1984). Die Swaarvoertuignabootsertoetse (SVN-toetse) op Pad 30, naby Hornsnek. NITRR Technical Note TP/3/84, Pretoria, CSIR, 1984.

DE BEER, M (1984(c)). HVS testing of National Road N2 Section 24 at Umgababa in Natal - Summary, RP/13/84.

FREEME, C R and WALKER, R N (1984 (a)). Economic design of bituminous pavements. Proceedings of 4th Conference on Asphalt Pavements for South Africa, Cape Town, 1984.

NETTERBERG, F (1984). Rapid Field Test for carbonation of lime or cement treated materials. RS/2/84, NITRR, 1984.

FREEME, C R et al (1984 (b)). State of the art on Heavy Vehicle Simulator testing in South Africa. Symposium on Recent findings of Heavy Vehicle Simulator testing, Annual Transportation Convention, Pretoria, 1984.

CHAPTER 6

SUMMARY, DISCUSSION AND RECOMMENDATIONS FOR FURTHER RESEARCH

CONTENTS

6.1 SUMMARY AND DISCUSSION

In this thesis the behaviour of mainly weakly cemented subbase layers in asphalt base pavements is discussed. The behaviour of these layers was studied with the aid of the Heavy Vehicle Simulator (HVS).

It was shown that the maximum horizontal tensile strain (ε_t) criterion is only applicable during the precracked (uncracked) phase of the weakly cemented subbase layers. This phase, however, constitutes less than 10 per cent of the total life of these layers. From this information the importance to quantify the behaviour of these layers in the postcracked (after traffic associated cracking) is realized. Extensive HVS testing on ten different HVS test sections showed that these weakly cemented subbase layers give adequate support to the asphalt base layer provided that;

(i) the subbase moisture condition is relatively dry,
(ii) no soft and wet interlayers exist between the upper layers in the structure,
(iii) initially the cemented layers not in a granulated (poor) state,
(iv) the cemented layers non-erodible (De Beer, 1985),
(v) the slope instabilities are minimized before the construction of the relatively rigid cemented layers,
(vi) adequate and more precise quality control during construction is done to avoid inadequate mixing depth or uncemented interlayers.

If above criteria are met the protection to the subgrade layers is also be adequate for this type of design (bitumen base structures).

Although the concept of equivalent granular state was proposed during the postcracked phase of these layers, the different assumed C and ϕ values (in the granular state) in Chapter 2

were not evaluated for applicability. This is an area for further research.

It was further shown that the relationship between effective elastic modulus of the weakly cemented upper subbase and the traffic loading is approximately hyperbolicly related during the postcracked phase in the dry state. Rapid detoriation (break down or degradation) of the modulus occurred during the excess porewater pressure (EPWP) state. This degradation was found to be linear at approximately 360 MPa per million E80s. It is however over conservative (and incorrect) to assume this rate of degradation for the "total life" of the weakly cemented layers. It is therefore proposed to incorporate alternative wet and dry periods during the "design life" of these layers in Chapter 4. The linear (wet) degradation is used during the wet periods and the hyperbolic (dry) degradation is used during the dry periods. It is however important to note that these calculations are dependant on the expected growth rate, i.e. in E80s, duration of wet periods and dry periods, initial traffic in E80s and the structural design period. The above factors must be assessed by the design engineer. After the calculation of the moduli values, linear elastic simulations can be done in the postcracked phase. The criteria during this state are the current maximum horizontal tensile strain (ε_t), criterion at the bottom of the asphalt base layer and the vertical compressive strain (ε_v) on top of the selected subgrade and subgrade layers. No other criterion is proposed for the weakly cemented layers in the postcracked phase at this stage. It is however believed that durability (erodibility) of the weakly cemented materials is one of the most important parameters to investigate in the future.

A very important aspect resulting from this study is the effect of relatively weak interlayers in this type of pavement design. The highest fatigue distress and permanent distress potentials occurs when the interlayer is positioned between the asphalt base layer and the weakly cemented upper subbase layer. The worst situation occurs when this interlayer is

thick and wet for pavements in this thesis. It is thus of utmost importance to avoid any interlayers in this type of pavement structure. This should be accomplished by adequate quality control and construction methods on site together with chemically stable cementing agents to be used in the weakly cemented materials.

6.2 RECOMMENDATIONS FOR FURTHER RESEARCH

As a result of discussions with Clauss (1982) and Savage (1985) the author belief that the following aspects of weakly cemented (and possibly strongly cemented) materials should be investigated further:

(a) The cementing agent chemistry and basic reactions on different types of weathered materials should be better understood.
(b) The critical factors to ensure stable cement reaction products should be established (organic impurities etc).
(c) The chemical and structural implications of both beneficial and detrimental carbonation.
(d) The rate of increase in the pH of the soil with increase in percentage stabilizer including determination of the initial consumption of lime (ICL) should be measured and analysed for the different weathered materials.
(e) The lime content when cementing reaction products start pozzalanic action to develop should also be established for these materials (cementing lime content, CLC).
(f) The lime content which completes modification, as defined by Clauss (1982) should also be established for these materials. (modification lime content, MLC).
(g) The effect of two phase reactions where lime is added initially to reduce the PI and then later the addition of cement to produce strength. This should be done over a range of delays between the adding of lime and cement; viz 12 hours, 24 hours, etc.
(h) The effects of delayed mixing and compaction on strength and the development non-traffic associated cracking.

(i) The effects of mixing and compaction moisture content which is relatively dry or relatively wet of optimum moisture content.

(j) The effects of particle size and mixing time of weathered soils.

(k) The swell and shrinkage characteristics of weakly cemented materials.

(l) Changes in effective elastic modulus of the weakly cemented materials, especially during the precracked phase.

(m) Erodibility of weakly cemented materials during the excess porewater pressure state (EPWP), both in the precracked and postcracked phases should be quantified. It is the author's belief that erodibility requirements must take precendence over strength requirements in weakly cemented materials in asphalt pavements. It is therefore necessary also to re-evaluate the applicability of existing durability test methods for cementitious materials such as the wet/dry durability test (NITRR, 1979). The possibility of additional new test methods such as the erodibility test (De Beer, 1985). A critical evaluation should be done of the current specifications for cementitious materials in South Africa.

(n) Different mixing and compaction methods to reduce the formation of weak interlayers, including the avoidance of smooth interfaces between the different structural layers in the pavement. The more friction between the layers the better.

6.3 REFERENCES

DE BEER, M (1985). Erodibility test. NITRR Report TP/100/85. New test methods. Pretoria, CSIR, 1985.

CLAUSS, K A (1982). Stabilization properties of dry processed, waste, carbide lime. NITRR Technical Report, RS/2/82 (Unpublished) CSIR, Pretoria, 1982.

SAVAGE, P F (1985). Personal communication.

NATIONAL INSTITUTE FOR TRANSPORT AND ROAD RESEARCH (1979). Standard Methods of Testing Road Construction Materials. Technical Methods for Highways, No. 1, CSIR, Pretoria, RSA. 1979.

APPENDIX A

PHOTOGRAPHIC RECORD OF HVS TESTS

HVS TEST AT MARIANNHILL, N3/1

SECTIONS

1 (215A3)

2 (217A3)

3 (218A3)

(a) Successful recovery of a solid block of stabilized material from the upper stabilized subbase layer.

(b) Successful recovery of a solid block of stabilized material from the lower stabilized subbase layer. Note smooth interfaces between the layers.

Stabilized subbase layers (weathered granite)

(c) Excavated depth profile of the road structure.

PLATE 1:

MARIANNHILL, N3/1: EXCAVATION OF A TEST PIT PRIOR TO HVS TESTING. NOTE THE TWO YELLOW-BROWN STABILIZED WEATHERED GRANITIC SUBBASES UNDERNEATH THE ASPHALT LAYER.

(a) General view of HVS test at Mariannhill, Section 3 (218A3).

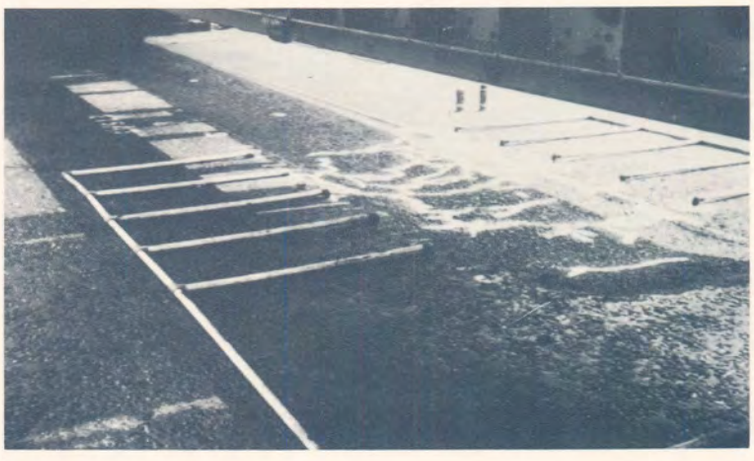

(b) HVS test 1 (215A3): Note the water inlet pipes on the front part of the test section. The white paint indicates the fatigue cracking of the asphalt during the wet test. The uncracked section at the back, is an indication of the surface during dry test conditions. E80s on dry test section: 21 × 10^6.

(c) 21 mm of permanent deformation (rut) on wet section. E80s on wet test section: 0,8 × 10^6.

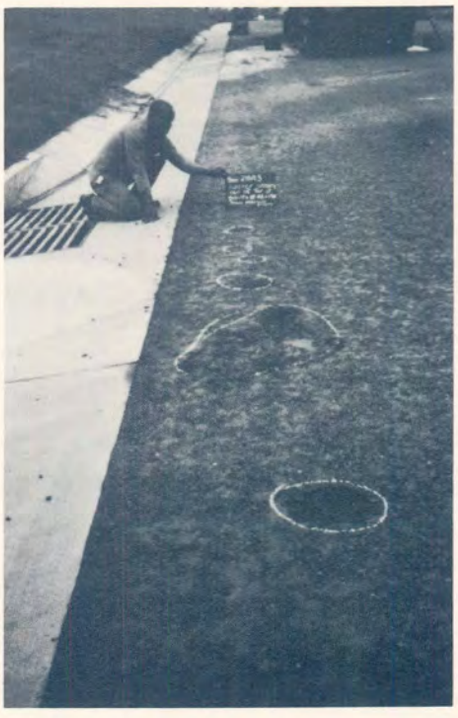

(d) Water seepage from the bottom of the asphalt layer, approximately 30 m from the actual HVS test section, during the wet test. The horizontal slope of the top of the subbase layers runs diagonally from the top right to the bottom left of the photograph.

PLATE 2:
HVS TESTS AT MARIANNHILL ON SECTION 1 (215A3) AND SECTION 3 (218A3).

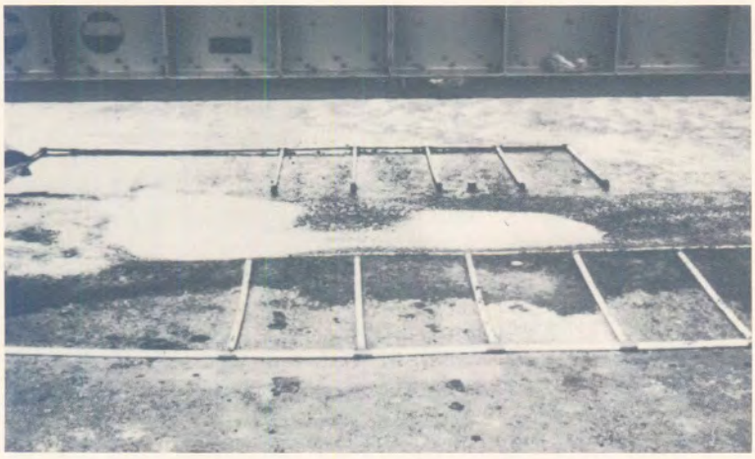

(a) Rutting of Section 1 during wet conditions. (Upper subbase saturated)

(b) Pumping from upper subbase during the wet test.

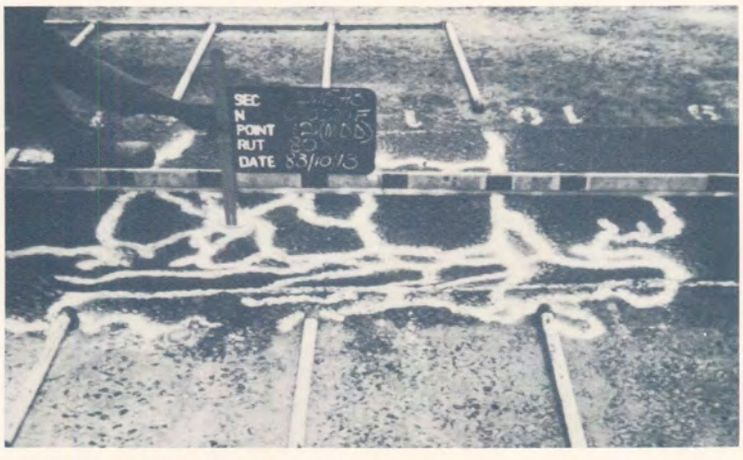

(c) Maximum rut of 80 mm on MDD12. Note the fatigue cracking of the asphalt layer. E80s on wet test section: $6{,}8 \times 10^6$

PLATE 3:
GENERAL VIEW OF THE BEHAVIOUR OF SECTION 1 (215A3), DURING THE WET TEST.

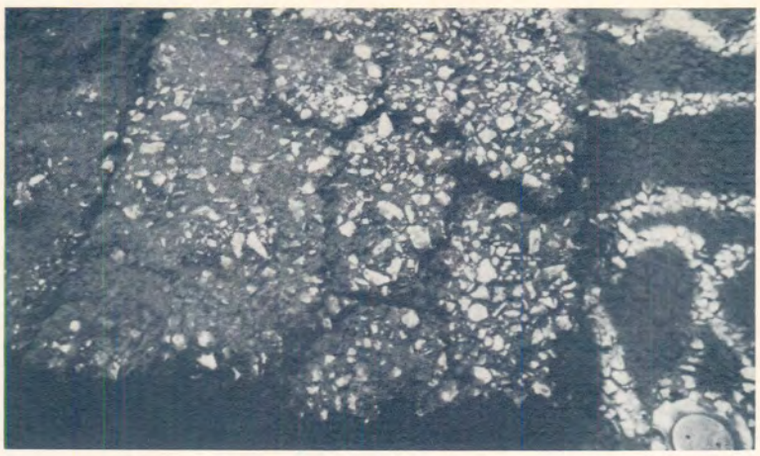

(a) Bottom of asphalt base layer. Note the fatigue cracks and some stripping of asphalt.

(b) Visible cracks on top of the upper stabilized subbase layer after the removal of the asphalt in (a).

(c) Recovered granulated upper subbase material within the trafficked area. Note blocks of the same material recovered from the untrafficked area.

PLATE 4:
EXCAVATED TRENCH ACROSS SECTION 1 AFTER THE WET TEST.

(a) Recovered cracked lower stabilized subbase layer within the trafficked area after the test. (Blocks on top of asphalt)

(b) Printed crack pattern of the bottom of the lower stabilized subbase on the top of the unexcavated selected subgrade layer.

PLATE 5:
EXCAVATED LOWER STABILIZED SUBBASE LAYER ON SECTION 1 AFTER THE WET TEST.

(a) General view of the surface of Section 2 (217A3) after 32 × 10^5 E80s in the dry state.

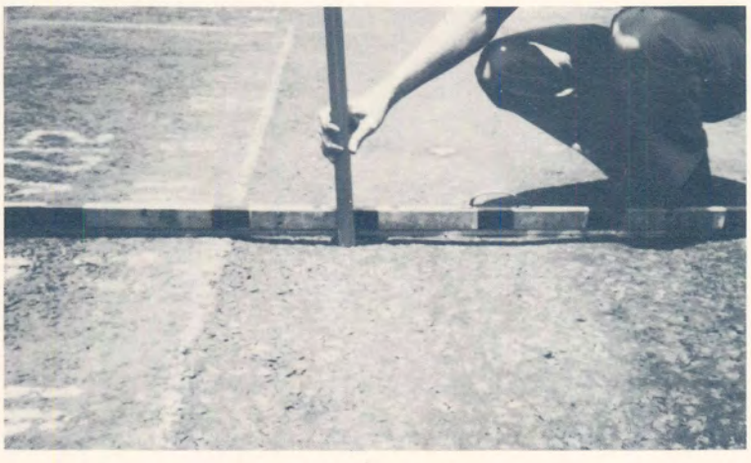

(b) Maximum rut of 20 mm on top of the asphalt layer. Rut originated from the asphalt surfacing and base layer only. (32 × 10^5 E80s)

PLATE 6:

VIEW OF THE SURFACE CONDITION ON SECTION 2 (217A3), AFTER THE HVS TEST IN THE DRY STATE. (NORMAL ENVIRONMENTAL CONDITIONS)

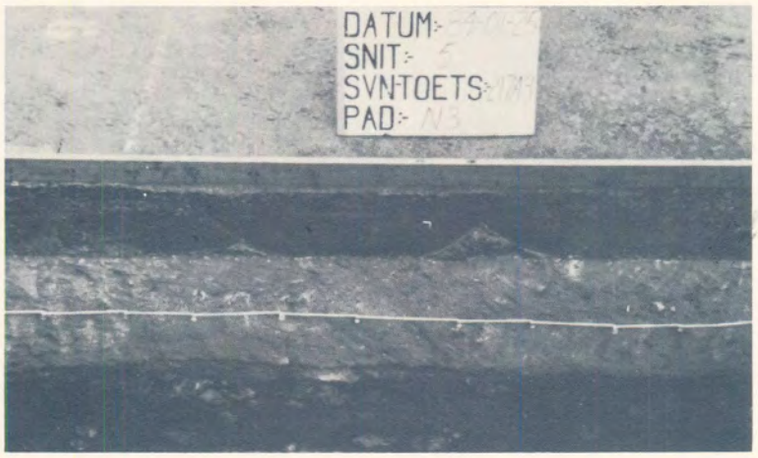

(a) Trench across the test section at the point of maximum rut (20 mm). Note the relatively perfect condition of the stabilized subbase layers, although cracked. (32×10^6 E80s)

(b) Recovered cracked upper stabilized subbase layer after $3{,}6 \times 10^6$ E80s.

PLATE 7:
EXCAVATED TRENCH ACROSS SECTION 2 (217A3) AFTER THE DRY TEST.

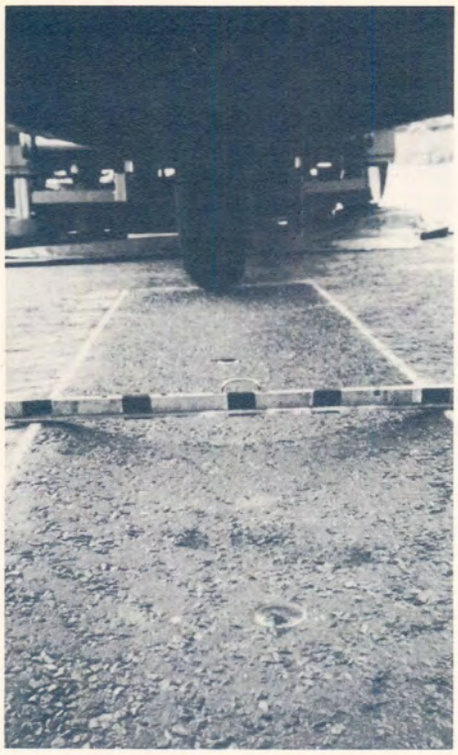

(a) General view of the surface of the test section after 32 000 actual repetitions with the single wheel load at 150kN. (Contact pressure: 1445kPa)

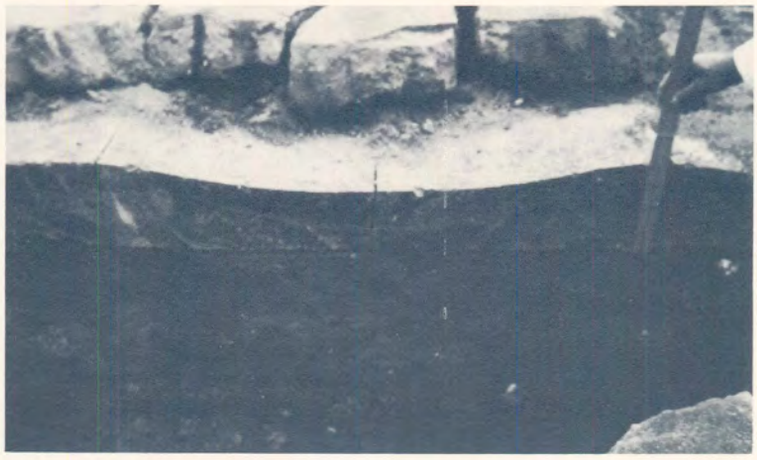

(b) Trench across test section after test. Note the excessive asphalt deformation, and the minimum amount of rut on top of the upper stabilized subbase. (No carbonation within stabilized subbase layers.)

PLATE 8:
HIGH SINGLE WHEEL LOAD TEST ON SECTION 3 (218A3) IN THE DRY STATE.

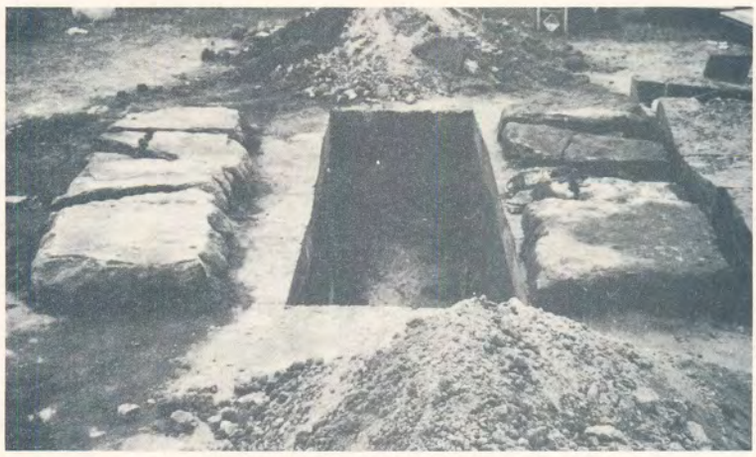

(a) General view of the recovered blocks of subbase material. Upper subbase on the right, lower subbase on the left.

Lower subbase →

Upper subbase →

(b) Note the relatively smaller blocks of recovered upper stabilized subbase material, due to fatique cracking and fracturing. The lower stabilized subbase experienced only fatigue cracking, hence the bigger blocks of material.

PLATE 9:

EXCAVATED TRENCH ACROSS TEST SECTION 3 (218A3), AFTER THE HIGH SINGLE WHEEL LOAD TEST.

HVS TESTS AT "FIGTREE", N2/24

SECTIONS

1 (223 A3)

2 (224 A3)

(a) View of HVS site on the fast lane of the south bound carriageway. Note the settlement cracks.

(b) General view of test on SECTION 1. Note the water inlet pipes on the side of the test section.

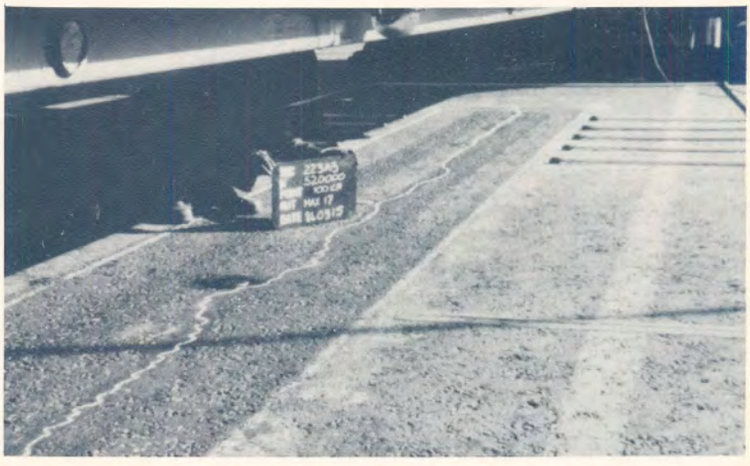

(c) Longitudinal crack on SECTION 1.

(d) Maximum permanent deformation of 17 mm after 520 000 repetitions of a 100kN dual wheel load (20 ME80s).

PLATE 1: FIGTREE, N2/24: General view of the HVS site and test sections. Note the longitudinal settlement cracks on both the site and test sections.

(a) Maximum permanent deformation of 38 mm at the crack after water introduction.

(b) Relative position of MDD8 on SECTION 1.

(c) Start of water pumping from the bottom of the crack on SECTION 1.

PLATE 2: Longitudinal crack and water introduction on SECTION 1.

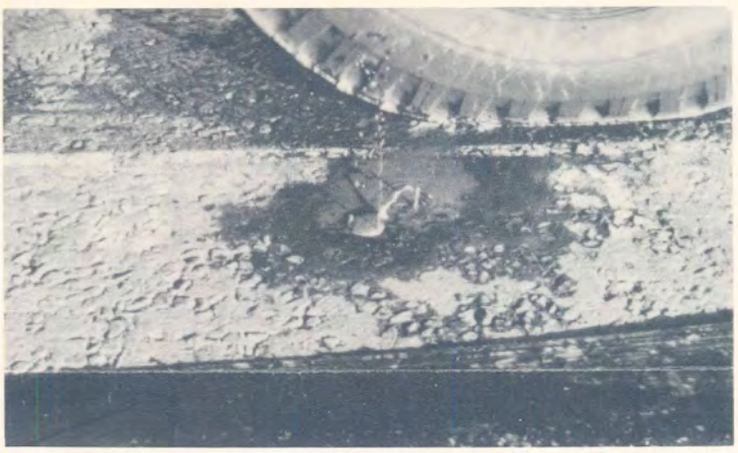

(a) Pore pressure release through nuclear moisture and density measuring hole, next to the HVS test section.

(b) Fines starting to pump through the longitudinal crack.

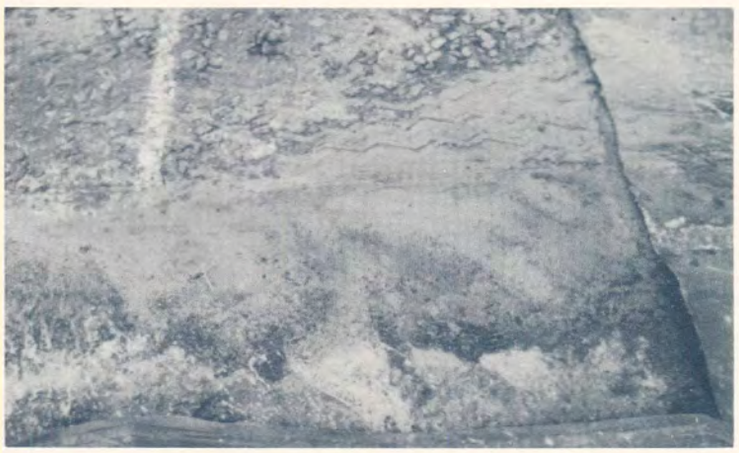

(c) Fines on the side of the test section after the "saturated" test.

PLATE 3: Pumping of fines from the upper lime-stabilized subbase layer (weathered Granite) on SECTION 1.

(a) Excavated test pit across the crack indicating that the crack exists in all the layers of the road structure.

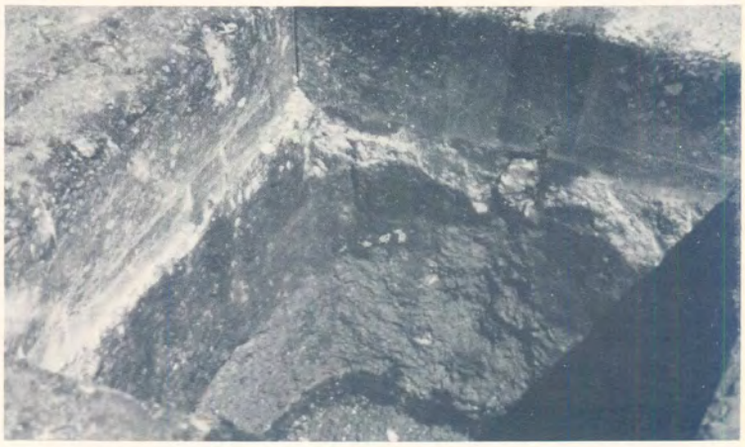

(b) Relative low pH zone at the position of the crack (dark red colour – high pH zone), determined with Phenolthalien.

(c) Note the discolouring on the side of the block next to the crack.

PLATE 4: TEST PIT across the longitudinal crack, between the two test sections.

(a) Face of the test pit, indicating the moisture regime at the position of the crack (point 1,0 on straight-edge). The light brown colour is the well-stabilized weathered Granite subbase layers.

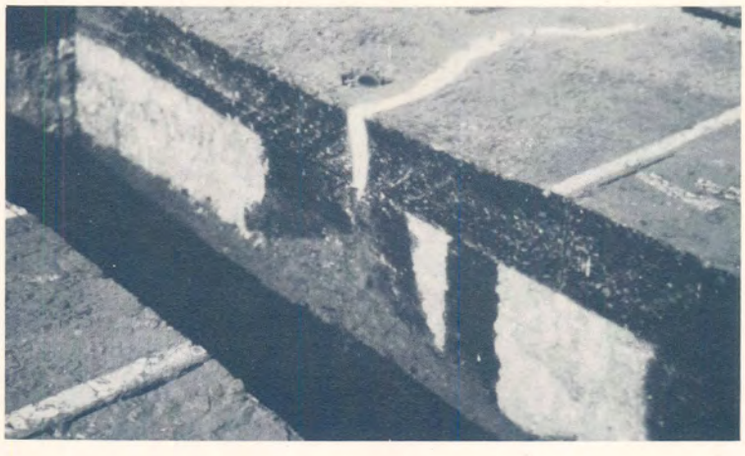

(b) Relative low pH zone at the position of the crack and the bottom of the lower subbase layer. This zone was carbonated, determined with HCL solution. The dark red area is the relative high pH zone.

PLATE 5: Excavated trench across SECTION 1 between measuring points 3 and 4.

(a) Moisture regime at the crack at measuring point 12 on SECTION 1.

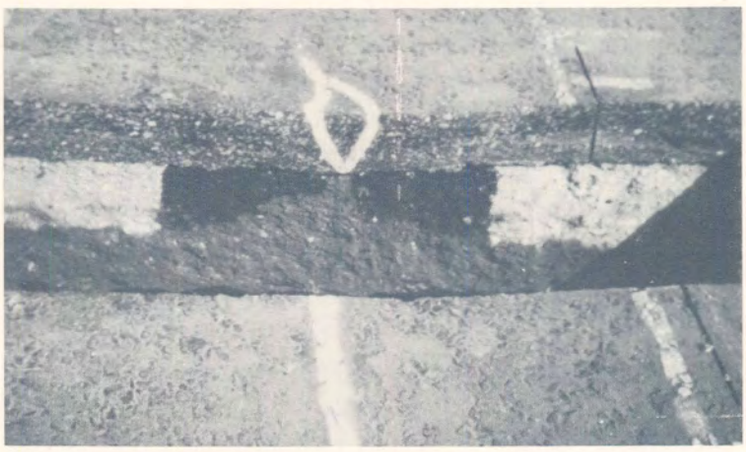

(b) Moisture regime (carbonated) at measuring point 19 on SECTION 2.

PLATE 6: Excavated trenches at measuring points 12 and 19 on SECTION 1 and 2 respectively.

(a) General view of section positions of the two trenches on section 1 and the recovered subbase material.

(b) Recovered upper subbase after 20,6 ME80s. (Semi-saturated). Note the position of the longitudinal crack. The other cracks are traffic associated. (Measuring points 3 to 4).

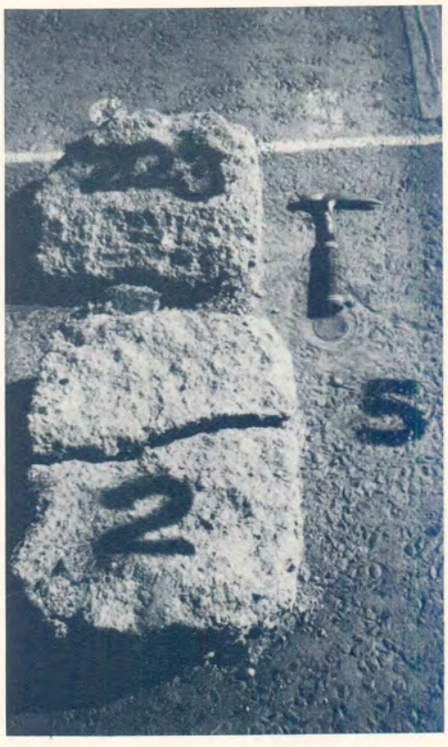

(c) Recovered lower subbase after 20,6 ME80s (Semi-saturated.) The two cracks are non-traffic associated. This layer was partially carbonated. (Measuring points 3 to 4).

PLATE 7: Recovered stabilized subbase layers on SECTION 1.

(a) Recovered upper subbase after 20,6 ME80s on SECTION 1 (saturated). Layer cracked and fractured (Measuring points 11 to 12).

(b) Recovered lower subbase layer after 20,6 ME80s on SECTION 1 (saturated) at measuring points 11 to 12.

(c) General view of recovered subbase layers on SECTION 2.

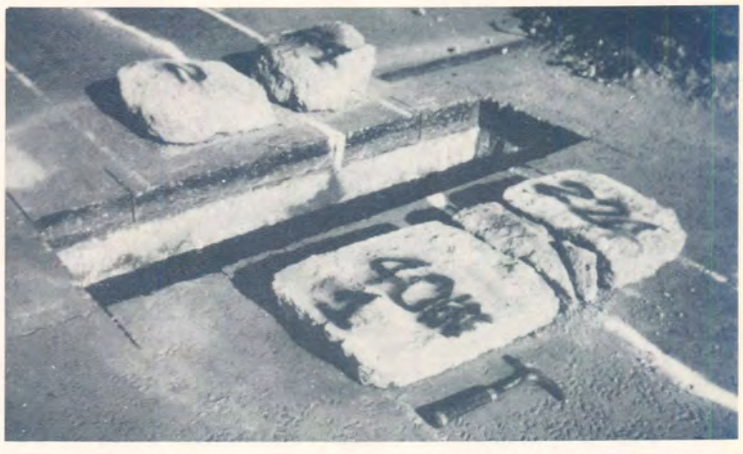

(d) Recovered upper and lower subbase layers from SECTION 2, measuring points 3 to 4, after 280 494 E80s. Note, only non-traffic associated cracks in the blocks.

PLATE 8: Recovered subbase layers from both TEST SECTIONS 1 and 2.

(a) Upper subbase layer cracked and fractured after 17 255 repetitions with 150 kN single wheel load.

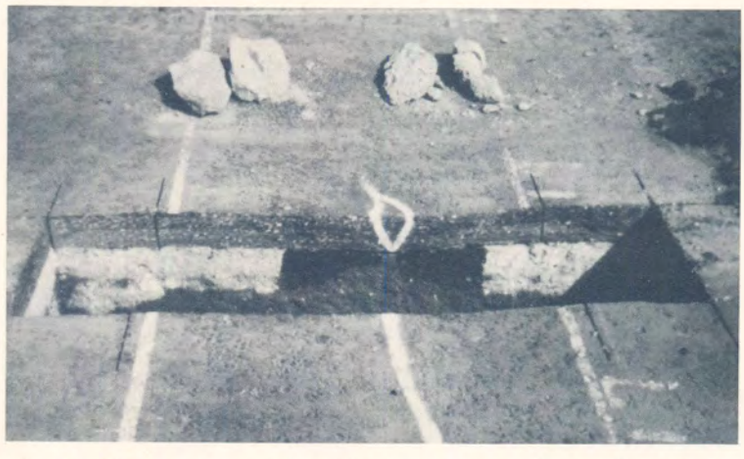

(b) Few blocks recovered from the lower subbase layer. The rest of the layer was soft, granulated and carbonated. Repetitions 17 255 with 150 kN single wheel load.

PLATE 9: Recovered subbase layers between measuring points 18 and 19 on SECTION 2 after 150 kN test during the "dry" conditions.

HVS TESTS AT UMGABABA, N2/24

SECTIONS

1 (227A3)

2 (259A3)

(a) Famous Berea Red Sand in a cutting at Umgababa HVS site.

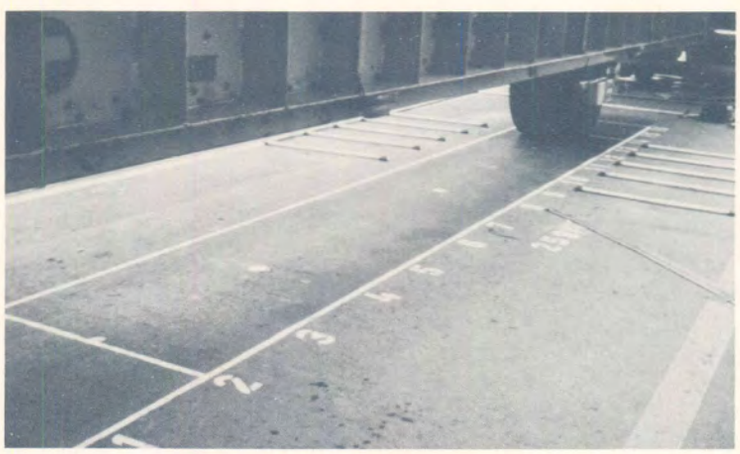

(b) Typical Surface condition of Section 2 in the dry state.

(c) Surface condition of Section 2 after Excess Pore Water Pressure (EPWP) state.

PLATE 1 : Berea Red Sand at Umgababa and the surface condition of Section 2.

(a) Surface condition of Section 1 after the EPWP state, (62 mm rut after 2067 repetitions at (100kN) Note the white water inlet pipes both sides of the Section.

(b) Pumping on Section 2 through MDD hole at measuring point 12 and longitudinal cracks.

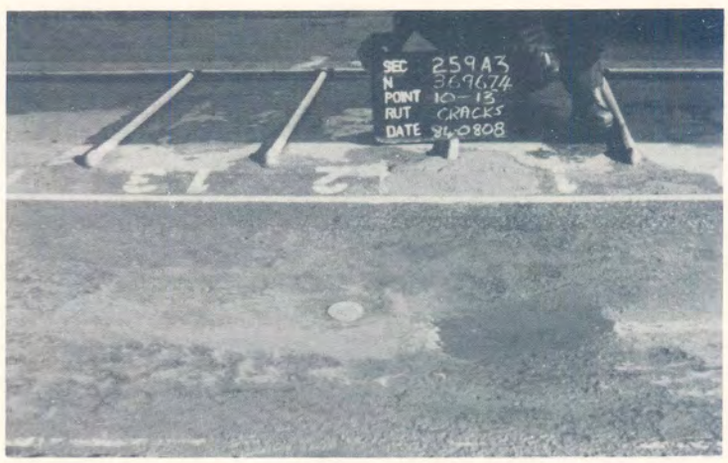

(c) Overhaul view of Section 2 after testing in the EPWP state.

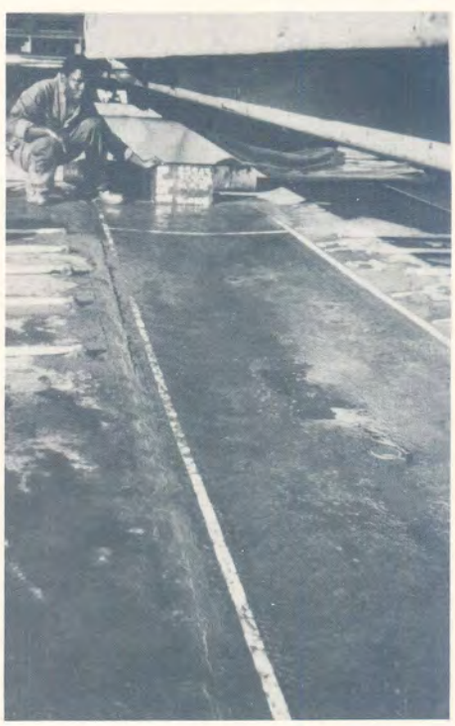

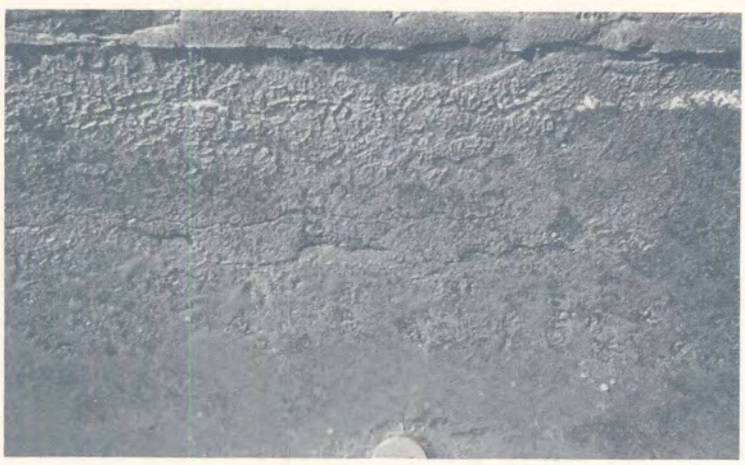

(d) Pumping through longitudinal fatigue crack on Section 2.

PLATE 2 : Pumping during the EPWP state on Sections 1 and 2.

(a) Cross Profiles made across Section 1 after HVS trafficking. NOTE the deformation and recovered stabilized Berea Red subbase material (cracked).

(b) Sideways (horizontal) pumping (erosion) of the lime treated Berea Red upper subbase at the bottom of the heaved asphalt on Section 1.

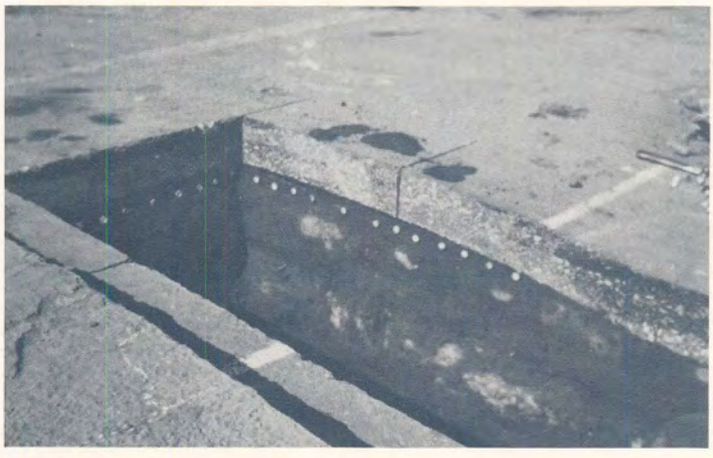

(c) White markers indicate top of upper subbase on Section 1. Above white markers is the soft pumped layer.

(d) Phenoltalien indication of relative high pH on the top of the upper subbase and the pumped layer.

PLATE 3 : Cross profiles made to study the failure mechanism at Umgababa.

(a) Cross profile across the test Section 1. Note the heaving of the asphalt as a result of the erosion action inside the trafficked area during the EPWP state.

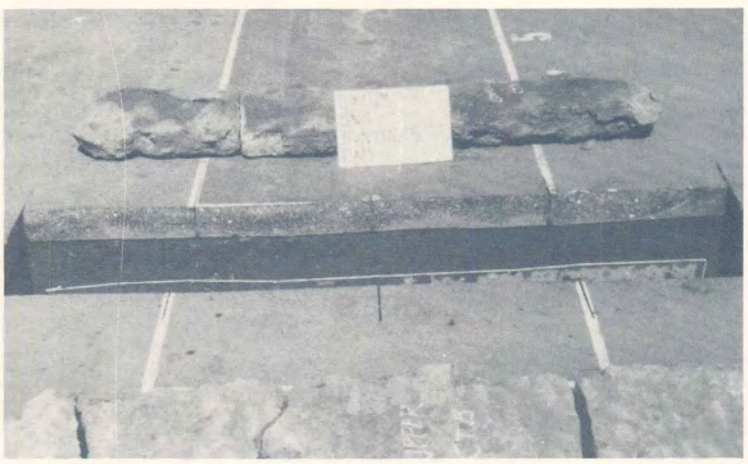

(b) Cross profile on Section 2 after the dry state. No deformation recorded on road surface.

PLATE 4 : Cross profiles on Section 1 and 2 after the EPWP and dry states, respectively.

(a) Cross profile after EPWP on Section 2. Note the thinner subbase inside the trafficked area.

(b) Recovered upper subbase material from Section 2. Note the thinner subbase inside the trafficked area.

(c) Phenolthalien indication of continious relative high pH within both the upper and lower stabilized subbase layers.

PLATE 5 : Cross profiles on Section 2.

(a) Fatigue cracking at the bottom of the asphalt base layer after the EPWP state on Section 2.

(b) Real road failure next to Section 2 in the normal trafficked lane during the time of HVS testing on Section 2.

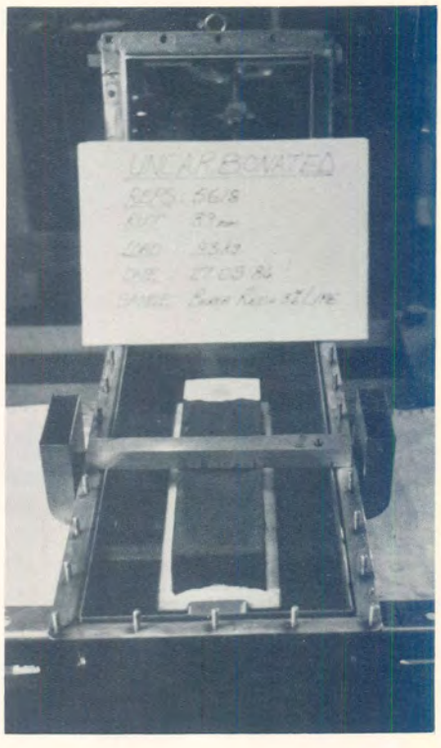

(c) Typical specimen of Berea Red material (recovered at Umgababa), after testing in the new Erosion test at NITRR.

PLATE 6 : Fatigue, real road failure and Erosion test specimen.

HVS TESTS AT VAN REENENS PASS, N3/6

SECTIONS

1 (233A3)

2 (234A3)

3 (235A3)

A.

B.

PLATE 1: Slope instabilities on National Route N3, at Van Reenens Pass. Note the crack width and the horisontal permanent deformation showed by the yellow line in photograph B.

A. UPPER SUBBASE

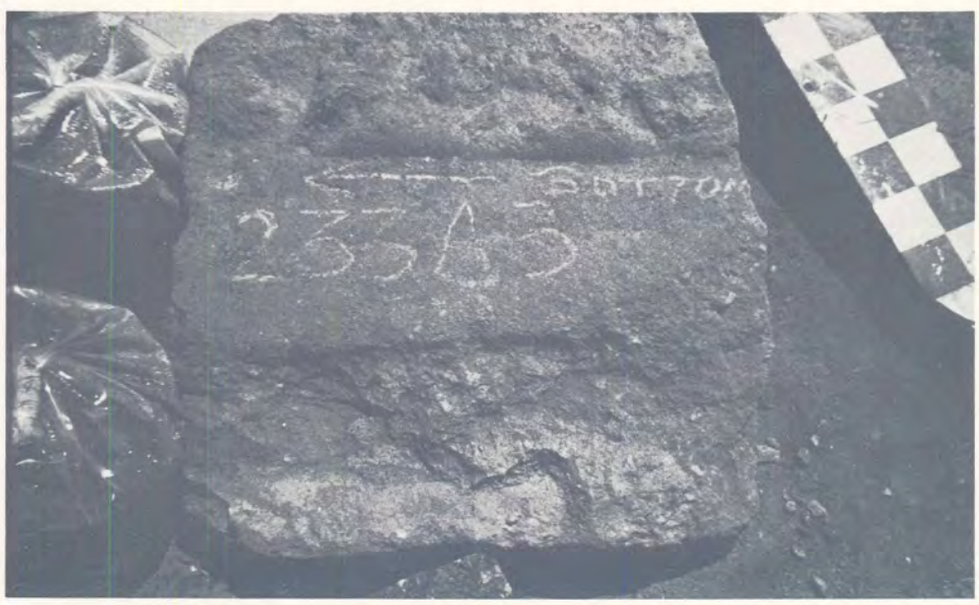

B. LOWER SUBBASE

PLATE 2: Upper and lower subbase material recovered from the test pit at Section 1 before any HVS trafficking. Note the white spots of badly mixed stabiliging agent in the upper subbase. The lower subbase show better cementing.

A.

B.

PLATE 3: **A.** Fatigue cracks on the surface of Section 1 after 279 795 actual repetitions of a 70 kN dual wheel load.

B. Closing of cracks at the surface after high temperatures applied to the road surface. Note the permanent deformation on the upper right of the photograph on the test section. The final actual repetitions of a 70 kN dual wheel load was 370 000, and the rut was 20 mm.

A.

B.

C.

PLATE 4:

A. Chemical phenol-test indicate well stabilized lower subbase, and poor stabilized upper subbase on Section 1.

B. Cross section profile on Section 1 after HVS test. Note the irregularities at the layer interfaces, and also the two recycled asphalt layers above the upper subbase.

C. Temperature rut at measuring point 8 on HVS Test Section 1. Note that most of the deformation was caused in the wearing course and not in the recycled asphalt base layer.

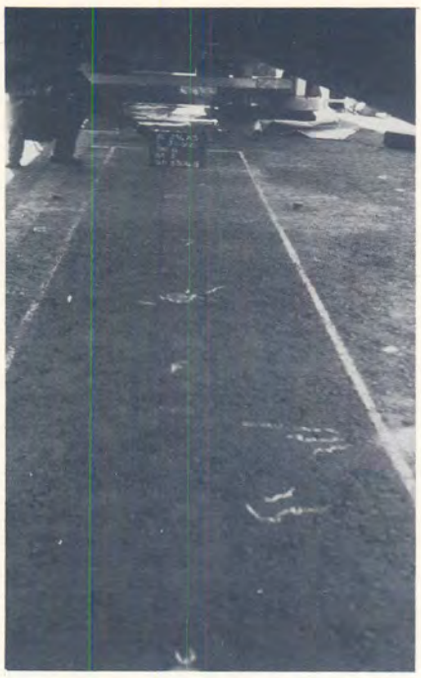

A.

B.

C.

D.

PLATE 5: Fatigue crack growth on HVS Test Section 2.

A. Fine hair cracks after 30 000 repetitions of a 70kN dual wheel load.

B. Sudden crack appearance on the surface after 100 000 repetitions of a 70 kN, and 201 488 repetitions of a 100 kN dual wheel load on Section 2.

C. Increased crack growth after 316 153 total repetitions.

D. Major increase in crack growth from 316 153 to 319 153 total repetitions.

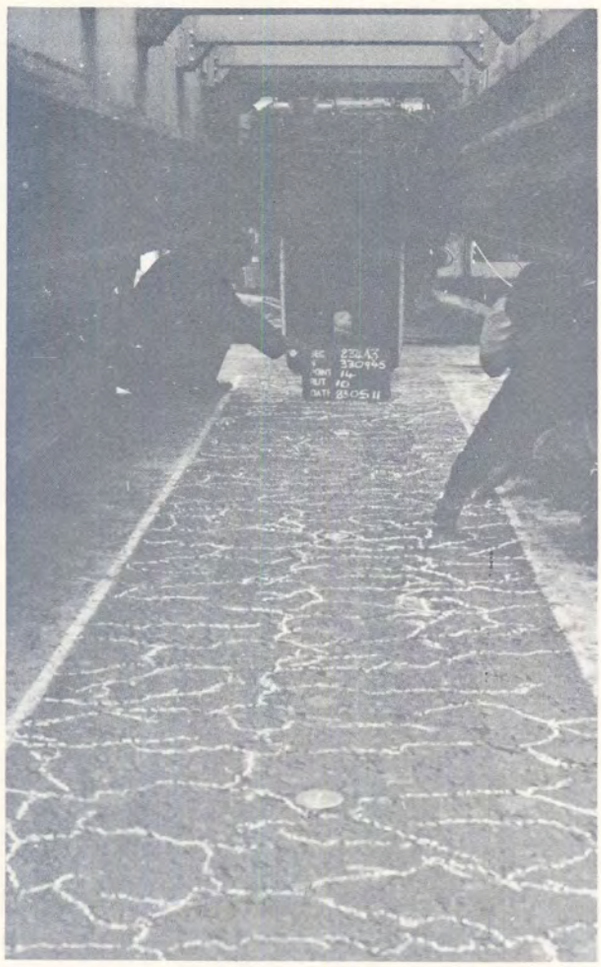

A.

B.

PLATE 6: **A.** Further increase in crack growth after 330 945 total repetitions. Surface water introduced at 330 945.

B. Crack pattern after 396 979 total repetitions. Note zero rut increase from 330 945 to 396 979 total repetitions, under wet surface conditions.

A.

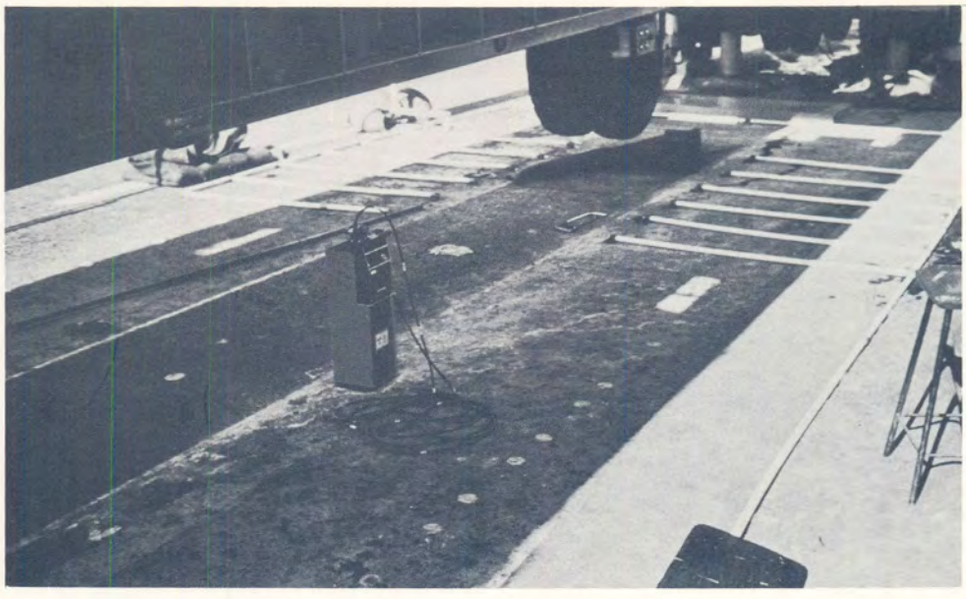

B.

PLATE 7: Surface and subsurface water introduced on Section 2 after 396 979 total repetitions.

A. Water fed-pipes for subsurface water, both sides of the lower end of the test section. Inlet-depth 440 mm.

B. Pumping of fines from the upper subbase through the cracks on the total test section.

A.

B.

C.

PLATE 8: **A.** Final crack pattern and permanent deformation on Test Section 2.

B. Longitudinal cracks on edge of Test Section 2 at point 9, where a local rut of 89 mm was formed.

C. Stripping and total failure of the upper recycled asphalt base layer, where poor aggregates was used.

A.

B.

C.

PLATE 9: FINAL CRACK PATTERN ON SECTION 2:

A. Final crack pattern on Section 2. Note the different block sizes of the cracks on the two halves of the test section. Note also the markers on the local rut areas.

B. Final crack pattern where surface and subsurface water was introduced (big and small blocks). Note the end test pit on the top of the photograph.

C. Final crack pattern where only surface water was introduced (big blocks).

A.

B.

C.

PLATE 10: **A.** Final crack pattern at the MDD at measuring point 8. On the left only surface water, and on the right surface and subsurface water was added.

B. Local rut of 65 mm at measuring point 6 (surface water).

C. Local rut of 89 mm at measuring point 9 (surface and subsurface water). Note the big blocks.

A.

B.

PLATE 11: **A.** Note the three layers in the asphalt. From top to bottom is the 40 mm wearing course and the two 50 mm recycled base layers. Note the middle layer of lighter colour. This is the weak zone in the base layer because of poor aggregates.

B. Fines pumped horisontally into the end test pit. Note the horisontal crack in the weak asphalt layer. Fines was pumped out of this horisontal crack as well as between the upper subbase and base, and between the two subbases.

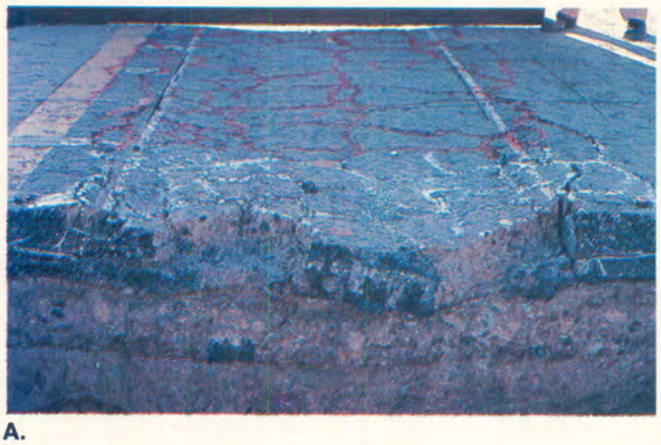

A.

B.

C.

D.

PLATE 12: CROSS PROFILES:

A. Cross profile on Section 2 at the end of the HVS test showing the vertical cracks from top to bottom where fines was pumped out to the surface. Note the stripping in the base layer on the left.

B. Weak zone start to fail forming smaller block sizes. The bottom of the base layer was not cracked and no fines allowed to migrate to the surface.

C and D: Weak zone stripped and failed. Note the fines at the interface of the recycled layers.

APPENDIX B

INPUT PROGRAM TO PLOT THE THREE DIMENSIONAL BEHAVIOURAL MODEL

B1. Input program

In order to plot the behavioural model in three dimensions, the computer program, DISSPLA, available at the Computer Centre at CSIR, was used. This progrm needs an input program (data) in a certain printout of the program MODEL is given in the following section. The parameters XX, YY and ZZ referred to Radius of Curvature, (RC), Elastic Modulus, (E) and Road Surface Deflection, (RSD), respectively. In the program equations 3.2 and 3.3 (see Section 3.2.14) are used to calculate the elastic modulus and road surface deflection, using the radius of curvature as input starting from 50 m to 940 m in steps of 10 m.

```
   PROGRAM MODEL       74/750  OPT=2,ROUND= A/ S/ M/-D,-DS      FTN 5.1+547          85/01/25. 08.48.04        PAGE      1
DO=-LONG/-OT,ARG=-COMMON/-FIXED,CS= USER/-FIXED,DB=-TB/-SA/-SL/-ER/-ID/-PMD/-ST,PL=50000
FTN5,I=MODEL,L=L.

      1                PROGRAM MODEL(INPUT,OUTPUT)
      2           C
      3                DIMENSION XX(811),YY(811),ZZ(811)
      4                DIMENSION NINCH(2)
      5           C
      6                WRITE(6,900)
      7                NPUNTE=90
      8                X=50.
      9                DO 10 I=1,NPUNTE
     10                     YY(I) = 5.52787639 **X  +2.51021E-03 * X * X
     11                     XX(I) = X
     12                     ZZ(I) =  1.064 * 136000. /X  - 1.563E-04 *136000/X*136000/X
     13                     WRITE(6,910) XX(I),YY(I),ZZ(I)
     14                     X = X + 10.
     15               10 CONTINUE
     16           C
     17                CALL CALCMP(NINCH,'P2967',10)
     18           C**       CALL TK41(41113)
     19                CALL UNITS('MM')
     20                CALL MX1ALF('L/CSTO','/')
     21                CALL MX2ALF('STAND','*')
     22                CALL PAGE(300.,210.)
     23                CALL INTAXS
     24                CALL PHYSOR(10.,10.)
     25                CALL AREA2D(290.,200.)
     26                CALL X3NAME('*RADIUS OF CURVATURE,RC(/M)$',100)
     27                CALL Y3NAME('*EFFECTIVE ELASTICE MODULUS(MPA)$',100)
     28                CALL Z3NAME('*ROAD SURFACE DEFLECTION,RSD(/MM)$',100)
     29                CALL VOLM3D(1.,7.5,2.)
     30                CALL VUA6S(30.,-31.,23.)
     31                CALL GRAF3D(0.,200.,1000.,0.,500.,7500.,0.,200.,2000.)
     32                CALL CURV3D(XX,YY,ZZ,NPUNTE,0)
     33           C      XY-VLAK
     34                CALL GRFITI(0.,0.,0.,1.,0.,0.,0.,1.,0.)
     35                CALL AREA2D(1.,7.5)
     36                CALL GRAF(0.,200.,1000.,0.,500.,7500.)
     37                CALL CURVE(XX,YY,NPUNTE,0)
     38                CALL END3GR(0)
     39           C      YZ-VLAK
     40                CALL GRFITI(0.,0.,0.,0.,1.,0.,0.,1.,1.)
     41                CALL AREA2D(7.5,2.)
     42                CALL GRAF(0.,500.,7500.,0.,200.,2000.)
     43                CALL CURVE(YY,ZZ,NPUNTE,0)
     44                CALL END3GR(0)
     45           C      XZ-VLAK
     46                CALL GRFITI(0.,0.,0.,1.,0.,0.,1.,0.,1.)
     47                CALL AREA2D(1.,2.)
     48                CALL GRAF(0.,200.,1000.,0.,200.,2000.)
     49                CALL CURVE(XX,ZZ,NPUNTE,0)
     50                CALL END3GR(0)
     51           C      Z-RIGTING
     52                CALL SETCLR('RED')
     53                DO 20 I = 1,NPUNTE,5
     54                     CALL RLVEC3(XX(I),YY(I),0.,XX(I),YY(I),ZZ(I),0)
     55               20 CONTINUE
```

```
      C     Y-RIGTING
            CALL SETCLR('GREEN')
            DO 30 I = 1,NPUNTE,5
               CALL RLVEC3(XX(I),0.,ZZ(I),XX(I),YY(I),ZZ(I),0)
         30 CONTINUE
      C     X-RIGTING
            CALL SETCLR('BLUE')
            DO 40 I = 1,NPUNTE,5
               CALL RLVEC3(0.,YY(I),ZZ(I),XX(I),YY(I),ZZ(I),0)
         40 CONTINUE
            CALL SETCLR('WHITE')
            CALL RLVEC3(0.,0.,2000.,0.,7500.,2000.,0)
            CALL RLVEC3(1000.,0.,2000.,0.,0.,2000.,0)
            CALL RLVEC3(1000.,0.,2000.,1000.,7500.,2000.,0)
            CALL RLVEC3(1000.,7500.,2000.,1000.,7500.,0.,0)
            CALL RLVEC3(1000.,7500.,2000.,0.,7500.,2000.,0)
            CALL RLVEC3(1000.,0.,2000.,1000.,0.,0.,0)
            CALL DASH
            CALL RLVEC3(0.,0.,0.,0.,7500.,0.,0)
            CALL RLVEC3(0.,7500.,0.,0.,7500.,2000.,0)
            CALL RLVEC3(0.,7500.,0.,1000.,7500.,0.,0)
      C
            CALL ENDPL(0)
            CALL DONEPL
            STOP
        900 FORMAT('1',/,7X,'X',14X,'Y',14X,'Z')
        910 FORMAT(3F15.5)
            END
```

--VARIABLE MAP--(LO=A)

-NAME-	--ADDRESS--	--BLOCK--	----PROPERTIES----	----TYPE----	--SIZE--	-NAME-	--ADDRESS--	--BLOCK--	----PROPERTIES----	----TYPE----	--SIZE--
I	55178			INTEGER		XX	7128			REAL	811
NINCH	55138			INTEGER	2	YY	23658			REAL	811
NPUNTE	55158			INTEGER		ZZ	40408			REAL	811
X	55168			REAL							

--PROCEDURES--(LO=A)

-NAME-	----TYPE----	--ARGS--	--CLASS--	-NAME-	----TYPE----	--ARGS--	--CLASS--
AREA2D		2	SUBROUTINE	MX1ALF		2	SUBROUTINE
CALCMP		3	SUBROUTINE	MX2ALF		2	SUBROUTINE
CURVE		4	SUBROUTINE	PAGE		2	SUBROUTINE
CURV3D		5	SUBROUTINE	PHYSOR		2	SUBROUTINE
DASH		0	SUBROUTINE	RLVEC3		7	SUBROUTINE
DONEPL		0	SUBROUTINE	SETCLR		1	SUBROUTINE
ENDPL		1	SUBROUTINE	UNITS		1	SUBROUTINE
END3GR		1	SUBROUTINE	VOLM3D		3	SUBROUTINE
GRAF		6	SUBROUTINE	VUABS		3	SUBROUTINE
GRAF3D		9	SUBROUTINE	X3NAME		2	SUBROUTINE
GRFITI		9	SUBROUTINE	Y3NAME		2	SUBROUTINE
INTAXS		0	SUBROUTINE	Z3NAME		2	SUBROUTINE

```
--STATEMENT LABELS--(LO=A)
 -LABEL-ADDRESS-----PROPERTIES----DEF        -LABEL-ADDRESS-----PROPERTIES----DEF

      10   INACTIVE    DO-TERM          15          40   INACTIVE    DO-TERM          65
      20   INACTIVE    DO-TERM          55         900     3428      FORMAT           81
      30   INACTIVE    DO-TERM          60         910     3468      FORMAT           82


--ENTRY POINTS--(LO=A)
 -NAME---ADDRESS--ARGS---

  MODEL       138       0


--I/O UNITS--(LO=A)
 -NAME--- PROPERTIES-------------

  TAPE6    FMT/SEQ


--STATISTICS--

  PROGRAM-UNIT LENGTH              5524B =  2900
  CM STORAGE USED                 51000B = 25088
  COMPILE TIME                    0.309 SECONDS
```

TABLE B2 - Calculated E and RSD values for the different RC values

RC (m)	E (MPa)	RSD (μm)
X	Y	Z
50.00000	282.66934	1663.72608
60.00000	340.70934	1557.32089
70.00000	399.25138	1439.46841
80.00000	458.29546	1328.19300
90.00000	517.84158	1228.08336
100.00000	577.88974	1139.45152
110.00000	638.43994	1061.28555
120.00000	699.49219	992.26356
130.00000	761.04648	931.10267
140.00000	823.10281	876.66710
150.00000	885.66118	827.98734
160.00000	948.72160	784.24825
170.00000	1012.28406	744.76800
180.00000	1076.34855	708.87640
190.00000	1140.91510	676.39543
200.00000	1205.98368	646.62288
210.00000	1271.55430	619.31871
220.00000	1337.62697	594.19412
230.00000	1404.20168	571.00256
240.00000	1471.27843	549.53256
250.00000	1538.85722	529.60184
260.00000	1606.93806	511.05259
270.00000	1675.52093	493.74753
280.00000	1744.60585	477.56678
290.00000	1814.19281	462.40517
300.00000	1884.28182	448.17017
310.00000	1954.87288	434.77897
320.00000	2025.96595	422.16206
330.00000	2097.56108	410.25183
340.00000	2169.65825	398.99200
350.00000	2242.25746	388.33074
360.00000	2315.35872	378.22188
370.00000	2388.96201	368.62378
380.00000	2463.06735	359.49886
390.00000	2537.67473	350.81312
400.00000	2612.78416	342.53572
410.00000	2688.39562	334.63864
420.00000	2764.50913	327.08834
430.00000	2841.12468	319.88553
440.00000	2918.24227	312.98489
450.00000	2995.86190	306.37489
460.00000	3073.98358	300.03760
470.00000	3152.60729	293.95652
480.00000	3231.73305	288.11647
490.00000	3311.36085	282.50344
500.00000	3391.49070	277.10446
510.00000	3472.12258	271.90756
520.00000	3553.25651	266.90161
530.00000	3634.89248	262.07631
540.00000	3717.03049	257.42207
550.00000	3799.67054	252.92997
560.00000	3882.81263	248.59169
570.00000	3966.45677	244.39949
580.00000	4050.60295	240.34612
590.00000	4135.25117	236.42481
600.00000	4220.40143	232.62921
610.00000	4306.05374	228.95339
620.00000	4392.20809	225.39177
630.00000	4478.86447	221.93912
640.00000	4566.02291	218.59052
650.00000	4653.68338	215.34134
660.00000	4741.84589	212.18722
670.00000	4830.51045	209.12407
680.00000	4919.67705	206.14800
690.00000	5009.34569	203.25536
700.00000	5099.51637	200.44268
710.00000	5190.18910	197.70672
720.00000	5281.36386	195.04436
730.00000	5373.04067	192.45268
740.00000	5465.21952	189.92892
750.00000	5557.90042	187.47043
760.00000	5651.08335	185.07471
770.00000	5744.76833	182.73941
780.00000	5838.95535	180.46225
790.00000	5933.64441	178.24111
800.00000	6028.83551	176.07393
810.00000	6124.52866	173.95678
820.00000	6220.72384	171.89381
830.00000	6317.42107	169.87725
840.00000	6414.62034	167.90742
850.00000	6512.32166	165.98272
860.00000	6610.52501	164.10162
870.00000	6709.23041	162.26264
880.00000	6808.43785	160.46440
890.00000	6908.14733	158.70556
900.00000	7008.35885	156.98483
910.00000	7109.07242	155.30100
920.00000	7210.28802	153.65288
930.00000	7312.00567	152.03935
940.00000	7414.22536	150.45934